Ouranos Mission

A mission to the Uranian system for in-situ atmospheric measurements

CAELUS: DSE Group 26

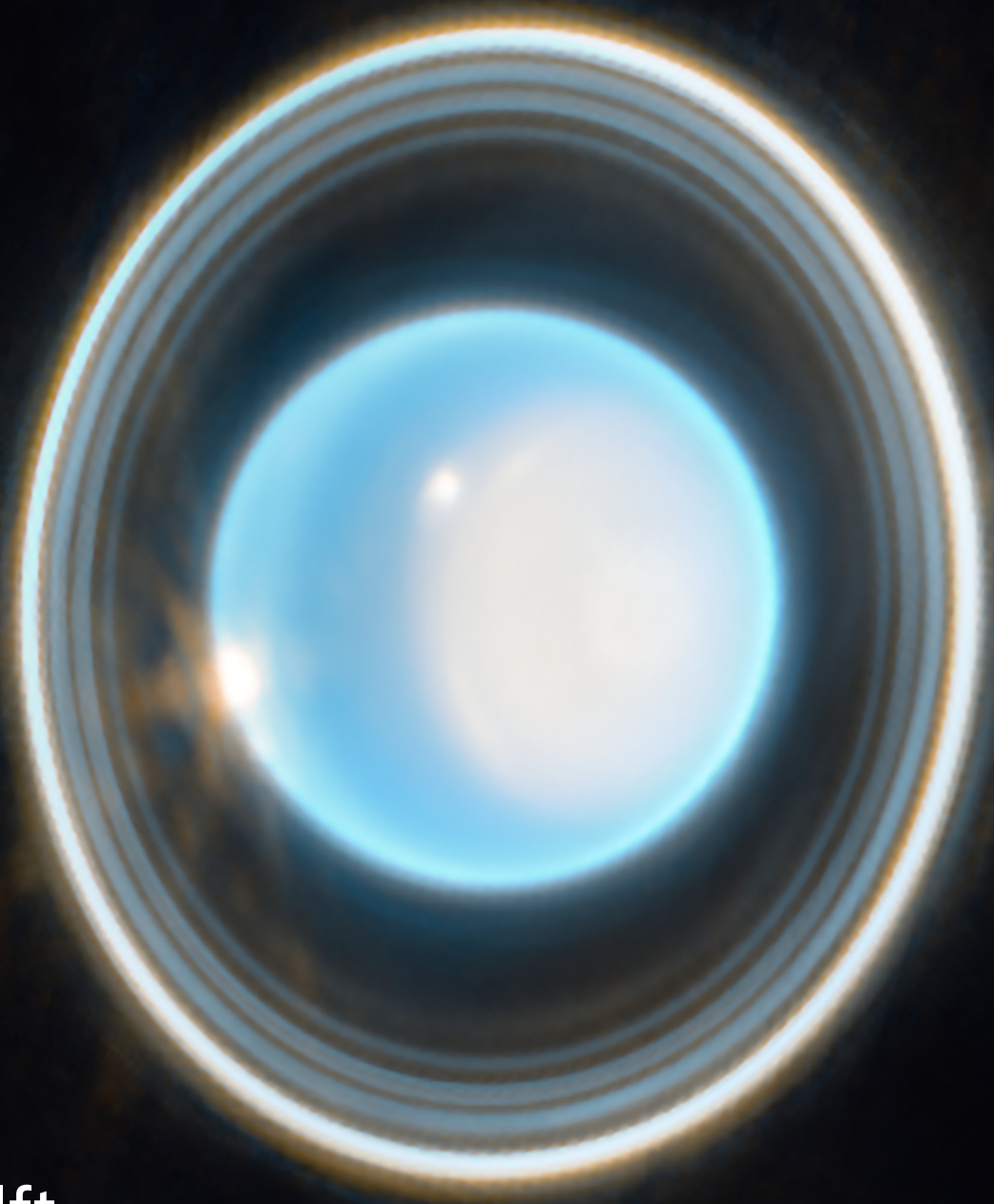

Technical University Delft

TU Delft

Ouranos Mission

A mission to the Uranian system for in-situ atmospheric measurements

by

CAELUS: DSE Group 26

Student Name	Student Number
Arnaud Mathieu	4860136
Arthur Van Der Steichel	5235227
Dennis Lappee	5204615
Elia Dalla Piazza	5228999
Felix Lagarden	4648943
Jeroen Dijkstra	5092604
Marco Zambolin	5250641
Noah Kaijser	5050944
Pierluigi Meneses	5006872
Stan Nuijten	5295556

Tutor: Dr.ir. Erwin Mooij
Coaches: Dr.ir. Erik-Jan van Kampen
Ir. Eva Smeets
Teaching Assistant: Austin Phillips
Institution: Delft University of Technology

TU Delft

Preface

This report marks the end of the Design/Synthesis Exercise of a space mission to Uranus, called *Ouranos*. The aim of the project was to learn to make a complete design of a spacecraft able to collect in-situ measurements of the atmosphere of Uranus. The result of the project, however, far exceeded these learning goals. It provided us with deep insight into the space engineering and exploration fields, as shared by world-leading experts.

Our gratitude towards those that made all this possible cannot be understated. First, we want to thank Austin 'TA Austin' Phillips for sharing his experience with a space-DSE project. Next, a big thank you to our coaches Eva and Erik-Jan who were present every week to provide us with feedback during our status meetings, which served as a welcome and much-needed sanity check. We are grateful to Monsieur Lebreton, whose enthusiasm continually motivated us and who provided us with his well-informed opinion. Not least of all, we cannot thank our tutor Erwin enough for the critical feedback, insights, sources, and all the other help that is now woven into the story of the report.

CAELUS: DSE Group 26
Delft, June 2023

The heavens themselves, the planets, and this centre
Observe degree, priority, and place,
Insisture, course, proportion, season, form,
Office, and custom, in all line of order.

William Shakespeare
Troilus and Cressida (Act I, Scene III)

Executive Summary

With the alignment of the planets in the 2030s, a perfect opportunity is presented to explore the outer reaches of the Solar System. With this, studying Uranus would become possible. With it being one of the least studied planets in the Solar System, the demand for accurate scientific data is high. This is where Ouranos comes in. This project has the specific purpose to design a scientific mission to Uranus, where measurements will be taken of its atmosphere. The summary below highlights the important parts and results of this report.

Science Objectives, Measurements, and Mission Requirements

For the market analysis, past and proposed missions were analysed. This allowed for the identification of extra functionalities or interested parties. One mission extension studies other planets than Uranus, done during the flybys of the relevant planets. Additionally, NASA was selected as an interest based on the fact that they have proposed a similar mission. This allowed for an increase in the budget.

The in-situ atmospheric measurements are known as priority 1 measurements. They are the basis for this mission. They are divided into composition, thermal and dynamical measurements of the atmosphere and composition beneath the clouds. The first measurements are the radiative net balance of the atmosphere, the vertical structure of the cloud and haze layers, and a number of cosmological and tropospheric abundant chemical species. Beneath the clouds, a number of isotopes, noble cases, and the He/H_2 ratio are measured.

For the Uranian system, a number of priority 2 measurements will be taken. For Uranus specifically, the magnetic field, its rings and acoustic oscillating modes will be measured. Over the course of the orbiter mission, it will perform flybys by the five major moons: Miranda, Ariel, Umbriel, Titania, and Oberon.

During its interplanetary trajectory, the space system makes use of gravity assists. Together with CNRS, it was decided that the space system's orbiter shall be in the same configuration during transit as it is during the Uranian orbit phase. This allows for the measurement of the magnetosphere and ionosphere of the planet, as well as performing radio science experiments on its atmosphere. Furthermore, the spacecraft will send its precise location to Earth using high-frequency bands. This aids the search for Planet 9. By measuring the deviation, the search window of Planet 9 could be shrunk immensely.

Deep space missions have a unique Return on Investment. Immediate financial returns are not provided, but the long-term return is outstanding, spanning over several decades, according to the National Space Society. The value lies in the gained knowledge and its subsequent impacts. This also extends beyond science and engineering. It also stimulates the economy by creating jobs and fostering businesses. Additionally, it requires international cooperation, leading to humanitarian actions and promoting diplomatic relations.

Technical Overview

The trade-off was done for system and mission concepts. The four system concepts consisted of a rotorcraft, a blunt body with a parachute, a winged body and additional CubeSats, and a rotorcraft combined with a blunt body. For the mission concepts, there was the choice between a direct transfer and gravity assists, chemical or electrical propulsion, an elliptical or circular orbit around Uranus, a V profile, a staircase profile, and a gradual descent for the atmospheric mission.

The results of the mission and system concepts trade-off can be seen in Table 1 and Table 2, respectively.

Table 1: System Trade-Off Results

Concept	Mass (15%)	Risk (10%)	Sust (5%)	Scientific Yield (40%)	Atmos. Vehicle Power (15%)	Cost (15%)	Total
Rotorcraft	4	1	3	3	1	2	2.5
Winged Body & CubeSats	3	2	3	4	4	1	**3.15**
Blunt Body	4	3	2	2	4	3	2.85
Blunt Body & Rotorcraft	4	2	2	3	1	2	2.55

Table 2: Mission Profile Concept Trade-Off Results. The acronyms are: DT=Direct Transfer, GA=Gravity Assist, RB=Retrograde Burn, DE=Direct Entry, DB=De-orbit Burn, V=V-profile, DD=Drag De-orbit, GD= Gradual Descent Profile, SP= Staircase Profile, ES = Early Separation

Concept	Cost (50%)	Risk (25%)	Mission Duration (15%)	Sustain-ability (10%)	Total
DT, RB, DB, V	1	1	3	3	1.50
DT, RB, DD, GD	2	3	3	3	2.50
GA, RB, DB, SP, GD	3	2	4	4	**3.00**
DT, DE, ES, DD, SP	2	2	3	3	2.25

From the trade-off, it was clear the winged body for atmospheric flight is the best concept. This was due to its score in the scientific yield category, which was also made evident in the sensitivity analysis. For the mission, concept 3 came out as the best. This was mainly due to it having a gravitational assist and the possibility for a secondary mission. However, during the sensitivity analysis, it often shared first place with concept 2. Both were used to optimise the mission profile for the system concept. During the mission profile optimisation, the Uranian orbit phase and the end-of-life phase were reconsidered. The former considered when to separate the atmospheric vehicle and the orbiter, and how to get captured in an orbit, while the latter considered how to dispose of the orbiter. The final concept consisted of an interplanetary gravity assist, with an early separation of the glider and orbiter. The glider will perform a direct entry, while the orbiter will perform an insertion burn. Once in the atmosphere, the glider will perform a gradual descent to measure the necessary scientific data between 0.1 and 20 bar. The orbiter will continue to orbit around Uranus while gathering experimental data on the Uranus system.

The mission starts with the launch from Earth, where it will be carried into a hyperbolic trajectory. After, the system will perform two gravity assists. First, it will swing by Mars, and after 2 years it encounters Jupiter, which sets it on a trajectory to Uranus. After 16 years it will approach Uranus. 20 days before arrival, the orbiter and entry capsule will split, and the orbiter will perform a small manoeuvre to increase. Subsequently, the capsule will enter the atmosphere while protecting the glider. After entry, the glider will be deployed in the atmosphere, where it will descend from 0.1 bar to 20 bar over the course of 4 days. At the same time, the orbiter performs its burn to be captured in an orbit around Uranus and it will send the data back to Earth. After the atmospheric mission has been completed, the orbiter will shift its focus to the moons and the rings. Upon completion of the secondary mission, the orbiter will slowly de-orbit and burn up in the Uranian atmosphere.

Both the orbiter and glider will have multiple payloads onboard to perform their respective measurements. The magnetometer will measure the magnetic field of Uranus in detail. The Net Flux Radiometer gathers data on the dynamics of the atmosphere. The camera will capture images of the major moons of Uranus. The nephelometer will measure the properties of Uranus' cloud and haze layers. The radio science experiment will be used to narrow down to search range for Planet 9, as well as the execution of the PRIDE experiment. The mass spectrometer and the tunable laser spectrometer will be used to measure the chemical composition of the atmosphere. The visible-IF imaging spectrometer will be used to provide spectral images of Uranus and its moons. Finally, the laser altimeter is used to map the height profile of the major moons.

To have a proper risk analysis, it was necessary to define likelihood and severity. These range from very likely (practically guaranteed) to negligible(never happened before), and from catastrophic (mission larger) to negligible (negligible impact). Each of the subsystem engineers identified possible risks for their respective subsystems, which were subsequently categorised. The risk was divided over the orbiter, capsule and glider.

The orbiter has a number of high-severity risks. As, there is significant experience with orbital vehicles, both in Earth orbit and to destinations further out, most systems have low probabilities of failure. These risks are the failure of the high gain antenna and the ADCS. These were mitigated by having redundancies in place.

The main risks for the capsule are that the heat shield would be too thin over its whole area, the glider might not deploy, and the structural failure of the backshell. To mitigate these the heat shield will have an additional thickness and the parachute should allow the capsule to descend over the desired pressure range in 2 h.

The glider is the riskiest part of the mission, both because the mission's success hinges on it and because it is the first glider outside of Earth's atmosphere. The most important risks are the thermal limits of the payload, batteries and structure being exceeded and wing or glider deployment failure. Several mitigations were put in place. Both the payload and batteries are both encased in thermal isolation. The mitigation for the glider is as follows: it will first be put under the capsule, but still attached to it. This allows for the testing of the deployment system and allows for the unfolding of the wing.

Before starting the final design of the different systems and subsystems, it was important to first establish the relevant subsystem requirements. This was done by splitting the group members according to their primary and secondary subsystems. Each individual came up with a list of relevant subsystem requirements. This was

done both by having general knowledge about their respective subsystem and performing a literature review. Most system requirements were still TBD at that time but were filled in over the course of the detail design phase.

Glider Design

Moving onto the glider design, to perform the necessary measurements, the glider has a number of instruments on board. These are a net flux radiometer, a nephelometer, an atmospheric structure instrument, a mass spectrometer, and tunable laser spectrometer and a radio science experiment, whose purpose has been described in the previous section.

Before sending the data to the orbiter, it must first be processed by the OBCs. In total three rad-hard RAD720 OBCs will be in place, where one is present for redundancy. This will result in a total bit rate of 2251 bit s^{-1}. It will also have the capability of storing the data gathered by the payload, as the glider and orbiter will not be in contact for 100 % of the mission time. Furthermore, the three OBCs will perform the same calculations and compare the data before sending it to the orbiter so as to guarantee the reliability of the received data on Earth.

For the glider communications, the communication frequency was first selected. This will be a one-way link, meaning the glider does not receive any communication, which decreases the mass and lessens the complexity of the design. The main phenomena to overcome are free space loss and atmospheric attenuation. In order to do so, the signal will be sent in the Ultra High Frequency region, at a frequency of 405 MHz and 326 MHz, and no compression of the data will be performed. Following this, the antenna design was considered. Due to the strong winds, achieving high pointing accuracy is problematic. To overcome this, an omnidirectional antenna was selected to allow communication at a large range of angles from boresight. Furthermore, the antenna will have a low or medium gain due to the large beam width of the signal. The antenna chosen is the quadrifilar helix antenna. It has a maximum angle from boresight of 70°.

As the glider descends to 20 bar, its atmospheric attenuation will worsen over time. However, most of the power of the signal is lost due to free space loss. With an antenna efficiency of 55 % it will have a pointing loss of −0.12dB. By also considering the total link budget, the total subsystem power can be determined. By considering a margin of 3 dB for the signal-to-noise ratio and a loss of 45 %, a total power of 181 W was calculated.

The first thing that was done, was selecting an appropriate airfoil for the glider's main wing, the horizontal stabiliser and the vertical stabiliser. This was done via inspection, based on the aerodynamic characteristics of the various airfoils chosen. The aerodynamic characteristics were determined by analysing the airfoils using the XFLR5 airfoil design tool. All the analyses were run with 150 panels, at a density of 0.05 kg m^{-3} and a kinematic viscosity of 2.25×10^{-5} m^2 s^{-1}. The main characteristic that was considered was the $\frac{C_l}{C_d}$ ratio, due to the gliding flight. From this, the FX62-K-153/20 airfoil was chosen for the main wing and the NACA0012 for both the horizontal and vertical stabiliser.

This was followed by estimating the dimensions of the wing. The wing area was calculated to be 2.91 m^2. With an aspect ratio of 26.4 , this results in a span of 8.56 m and a mean chord of 0.32 m. As the glider has no quarter chord sweep, the taper ratio becomes 0.4 From here, the root and tip chord were calculated to be 0.43 m and 0.17 m, respectively. Using the aerodynamic and geometry values of the glider, both the time of flight and glide range could be determined. These are 4 d, 1 h and 15 min, and 8541 km.

Next, the stability of the glider was analysed in XFLR5. As there is no active control, it is especially important for the glider to be both statically and dynamically stable. It is desired to have a negative slope in the C_m vs α curve, and the real parts of the eigenvalues be negative. This was done by iterating over different glider geometries and centre of gravity positions, which resulted in a statically stable glider. For dynamic stability, XFLR5 uses a linearised model. It analyses two longitudinal eigenmotions (phugoid and short-period) and three lateral eigenmotions (spiral, roll damping, and Dutch roll modes). After iterating through various parameters, such as dihedral, sweep, and horizontal stabiliser angle of incidence, a dynamically stable glider was found. The final wing, vertical and horizontal stabiliser parameters can be found in Table 3

Before starting the structural analysis of the glider, it was first important to choose the appropriate materials. The aluminium alloy Al-Cu 2024 and titanium alloy Ti-6Al-4V were chosen as the used materials. Both have good properties with regard to specific normal and shear strength and are thus considered. Two other alloys were briefly considered (Al-Cu 2324-T19 and Al-Cu 2224-T351X), however, not all relevant properties could be found, and as such were discarded. Furthermore, per the ECSS-E-30 stands, a safety factor of 1.3 will be applied to any thickness calculated and a factor of 1.1 applied to stress.

The wing analysis was split up into multiple parts. First, the cross-sectional area was defined. For simplicity, the cross-section of the wing was assumed symmetric, as well as the resultant force acting halfway through the horizontal section. The cross-section consists of three parts: a half circle, a rectangle, and an isosceles triangle. Because of this simplification, the analysis will be more accurate for symmetric airfoils than for cambered ones. This would lead to an overdesign in the structure for the case in which an asymmetric airfoil is selected, which is preferred to underdesigning. The first step in the analysis was to consider the shear stress due to the torsion

Table 3: Overview of the Aerodynamic Parameters of the Glider

(a) The Aerodynamic Parameters of the Wing and Other Aerodynamic Dimensions

Wing parameters	
b [m]	7.45
c_r [m]	0.407
c_t [m]	0.163
Γ [deg]	-0.5
Λ_{c2} [deg]	0.996
AR [-]	26.2
Static Margin [%]	0.15
$\overline{c}$ [m]	0.302
Other parameters	
l_f [m]	1.675
d_f [m]	0.7
$l_{connection}$ [m]	1.675

(b) The Aerodynamic Parameters of the Horizontal and Vertical Stabiliser

Vertical stabiliser parameters	
b_v [m]	0.671
c_{r_v} [m]	0.373
c_{t_v} [m]	0.15
Horizontal stabiliser parameters	
b_h [m]	1.36
c_{r_h} [m]	0.267
i_h [deg]	3
c_{t_h} [m]	0.15

Table 4: Overview Main Budgets Glider

Budget	Value
Power [W]	323
Mass [kg]	330.8
Cost [M€ FY22]	50.74

caused by lift. Second, the transverse shear due to lift was considered. For this, structural idealisation was used to estimate said shear. Third, the normal stress due to bending was analysed. The wing was approximated as a cantilever beam to ease the analysis. Fourth, buckling was considered, for which only the spars were analysed. The analysis results in a minimum thickness for the spars. Last, the thermal stresses were taken into account, by considering the temperature differences the glider will experience.

The fuselage analysis was next. It has a length of 1.675 m and a diameter of 0.56 m. Its thickness was computed based on torque and pressure loads. However, the fuselage has a small surface, and therefore any aerodynamic loads can be neglected. Furthermore, the fuselage will contain holes, such that no pressure difference is present. This means the thickness is limited by manufacturing and thus will be 0.8 mm. From these calculations, a number of parameters were determined. The fuselage has a required thickness of 0.8 mm and the wing a thickness of 1.4 mm. This led to a total mass for the glider structure of 172 kg.

The glider has to operate between 273 K and 293 K for the subsystems and payload to operate properly. For the analysis, it was assumed that the skin surface of the glider is at the same temperature as the outside air and that the payload and subsystems are contained in cylinders, whose centre is aligned with the centre of the fuselage. The length of this cylinder is the total length of the payload placed in sequence (0.5072 m). The largest width dimension is 0.20 meter, which results in a clearance of 0.138 m between the cylinder and the fuselage. The same calculation was made for the subsystem cylinder, which resulted in a length of 0.8 m and a radius of 0.1 m. Thermal management subsystems normally either add heat or remove heat by radiating it away. For this, the heat flux due to radiation, and the heat loss due to conduction are considered, as were the heat generated by internal electrical inefficiencies. The calculations were done for a payload temperature of 276.5 K and a subsystem temperature of 283 K. From the subsystems, it was determined that the minimum power generation at all times is 5.234 W, and the maximum heating power required is 14 W. To provide part of this thermal minimum a Radioisotope Heating Unit was selected. The isotope used is americium-241, which has a half-life of 430 yr. RHUs are produced in units of 3 W, which each weigh 200 g. The remaining heating is performed by onboard heaters, which provide up to 11 W of heating power over the mission.

For the glider power, the different subsystems and the payload were considered. For the total flight time of 97.25 h and the time between separation and entry being 20.7 h, the total required energy storage is 33.8 kW h. For this, a non-rechargeable lithium carbon monofluoride battery was selected. The selected battery has a specific energy of 710 W h kg^{-1}, an energy density of 1000 W h L^{-1} and a capacity of 51 W h.

An overview of the most important budgets of the glider can be found in Table 4.

Atmospheric Entry

For the modelling of the atmospheric entry, it was first important to have a reliable model of the atmosphere of Uranus. For this, NASA's General Reference Atmosphere Model (GRAM) was used (Justh et al., 2021). It uses a list of altitude, latitude and longitude as input and gives atmospheric properties (pressure, density,

temperature, etc.) as outputs. One feature the Uranus GRAM is missing is the modelling of winds, which is due to a lack of data. The trajectory model simulates how the capsule moves over time. For this, it was decided to use Tudat to simulate the capsule movement. Using this, the entry of three different segments could be simulated. The ballistic entry has a duration of about 7 min. This is followed by a descent with a supersonic parachute, which takes a little over 1 min. Finally, the capsule descends with a normal parachute until the required pressure level. This takes 4 min. In total, the atmospheric entry has a duration of around 12.5 min.

Aeroshell Design

The main purpose of the capsule is to protect the glider during entry. For this, a simulation used for the atmospheric entry was run. The equations used for convective heat flux and radiative heat flux were originally optimised for Jovian entry and are not necessarily indicative of the heating in the Uranus atmosphere. However, both atmospheres are primarily made up of hydrogen and helium, which justified their use. It was found that the radiative heat flux was a magnitude larger than the convective heat flux. It also affects the capsule of a larger altitude range. The convective and radiative heat flux peak at 4.9 $MW\,m^{-2}$ and 5.0 $MW\,m^{-2}$. With these values, the total heat load of the entry trajectory was calculated to be 221 $MJ\,m^{-2}$, from which the required heat shield thickness was determined. For this the heat shield material PICA was chosen, as it is a very well-understood material and it has a low density. By applying a safety factor of 11.7 %, a thickness of 5.98 cm was found. This also resulted in a total heat shield mass of 181 kg, which is 50 % of the total capsule mass.

For the parachute design, three considerations were taken into account: shock loads are created during deployment, an increase in stability, and it will act as a backup during descent in case the glider deployment fails. It is expected that the capsule will be unstable during transonic flight, which necessitates the use of a supersonic parachute, which will be deployed at Mach 2.0 The parachute diameter was dictated by it being a backup to the glider. For this, it has to descend to the 20 bar level in at least 4 h. This resulted in a diameter of 11.2 m. By using the PIA.C-44378 Type III fabric, the total mass became 6.92 kg.

The second part that should be considered is the suspension. For this 8-strand nylon ropes with a diameter of 0.5 cm were used. The low diameter was chosen based on redundancy, as more lines could be used, than when using a high diameter. Using a safety factor of 3 on the line count, results in a total of 54 lines, with a total mass of 46.2 kg

The aeroshell consists of two main elements: the heat shield as discussed earlier, and the backshell. The backshell is further divided into a top, middle and bottom shell. The first two were assumed to have a trapezoidal shape. The geometry is constrained by the glider size, the size of the parachute, and entry characteristics. Furthermore, the height of the middle shell is constrained by the height of the folded wings. The lower and upper radius of the top shell was constrained by the parachute and were found to be 0.5 m and 0.6 m. The remaining dimensions were calculated by using a taper ratio of 0.66 based on the MSL entry capsule.

The top and middle shell experience two main loads: axial shock loads during parachute deployment and pressure loads in the atmosphere. The pressure loads result in the minimum thickness of both parts. The axial stress acts on the top shell, which results in its smaller radius.

The bottom shell was designed next. It supports the thermal shield and thus has the same shape. The main loads analysed are those from the entry accelerations and the atmospheric pressure. The bending stresses are the critical stresses, which resulted in a minimum thickness of 7 cm.

Lastly, the thermal loads generated during entry were considered with a peak temperature change of 200 °C. As a result, it was decided to use a hypocrystalline ceramic aerogel, due to its low coefficient of thermal expansion and low density. The insulation layer formed by the gel was determined to be 4 cm. From this, the total structure mass could be computed to be 41.6 kg.

The stability of the capsule is important to guarantee that it enters the atmosphere at the correct orientation. For this, it is important to consider the location of the centre of mass (CM) and the centre of pressure (CP). The more aft the CP is located with respect to the CM, to more stable the capsule is. Additionally, to ensure the capsule does not enter the atmosphere at a fixed angle of attack due to a laterally offset CG, it was also necessary to add a large mass of 38.2 kg.

Before the glider starts its mission, its wings should be able to unfold first. As such, the glider will first stay attached to the capsule during entry so it can survive the loads. During the entry phase, the glider will be attached to the capsule at multiple points to avoid collisions with other subsystems. A mechanism needs to be in place to get rid of the heat shield. This will be done by using a pyro. The second mechanism is a rail over which the glider can gain an initial velocity before starting its flight. To prevent damaging the fuselage, it will slide upon a cart over the rails. The third mechanism has to be present to open the bottom of the capsule. The last mechanism is related to the unfolding of the glider. The wing span is too large to fit within the capsule, and thus the wings must be folded. For this, an electroactive high-temperature shape memory polymer reinforced with carbon fibres will be used. By running a current of 15 V through the wings, they will deploy by themselves, preparing the glider for the mission.

Table 5: Launcher Trade-Off

Launcher	**Cost (40%)**	**Payload (45%)**	**Sust. (15%)**	**Total**
Falcon Heavy	4	2	3	2.95
Falcon Heavy Expendable	3	4	2	**3.3**
Vulcan	2	2	1	1.85

Table 6: Properties of the Three Most Promising Gravity Assist Trajectories and a Direct Transfer for Reference.

Planets	**ΔV transfer [m s^{-1}]**	**ΔV capture [m s^{-1}]**	**Flight time [yr]**
EU	1817	997	19.79
EJU	132	493	21.62
EMJU	170	783	16.10
EVVEJU	3	550	26.26

Table 7: Orbital characteristics of the Capsule Trajectory up to Entry Around Uranus

Capsule orbital characteristics			
V_∞ [m s^{-1}]	**Periapsis** [km]	**Atmospheric entry velocity** [km s^{-1}]	**entry flight-path angle** [°]
4240	19.400	26,600	-33.0

Astrodynamics Design

First, it was important to have a trade-off between the possible launchers. The launchers chosen were the Falcon Heavy, in both reusable and expendable configurations, and the Vulcan launcher. The results of the trade-off are presented in Table 5. The winner is the Falcon Heavy in its expendable configuration. This is due to its scoring in the cost and payload criteria.

As Falcon Heavy came out as the best launcher from the trade-off, its payload mass to Uranus can be estimated. This is because no values are given, only to Earth orbits, Mars and Pluto. By using the data available on the launch capabilities and the ΔV required, a tool was developed to estimate the launch ΔV required based on the total system mass. This tool was used during the design of the interplanetary trajectory.

To design the interplanetary trajectory the Tudat package was used for the modelling and Pygmo was used for the optimisation of said trajectories. For the trajectory design, many gravity assists are possible. A single flyby is only possible if either Jupiter or Saturn is used. Using the inner planets can lower the required propellant at the cost of transfer time. However, the inner planets are unlikely to efficiently bring the spacecraft to Uranus. Therefore, only trajectories including Jupiter, Saturn or both are considered. Furthermore, only three flybys of the inner planets are considered. There are also limits set to the flight time: between 30 and 500 d for the inner planets and between 400 and 2000 d for Jupiter and Saturn. The time until Uranus is between 3 and 20 years. The four most promising trajectories are shown in Table 6, where V refers to Venus, E to Earth, M to Mars, J to Jupiter and U to Uranus. It was assumed that the launch provided a total ΔV of 6264 m s^{-1}. The Jupiter assist requires a small burst at Earth departure but has the smallest capture burn. The trajectory along Mars has the largest capture burn but compensates with the lower flight time. The longest assist requires the lowest propellant, but a lot of flight time. This is a big advantage with the use of an RTG, as its power output decreases exponentially over time.

Again Tudat was used for the simulation. The capsule trajectory was simulated up to atmospheric entry. Once it passes a preset height above 1 bar, the state of the capsule is given as input to the atmospheric entry mode. After, the required burn manoeuvre for the orbiter is determined. Its state is propagated up to its periapsis, where it is assumed to be in its orbit. The main parameter for the orbit selection is the entry angle. It being either too shallow or too steep will be catastrophic for the mission. The bounds for the simulation were set between 30° and 35°, which is controlled by setting the periapsis. The entry velocity and position follow from the orbit. Furthermore, the atmosphere was considered to start at 1000 km above the 1 bar line. The results are displayed in Table 7.

Next, the orbit of the orbiter was designed. Any corrective burns will be performed far away from Uranus, as to decrease the cost of any correction manoeuvre. After periapsis, the orbiter enters a captured orbit. The final orbital characteristics are displayed in Table 8.

The final orbit of the orbiter is a major factor in the designing of the communication system of the glider. For this, the distance between the glider and the orbiter and the angle between radial out at the glider and the vector from the glider to the orbiter is determined at all points of the entire atmospheric mission. These distances and angles were subsequently checked with the constraints of the glider communication system. This results in a list of communication intervals. The characteristics can be found in Table 9.

Table 8: Orbital characteristics of the Orbit the Orbiter Will Enter During the Atmospheric Mission

Orbiter orbital characteristics					
V_∞ [m s^{-1}]	**periapsis** [km]	**apoapsis** [km]	**inclination** [°]	**argument of periapsis** [°]	**orbital period** [h]
4240	26,900	240,000	81	118	35.3

Table 9: Properties of the Orbit Relevant to the Communication Design

Part of mission in contact with orbiter [%]	**Maximum distance** [km]	**Maximum angle** [°]
40	225,000 km	70

After the atmospheric mission has been concluded, the orbiter will continue to investigate Uranus and its moons for 3 more years. The initial inclination of the orbit of the orbiter is at 81°, which complicates manoeuvres to encounter any of the moons. Additionally, its low apoapsis places only Miranda and Ariel in range for an encounter. Therefore, to preserve fuel it is advised to perform flybys of either Miranda or Ariel. These encounters can be performed by adjusting the orbit at either periapsis or apoapsis. These manoeuvres should be repeated for the duration of the mission in Uranian orbit. During the manoeuvres, the orbiter should take care to avoid the rings, to prevent any unnecessary risks. In the initial orbit, this is easy, but as the inclination decreases due to successive flybys, a manoeuvre to increase the periapsis to a point higher than the rings should be considered to solve this problem

Orbiter Design

The orbiter will have the magnetometer, camera, radio science experiment, visible-IF imaging spectrometer and a laser altimeter onboard. These are necessary to perform the secondary mission. This results in a total payload mass of 28.78 kg and a power of 16.2 W

Similar to the glider, the orbiter will also need a data handling system. The payload will generate a maximum bit rate of 40 Mbit s^{-1}, from which the camera generates the most. The orbiter will perform flybys of the moons and take images with said camera. Together with the company Edgise, it was determined to use region-of-interest compression to lower the data generated by the images. This results in a total of 35MB per flyby. The NanoXplore NG-Large will be used to compress the data, whereas the OBC will deal with the scientific data and the telemetry of the subsystems. The communications subsystem then sends a downlink to the ground station network.

The communications subsystem is responsible for sending all the gathered data to Earth. To have it reliably sent to Earth, the uplink and downlink must be designed correctly. For this, the signal-to-noise ratio, the antenna gain and the pointing loss are considered. It was necessary to have a pointing loss of less than 1dB, which results in a pointing accuracy of 0.769 m rad. The analysis performed was done for both a high gain and a low gain antenna. The antenna configuration is similar to that of Cassini, where one LGA is mounted on top of an HGA, with a second LGA placed on the other side of the orbiter. The HGA operates at X- and Ka-band, while the LGA operates only at X-band. With both having an amplifier with an efficiency of 0.6 , a transmitted power of 50 W and an input power of 84 W is required. The total subsystem has a mass of 121.1 kg and a peak power consumption of 116.6 W.

The Attitude Determination and Control Subsystem (ADCS) is important to guarantee pointing accuracy, accurate manoeuvring, and disturbance resistance. For the attitude determination, it is required to have the orbiter orientation known to 0.7 mrad. The attitude will primarily be determined using star sensors and gyroscopes. A total of three star sensors will be present, with one for redundancy. In addition to that, there are also two inertial reference units, made up of two gyroscopes each. They have a tendency to drift and therefore require periodical information from the star sensors to recalibrate. When in orbit around Uranus the ADCS also needs to counter disturbance torques. The disturbances considered are a gravity gradient torque, a magnetic disturbance torque, atmospheric drag, a torque due to solar pressure, and a thrust-misalignment torque. With these disturbances, the attitude control configuration can be found. For this four blocks of four thrusters are placed on the outer edges of the orbiter to give it full control. These are the MC-111C thrusters. Although 12 would be enough for full control, 16 thrusters are needed to guarantee a large misaligned torque is sufficiently countered. For this a propellant mass of 15.4 kg is needed.

The orbiter will use RTGs for its power generation, therefore it was necessary to perform two trade-offs. The first trade-off resulted in the used isotope. This trade-off was based on the power density of the different considered isotopes after 20 years. From this, it was decided to use plutonium-238, as its power density after 20 years was more than double the second-best option. The main problem is that plutonium-238 is scarce, but NASA has started to produce more plutonium-238, with the possibility to increase the production rate. The second trade-off is the RTG type which was based on power density and cost. From this, it was decided to go with the GPHS-RTGs as it has the highest BOL power. Based on the required power of 466.3 W, a total of 3

Table 10: Final Propellant Tanks Dimensions

Propellant	Tank Radius [m]	Tank Length [m]	Wall Thickness [mm]
N_2O_4	0.5	0.05	1.8
MMH	0.5	0.04	1.8

Table 11: Overview Main Budgets Aeroshell

Budget	Value
Power [W]	466.3
Mass [kg]	2709
Cost [M€ FY22]	1162.3

RTGs will be used, with a PCDU to distribute the power. Finally, the power system has a mass of 217.1 kg.

The propulsion system is required to perform manoeuvres during the mission, with the largest being orbital insertion (ΔV = 1398 m s^{-1}). Based on CNRS03.08-O-PRP.01, the propulsion system shall provide a minimum thrust of 400 N. This is only possible with chemical propellants. To fulfil both the thrust and specific impulse requirement, the bipropellant N_2O_4/MMH was found as a suitable propellant.

Next, the engine was chosen, which is also based on the thrust and specific impulse requirements. It also depends on the burn time of a single burn, which cannot exceed 96 min. From this, the Apogee motor S400-15 was chosen for this mission.

The orbiter structure was decided to have an integral structure, meaning the tank surfaces act as load-bearing elements. This allows for the saving of mass and cost, as less material will be required. With this, the tanks will be optimised to withstand axial, lateral and pressure loads that could be encountered during operations. It was decided to have the tanks with a cylindrical body and two spherical caps. The volume of the tanks was based on the densities of N_2O_4 and MMH. For pressurising the gas, isothermal expansion was assumed. To find the radius and length of the tanks, an optimisation was implemented to minimise the tank mass.

Next, the thickness of the tanks was determined by considering the launch loads of the Falcon Heavy and the pressure at the propellants that have to be stored. A safety factor of 1.3 was applied to the final value of the thickness. With the thickness, the radius and length could be determined. This was done by considering the critical bending stress and critical buckling stress.

Lastly, a vibrational analysis was performed on the tanks. This was done by checking the natural frequency of the structure against the vibrational loads experienced during launch. With these analyses, the final dimensions were calculated and they are presented in Table 10.

For the thermal management of the orbiter, three components were considered: the absorbed energy, the emitted energy, and the heat dissipated by the various subsystem on board the spacecraft. The absorbed power consists of solar radiation, the albedo radiation of the planet encountered and the planet flux. For the emitted power, the orbiter is assumed to have a cylindrical shape, from which the radiative and absorptive area can easily be found. Before starting the calculations, it is important to determine what type of multi-layer insulation will be used because it highly influences the thermal balance. Due to its large distance from the Sun, the orbiter will need insulation that allows a very high absorptivity and very low emissivity. For this, aluminised Kapton foil was selected. This resulted in an absorbed power of 3.28 W, an emitted power of 133.8 W and a required thermal power of 130.6 W to heat up the spacecraft. This heat will be generated by the RTGs, which will be placed at a distance of 2.7 m from the spacecraft. However, due to its trajectory and the fixed RTG distance, the spacecraft will make use of louvres, which are metal strips which are forced open upon a specific thermal heat. The total mass of the subsystem becomes 69.8 kg.

An overview of the most important budgets of the orbiter can be found in Table 11.

Project Management

The reliability of the glider, aeroshell and orbiter has already been discussed in their respective sections and will not be repeated here. For availability, it is more interesting to look at the individual subsystems instead of the full system, as the design will be used once. Once it is assembled, the total system should have an extremely high availability. Off-the-shelf components and subsystems will be preferred due to the cost decrease. The glider requires little development time, as most subsystems do not require new technology. The only component that is relatively new is the RHU, however, it is still easily available as it is used on an industrial scale. The aeroshell needs to be custom-made, but it is a standard type structure and thus has a high availability. The desired gel has a lower availability. Another component that is limited is the parachute. The orbiter has limited availability and limited development time as well. All subsystems except for the power system are easily available. This is due to the scarcity of Plutonium-238.

Maintainability concerns itself with the maintenance of the system; both on Earth and during the mission. The subsystem with the lowest maintainability of the glider is the structure. Due to the integration of the other subsystems, the inspection can only be done by removing these subsystems. For the aeroshell, maintenance of the explosive used to release the parachute and the heat shield is the most difficult. Maintenance of the heat shield itself is also difficult. The maintenance of the orbiter is similar to that of the glider.

Finally, safety was considered. The main component of the glider that could cause harm is the RHUs. When the radioactive material gets exposed, it poses possible safety issues. However, the risk is lower due to the high amount of safety tests. For the aeroshell, the explosives are the components that could cause harm. Finally, for the orbiter, the RTGs could harm the environment as well. Similar to the RHUs, the risk is low due to the many safety procedures.

The logistics consist of multiple parts to be considered. The first part is the testing facilities, which will be the testing facilities at ESTEC. This is for the integration of the main orbiter and glider subsystems. However, for the capsule, Langley Research Center will be used due to its high expertise. After the testing phase, the spacecraft needs to be delivered at Kennedy Space Center (KSC) four weeks before launch. Here the spacecraft will be integrated into the launcher at the Horizontal Integration Facility. After integration, the communication and operations are analysed. Three main facilities are critical and these are the Spacecraft Operations Control Center (SOCC), the Payload Operations Control Center (POCC) and the Mission Control Center, which are located at ESOC. Additionally, the data server will be set up at the MCC, with an additional SOCC at the Launch Control Center at KSC.

The operations consist of all the people and activities necessary to make the spacecraft and atmospheric vehicle fulfil the pre-selected functions and mission objectives. Throughout the mission, a very different amount of people will be required to work at the MCC, SOCC and POCC depending on the phase of the mission. The most crowded phases will be the launch and early mission operations due to the many checks and in-orbit tests, the two fly-bys at Mars and Jupiter where many measurements data will be gathered and finally during operations at Uranus. This last phase will be the longest one, therefore leading to a very high operational cost.

The production concerns itself with the main structural elements of the Ouranos mission. These are the glider wing, glider fuselage, glider T-tail, backshell structure, thermal shield, and orbiter structure.

First, the glider wing, which consists of four skin panels, four ribs and should be made of Ti-6Al-4V. The skin panels are flat plates that can be manufactured using separating by the mechanical removal from a bigger panel with a constant thickness. The post-processing should consist of removing burr or inaccuracies at the edges by sanding. The production of the ribs will be different, as they require a higher thickness and a very specific complex shape. For this extrusion will be used. Once both have been manufactured, they will be assembled. The skin panels are linked via friction stir welding and the ribs are connected using common welding.

The fuselage will be cylindrically shaped and made out of Al-Cu-2024. Rolling manufacturing can be used to get the plate into the desired shape. It can be closed by friction stir welding or common welding techniques. With the same process, the nose can be connected to the cylindrical section. Then, the production of the T-tail is considered. Due to the similarities between loads and geometry, the same manufacturing processes used for the wing are applied to this structure.

The backshell of the aeroshell is considered next. Due to the high aerodynamics, pressure and thermal loads, it is critical to choose the right manufacturing process. As such, it should be made an integral structure to avoid any heat or cracks propagating through the backshell. As a result, metal forming is the only manufacturing process that can be used, where a specific mould should be created.

After, the thermal shield is considered. The required manufacturing process can be determined based on previous deep space missions. Due to the similarities between the panels used in the Ouranos mission and the Space Shuttle, the manufacturing process can be derived from this.

Finally, the orbiter structure has to be produced. It was decided to make this an integral structure with the propellant tanks. As this is an element that is commonly used, the casting of the tanks can be done via a private company. For the closing of the spherical caps and the cylindrical sections of the tanks, friction stir welding will be required.

Many different aspects were taken into account during the design for the sustainability of this mission. The impacts of the requirements were considered first. The requirements that would be problematic are ESA03 and ESA03.07. This former was concerned with the usage of toxic materials. Early on this was identified as unfeasible and it was changed to a restraint to keep toxic material usage to a minimum. The latter concerned itself with the reusability of the launcher. With the total system mass, the reusable form of the Falcon rocket could prove to not be able to launch the system. During the design phase, sustainability was used as one of the trade-off criteria. This was most important during the trade-off of whether or not to use a kick stage and when considering the propulsion type (chemical vs electrical).

The impact of the manufacturing phase was also considered. Although the total system is very complex, it has a high manufacturing readiness level due to decades of space exploration. The manufacturing of the glider is relatively straightforward as aircraft and glider manufacturing is well developed. However, due to the novelty of the design, intensive testing will be required. In the case of the manufacturing plan of the Ouranos mission

systems, since their structural characteristics are extreme, the processes used will result in a lot of material waste. This will have a negative impact on the sustainability of the mission.

The selection of the launch vehicle was also considered. The main characteristics for these would be the reusability of the launcher and the CO_2 emissions produced during the launch. For reusability, the most obvious choice would be SpaceX's Falcon launcher series as these are designed specifically for reusability. Although, from a fuel standpoint it is not necessarily more sustainable than other launchers, as it still produces CO_2 during launch.

The end-of-life phase of this mission was also considered and was split into the space part and the atmospheric flight part. For the space part, the possibilities of secondary scientific missions were considered. These include flybys of Uranus' moons and a separate mission for the orbiter itself. The atmospheric flight had different aspects to consider. Due to the gradual descent flight profile, the option for a secondary mission presents itself more easily. As the glider is unpowered, the mission duration becomes a design variable.

Lastly, the operations and logistics were analysed. With the SOCCC, POCC and MCC being at the same location, positive strides toward sustainability have been made. Furthermore, the testing locations for the orbiter and glider are located in Europe. However, the testing of the parachute and capsule will be performed in America. This does mean that the net carbon footprint will be smaller as fewer systems will have to be transported to the KSC.

Conclusions and Recommendations

The current design uses a glider, which will greatly exceed the required time span within the Uranian atmosphere. This glider would allow for the most comprehensive and in depth understanding of an outer planet in addition to the first in-situ measurement of an ice giant. In addition, the determined cost of the mission is lower than the projected budget of the mission. The mass could also be increased by a significant amount without increasing the Δv budget. These factors mean that the scientific yield of the mission could be expanded without going beyond the cost budget.

Many recommendations were done for a continuation of the design. Only the most important ones will be presented here. Regarding the propulsion subsystem of the orbiter, the use of the green monopropellant ASCENT could be considered: at the moment a 100 N thruster is developed, hence it can be considered to cluster four of these together and function as the main engine to provide enough thrust.

Regarding the aeroshell, Computational Fluid Dynamics (CFD) shall be used to better quantify the highest heat flux and its point of action. On the other hand, as far as the decelerator is considered, deployment mechanisms have not been designed for the parachute, which shall be investigated for it to properly work.

Finally, for the glider, RTGs might be considered as power sources, once enough radioactive material would be available: it would not only allow for a larger mission duration but also for less complicated thermal management. From a structural point of view, horizontal and vertical stabilisers have not been analysed due to time constraints: for completeness, their contribution to load bearing, total mass and cost shall be included; finally, the load transfer between wings, tail and fuselage has been left out: that is something that should be seriously designed since that is where usually peak stresses arise.

List of Symbols

The lists below describe several symbols and abbreviations used within the body of the document

Constants

π	3.141592654....	[-]
σ	Stefan Boltzmann constant $5.670374419 \times 10^{-8}$	[W m^{-2} K]
c	speed of light 2.99792458×10^{8}	[m s^{-1}]
g	Earth gravitational acceleration 9.806 65	[m s^{-2}]
I_{xz}	Polar mass moment of inertia (Y-axis)	[kg m^2]
k	Boltzmann constant 1.380649×10^{-23}	[J K^{-1}]
k	Coefficient of thermal conductivity	[-]

Symbols

$\bar{c}$	Mean chord	[m]
Δh	Altitude difference	[m]
ΔV	Change in velocity	[m s^{-1}]
$\frac{C_L}{C_D}$	Lift over drag ratio	[-]
$\frac{W}{S}$	Wing loading	[N m^{-2}]
$\overline{c}$	Mean Aerodynamic Chord	[m]
$\overline{P}$	Pressure normalised by the stagnation point pressure	[-]
A	Surface Area	[m^2]
a	Semi-major axis	[m]
a	Speed of Sound	[m s^{-1}]
a_2	Length of Rectangular Portion of Airfoil Cross-section	[m]
a_3	Length of Triangular Portion of Airfoil Cross-section	[m]
a_s	Albedo Radiation Flux	[W m^{-2}]
acc	Acceleration	[m s^{-2}]
AR	Aspect ratio	[-]
b	Wing span	[m]
C_D	Drag coefficient	[-]
C_L	Lift coefficient	[-]
C_p	Pressure coefficient	[-]
C_r	Root chord	[m]
C_t	Tip chord	[m]
C_{D0}	Zero lift drag	[-]
D	Antenna diameter	[m]
E	Elastic modulus	[GPa]
e	Oswald efficiency factor	[-]
e	Pointing accuracy	[rad]
E_b/N_0	Signal-to-noise ratio	[-]
F	Visibility Factor	[-]
f	Frequency	[Hz]
G	Gain	[dB]
G	Shear modulus	[GPa]
g	Gravitational acceleration	[m s^{-2}]
h	Heat load	[J m^{-2}]
h_{range}	Vertical distance	[m]
I_{sp}	Specific impulse	[s]
I_{xx}	Area Moment of Inertia (X-axis)	[m^4]
I_{xx}	Mass Moment of Inertia (X-axis)	[kg m^2]
I_{yy}	Area Moment of Inertia (Y-axis)	[m^4]
I_{yy}	Mass Moment of Inertia (Y-axis)	[kg m^2]
I_{zz}	Area Moment of Inertia (Z-axis)	[m^4]
I_{zz}	Mass Moment of Inertia (Z-axis)	[kg m^2]
J_s	Solar Radiation Flux	[W m^{-2}]
J_{IR}	Infrared Radiation Flux	[W m^{-2}]
L_a	Atmospheric attenuation	[dB]
L_l	Transmitter loss factor	[dB]
L_pr	Pointing loss	[dB]
L_r	Receiver loss factor	[dB]
L_s	Space loss	[dB]
L_{distr}	Distributed Lift Force	[N m^{-2}]
L_{res}	Resultant Lift Force	[N]
M	Mach number	[-]
m	Average Molecular mass	[-]
m_h	Horizontal stabiliser mass	[kg]
m_w	Wing mass	[kg]
$M_{bending}$	Bending Moment	[N m]
p	Pressure	[N m^{-2}]
P_0	Beginning-of-life power	[W]

q	Heat flux	[W m^{-2}]
q_b	Basic Shear Flow	[N m^{-1}]
q_{s_0}	Equivalent Shear Flow	[N m^{-1}]
R	Gas constant	[J kg^{-1} K^{-1}]
R_N	Surface normal distance to the centre line	[m]
R_{glide}	Glide range	[km]
r_{tank}	Tank Radius	[m]
S	Wing area	[m^2]
s	Surface distance from the stagnation point	[m]
T	Orbital period	[s]
T	Temperature	[K]
t	Airfoil Maximum Thickness	[m]
t	Thickness	[m]
t	Time of flight	[s]
t_b	Burn time	[s]
T_s	System noise temperature	[K]
t_t	Skin Thickness	[mm]
TH	Heat shield thickness	[cm]
V	Flight Velocity	[m s^{-1}]
v	Velocity	[m s^{-1}]
V_∞	Hyperbolic excess velocity	[m/s]
V_{prop}	Pressurising Gas Tank Volume	[m^3]
V_{prop}	Propellant Tank Volume	[m^3]
x_c	X-location of the Centroid	[m]
$x_{a.c.}$	Longitudinal position of the wing aerodynamic centre	[m]
$x_{c.g.}$	Longitudinal position of the centre of gravity	[m]
$x_{n.p.}$	Longitudinal position of the neutral point	[m]
Y	Molecular mass fraction	[-]
SM	Static Margin	[percent]

Greek Symbols

α	Coefficient of Thermal Expansion	[K^{-1}]
α_{IR}	Absorptivity	[-]
β	Surface angle with respect to the centre line	[rad]
ϵ_{IR}	Emissivity	[-]
η	Efficiency	[-]
Γ	Dihedral	[rad]
γ	Flight path angle	[rad]
γ	Specific Heat ratio	[-]
λ	Taper ratio	[-]
λ	Wavelength	[m]
λ_n	Eigenvalue	[-]
$\Lambda_{c/2}$	Half chord sweep	[rad]
$\Lambda_{c/4}$	Quarter chord sweep	[rad]
μ	Gravitational parameter	[m^{3}s^{-2}]
ν	Poisson's ratio	[−]
ω_n	Frequency	[Hz]
ρ	Density	[kg m^{-3}]
ρ_{avg}	Average density	[kg m^{-3}]
σ_y	Yield Stress	[MPa]
τ_y	Yield Shear Stress	[MPa]
$\tau_{1/2}$	Half life	[years]
ε	Emissivity factor	[-]
ε	Strain	[-]
ζ	Damping Ratio	[-]

Abbreviations

ADCS	Attitude Determination and Control Subsystem
ASCENT	Advanced Spacecraft Energetic Non-Toxic
BOL	Beginning-of-Life
CAELUS	Comprehensive Atmospheric and Environmental Learning of Uranian System
CFD	Computational Fluid Dynamics
CM	Centre of Mass
CNRS	Centre national de la recherche scientifique
CP	Centre of Pressure
DGB	Disk-Gab-Band Parachute
DNA	Deoxyribonucleic Acid
DR	Data Rate
DSN	Deep Space Network
EOL	End-of-Life
FH	Falcon Heavy
FOS	Factor of Safety
GRAM	General Reference Atmosphere Model

HGA	High Gain Antenna
HIF	Horizontal Integration Facility
IRU	Inertial Reference Unit
JWST	James Webb Space Telescope
LEO	Low Earth Orbit
LGA	Low Gain Antenna
MMH	Monomethylhydrazine
MMOI	Mass Moment Of Inertia
MSL	Mars Surface Laboratory
NAC	Narrow Angle Camera
NASA	National Aeronautics and Space Administration
NFR	Net Flux Radiometer
PCDU	Power Conditioning and Distribution Unit
PICA	Phenolic Impregnated Carbon Ablator
RCS	Reaction Control System
RHU	Radioisotope Heating Unit
ROI	Return on Investment
RSE	Relative Standard Errors
RTG	Radioisotope Thermoelectric Generator
SMA	Shape Memory Alloy
SPICE	Spacecraft, Planet, Instrument, Camera Matrix and Events
ToF	Time of Flight
TRL	Technology Readiness Level
Tudat	TU Delft Astrodynamics toolbox
TWTA	Travelling Wave Tube Amplifier
UHF	Ultra High Frequency
VLBI	Very Long Baseline Interferometry
WAC	Wide Angle Camera

Contents

1. Introduction

Inherent in our human DNA is the drive to understand where we come from and to explore what we don't know. This can be seen all throughout history; from the time we left the mainland of Africa to landing on the surface of the Moon. The latter is considered the pinnacle of human exploration efforts but often overshadows other giant leaps taken in space science and engineering. At the start of the 1990s, the first exoplanet was detected. Later that decade until now, many thousands have been confirmed after dedicated exoplanet telescopes were used. More than 30 % of exoplanets are labelled as *Neptunian* exoplanets[1]. Investigating the Neptunian planets in our Solar System, i.e. Uranus and Neptune, widens our understanding of them and the formation of the star system we call home.

William Herschel discovered Uranus in 1781 while probing the night sky in search of binary star systems. At first, he thought that the newly detected celestial body was a comet, but after weeks of verification with other astronomers, it was confirmed to be a planet[2]. In the last 200 years, up until Voyagers' flyby of the planet and recent observations by the James Webb Space Telescope (JWST), its general planetary characteristics could be determined. Compared to Earth, it is 4 times wider and has a mass of around 14.5 Earth masses. It is located at 19.8 astronomical units from the Sun, at an inclination of 97.77° with the Ecliptic. A Uranian day lasts a little more than 17 h, and a year of roughly 84 Earth years. Uranus has a ring and an extensive moon system; 5 major moons accompanied by 21 smaller ones. Similarly to the other Gas Giants, Uranus' atmosphere consists of mostly hydrogen and helium, with traces of ammonia, water, and methane. The latter gives Uranus its blue colour[3].

Following the Mission Need Statement, this report aims to provide the full design cycle of a deep space mission that will explore the Uranian system and take in-situ measurements of the atmosphere. Both mission and system design principles are used to form a detailed overview from the moment the spacecraft leaves Earth to the final mission phase at Uranus. Interplanetary trajectories, an atmospheric entry, and a flight path were optimised to fulfil the mission objectives of the orbiter, aeroshell, and glider. The orbiter is called Herschel, named after the scientist, whereas the glider is named Prometheus, signifying that it brings knowledge about Uranus. These objectives are driven by different stakeholders from many different fields; from the customer CNRS in Orleans to world-leading experts from across the world. In line with the Project Objective Statement, the detailed design and reporting were done by CAELUS (Comprehensive Atmospheric and Environmental Learning of Uranian System) which consists of 10 students from the Aerospace Engineering faculty of the Delft University of Technology, over a time span of 10 weeks. This final part of their Design/Synthesis Exercise marks the end of the bachelor's curriculum.

The report has the following structure. It is divided up into four parts. Part I starts with the scientific objectives and mission requirements presented in Chapter 2. Then, it gives a technical overview of the mission and system architecture in Chapter 3. Part II covers everything related to the atmospheric mission. Chapter 4 discusses the glider design. Then, the atmospheric entry is illustrated in Chapter 5 which is followed by the aeroshell design in Chapter 6. Next, Part III explains the space mission aspect by giving the astrodynamic design in Chapter 7 and the orbiter design in Chapter 8. Part IV presents the final chapters concerning the assembly, operations, and organisation by providing a complete configuration overview in Chapter 9 and the general management of the Ouranos mission in Chapter 10. An extensive conclusion with recommendations is given in Chapter 11.

[1] URL: https://exoplanets.nasa.gov/what-is-an-exoplanet/planet-types/neptune-like/ [cited 21/06/2023].

[2] URL: https://www.nationalgeographic.com/science/article/uranus#:~:text=Uranus%20was%20the%20first%20of,mistaking%20it%20for%20a%20comet. [cited 27/06/2023].

[3] URL: https://solarsystem.nasa.gov/planets/uranus/in-depth/#:~:text=The%20seventh%20planet%20from%20the,the%20plane%20of%20its%20orbit. [cited 27/06/2023].

PART I

MISSION CONCEPT TO URANUS

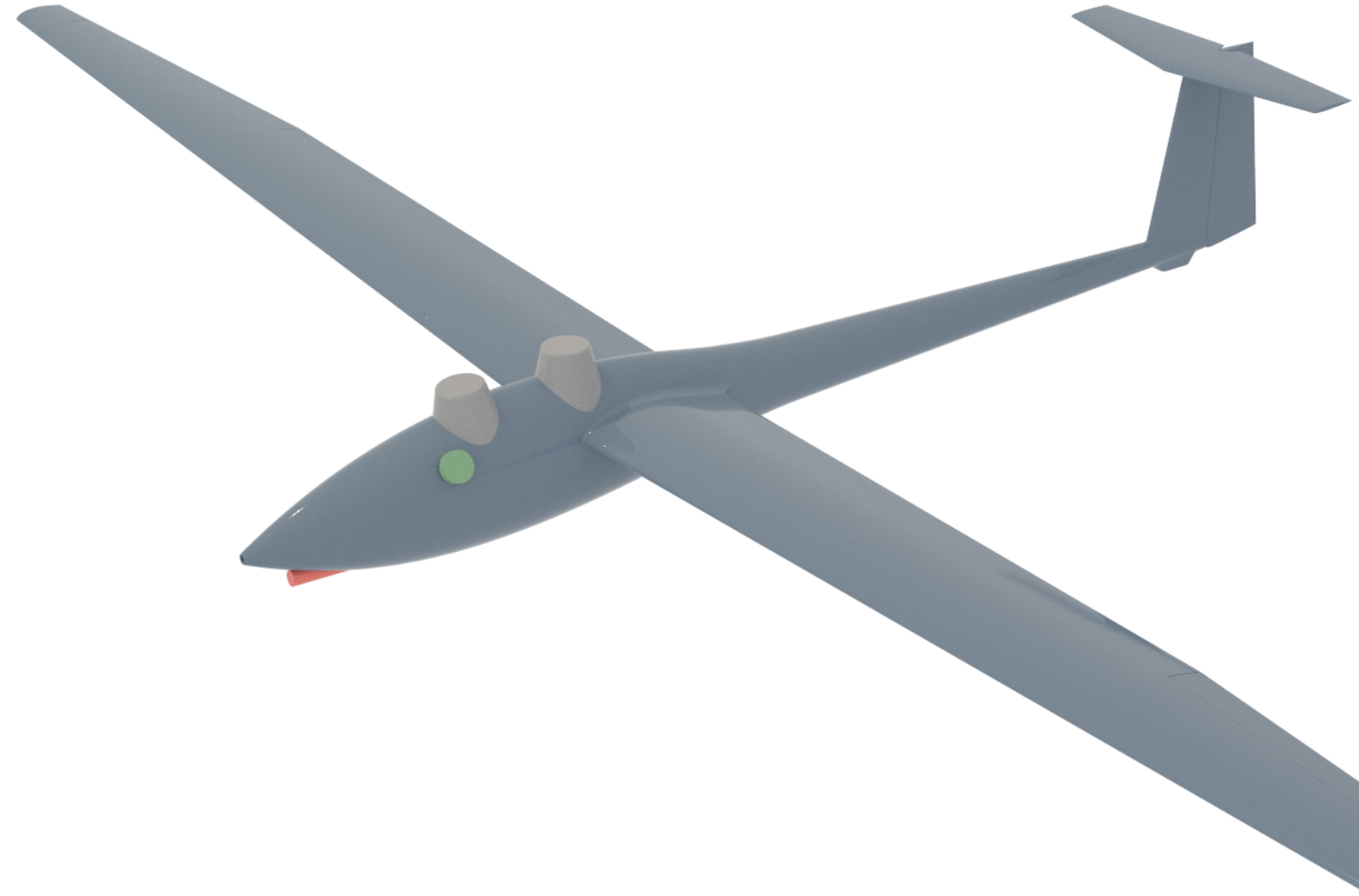

2. Science Objectives, Measurements, and Mission Requirements

Ouranos is a science mission by nature. All engineering functionality developed in the following chapters is in service to the scientific goals and objectives that were set together with the customer, experts in the field from the Delft University of Technology, and other stakeholders in the scientific community. CNRS was the primary source to determine these objectives, with Dr. Lebreton as the project scientist and contact point. First, a market analysis is described in Section 2.1 to identify additional mission goals and stakeholders. Second, Section 2.2 presents the priority 1 objectives and measurements taken by Ouranos, which justifies a deep space mission to Uranus set by the stakeholders and deals with in-situ measurements of the glider. Next, Section 2.3 covers the priority 2 science, which was determined after discussions with experts in the field to make full use of the orbiter within the budget constraints. After that, Section 2.4 explains how the current payload suite could be used for extra science, which does not necessarily concern a Uranus mission and therefore got labelled with priority 3. Then, Section 2.5 talks about mission justification. Lastly, Section 2.6 discusses the return on investment of this scientific mission to Uranus.

2.1 Market Analysis

A market analysis was performed to ensure a competitive design. Past and proposed missions were analysed to identify extra functionalities and other interested parties. Studying a larger part of the Uranian system, instead of focusing only on Uranus, was identified as an extended mission possibility while studying the magnetic and gravitational field was classified as a secondary mission and set as a requirement. Both of these types of missions would require an orbiter and it was therefore set as a constraint.

NASA was selected as a party that would have an interest in Ouranos based on the fact that they are proposing a very similar mission (Simon et al., 2021). It was estimated that they would pay M€500 to make such a mission reality. This increase in budget could be used to improve the quality of the primary mission by designing a better-performing atmospheric vehicle, to improve the secondary mission by doing extra measurements or to increase the extended mission possibilities. Additionally, funding by NASA could be spent to cover the cost of the payload.

2.2 In-situ Measurements of Uranian Atmosphere

The findings of Voyager 2's remote measurements had error bars that were too big to discern between the abundances of small protosolar and supersolar chemical species, causing difficulties in properly providing models of Uranus' interior (Mousis et al., 2018). Previous missions resolved this issue for other gas planets by sending scientific probes that took in-situ measurements, as illustrated by Galileo and Cassini. In-situ measurements provide valuable information about a planet's compositional, thermal, and dynamical structure, as well as the vertical distribution of some gases and details about processes in the far deeper atmosphere. Inspired by (Atkinson et al., 2020), Section 2.2.1 and Section 2.2.2 cover the priority 1 measurement of the Ouranos mission.

2.2.1 The Compositional, Thermal, and Dynamical Atmospheric Structure

By measuring the altitude profile of the net radiative balance between solar and visible insulation and upwelling thermal infrared radiation, the glider will provide data to investigate the radiative net balance of the atmosphere. The vertical structure of the cloud and haze layers will also be determined, next to its composition and properties by collecting aerosol optical properties, size distribution, number and mass densities, and composition.

Another aspect of this scientific objective is the questions concerning the stability and vertical structure of the temperature and pressure up to 20 bar. The atmospheric winds and wave phenomena variations as a function of depth need to be investigated by Doppler wind experiments between the glider and the orbiter, also from 0.1 to 20 bar. How the distribution of chemical species in the atmosphere is shaped by these convective motions and vertical mixing, will be resolved by sampling

- the cosmological abundant species CH_4, NH_3, H_2S, H_2O, and
- the tropospheric abundant species CO, PH_3, AsH_3, GeH_4.

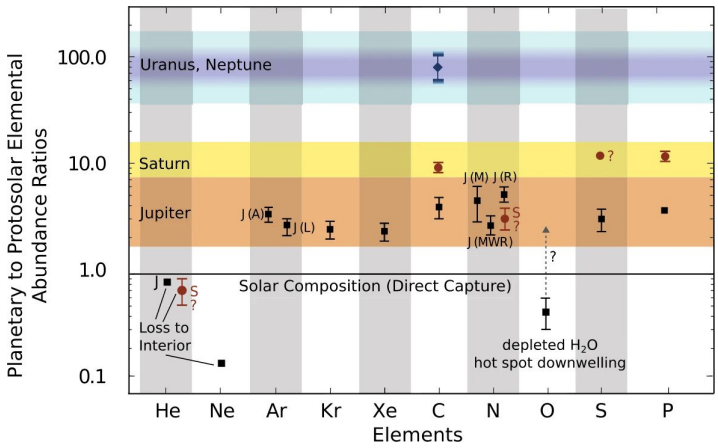

Figure 2.1: Element abundances for different Solar System bodies (Atreya et al., 2020)

2.2.2 Composition beneath the Clouds

In-situ measurements allow investigation of the deeper troposphere by breaking through the layers of haze and clouds, beyond the reach of flyby spacecraft. Heavy noble gases are particularly significant, together with the most important reservoirs of the main isotopes of H, C, O, and Ne. Therefore, for the glider to meet the final priority 1 science objectives, it will sample

- the isotopes $^{14}N/^{15}N$, $^{12}C/^{13}C$, D/H, $^{3}He/^{4}He$, Ne, Ar, Kr, Xe, $^{18}O/^{17}O/^{16}O$,
- the well mixed abundances of the noble gases He, Ne, Xe, Kr, Ar,
- the cosmic abundance ratio He/H_2.

The region that is considered to be beneath the clouds starts from roughly 10 bar and below. This is far into the mission duration of the glider, and the probability of receiving altered data from the attenuation of the atmosphere only increases from here. The orbiter will therefore also include payload instruments that can pierce through the upper cloud layers to accompany the glider in gathering information about the lower atmosphere. Looking at Figure 2.1, it is clear that the abundance ratios in the atmosphere of Uranus either have a large error bar or are unknown. The figure also compares the ratios per element for all the outer planets. It is taken from a paper which focuses on critical in-situ science of the Icy Giants (Atreya et al., 2020). Next to the isotopes and noble gases given in the figure, the paper also covers the cosmological and tropospheric abundant species. All the science measurements mentioned in this section can be found in the Science Traceability Matrix in Appendix B. The mission objective is met if all these measurements are performed in a 2-hour window, in pressure ranges of 0.1 to 20 bars.

In summary, Ouranos shall

- Measure the radiative energy balance of the atmosphere.
- Measure the Doppler frequency shift between the orbiter and glider.
- Determine the composition of the atmosphere, clouds, and haze layers.
- Investigate the vertical profiles of the thermal and dynamical atmospheric structure.
- Sample and monitor the vertical profile and abundance of heavy noble gases and chemical species.

2.3 Explore the Uranian System

This section covers all the priority 2 measurements that will be performed in the Ouranos mission. They are not part of the original justification of this mission but were determined in cooperation with Dr. Lebreton as they are of great interest to CNRS and the scientific community in general.

2.3.1 Magnetic Field Interactions

This priority 2 measurement has the same scientific objective as the priority 1 measurement about the radiative net balance, namely determining how the magnetic field interacts with the upper atmosphere. It is, however, part of the orbiter payload and not the glider system, since the orbiter can add valuable information by measuring the magnetic particle fluxes and how they change in different orbital ranges.

The space system will measure Uranus's magnetic particles and fields and how those concentrations change over different ranges of time and space. These experiments will enable scientists to determine how the magnetic field interacts with the solar wind.

2.3.2 Magnetic Field Formation

The final part of the study of the magnetic field concerns its formation. It is tilted with respect to Uranus' rotational axis, so gathering information about its formation could provide an answer to this weird anomaly. This objective can be achieved by indirectly measuring the material inside the core of Uranus, through Gravity / Radio Science Experiments. In other words, the orbiter will remotely measure and map the internal magnetic field structure.

2.3.3 Acoustic Oscillating Modes of Gas Giants

The interior of the outer planets of our Solar System is thought not to be homogeneous. This means that no conclusions can be made about the core from measuring the abundances in the atmosphere, presented in Section 2.2, alone (Gaulme et al., 2014). To understand the formation of planetary systems like our own, a proper study of the interior of the system's celestial bodies is required. Therefore, another way of determining the interior of the planet is taken into account in the orbiter's scientific objectives.

This will be done through helioseismology. It has been proven useful when studying the photometric light curve of other stars. Similarly for Jupiter and Saturn, as gas planets are mostly fluid and convective resulting in their seismology resembling that of stars more than terrestrial planets. According to (Gaulme et al., 2014), gas planet-seismology is made possible by the resonant cavity and a mechanism to make it possible to produce acoustic modes. The first can be thought of as a large echo chamber inside the planet; wavelengths of sound get trapped inside a region which can be caused by a difference in temperature or density. The latter can be expected to be present as the infrared emitted by the planet is higher than expected based on the temperature alone, although for Uranus the excess is only 6 %. This excess energy is radiated out as acoustic waves (Goldreich et al., 1994), in the order of μHz. Comparing the excess with other gas planets, it is clear that Uranus is on the lower side, meaning that it almost is at thermal equilibrium. Hence, the orbiter will probe the photometric light curve of Uranus to check if it has acoustic oscillating modes at all.

2.3.4 Moon Science: Oberon, Titania, Umbriel, Ariel, and Miranda

Inspired by the JUNO mission, Ouranos will perform flybys of Uranus' five major moons, namely Miranda, Ariel, Umbriel, Titania, and Oberon. Compared with JUNO, which did not carry instruments dedicated only to moon science, Ouranos will perform measurements focused on answering as many questions about the moons. What is the internal magnetic field structure of the moons? What is their core made of? What are their height profile, composition, and physical properties? Therefore, many of those instruments will be based on the payload suite of JUICE, which has been designed to explore the Jovian moon system. These scientific data are very important to the scientific community because most of the Uranian moons could host a residual ocean a few tens of kilometres thick which could potentially harbour life (Castillo-Rogez et al., 2023). Other payload instruments onboard Ouranos that are part of the priority 2 suite can be used to further investigate the moons.

2.3.5 Uranian Rings

Ouranos will lastly look into the rings of the Uranian system. Two sets of rings are present: inner and outer rings and they most likely consist primarily of black radiation-processed organics mixed with water ice. Nine rings in the inner set have a dark colour while the outer set has two rings with distinct colours; the innermost is reddish, and the outer one is blue, like Saturn's E ring. The Bond albedo of the rings' particles is below because of how dark the rings are. Figure 2.2 shows an image of Uranus with its rings taken by JWST[1]. Next to verifying the composition, Ouranos will also determine the structure of the rings using radio occultation. Such an experiment could be very useful to study the origin, age, and shaping process of the rings.

Understanding this, together with previously mentioned science objectives concerning the Uranian system can contribute to our knowledge of the formation of Uranus and its orbiting neighbours. More generally, strengthening our grasp on the dynamics of complex planetary systems inside the Solar System presents a strong base to study exoplanets.

[1] URL https://www.nasa.gov/feature/goddard/2023/nasa-s-webb-scores-another-ringed-world-with-new-image-of-uranus [cited 13/06/2023]

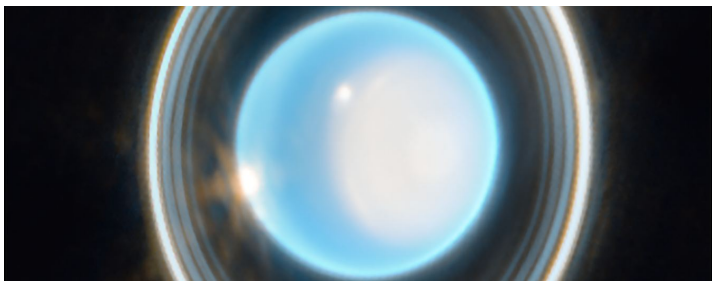

Figure 2.2: Uranus and its rings captured by Webb's Near-Infrared Camera (NIRCam) on February 6, 2023

In summary, Ouranos shall

- Determine the formation and different interactions of the magnetic field to explain its tilted orientation compared to the planet's rotational axis.
- Measure the photometric light curve of Uranus.
- Investigate the atmosphere and ionosphere of Uranus, its moons and the ring system to complete the Uranian system exploration.

2.4 Investigate Solar System Bodies during Interplanetary Flybys

A large contribution, that makes the Ouranos mission interesting for the stakeholders, is its possibility to add scientific objectives as secondary mission requirements, without the need to add new payload instruments. This defines Ouranos' priority 3 measurements. First, this section briefly mentions what experiments will be performed during the gravity assists, after which it covers the search for Planet 9 during the whole period of the interplanetary phase.

2.4.1 Gravity Assists

For its transfer to Uranus, Ouranos will use gravity assists. An advantage of this over direct transfer like Hohmann, for example, is a reduced ΔV budget and an extra possibility to make more planetary measurements and extend the mission's scientific objectives.

Together with CNRS a mission requirement was made, for such a mission phase, which states that the orbiter space system shall be in the same measuring configuration between the transfer and operational phase. This means that Ouranos will measure the magnetospheres and ionospheres of the planet, perform radio science experiments on their atmospheres, and in the case of Gas Giants, collect photometric light curves to probe for acoustic oscillating modes.

2.4.2 Planet 9

Ouranos can address the search for Planet 9 during its interplanetary mission phase. Certain Kuiper Belt objects in our outer Solar System follow a trajectory that can't be modelled by readily-predictable orbital behaviour based on the planets and other trans-Neptune heavy bodies (Batygin et al., 2019). These anomalies in the gravitational field of the solar system could be caused by Planet 9, which has a mass of approximately 6.2 Earth masses, a semi-major axis of approximately 380 astronomical units (AU) with a perihelion of 300AU, and an inclination between 11 and 21 degrees with the Ecliptic (Brown & Batygin, 2021). Figure 2.3 shows the hypothetical orbit of the planet compared to known outer Solar System objects. Planet 9 would also alter the path of the Ouranos spacecraft during its travel between Jupiter and Uranus, compared to its nominal trajectory which doesn't consider this extra planet for the computations.

The spacecraft will use high-frequency bands to send its precise location to Earth, where any deviation will be noticed and any relation with Planet 9 investigated. The gathered data by Ouranos could shrink the search window of Planet 9 a thousandfold and make hunting for the planet with high-powered telescopes much more feasible[2].

In summary, Ouranos shall

- Perform priority 2 measurements during planetary flybys, relevant to the swingby planet.
- Probe for hints of the existence of Planet 9.

[2]URL https://eos.org/articles/a-mission-to-uranus-could-help-find-planet-9 [cited 12 June 2023]

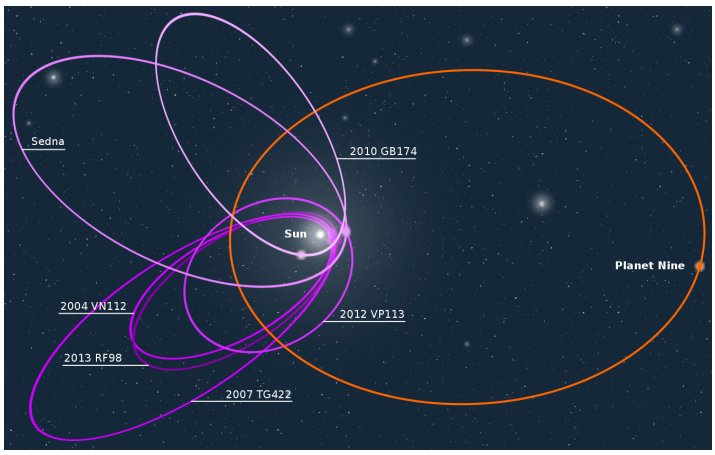

Figure 2.3: The orbit of Planet 9 compared to known outer Solar System objects

2.5 Mission Justification

All the scientific objectives mentioned in the previous sections were translated from six science goals. The science goals can be seen in the Scientific Traceability Matrix in Appendix B as well. The science goals share the same priority label as their corresponding objectives. The priority 1 goals are studying Uranus' atmosphere and sampling its composition. Then, the priority 2 goals are studying the magnetospheres, the major moon system and its rings. Lastly, the priority 3 goal is to study outer Solar System bodies.

These scientific goals will lead to a more complete knowledge of the Uranian System. As mentioned before, a general understanding of such *Neptunian* planets helps to analyse exoplanets in return. Both studies gain insight into the origin of protosolar systems and the formation of their planets. This is used by scientists to investigate the origin and evolution of the Earth itself. Linking back to what was said in the introduction in Chapter 1, which stated that knowing where we come from is inherent in being human; knowing our place in the Universe starts by understanding the place we call home, the Earth.

2.6 Return on Investment

Deep space missions, like expeditions to Uranus, have a unique Return on Investment (ROI) character. They don't provide immediate financial returns, but the National Space Society argues that the long-term return is outstanding, occurring over decades[3].

The value of deep space missions lies in the knowledge gained and subsequent impacts. Scientific experiments on spacecraft provide valuable data, but the true ROI comes from utilising this knowledge. It not only enriches our grasp on our place in the universe and the formation of the Solar System but also benefits non-space and science-related industries. The benefits extend beyond space engineering and science. Knowledge gained from missions stimulates the economy, creating high-skilled jobs and fostering new businesses. Advancements in power and fuel optimisation have practical applications in industries like fuel production, showcasing the tangible benefits of space exploration. Deep space missions often involve international cooperation, which fosters the improvement of diplomatic relations. Exploring distant worlds like Uranus brings people from all over the world together, fostering unity and global cooperation.

In summary, deep space missions may lack immediate financial returns, but their long-term ROI is exceptional. They drive knowledge and scientific discovery, enhance our understanding of the universe, stimulate the economy, create jobs, advance technologies, and foster international cooperation. Investing in space exploration yields benefits beyond our terrestrial boundaries.

[3]URL https://space.nss.org/settlement/nasa/spaceresvol4/newspace3.html#:~:text=Estimates%20of%20the%20return%20on,driving%20productivity%20growth%20is%20technology. [Cited 23 May 2023].

3. Technical Overview

This chapter presents a mission-wide technical overview to offer the reader a high-level technical overview of the system that will perform the Ouranos mission outlined in Chapter 2. In Section 3.1 the trade-off summary is presented. This consists of a discussion on the trade-off criteria, a summary of the different mission and system concepts, and the actual trade-off and mission optimisation. Then a high-level overview of the mission architecture and configuration is presented in Section 3.2. After a description of the different scientific measuring instruments is given in Section 3.3. This is followed by Section 3.4 and Section 3.5, where the functional flow diagram and functional breakdown structure are presented. Then, in Section 3.6, the overall risks of this mission are discussed, after which the numerous subsystem requirements are presented in Section 3.7.

3.1 Concept Trade-off Summary

Before arriving at the final design, a trade-off was done between four system concepts and four mission concepts. This process will be summarised in this section. The trade-off criteria are discussed in Section 3.1.1. Then, the mission concepts are analysed in Section 3.1.3. This is followed by the analysis of the common components of the four concepts in Section 3.1.4. Section 3.1.5 through Section 3.1.8 contain an analysis of the four different system concepts. Finally, Section 3.1.9 presents the trade-off process that was followed.

3.1.1 Trade-off Criteria

Before starting with the preliminary design, it is important what the different trade-off criteria will be. These criteria are the backbone of the preliminary design, as the trade-off will be dictated by these criteria. Due to the nature of the concept generation, the trade-off criteria have been split between the system concepts and the mission concepts.

Mission Concept Trade-off Criteria

The four mission concepts have varying astrodynamics components. The interplanetary trajectory can be performed with either a direct transfer or with gravity assists. Orbital capture at Uranus can also be performed in various ways. The orbital and atmospheric systems could either be separated before or after the system is in orbit. The atmospheric mission itself will be dictated by the possible flight profiles, and the End-of-Life (EOL) strategy of the orbital system can vary. To properly evaluate each mission concept, the following trade-off criteria have been identified:

Cost **Weight: 50%**. The cost for this mission is divided into several components, and for the mission cost the operational costs are leading. This criterion is evaluated qualitatively, as at this stage it was not possible to evaluate the cost.

Risk **Weight: 25%**. The risk of this mission is driven by ESA04, found in Table A.1, as the atmosphere of Uranus has many unknowns. This makes risk a natural trade-off criterion for this mission. Due to the lack of data, this analysis is performed qualitative

Mission Duration **Weight: 15%**. The duration of the space mission affects many different parts. For example, having a longer mission, increase the operations costs. Longer missions are also more demanding for the subsystems, increasing the chances of malfunction or failure. This criterion is assessed quantitatively.

Sustainability **Weight: 10%**. The mission concepts have different environmental impacts. This criterion is assessed based on the required ΔV. This part can be analysed quantitatively. Another part of sustainability is the ability to gather additional data due to the interplanetary trajectory. This part is assessed quantitatively.

3.1.2 System Concept Trade-off Criteria

The four mission concepts also have varying components. The space system may be a singular custom space system, or may also include multiple CubeSats. The atmospheric vehicle may be a rotorcraft, blunt capsule, or a wing body. For these concepts, a total of six trade-off criteria have been identified:

Scientific Yield **Weight: 40%**: The reason for this mission is the scientific interest in gaining knowledge on the formation of the Solar System. The aim is to comply with the scientific requirements, which are derived from the lack of knowledge of the Uranian atmosphere. The system's ability to collect scientific data is therefore leading. This is assessed via argumentation.

Cost **Weight: 15%**. At the time, the budget for the mission was limited to 1.5 Billion Euros. This is excluding possible collaborations with external parties. Because of the limited budget, the cost becomes a trade-off criterion. This can be assessed quantitatively based on estimated system costs.

Table 3.1: Interplanetary Gravity Assist Parameters

Planet swingbys	ΔV [km/s]	Travel time [years]	Departure date
Venus, Earth, Jupiter	7.1	27	May 2034
Earth, Earth, Jupiter	7.3	21	December 2033
Mars, Venus, Earth	7.0	16	August 2034
Mars, Earth, Earth, Jupiter	6.2	28	January 2034
Mars, Earth, Mars, Jupiter	6.1	28	March 2035
Mars, Jupiter, Saturn, Earth	7.5	29	October 2033
Jupiter	7.3	21	June 2034
Direct transfer	13.7	20	November 2040

Table 3.2: Arrival Trajectory Characteristics Summary

Orbit Type	Periapsis Radius [km]	Apoapsis Radius [km]	Hyperbolic Orbit Periapsis Velocity [km s^{-1}]	Elliptical Orbit Periapsis Velocity [km s^{-1}]	Orbital Insertion Burn ΔV [km s^{-1}]	Orbital Period [h]
Circular	27 000	-	21.2	-	6.6	3.2
	39 000	-	17.8	-	5.7	5.6
	98 200	-	11.8	-	4.1	22.3
	82 665	-	12.7	-	4.3	17.2
Elliptical	27 000	583 000	21.2	20.3	1	122.1
	39 000	583 000	17.8	16.7	1.2	125.8
	27 000	98 200	21.2	18.3	2.9	11.4
	39 000	98 200	17.8	14.6	3.3	12

Mass **Weight: 15%**. Mass is one of the main restrictions for space missions. Due to the nature of Tsiokovsky's equation, any addition of mass exponentially increases the required propellant mass. Thus, the mass should always be minimised. This can be assessed with mass estimation methods.

Power **Weight: 15%**. The performance of the system is in large parts related to the power. As an RTG has been chosen as a power source, the total required power dictates its sizing. RTGs are both expensive and limited in their power output, making the required power of primary importance. This can be assessed through statistical and empirical relations.

Risk **Weight: 10%**. Similar to the mission, this is also driven by ESA04, and results in the same argumentation. Although some statistical estimates can be made on reliability, the uniqueness of the mission makes it difficult to quantify.

Sustainability **Weight: 5%**. The production of the system should be sustainable, and comply with the sustainability requirements. This cannot be assessed numerically, as only a preliminary design is considered. It is therefore assessed qualitatively.

3.1.3 Mission Concepts

The analysis of the mission profile encompassed two aspects: astrodynamic trajectories and atmospheric flight. Initially, the focus was on interplanetary transfer trajectories. This involved examining a direct Hohmann transfer from an Earth parking orbit situated at an altitude of 185 km. The calculated ΔV for this transfer was 7.996 km s^{-1}. Additionally, the study explored gravity assists, which yielded ΔV values ranging from 6.051 km s^{-1} to 7.469 km s^{-1}. Seven combinations of gravity assists were considered, involving swingbys of Venus, Mars, Earth, Jupiter, and Saturn. The detailed results can be seen in Table 3.1. As can be seen, all gravity assists need significantly lower ΔV than the direct transfer. However, they do take longer than the direct transfer, except for the combination Mars, Venus, Earth. All the gravity assists have a launch date between 2033 and 2035, as to make use of the position of the planets.

Two types of orbits were evaluated for the spacecraft around Uranus: circular and elliptical orbits. The parameters of these orbits, including radius, periapsis, and apoapsis, were determined based on the dimensions of the inner and outer rings, the atmospheric height, and safety margins. Subsequently, the arrival trajectory was examined, which plays a crucial role in the atmospheric entry of the spacecraft. The outcomes for the different circular and elliptical orbits are summarised in Table 3.2. The primary focus is on the required ΔV, which is noticeably lower for the elliptical orbits compared to the circular ones.

Moving forward, the analysis shifted towards a direct entry trajectory, which posed the challenge of handling significant deceleration estimated at around 100-200 g. The atmospheric flight analysis commenced with the

Table 3.3: Overview of the numerically estimated parameters of system concept 1, to be used for the trade-off

Total Mass [kg]	Atm. Vehicle Propulsion Power [W]	Total Cost [€M]	TRL [-]
2762	34000	3273	7

examination of de-orbiting procedures. Firstly, aerobraking was considered due to its potential to substantially increase the payload capacity to Uranus by reducing the required ΔV. The other method explored was the de-orbit burn, which necessitated a ΔV ranging from 100 m s^{-1} to 2737 m s^{-1}, depending on the chosen Uranus orbit. Subsequently, various flight profiles were evaluated. The V profile offered advantages in terms of data collection but demanded significant power for an ascent. On the other hand, the staircase profile presented a simpler approach, requiring a constant altitude and descent. While it also provided enhanced measurement data, it introduced complexity through the need for active control and guidance. Lastly, the gradual descent profile was considered, which stood out for its simplicity. Although it did not offer notable scientific advantages compared to the other profiles, its reliability was a key advantage. The discussion then shifted to the secondary mission. The possibility of a secondary mission or mission extension depended on the chosen atmospheric vehicle. A winged body had a higher likelihood of an extension mission compared to a blunt capsule.

3.1.4 System Concepts Common Analyses

A dedicated chapter was devoted to exploring the commonalities among various concepts. The chapter begins by presenting payload information, including mass, bit rate, and power usage. Subsequently, the mass budget is treated. A high-level mass estimate was conducted for the rotorcraft, utilizing a regression line established from the Dragonfly, Ingenuity, Ehang 184, and Ehang 216 missions. An iterative stress analysis based on hoop and bending stresses was performed, yielding a mass estimation. Similarly, for the aeroshell and orbiter mass, regressions were carried out using data from different missions (with relative standard errors (RSE) of 42.5 % and 43.3 % respectively) to estimate their masses. Next, a comprehensive analysis of the rotorcraft's power budget is presented and validated using data from the Ingenuity mission. Additionally, a cost analysis was conducted, applying a 20% cost margin based on NASA's Green Book (Ryschkewitsch, 1992). The cost estimations for the rotorcraft were based on available missions such as Ingenuity and DragonFly, while for the blunt capsule, estimations were derived from missions such as Huygens, Galileo, Viking, and Pioneer Venus. The main space vehicle's cost was estimated using linear regression with data from Galileo, Cassini, Juno, and Lucy missions. Lastly, the kick-stage cost analysis focused on the Astris kick-stage, considering ESA's involvement as a key stakeholder. Moving on, the chapter assesses the risks associated with the space system and the electrical propulsion system. Both systems were deemed highly reliable, with a low number of failures compared to the total number of launches. Sustainability was also analysed, starting with the kick stage, where the Astris kick stage was considered due to its expected higher sustainability compared to other alternatives. The impact of fuel, such as hydrazine's toxicity and the unknown effects of xenon ion thrusters on Earth's atmosphere, were taken into account for chemical and electrical propulsion systems, respectively. Finally, a feasibility analysis was conducted. The maximum vertical descent rate was determined to be 23.6 m s^{-1}. It was concluded that electric propulsion is not feasible for this mission due to the required operating power, which ranges between 500 W and 9000 W, which could not be provided by RTGs.

3.1.5 System Concept 1

The initial concept explored was that of the rotorcraft. The analysis began with the mass budget, utilising the findings from the common analysis chapter. The rotorcraft's mass was determined to be 68 kg. For the aeroshell and orbiter, regressions were employed, resulting in masses of 422 kg and 2762 kg, respectively. Next, the required power for the rotorcraft was quantified, as it was the only component considered in this aspect. To achieve a flight time of 2 h, each motor would need to be supplied with 2770 W. Moving on to cost estimation, assessments were made for both the aeroshell and the orbiter. The cost for the aeroshell was estimated to be M€ 850, while the cost for the orbiter was determined to be M€ 3273. The analysis then focused on risk assessment, identifying the rotorcraft as the component with the highest risk. This is attributed to several factors: limited flight history with only one proven rotorcraft, multiple rotors introducing multiple potential failure points, and the use of an experimental battery in the calculations. Finally, the feasibility of the battery was considered. The only way to address this concern was to utilise an experimental high-capacity lithium-sulfur battery. The key findings and values have been summarized in Table 3.3.

3.1.6 System Concept 2

The second concept involved a combination of a winged body and CubeSats. The analysis began with the mass budget. Initially, the winged body's mass was based on a paper about a glider on Uranus, estimated at 234 kg. However, through iteration, the final mass was revised to 93 kg. The aeroshell mass was determined to be 472 kg. Additionally, considering the inclusion of 12 MarCo satellites, the total mass of the CubeSats

Table 3.4: Overview of the numerically estimated parameters of system concept 2, used for the trade-off

Total Mass [kg]	Atm. Vehicle Propulsion Power [W]	Total Cost [€M]	TRL [-]
3345	0	3759	8

Table 3.5: Overview of the numerically estimated parameters of system concept 3, used for the trade-off

Total Mass [kg]	Atm. Vehicle Propulsion Power [W]	Total Cost [€M]	TRL [-]
2514	0	2717	9

Table 3.6: Overview of the numerically estimated parameters of system concept 4, used for the trade-off

Total Mass [kg]	Atm. Vehicle Propulsion Power [W]	Total Cost [€M]	TRL [-]
2713	26000	3349	8

amounted to 162 kg. Finally, the mass of the orbiter was calculated to be 2898 kg. Moving on to the power budget, the required power for the winged body, CubeSats, and the orbiter was determined. The winged body required 152 W, the CubeSats required 300 W, and the orbiter required 9197 W. The cost estimation for this concept presented some challenges, particularly for the winged body due to the lack of reference data. However, assuming its cost was equivalent to that of the rotorcraft, it was estimated at M€ 374. The aeroshell's cost was estimated at M€ 960, the CubeSats at M€ 122, and the orbiter at M€ 3759. A risk analysis was conducted for the CubeSats and the atmospheric vehicle. The CubeSats were found to have a relatively high number of failures, while the atmospheric vehicle was deemed highly risky as it has never been attempted before. Feasibility analysis followed, starting with the analysis of atmospheric operations. The optimum angle of attack, calculated to comply with the maximum descent rate, was found to be around 37.6°. However, it was determined that this angle exceeded the wing's stall limit, and thus it was reduced to 15°. Furthermore, communications feasibility was examined to determine the maximum distance between the atmospheric vehicle and the CubeSats, which was found to be 355 km. This is smaller than any of the considered orbital altitudes. As a solution, it was proposed to place the CubeSats in a lower orbit, acting as relays between the atmospheric vehicle and the orbiter. From this it was determined that the optimum number of CubeSat clusters would be three. The important values have been summarised in Table 3.4.

3.1.7 System Concept 3

Concept 3 focuses on a blunt capsule. The mass budget estimation yielded a mass of 333 kg for the blunt capsule itself and 2514 kg for the main space vehicle. Regarding the power budget, determining the power requirements for the blunt capsule was relatively straightforward since it only carries the payload. Consequently, it would receive the highest possible score in the trade-off analysis. The cost analysis involved the kick stage, blunt capsule, and main space vehicle. The cost of the kick stage was based on the Astris, estimated at M€ 138. The blunt capsule was estimated to cost M€ 640, while the main space vehicle was projected to cost M€ 1935. The total cost for the concept amounted to M€ 2717. The risk analysis concluded that the blunt body posed very little risk, as it has been utilised numerous times and proven highly reliable. The only potential concern was its utilisation in the atmosphere of Uranus, which has not been previously tested. Lastly, a feasibility analysis was conducted. This analysis resulted in determining a minimum parachute diameter of 2.5 m. The important values have been summarised in Table 3.5.

3.1.8 System Concept 4

Concept 4 combines a blunt capsule with a rotorcraft. The estimated mass of the rotorcraft is 71 kg, while the blunt capsule weighs 404 kg, and the orbiter has a mass of 2713 kg. Determining the power budget for the rotorcraft involved considering the power requirements of the measuring instruments and motors. This resulted in a constant power supply of 2160 W to each motor. The cost estimation for the concept utilized the regression analysis mentioned earlier. The blunt capsule was estimated to cost M€ 810, the orbiter M€ 2029, the rotorcraft M€ 374, and the kick-stage M€ 108. The total cost for the concept amounted to M€ 3349. The risk analysis mainly focused on the rotorcraft, which led to a similar conclusion as in concept 1. Additionally, the introduction of a blunt capsule increased the number of potential points of failure, thus reducing overall reliability. The feasibility analysis of the rotorcraft involved estimating the parachute diameter, resulting in a diameter of 4.6 m. Lastly, the minimum thrust and corresponding pitching angle were determined, considering the worst-case scenario of head-on wind. The minimum thrust was found to be 3.94 kN at a pitching angle of 52.7°. The important values have been summarised in Table 3.6.

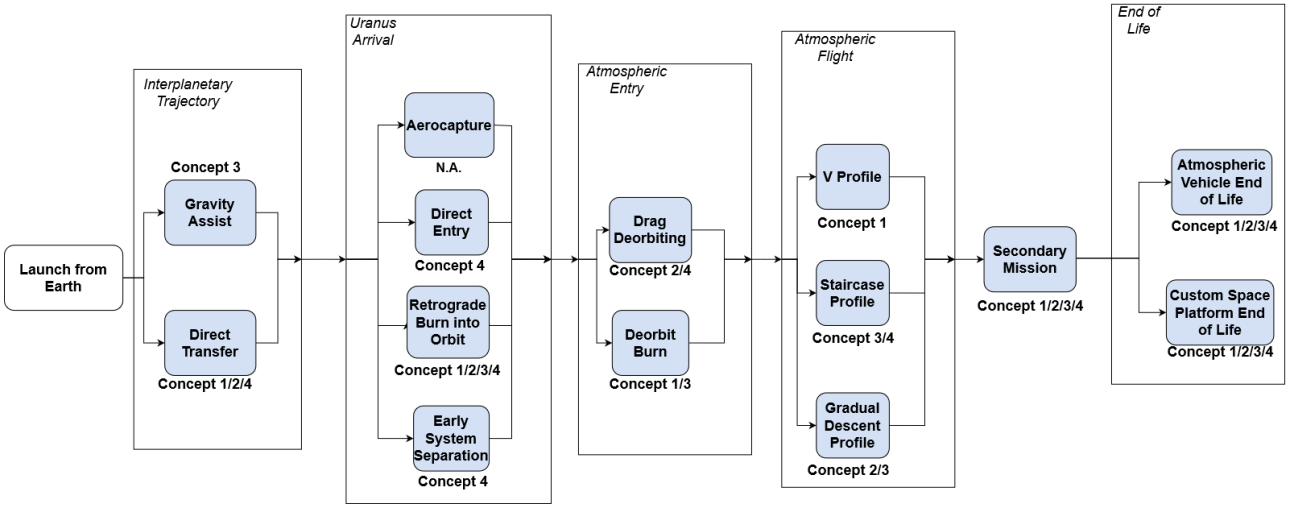

Figure 3.1: Mission Concept Timeline

Table 3.7: System Trade-Off

Concept	Mass (15%)	Risk (10%)	Sust (5%)	Scientific Yield (40%)	Atmos. Vehicle Power (15%)	Cost (15%)	Total
Rotorcraft	4	1	3	3	1	2	2.5
Winged Body & CubeSats	3	2	3	4	4	1	**3.15**
Blunt Body	4	3	2	2	4	3	2.85
Blunt Body & Rotorcraft	4	2	2	3	1	2	2.55

3.1.9 Trade-off Process

The trade-off process describes the steps that were taken to arrive at the final concept. The concepts were scored on a scale of 0 to 4, where 0 means it cannot meet the requirements and 4 means that it exceeds the requirements. First, the mission profile was considered, followed by the system concepts. Then the mission profile was optimised such that it would fit the system concept. Last, the complete concept is summarised.

3.1.10 Mission Profile Concept Trade-off

Here the trade-off process for the mission concepts is described. The flow of the different mission concepts can be seen in Figure 3.1 and an overview of the results from this trade-off can be seen in Table 3.9.

Concept 1 was scored lowest. This was due to its scoring in the cost (1) and risk (1) criteria. The scoring for cost was due to the V profile and the direct interplanetary transfer. The V profile is a high-risk manoeuvre, and by using a direct transfer the ΔV required becomes too high. For mission duration and sustainability, it scored a 3. This is due to the relatively short time it takes for a direct transfer, and the ΔV required per mission phase.

This was followed by concept 2. Similarly to concept 1, it needs a high ΔV and was thus scored a 1 in cost. For risk, it was given a 3 as a Hohmann transfer carries less risk than a gravity assist. Additionally, a gradual descent is considered less risky. For mission duration, it was given a 3, as it performs well, but is not the best. For sustainability, it is similar to concept 1 and was given a 3.

Continuing with concept 3, it was scored a 3 in cost, due to its low ΔV usage. In risk, it was scored a 2, which was due to the usage of gravity assists and the staircase profile. In mission duration, it has a 4, as its shortest gravity assist is shorter than a direct transfer. In sustainability, it was scored a 4 and follows the same argumentation as previous concepts.

Finally, concept 4 was scored. For the cost, it was scored a 2, with the same explanation as concept 2. In risk, it was given a 2, which was due to the staircase profile. For mission duration, it is similar to concepts 1 and 2 and thus scored a 3. Finally, sustainability is similar to concepts 1 and 2 and was also given a 3.

Following this, a sensitivity analysis was performed. This was done by switching the places of the weight.

Table 3.8: General overview of all the important values of the system concepts that helped in the trade-off process

	Concept 1	Concept 2	Concept 3	Concept 4
Total Mass [kg]	2762	3345	2514	2713
Total Cost [€M]	3273	3759	2717	3349
Atm. Vehicle Propulsion Power [W]	34000	0	0	26000
TRL	7	8	9	8

Table 3.9: Mission Profile Concept Trade-Off Results. The acronyms are: DT=Direct Transfer, GA=Gravity Assist, RB=Retrograde Burn, DE=Direct Entry, DB=De-orbit Burn, V=V-profile, DD=Drag De-orbit, GD= Gradual Descent Profile, SP= Staircase Profile, ES = Early Separation

Concept	Cost (50%)	Risk (25%)	Mission Duration (15%)	Sustain-ability (10%)	Total
DT, RB, DB, V	1	1	3	3	1.50
DT, RB, DD, GD	2	3	3	3	2.50
GA, RB, DB, SP, GD	3	2	4	4	**3.00**
DT, DE, ES, DD, SP	2	2	3	3	2.25

Additionally, one criterion was removed each time. From this, concept 2 was still runner-up, but the scoring was closer to concept 3. In some cases, both would share first place. Therefore, the mission optimisation will be done by using both concepts 2 and 3.

3.1.11 System Concept Trade-off

The mission trade-off was followed by the system trade-off. Table 3.8 shows the important quantities used for the trade-off and the result of the trade-off is shown in Table 3.7.

Due to the quantitative nature of some of the criteria, margins had to be implemented to give a fair scoring. If the concept would within a certain percentage of the requirement, it would be scored a 3. For mass, this margin was 10 % and for cost 20 %. The score would be lowered by one when the value deviates from this margin.

First, the rotorcraft was analysed. Because of the requirements and margins, it scored a 4 in mass and a 2 in costs. For power, it scored a 1, as the required power was too large. The same score was given for risk, due to the novelty of the concept, and it having the lowest TRL out of all the concepts. In scientific yield, it was scored a 3, as it meets the requirements and not much more. For sustainability, it was also scored a 3, due to the balance between mission extension and production of specific parts.

Second, the winged body and CubeSats combination concept was scored. In mass, it was scored a 3 and cost a 1. In risk, it was scored a 2, due to the presence of a paper on a glider in Uranus' atmosphere (Bessette, 2022). In sustainability, it scored a 3. CubeSats can be bought off the shelf, and the glider has a huge potential for a mission extension. However, it was slightly brought down due to the possibility of specialised manufacturing. In scientific yield, it scored a 4. This was again due to the paper, which stated it could fly for up to 12 days, increasing the amount of data gathered. It also scored a 4 in vehicle power, as it only needs 0.3 kW h to be operational. Finally, in cost, it scored a 2, as it exceeds the 20 % margin.

Third, the blunt body was scored. For both mass and power, it scored a 4, due to the low values for both. It also scored a 3 in cost, as it meets the requirements. For risk, it was scored a 3. Normally, it would get a 4 as blunt bodies have been used many times, but they have not been used in Uranus' atmosphere, thus lowering the score. For sustainability, it scored a 2. Although its manufacturing is easy and straightforward, there is no possibility for a mission extension, thus lowering its score. Lastly, in power, it scored a 4, as it has the same power usage as the winged body.

Lastly, the blunt body and rotorcraft combination was scored. For mass, it scored a 4, as it is 10 % below the LAU07 constraint. In risk, it was scored a 2, and this was due to the rotorcraft being a vulnerable system. It was scored similarly in sustainability. This was again due to the rotorcraft, and due to the manufacturing of multiple vehicles. For scientific yield, it was scored a 3. This was due to the combination of vehicles, but it does not exceed the science requirements. For the power criterion, it scored a 1 due to its extreme power requirement. Finally, for cost, it scored a 2, as it was above the 20 % margin.

After the trade-off, the sensitivity analysis was performed. This was done by changing the weights and removing criteria. By reducing the weight of scientific yield, and treating Ouranos as any other space mission concept 2 becomes the winner. Similarly, by switching around other weights and removing criteria, concept 2 comes out as a winner. Concept 3 is best merely because of the scientific yields it can provide.

Table 3.10: Uranian Orbit Phase Qualitative Trade-Off Results

Method	Mass (25%)	Risk (25%)	Cost (25%)	Sust. (15%)	Compl. (10%)	Total
Early Separation						
Direct Entry & Orbit Insertion Burn	3	2	3	2	3	**2.6**
Late Separation						
Aerocapture	4	1	1	4	2	2.3
Orbit Insertion Burn	1	4	1	2	4	2.2

Table 3.11: EOL Phase Trade-Off Results

Method	Cost (40%)	Scientific Yield (30%)	Risk (20%)	Sust. (10%)	Total
Drag De-Orbit	3	4	3	3	**3.3**
De-Orbit	2	2	3	2	2.2

3.1.12 Mission Profile Concept Optimisation

Mission concept 3 and system concept 2 were selected from the trade-off. However, they are not 100 % compatible, and thus certain elements have to be adjusted. The first mismatch is in the atmospheric flight. Concept 3 uses two flight profiles (staircase and V profile), which is not possible with one vehicle. Furthermore, both profiles do not fit a glider and thus were switched out for the gradual descent. Further optimisation was performed by considering various methods of entering Uranus orbit. The results of this trade-off are shown in Table 3.10. For the early separation, the atmospheric vehicle would perform a direct entry, and the orbiter an injection burn. For late separation, both an aerocapture manoeuvre and orbit insertion burn were considered. Starting from the cost score, the orbit insertion burn option is considered to be a 1 as it requires the highest ΔV. The aerocapture trajectory was also given a 1, as this would require a custom aeroshell. Finally, there is direct entry combined with orbit insertion burn, in the early separation category. This still requires fuel for the orbiter capture, but it does not need to carry the atmospheric vehicle during this burn. Furthermore, this concept has already been used before, which reduces development costs. The mass score is also based on the amount of fuel required. As such, the scores of the early separation option and the combined orbit insertion burn option are both 3. In contrast, the aerocapture option becomes ideal as the aeroshell is likely less massive than the propellant required for the early separation. The orbital insertion burns for the entire system and requires the most fuel mass. Regarding the risk score, both aerocapture and direct entry are purely dependent on estimations. If there are unexpectedly large deviations from the estimation this could impede mission success. However, during direct entry, the orbiter does not have any risks related to the atmosphere, which is the case for aerocapture. Therefore, they respectively score 2 and 1. Meanwhile, since the orbital insertion burn option allows for correction upon arrival to Uranus, it presents a lower risk, thus scoring a 4. For the sustainability score, the possibility of an extended mission was considered. Both the direct entry and orbital insertion burn require significant amounts of fuel, which is unsustainable. Even with less fuel required, direct entry limits the option of an extended mission compared to other options. Therefore, both receive a 2. Aerocapture does not require fuel, can take scientific measurements during entry and can extend the mission, which is why a 4 is given. Lastly, the complexity of the design was considered. The aerocapture requires a totally innovative aeroshell and thus receives a 2. Direct entry still has some complexity due to the early separation, and thus only receives a 3. An orbital insertion burn only requires an engine, which does not add much complexity and is therefore scored a 4.

Lastly, the EOL phase was optimised. Two options are considered: drag de-orbiting and a retrograde de-orbit burn. First, the cost score was considered. The satisfactory score of the retrograde de-orbit burn is due to the fact that additional fuel would be needed, increasing the cost. Drag de-orbiting, on the other hand, will make use of the planet's atmosphere to slowly de-orbit. As such, it is considered a good option. Next, the scientific yield was scored. A retrograde de-orbit burn will ensure the fastest disposal, but it does not permit the gathering of any secondary experimental mission data, hence being only satisfactory. Drag de-orbiting allows the orbiter to gather data over a longer period of time than the mission duration. This entails that it is an ideal choice as it maximises the scientific yield of the mission. In terms of risk score, both concepts are considered to be good since both ensure the safe disposal of the spacecraft, the only difference being the speed at which this process is completed. Lastly, in terms of sustainability, since drag de-orbiting only involves the use of the atmosphere to dispose of the spacecraft, it is considered a good choice. A retrograde de-orbit burn, on the other hand, requires some fuel to perform the manoeuvre, whose production procedure on Earth is oftentimes

polluting. Therefore, it is considered a satisfactory choice.

3.1.13 Final Concept Overview

The final mission concept chosen entails an interplanetary gravity assist with a launch window between 2033 and 2035 whose travel time will be in the range of 16 to 29 years depending on the trajectory selected. Once the spacecraft reaches Uranus, the orbiter will separate from the glider and perform an insertion burn into a highly elliptical orbit. The glider, after separating from the orbiter, will perform a direct entry into the Uranian atmosphere, during which an aeroshell will ensure protection during its steep entry. After bleeding off enough of the atmospheric entry velocity, possibly with an additional parachute, the glider will perform a gradual descent from the 0.1 bar region to the 20 bar region in a time period of 2 hr. Once the scientific operations time period is over, the glider will continue to dive deeper into the atmosphere until it loses contact and is disposed of. Finally, the orbiter will continue to orbit around the planet, while gathering scientific data on Uranus and its surrounding environment until after the secondary and extended mission it will plunge to its end in the atmosphere of Uranus. The duration of this part of the mission has not been determined yet but it will be analysed in Section 7.4.

3.2 High-level Mission Architecture and Configuration

The mission will start with the launch of the system into low Earth orbit. From this orbit, the entire system will be carried by the launcher into a hyperbolic trajectory, leaving behind Earth. After leaving Earth, the system will perform 2 gravity assist trajectories to raise its apoapsis. First, it will swing by Mars and perform a manoeuvre at periapsis to raise its apoapsis for a Jupiter encounter. After coasting for another 2 years, the system will swing by Jupiter, and leave on a trajectory to Uranus. 16 years after launch, the system will approach Uranus. 20 days before arriving at the Uranus periapsis, the orbiter and entry capsule will split, and the orbiter will perform a small manoeuvre to increase the periapsis of its orbit. Then, the capsule will enter the atmosphere and protect the glider, before opening the bottom and deploying the glider. The glider will then glide from 0.1 bar to 20 bar over the course of 4 days. At the same time, the orbiter will perform its capture burn and enter an orbit around Uranus. During the atmospheric mission, the orbiter will receive data from the glider. The orbiter will transmit all data to Earth. After the atmospheric mission has been performed, the orbiter will focus on the moons, performing manoeuvres and moon swingbys to gather further scientific information on Uranus, its rings and its moons. There is a possibility of extending this mission if this proves feasible. After the mission and possible extended missions have been completed, the glider will lower its periapsis to encounter the atmosphere. Over the course of several passes, during which additional scientific information can be gathered, the orbit of the orbiter will decrease in altitude, until the orbiter will burn up in the Uranian atmosphere.

3.3 Payload Suite

A payload suite was carefully selected for the detailed design to meet the mission objectives mentioned in Chapter 2. Most instruments are based on previous deep space missions, and some are suggested by the customer which are not published yet. In that case, as much information from private communication is mentioned and missing parameters are taken from similar instruments.

3.3.1 Magnetometer

The magnetometer is based on MAG of the MESSENGER mission. It is a 3.6-meter-long boom with a sensor used to measure the magnetic field. It's a low-noise tri-axial fluxgate magnetometer. It has a mass comprised of a 2.66 kg boom, a 1.24 kg electronics box with cables, and a 0.18 kg sensor making it a total of 4.09 kg. It has a power usage of 4.2 W and a data rate of 960 kbit s^{-1} (Anderson et al., 2007).

MAG has two measurement ranges: a coarse range used for pre-flight testing (51 300 nT full scale, 1.6 nT resolution) and a fine range for Mercury operation (1530 nT full scale, 0.047 nT resolution). A magnetic cleanliness program was followed to minimise interference from spacecraft-generated magnetic fields. The instrument's analogue signals are low-pass filtered (cutoff at 10 Hz) and sampled simultaneously by three 20-bit analogue-to-digital converters every 50 ms. This allows for capturing detailed changes in the magnetic field over time.

3.3.2 Net Flux Radiometer

The Net Flux Radiometer (NFR) created specifically for the Galileo spacecraft will be used for the Ouranos mission. Its main objective is to determine the vertical profile of upward and net radiation fluxes in five distinct spectral bands, which range from solar to far-infrared wavelengths. It has a total mass of 3.13 kg, a peak power consumption of 6.3 W, and a data rate of 55 $bits^{-1}$. The information about this instrument is gathered from a study on an advanced Net Flux Radiometer on a future Ice Giants probe mission (Aslam et al., 2020).

The NFR instrument gathers unique measurements that advance our understanding of atmospheric dynamics. It helps identify cloud layers and estimate their opacities, shedding light on cloud development, evolution,

and distribution in Uranus' atmosphere. The NFR also aids in determining water vapour abundance in Uranus' atmosphere, which is crucial for understanding its chemistry and composition. By measuring radiation fluxes across different spectral bands, the NFR provides valuable data for calculating water vapour abundance and distribution. Overall, the Net Flux Radiometer enhances our understanding of Uranian atmospheric dynamics, cloud layers, and water vapour abundance. This knowledge contributes to broader research on planetary atmospheres.

3.3.3 Camera

The camera that will be used onboard the orbiter is taken from the European Space Agency (ESA) spacecraft Rosetta. The OSIRIS (optical, spectroscopic, and infrared remote imaging system) camera was developed for the comet 67P/Churyumov-Gerasimenko mission and will be augmented for the orbiter's imaging equipment (Keller et al., 2007). The Narrow Angle Camera (NAC) and Wide Angle Camera (WAC) are two different types of cameras that are part of the system. NAC has a mass of 13.2 kg, WAC has a mass of 9.48 kg. It has a power consumption of 34 W and a data rate of 40 Mbit s^{-1}. This makes the imaging instrument the most crucial part of the data handling of the orbiter.

For this mission, the NAC travels from near flybys of the comet's largest moons to varied distances from the comet's surface. Its primary objective is to capture images of the surface at a remarkable resolution of up to 2 cm per pixel. The topography and geological properties of the moons may now be thoroughly analysed and mapped. It will also measure the photometric light curve of Uranus, to probe if the planet has acoustic oscillating light curves. On the other hand, the WAC is designed to take pictures of the gas and dust that surround Uranus and its moons. The NAC and WAC now come with filter wheels, enhancing their utility for scientific study. The near-infrared through near-ultraviolet regions of the electromagnetic spectrum can be chosen for certain imaging wavelengths thanks to the filter wheels. By employing various filters, it is possible to learn about the surface properties and composition of the planets and moons, as well as the surrounding gas and dust.

3.3.4 Nephelometer

The glider will use a state-of-the-art instrument which will determine the vertical structure, composition, and properties of Uranus' cloud and haze layers. It was assumed that LONSCAPE can provide this information similarly to a traditional nephelometer, but it is constrained in a mass and power budget (Renard et al., 2020). Private conversations with Dr. Lebreton[1] confirm that the mass will be around 1.5 kg and power consumption 2 W. The data rate and dimensions, however, are taken from the Galileo mission to base the data handling on and accommodation of LONSCAPE in the glider. It has a bit rate of 10 bit s^{-1} with an overall accuracy range from less than ±5 % for the 5°, 15°, and 180° channels to less than 10 % for the 40° and 70° channels[2].

3.3.5 Radio Science Experiment

Radio science Experiments (RSE) will both be done on the orbiter and the glider. For the orbiter, it will be based on 3GM from Juice. 3GM is an assembly of 2 instruments. From private communication with Dr. Lebreton and Dr.Ir. Dirkx (TU Delft), the working principles of radio science and the needed instruments became clear and will be used as the primary source for this section.

The first instrument is a transponder, for the orbiter it is a Ka-band transponder and for the glider a UHF one. This allows for very precise measurements of the velocity of both systems. It has an accuracy of a few μm^{-1}. The second instrument is the Ultra Stable Oscillator (USO). It provides a minimum frequency stability of 2×10^{-13} from 1 s to 100 s integration time, and 6×10^{-13} for up to a 1000 s (Hussmann et al., 2014). This will probe Uranus's atmosphere and ionosphere and its moons and rings. By measuring how Ouranos will fall into the gravity of Uranus, its moons, and possibly Planet 9, clues can be found about the interior structure of the different bodies of the Uranian system. Or in the case of Planet 9, if it could provide hints of its existence.

Something else Ouranos will perform, originally from the JUICE mission, is the PRIDE experiment. PRIDE is a combination of radio astronomy instrumentation and telescopes from all over the surface of the Earth. PRIDE will employ instrumentation developed for VLBI, which combines many different radio telescopes to work together as a single system. In general, the resolution of a measurement is proportional to the wavelength of the signal and inversely proportional to the size of the telescope. With PRIDE, a larger network than, for example, DSN is synthesised and able to support science activities on a scale never seen before. Precision normally applicable for Earth-orbiting spacecraft, can now be achieved anywhere in the Solar System. PRIDE measures the spacecraft's radial velocity with an accuracy of a couple of μm^{-1}, handy for its Doppler shift measurements. With this high accuracy, even a small deviation from the nominal trajectory from Jupiter to Uranus will be detected on Earth.

[1] Email conversation in May and June of 2023, and a meeting on 16/06/2023.

[2] URL: https://pds-atmospheres.nmsu.edu/data_and_services/atmospheres_data/Galileo/nep.html [cited 20/06/2023].

3.3.6 Mass Spectrometer

The Mass Spectrometer (MS that will be used is the one from the Cassini-Huygens mission, known as the Gas Chromatograph (GC) Mass Spectrometer. It has a mass of 17.3 kg, an average power consumption of 41 W, and a data rate of 1741 bit s^{-1} (Bauer et al., 1997). For the Huygens mission, the GCMS was used to analyse the composition of Titan's atmosphere. Titan and Uranus are completely different worlds; one is a terrestrial moon and the other an icy gas planet. Therefore, augmentation to this instrument which is specifically designed for Titan is needed to use it in Uranus' atmosphere.

In general, a gas chromatograph improves the capabilities of a mass spectrometer by separating complex mixtures, offering selective analysis, concentrating chemicals, and reducing general measuring errors. This way, gas chromatography and mass spectrometry can be used together to analyse a variety of materials, including environmental, biological, and chemical samples, with greater accuracy and dependability. For the Ouranos mission, however, it is required to measure the main isotopes of H, C, O, Ne, and the heavy noble gases and in this context, the GC may not be helpful as it was for the Huygens mission. For these isotopes and the heavy noble gases, a mass spectrometer can directly ionise the gas sample and measure the composition. This is achieved within the mass spectrometer itself, without the need for a gas chromatograph.

This would result in a mass spectrometer instrument which is lighter and has a lower power consumption and data rate. Unfortunately, it is rather difficult to find these values excluding the gas chromatograph without contacting the payload manufacturer. Further calculation in this report will thus be done using the full GCMS configuration.

3.3.7 Tunable Laser Spectrometer

The tunable laser spectrometer (TLS) was taken from Curiosity's SAM suite (Mahaffy et al., 2012). It is very complementary to the MS and would provide an accurate latitude profile of the species mentioned in the Scientific Traceability Matrix in Appendix B. It has a similar in-and outlet to the MS. During private communication with Dr. Lebreton it was shared that nowadays, TLS instruments have a mass of 1 kg but they are not published yet so the properties from SAM will be used. It has a mass of 3.7 kg, a power consumption of 34 W, and a data rate of 70 bit s^{-1}.

To analyse samples obtained from the glider, the TLS is frequently used in conjunction with a Mass Spectrometer. For highly sensitive measurements of the cosmological abundant species, namely CH_4, NH_3, H_2S, and H_2O. It was found that the maxing ratio of these chemical species is much lower than other elements that are measured by the MS (Guillot, 2022).

The general idea of a TLS is based on how individual rotational lines within a molecule's vibrational band absorb IR laser light. Each molecule has its own set of rotating lines that match the various energy levels in the molecule. The TLS can selectively measure the absorption of a molecule of interest, making it possible to detect and study, by adjusting the laser's frequency to coincide with its rotational lines. The great sensitivity of a TLS is one of its main benefits. The TLS is a non-invasive approach since it can offer direct readings without the requirement for sample preparation. This is especially helpful for analysing fragile or small samples. The TLS is also reasonably simple to calibrate, ensuring precise measurements.

3.3.8 Atmospheric Structure Instrument

An augmented Atmospheric Structure Instrument based on the *Huygens HASI* is specifically made for possible Uranus and Neptune missions. The Ice Giants Atmospheric Structure Instrument, or IG-ASI, will therefore also be included in the glider. It has a total mass of 1.5 kg, a power consumption of 10 W, and a data rate of 250 bit s^{-1} (Ferri et al., 2020).

The ASI can work at high entry speeds, already. From the three measured state variables, temperature, pressure, and density, the atmospheric mean molecular weight may be determined. Other instruments on the glider, including the mass spectrometer and the TLS, will probably determine the molecular weight more accurately, however. In these circumstances, the accelerometer data may be used to define the magnitude of large vertical winds in waves or gusts. The data from ASI will be used to determine the altitude of the measurements of other instruments as well, and also the rate of descent for the Doppler and wind experiments between the orbiter and the glider. ASI's capabilities and accuracy, based on the ASI from Galileo:

1. To accurately define the state properties as a function of altitude below the 0.1 bar level to approximately 20 bar
2. To define the currently highly uncertain state properties of the upper atmosphere
3. To measure the stability of the atmosphere, and identify convective layers and stable layers, where they exist
4. To detect cloud levels from changes in lapse rate at their boundaries
5. To define state properties within the clouds, and thus provide supplementary information on cloud composition

6. To search for and characterise wave structures in the atmosphere
7. To search for and measure the intensity and scale of turbulence in the atmosphere
8. To measure vertical flow velocities above a threshold of about 0.3 m s^{-1}
9. To establish an altitude scale for use in correlating all glider experiment data
10. To define the probe vertical velocity, necessary for the analysis of the Doppler wind experiment as part of the RSE mentioned in Section 3.3.5

3.3.9 Visible-IF Imaging Spectrometer

The visible-IF imaging spectrometer is based on the MAJIS instrument onboard the JUICE mission. It was designed to provide spectral imaging of all the bodies of interest in the Jovian system. MAJIS consists of three main components: the main electronics module, the proximity electronic module, and the optical head and radiators. The command and control processing unit manages uplink and downlink with the spacecraft and controls the main electronics. Through a Power Conditioning and Distribution unit, it is turned off and on. The data gathering from the detectors and auxiliary mechanisms is controlled by the proximity electronics. To use the spectrometer, a total of 12 W needs to be supplied by the power system, and it has a bitrate of 3000 bit s^{-1} (Hussmann et al., 2014).

By providing spectral images, MAJIS can help identify specific characteristics of Jupiter's moons. More specifically, it helps identify the composition and properties of the surfaces and possible atmospheres of the relevant moons. Similarly, the visible-IF imaging spectrometer for the Ouranos mission has two purposes. The first is to take measurements of Uranus and the second is for measurements of its moons. For the measurements of Uranus, its purpose is to determine the compositional thermal and dynamical structure of its atmosphere. Specifically, the vertical structure, composition and properties of the cloud and haze layers are of interest, as well as the atmospheric temperature, stability, and any winds and wave phenomena. For the moons, its task is to investigate their surface. Meaning, it will determine its composition and physical properties by measuring the albedo and the presence of ice, salts, minerals, and possible organic compounds.

3.3.10 Laser Altimeter

For the laser altimeter, the Ganymede Laser Altimeter (GALA) onboard the JUICE mission was taken as a reference. It has a power usage of 51 W. Its purpose is to map the height profile of the moons Ganymede, Europa, and Callisto. This is done by sending out a laser pulse and measuring its time of flight and combining different ground tracks it will generate. Additionally, information about the albedo can be obtained at the specific wavelength of the laser (Hussmann et al., 2014).

These measurements are similar to the measurements that will be performed during the Ouranos mission. Using the laser altimeter, the surfaces of the major moons of Uranus will be studied. Specifically, the height profile will be measured by measuring the time of flight of a laser pulse, and the composition of said moons can be determined by measuring its albedo.

3.4 Functional Flow Diagram

The functional flow diagram for the final design of the Ouranos space mission is displayed in Figure 3.2 and 3.3. It shows the whole mission sequence of events and milestones, starting from F0, where the pre-launch activities are presented, and ending with F8, where the End of Life of the orbiter is performed. Each white box, besides presenting the Level 1 function and its corresponding ID, presents a rectangular grey box at the lower edge: here the system(s) performing the function and the corresponding subsystems involved are presented. For the subsystems, the abbreviations explained in the legend are used. In some instances there are some functions which are being repeated: for those cases, the repeated function is enclosed by a rectangular frame and a circle with the corresponding letter is used for the following cases in which the function would appear.

3.5 Functional Breakdown Structure

The functional breakdown structure is an extension of the functional flow diagram presented in Section 3.4. It extends the functions by an additional level by sacrificing the visual elaboration on the temporal flow that is shown in the Functional Flow Diagram and replacing it with a visualisation showing how functions are related to their parent function. The resulting diagram is shown in Figure 3.4 and Figure 3.5. If a second-level function does not indicate any third-level functions it was deemed to be such a low-level task that it could not be further broken down.

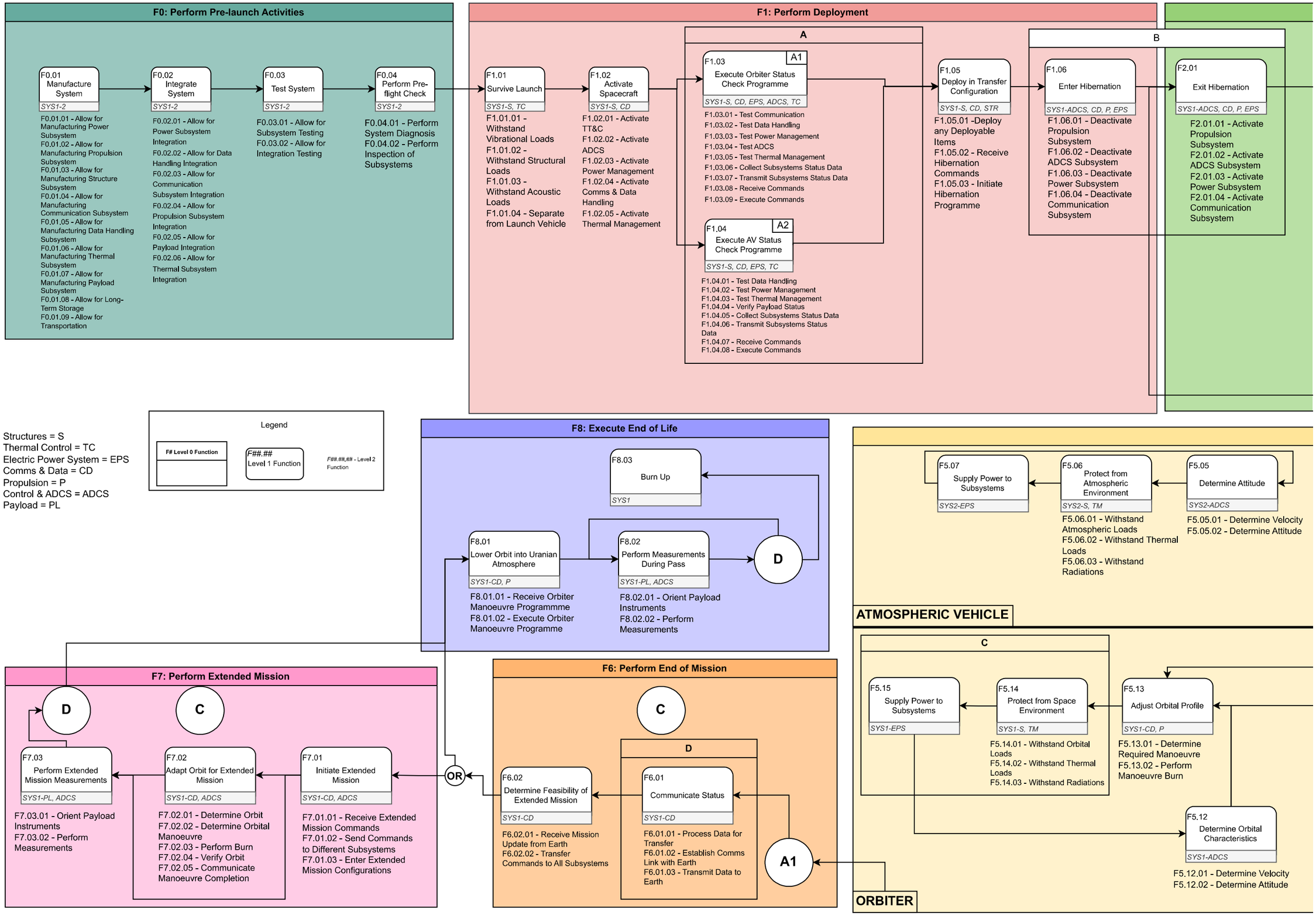

Figure 3.2: Functional Flow Diagram (part 1)

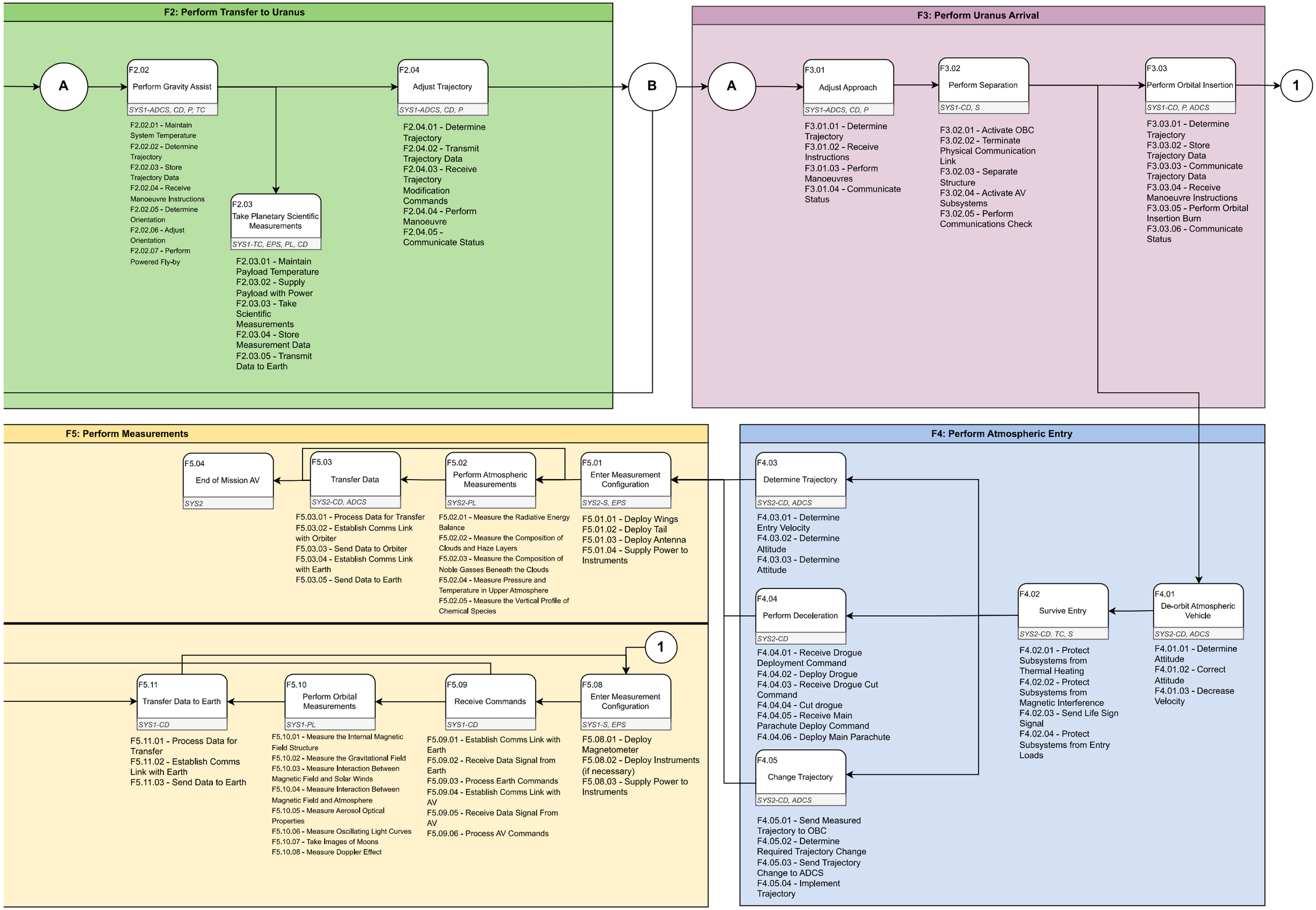

Figure 3.3: Functional Flow Diagram (part 2)

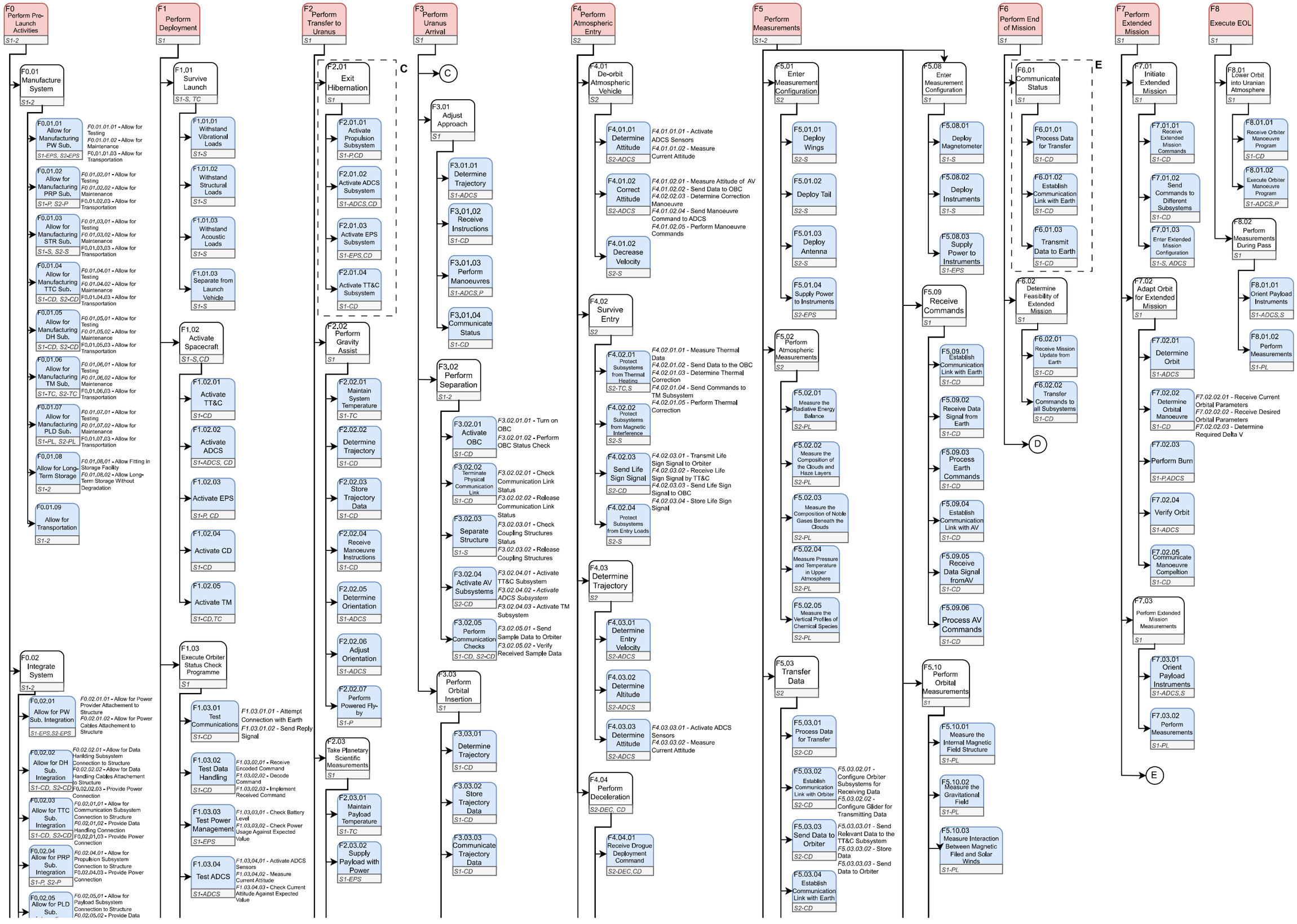

Figure 3.4: Functional Breakdown Structure (part 1)

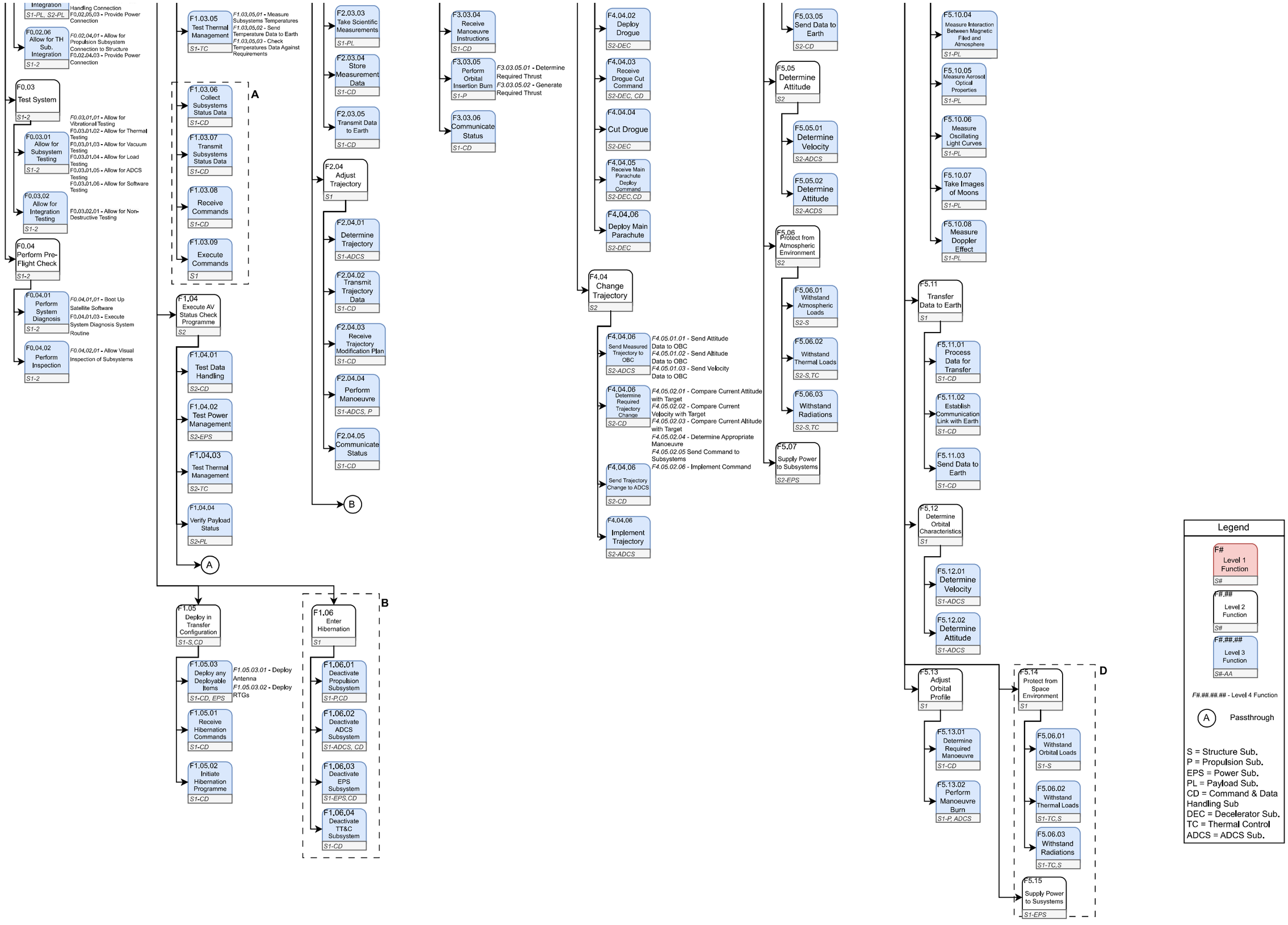

Figure 3.5: Functional Breakdown Structure (part 2)

Table 3.12: Definitions of severity and likelihood designations

Likelihood		**Severity**	
Very Likely	Practically guaranteed	Catastrophic	Complete Primary mission failure
Likely	Very high chance of occurring, occurs in most missions	Severe	Partial Primary mission failure
Moderate	Has occurred in multiple previous missions	Moderate	Secondary mission failure
Unlikely	Has occurred in previous missions	Low	Negative impact on mission but no mission failure
Negligible	Has not happened in previous missions	Negligible	Negligible impact on mission performance

Table 3.13: Orbiter risks

ID	Risk	Severity	Likelihood
OR01	Antenna fails to deploy	Catastrophic	Negligible
OR02	Attitude determination component failure	Catastrophic	Negligible
OR03	Attitude control component failure	Catastrophic	Negligible
OR04	Momentum dump thrusters' propellant usage exceeds limits	Moderate	Unlikely
OR05	RTG power output lower than expected	Severe	Unlikely
OR06	RTG fails to deploy	Severe	negligible
OR07	Interference of Magnetometer due to other subsystems	Moderate	Unlikely
OR08	Science component fails to activate	Severe	Negligible
OR09	One processor fails	Severe	Unlikely
OR10	Radiator component failure	Low	Moderate

3.6 Risk Analysis

In this section, the risk analysis of the systems is presented. The basis of this risk analysis was the risks analysed in previous steps of the design. The risks were reviewed and evaluated in cooperation with the subsystem engineers, following which the likelihood and severity of all risks were discussed. For those risks that are unacceptable possible mitigation strategies were discussed. The already implemented mitigation strategies were documented, and newly identified mitigation strategies were implemented in the design. This leads to a system with acceptable risks. Only the risks related to the actual detail of the design were included, as further risk analysis would not result in meaningful mitigation strategies for the design presented in this report.

3.6.1 Risk Qualification

First of all, the measurements of the risks in likelihood and severity need to be established. These definitions were the basis for the ratings given to all risks, and the division into acceptable and unacceptable risks. While not all definitions are equally applicable to all subsystems, they give an impression of the risks and a more objective framework than merely using the ratings on their own. The definitions used with regard to likelihood are intended to be about a system used commonly in deep space missions. The design and components were included in this evaluation. Furthermore, the identified risks were mapped in a risk map, where the risks requiring mitigation were determined. Risk mitigation strategies were developed and implemented where applicable

3.6.2 Orbiter Risks

The orbiter has several risks with high severity. However, there is significant experience with orbital vehicles, both in Earth orbit and to destinations further out. Therefore, most systems have low probabilities of failure. In addition, numerous subsystems will use off-the-shelf components, further increasing reliability. The most critical failures are associated with the communication subsystem, attitude determination and control and power generation. With the failure of any of these systems, the mission would be a failure. The risks are summarised in table 3.13.

From these risks, an orbiter risk map was generated fig. 3.6. This shows that there are 5 risks in need of mitigation. The antenna, while an off-the-shelf part that has been used before in the Cassini mission (Taylor et al., 2002). It is, however, too mission-critical to risk complete failure. Therefore, a low-gain antenna shall be included as a backup solution. This antenna would still decrease the science yield, especially during the atmospheric mission, where communication time with the glider is limited, but allow a partial mission success in case of failure, therefore lowering the severity. The attitude determination and control subsystem is important for allowing the communication subsystem to achieve the required pointing accuracy to communicate with Earth and is thus also mission critical. Therefore, both for attitude determination and attitude control redundant

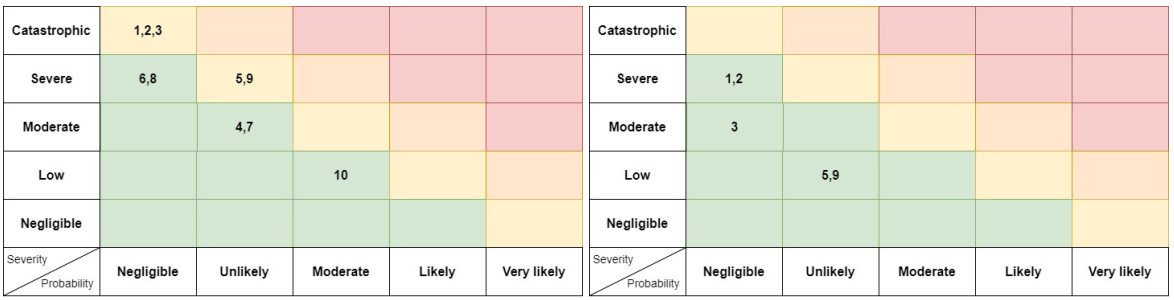

(a) Unmitigated risk map

(b) Mitigated risk map

Figure 3.6: The risk maps of the risks concerning the orbiter.

Table 3.14: Orbiter risk mitigation

ID	Risk mitigation strategy	Severity (unmitigated severity)	Likelihood (unmitigated likelihood)
OR01	A low gain antenna shall be used as the backup for the high gain antenna	severe (Catastrophic)	Negligible (Negligible)
OR02	There shall be redundant attitude determination components	Severe (Catastrophic)	Negligible (Negligible)
OR03	There shall be redundant attitude control components	Moderate (Catastrophic)	Negligible (Negligible)
OR05	An additional RTG shall be used for redundancy	Low (Severe)	Unlikely (Unlikely)
OR09	Three processors shall be used for redundancy	Low (Severe)	Unlikely (Unlikely)

components shall be used. Furthermore, the orbiter shall be able to recover if it loses control for a period of time. The power subsystem, too, is mission-critical and thus requires risk mitigation. Therefore, to have a sufficient margin of power generation, one RTG more than actually required shall be carried by the orbiter. Last, of all, the processors are mission-critical too. Therefore, a setup will be used where three processors shall run all computations of the orbiter. If one processor fails, the other two will still determine the correct answer, thus enabling operations with one failed processor. These risk mitigation strategies are summarised in table 3.14

3.6.3 Capsule Risks

While entry capsules are not novel concepts, most entry protection has been done for Earth re-entry. A decent amount of missions have been sent to Mars. However, missions to other planets are more rare, with a limited amount to Venus, one to Titan and one to Jupiter. Therefore, fewer previous designs and experiences are available to analyse to increase reliability. The different atmospheric makeup and major temperature gradient complicate the capsule design for Uranus. Furthermore, uncertainties about the atmosphere might negatively affect the performance of the heat shield and decelerator. Furthermore, the decelerator could fail to deploy, which would cause the mission to fail. Lastly, the glider might fail to deploy, causing the flight mission to fail. These risks are summarised in table 3.15

These risks have been mapped in a risk map, identifying which risks require mitigation. The heat shield risks are dealt with by implementing margins on the thickness of the heat shield, both overall, to take into account an increased heat load. In addition, the peak heat flux might not be at the stagnation point. This risk is mitigated by increasing the heat shield thickness at the edges of the heat shield. To mitigate the glider deployment failure risks, the parachute has been designed to allow the system to descend slower than two hours through the area of interest, allowing scientific measurements to be done, in a limited fashion, in case of glider deployment. These risk mitigation strategies are summarised in table 3.16 The risk associated with the failure of the decelerator to deploy could be mitigated. With a second decelerator and deployment system, this was not considered feasible. Therefore, this risk remains in the yellow category without mitigation. In addition, the heat shield could be impacted by a (micro) meteorite. This risk, too, remains unmitigated. While an impact of a micrometeorite would be disastrous for the atmospheric mission, mitigation would require the shielding

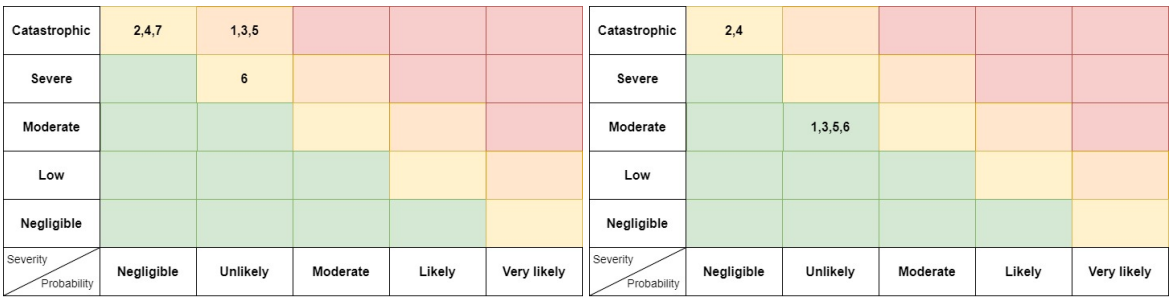

(a) Unmitigated risk map

(b) Mitigated risk map

Figure 3.7: The risk maps of the entry capsule.

of the heat shield. The feasibility and benefit from this should be further investigated in later analysis. This analysis could be done using the models identified in (Rodmann et al., 2021).

3.6.4 Glider Risks

The glider is the riskiest part of the mission, both because it depends on the other systems for its mission success, and due to the fact that no glider has been deployed outside of Earth's atmosphere. This, combined with the uncertainties on the properties of the Uranian atmosphere, makes the glider a risky component of the mission. These risks are some risks that any mission into the Uranian atmosphere would encounter, such as the thermal limits of either the payload, batteries or structure, or either the battery cells, communication subsystem or processors failing. The risks with failure of subsystems failing have a low probability, but are still higher than the orbiter, as the Uranian atmosphere can negatively affect the performance of these systems. The risks associated with the thermal situation are more likely, as the payload and batteries will be relatively thermally isolated inside the capsule, and hydrogen gas is not a great heat conductor. Other risks are associated explicitly with the glider aspect, such as risks associated with the flight path and stability, or general deployment of the wings and glider. The deployment risks are low, but after 16 years inside the capsule, proper performance is hard to guarantee. While glider performance is quite well known, the combination of the radically different

Table 3.15: Capsule risks

ID	Risk	Severity	Likelihood
CA01	Heat load exceeded limits	Catastrophic	Unlikely
CA02	Micrometeorite impact	Catastrophic	Negligible
CA03	Heat flux peak not at the stagnation point	Catastrophic	Unlikely
CA04	Decelerator fails to deploy	Catastrophic	Negligible
CA05	Decelerator ripped apart	Catastrophic	Unlikely
CA06	Glider deployment failure	Severe	Unlikely
CA07	Backshell structural failure	Catastrophic	Negligible

Table 3.16: Capsule risks

ID	Risk mitigation strategy	Severity (unmitigated severity)	Likelihood (unmitigated likelihood)
CA01	Additional thickness of heat shield	Moderate (Catastrophic)	Unlikely (Unlikely)
CA03	Additional thickness on the edge of the heat shield	Moderate (Catastrophic)	Low (Low)
CA05	Redundant parachute chords	Moderate (Catastrophic)	Unlikely (Unlikely)
CA06	Decelerator to allow for 2 hours of descent in case of glider deployment failure	Moderate (Severe)	Unlikely (Unlikely)
CA07	Increased safety margins	(Catastrophic)	(Negligible)

Table 3.17: Glider risks

ID	Risk	Severity	Likelihood
GL01	Science component failure	Catastrophic	Negligible
GL02	Compromised flight path angle	Catastrophic	Moderate
GL03	Lateral instability	Catastrophic	Moderate
GL04	Gust induced instability	Catastrophic	Low
GL05	Atmospheric attenuation loss	Catastrophic	Low
GL06	Transmitter failure	Catastrophic	Low
GL07	Temporary connection loss	Moderate	Moderate
GL08	Thermal limits payload exceeded	Catastrophic	Low
GL09	Thermal limits batteries exceeded	Catastrophic	Low
GL10	Thermal limits structure exceeded	Severe	Negligible
GL11	Battery cell failure	Severe	Low
GL12	Processor failure	Catastrophic	Negligible
GL13	Wing deployment failure	Catastrophic	Low
GL14	Glider deployment failure	Catastrophic	Low

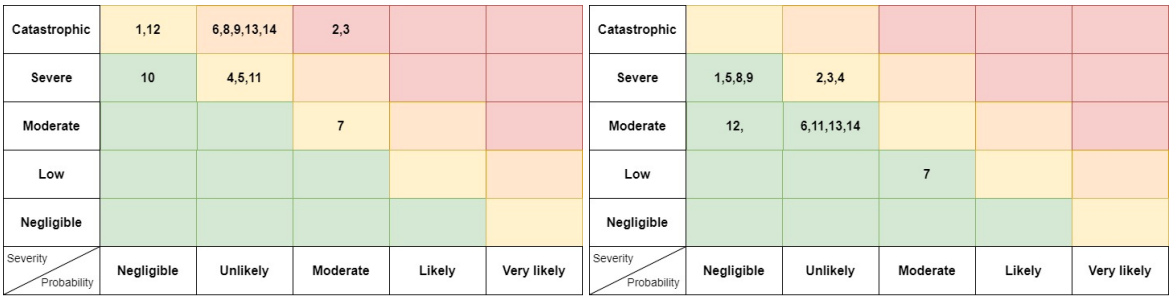

(a) Unmitigated risk map

(b) Mitigated risk map

Figure 3.8: The risk maps of risks concerning the glider.

Uranian atmosphere and a large range of pressure and density complicates this. These risks are summarised in table 3.17

From these risks, a risk map has been made to identify the risks requiring mitigation. As expected, there are numerous risks that require mitigation. For the most important part of the glider, the scientific payload, there are redundant instruments. For the tunable laser spectrometer, the measurements are also done on the mass spectrometer. In addition, the atmospheric structure instrument can gather some data on the atmosphere. The next step in mitigation is to encase the payload and batteries inside of thermal isolation and install a thermal moderator to moderate the temperature inside of this environment. While some openings are required for the payload to interact with the atmosphere and the batteries to provide power to the other subsystems, the thermal moderation will greatly decrease the risk of exceeding thermal limits, and allow for recovery to this range if a failure does occur, reducing the damage. To mitigate the risk of battery failure, the battery cells will be installed in parallel, so that 10 % of battery cells can fail without affecting glider performance. Even if more cells fail, power conditioning and distribution shall be used to redirect power to the most critical systems, shutting down less important systems. The processor shall have three processors, with all three doing all computations. If one of them fails, the other two will agree on a correct answer, and the correct answer can still be used. The communication subsystem has a redundant subsystem, that can independently transmit the data. It shall also transmit the data at a slight delay so that temporary connection outages shall have a much lower impact. Furthermore, the communication subsystem shall transmit at two low frequencies to decrease the impact of attenuation losses. The risks most difficult to mitigate are the ones regarding the deployment of the glider and the flight inside the atmosphere. With regard to the deployment of the glider, there will be a two-step deployment. First, the glider will be brought into a state below the capsule where the working of the deployment system can be tested, and the wings can be deployed, but the glider is still attached to the capsule. If at this point some part of the deployment fails, the decelerator shall allow for the system to descend slower than two hours through the area of interest. These risk mitigation strategies are shown in table 3.18 The flight path risks shall be mitigated by further aerodynamic analysis and, if necessary, the design, of the glider. The glider aerodynamics should be further developed to guarantee stability in a wide range of flight path angles, bank angles, sideslip angles and other conditions caused by sudden gusts. These risks should be further mitigated in further design iterations. Therefore, these risks shall, for the current design, remain in the yellow category.

Table 3.18: Glider risks mitigations

ID	Risk mitigation strategy	Severity (unmitigated severity)	Likelihood (unmitigated likelihood)
GL01	Redundant instruments and orbiter observation	Severe (Catastrophic)	Negligible (Negligible)
GL02	Further aerodynamic analysis and longitudinal control	Severe (Catastrophic)	Low (Moderate)
GL03	Further aerodynamic analysis	Severe (Catastrophic)	Low (Moderate)
GL04	Further aerodynamic analysis	Severe (Severe)	Low (Low)
GL05	Double frequency transmission, low frequencies chosen	Severe (Severe)	Negligible (Low)
GL06	Redundant transmission subsystems	Moderate (Catastrophic)	Low (Low)
GL07	Delay in transmission between two transmission subsystems	Low (Moderate)	Moderate (Moderate)
GL08	Payload isolated in thermally regulated environment	Severe (Catastrophic)	Negligible (Low)
GL09	Batteries isolated in thermally regulated environment	Severe (Catastrophic)	Negligible (Low)
GL11	Battery cells installed in parallel	Moderate (Severe)	Low (Low)
GL12	Three processors for error correction	Moderate (Catastrophic)	Negligible (Negligible)
GL13	Two-step deployment, possibility of parachute descent	Moderate (Catastrophic)	Low (Low)
GL14	Two-step deployment, possibility of parachute descent	Moderate (Catastrophic)	Low (Low)

3.7 Subsystem Requirements

Most of the subsystem requirements for both the glider and orbiter were initially defined based on past space missions, such as Cassini-Huygens, Galileo and Juno. They were classified into six different categories, based on the field they constrain: those were performance, safety and reliability (considered as a whole), sustainability, science, schedule and engineering budget. The values that could not be filled in based on previous instances were left as TBD (to be decided) and were completed during the detailed design phase, whereas the ones based on the past missions were set as TBC (to be confirmed) and then modified at a later time when more knowledge was gathered upon the topic. There were still many requirements that were highly specific to the Ouranos mission, such as the science requirements, which were defined early in the design process after numerous discussions with the client.

The subsystem requirements are fully listed in Appendix A. Furthermore, a brief summary is presented at the beginning of each subsystem section which shows the relevant key requirements.

PART II

ATMOSPHERIC MISSION

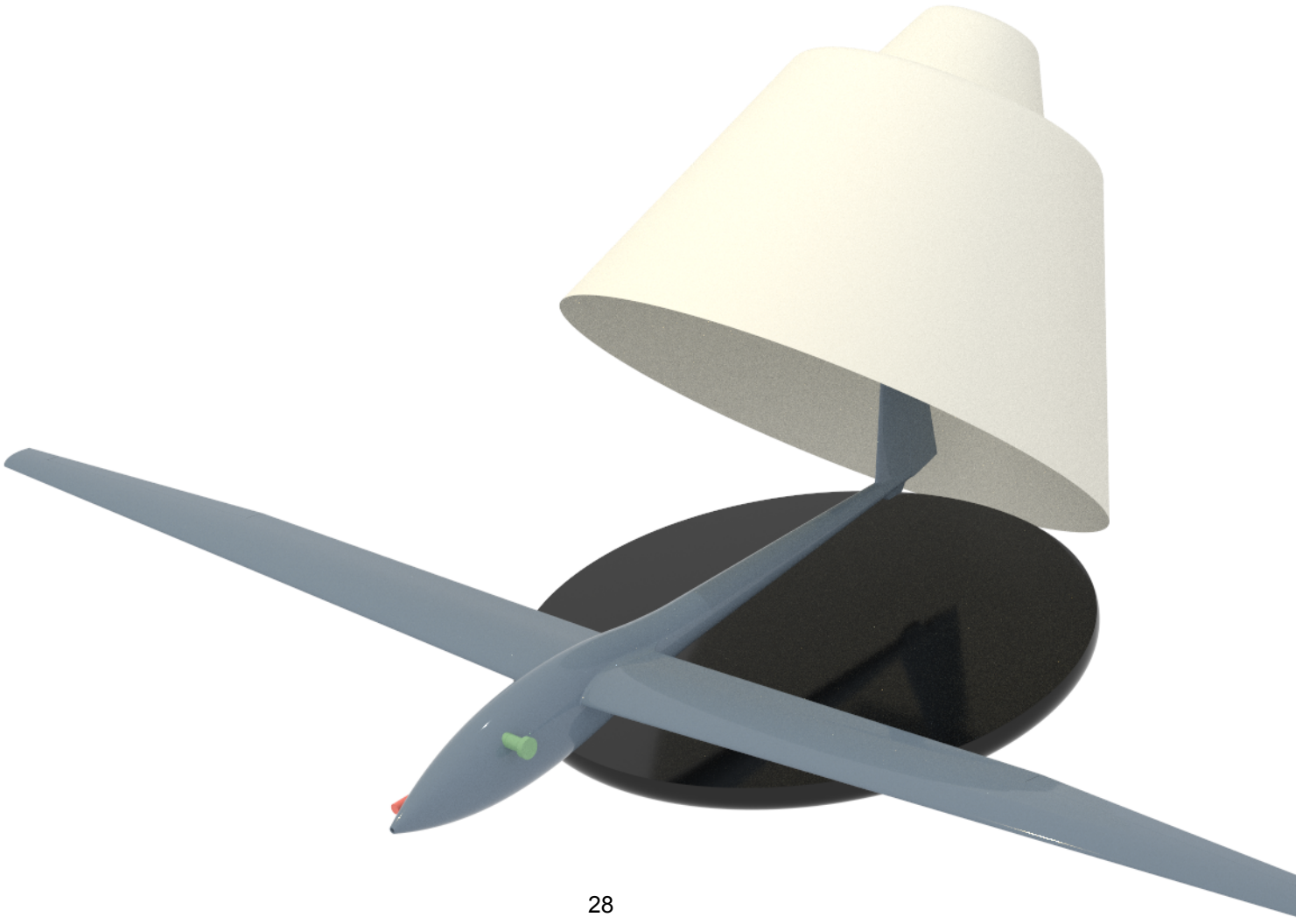

4. Prometheus Glider Design

In this chapter, the design of the atmospheric vehicle that will gather scientific data on Uranus' atmosphere is presented. To tackle such a design task, a number of aspects pertaining to the functions to be performed by the vehicle were taken into consideration.

In Section 4.1, the payload that will be carried onboard by the atmospheric vehicle, as well as the impact this will have on the remaining subsystems, is detailed. This is followed by an analysis of how the atmospheric vehicle will process the atmospheric data gathered in Section 4.2. Next, the ways in which the atmospheric vehicle will transmit the processed data are investigated in Section 4.3. This is followed by an analysis of the power required by the onboard payload, data handling and communications subsystems in Section 4.7.

As was mentioned in Section 3.1, the final choice for the atmospheric vehicle, after having completed the trade-off process, is a glider. Consequently, for the final design of the atmospheric vehicle, it was imperative to perform an analysis of the aerodynamic properties and characteristics of such a glider. This was considered and detailed in Section 4.4. Following the aerodynamic analysis, a structural analysis of the glider, where its ability to withstand the different loads it must overcome throughout the mission is described in Section 4.5. This is followed by an analysis of the thermal management subsystem, which takes into consideration the various thermal constraints imposed by the scientific payload and materials being used in Section 4.6.

Before diving into the subsystem design, it is important to understand that the glider will have to fulfil multiple functions and many requirements constrain the design space. These are presented in Table A.12 and summarised below. For all the systems and subsystems presented from now on, a summary box will be presented first to show what are the main functionalities the system/subsystem has to comply with. Due to its nature of summary, the content in the box will not include any specific values and this can be found in Appendix A. The mass, power and cost of each subsystem are checked with the requirements and if it complies, then the requirement is checked off with an 'X' in the verification column in Appendix A.

In summary, the glider shall

- Gather scientific data for at least 2 hours at specific pressure and temperature levels.
- Transmit all science and housekeeping data to the orbiter.
- Withstand the harsh conditions of deep space.
- Stay within the mass, power and cost budgets with a reliability of 95%.
- Withstand atmospheric entry loads.
- Have dimensions less than 4.5 m × 4.5 m × 4 m when integrated with the aeroshell.
- Separate from the aeroshell after entry into Uranus' atmosphere.
- Be evaluated in a testing campaign simulating the mission.
- Maintain its subsystems within their operating temperatures during the entire mission.
- Comply with the Planetary Protection Guidelines.
- Be delivered at the launch site 4 weeks before the launch and be easily transportable.

4.1 Onboard Payload

The glider's payload suite consists of the Net Flux Radiometer, LONSCAPE instrument, Atmospheric Structure Instrument, Mass Spectrometer, Tunable Laser Spectrometer, and instruments for the Radio Science Experiment. Based on the values given in Section 3.3, the total payload mass is 28.2 kg, has a total power consumption of 95.8 W, and a total data rate 2251 bit s^{-1}. On average, the operational temperature range of all the instruments is between 253 and 300 K. Important to remember is that the minimum required measurement period is 2 hours and that the glider will be designed around that. After that period, it will disappear into the abyss of Uranus. Proper data handling and relay with Earth/the orbiter will be of great importance.

4.2 Data Handling

Due to the high value of the data collected by the glider, data handling is an important part of the science mission. The glider will generate numerous different data when performing its measurements, and having them handled and sent correctly to the orbiter is something that should be carefully considered. The first step for the Data Handling subsystem design is the requirements shown in Table A.13, which are also presented hereafter.

In summary, the glider Data Handling subsystem shall

- Remain within the mass, cost, and power budget with a reliability of 99.4%.
- Be modifiable up until the start of the entry phase.
- Collect data from all the subsystems.
- Activate all glider subsystems upon arrival at Uranus.
- Determine any trajectory changes required for atmospheric flight.
- Send all required trajectory changes to the ADCS subsystem.
- Process all measurement data for Earth transmission.
- Have at least 2 GB of data storage.
- Have at least 250 MB of program memory.
- Process at a rate of at least 110 MHz.

From the different instruments, the total bit rate of the glider will be 2251 bit. The glider will also be able to store the data since, due to the time of flight and the orbit of the orbiter, the two systems will not be in contact throughout the entire atmospheric operation time.

To handle this data, three On Board Computers (OBC) will be used, where one will act as redundancy. The three OBCs will perform the same calculations before sending the data to the orbiter, to ensure data reliability and accuracy. If one of the OBCs were to have a discrepancy in data, the last two can still compare their information before sending it to the orbiter. The selected OBC is the Rad-hard *RAD750* manufactured by BAE Systems[1]. This one was chosen as it is cheap, small, requires a low amount of power and is an off-the-shelf component, which is one of the sustainability goals of this project. This OBC has been used on numerous missions before, such as the Perseverance Rover and the James Webb Space Telescope. It can withstand a total radiation dose of 1 Mrad, and a processing speed of 200 MHz. Additionally, it has an operating temperature between 218 K and 398 K. When the total picture of the data handling is sketched, the data handling diagram will be shown.

4.3 Communications

This section will discuss the design of the communications subsystem. First, the selection of the frequency will be discussed in Section 4.3.1, the antenna selection in Section 4.3.2, the noise and losses in Section 4.3.3 and afterwards, the link budget will be discussed in Section 4.3.4. The communication diagram will be discussed later in Section 8.3.

In summary, the glider communications subsystem shall

- Have a low and high gain antenna to transmit data to the orbiter with specific gain and bitrate.
- Be able to transmit data via the UHF band.
- Receive all data from the OBC.
- Have a signal-to-noise ratio of at least 4.00 dB .
- Operate in the harsh conditions of the atmosphere of Uranus.
- Stay within the mass, power and cost budget with a reliability of 99.4%.

4.3.1 Frequency selection

The communication subsystem of the glider is responsible for transmitting the gathered scientific data to the orbiter. This relay link is a one-way link, the glider will thus not receive signals from the orbiter. Because there is no need to receive signals, the glider's mass reduces and the communication link becomes less complex. A receiving dish would have a negative effect on the aerodynamic performance of the glider. The signals transmitted from the glider need to overcome the free space loss and atmospheric attenuation. At higher frequencies, the atmospheric attenuation increases. This is due to the opacity of trace elements in the atmosphere (Mousis et al., 2018). Because this attenuation increases with the square of the frequency, signals in the S-band will already have a loss of −200 dB around 10 bar (Saikia, 2016). 405 MHz is therefore selected for communications, to minimise this loss. The signal will be in the Ultra High Frequency (UHF) region. No compression will be used to ensure no loss of data, combined with a spectrum utilisation of 1 bit Hz^{-1} and the data rate of 2251 bit/s], this gives a required bandwidth of 2.251 kHz.

This same signal will be used for the Radio Science Experiment (RSE). The difference is that less data needs to be transmitted for this. The only thing of interest is the change of signal. A lower bit rate of 100 bps

[1] URL: https://www.baesystems.com/en/document/space-products-rad750 [cited 21/06/2023].

can therefore be used to check if this signal is still strong for transmission to Earth.

4.3.2 Antenna Selection

Due to the strong winds in the atmosphere, a high pointing accuracy for communication with the orbiter is problematic, especially when no signal is received. An omnidirectional antenna will be selected to allow communication at a large range of angles from boresight. The antenna will consequently have a low or medium gain due to the large beam width of the signal. Having a large beam is also beneficial for the RSE between Earth and the glider. It eliminates the need for a separate signal when the angle between Earth and the orbiter is large from the reference frame of the glider. The same signal can potentially be transmitted to Earth at a lower bitrate, without the need for pointing at the glider or Earth specifically.

The selected antenna to do this is the quadrifilar helix antenna that is designed for the Trace Gas Orbiter. Including the cabling to the transceiver which was discussed in Section 3.3, that orbiter's antenna has a mass of 0.7 kg and an efficiency of 76% (NASA, 2019). Although it is omnidirectional it sends most of the signal directly upwards in a wide beam. At boresight, this antenna has a gain of 7.5 dB and at an angle from boresight of 70° it has a gain of 0.0 dB (Cappellin et al., 2015). This allows for a longer communication window. To ensure that all the scientific data is received by the orbiter, the system will be fully redundant. The second quadrifilar helix antenna that will be used, will transmit at a frequency of 326 MHz, the lowest frequency that can be picked up by the VLBI networks on Earth. This lower frequency will experience even less atmospheric attenuation than the one selected for the first antenna in Section 4.3.1. The transmission of two frequencies decreases the chance of errors in the received data. The second signal will be transmitted with a delay of 6 s just like the Cassini-Huygens relay link (Taylor et al., 2002). This prevents the loss of data when there is a short loss of signal.

4.3.3 Noise and Losses

The system noise temperature is dependent on the cosmic microwave background noise temperature, the atmospheric noise temperature, and the physical temperature of the antenna. As a reference, the determined values for the similar OCEANUS mission are used (Saikia, 2016). Ouranos differs from this mission since it would only go down to 10 bar, while Ouranos goes down to 20 bar. This means that the CAELUS glider would travel deeper into the atmosphere and thus experience more atmospheric attenuation than the 9.48×10^{-3} dB that the OCEANUS mission would experience. The atmospheric attenuation in decibels scales linearly with the distance through the medium. The distance between 1 bar and 10 bar and between 1 bar and 20 bar, is 97 km and 144 km respectively (Justh et al., 2021). Scaling the atmospheric attenuation with respect to this difference in distance gives an atmospheric attenuation of 1.41×10^{-2} dB for the Ouranus mission. When combining this with a physical temperature of 193 K, the atmospheric noise temperature can be determined. This can be done with the following equation (Saikia, 2016):

$$T_{Atm} = T_p(1 - 10^{A/10}) \tag{4.1}$$

where T_{Atm} is the atmospheric noise temperature in K, T_p is the physical temperature in K and A is the atmospheric attenuation in dB. This results in a total system noise temperature of 103.34 K. The difference in atmospheric noise temperature, therefore, increases with only 0.19 K.

Most of the power of the signal is lost due to free space loss. This loss is determined with the following equation (Taylor, 2014):

$$L_s = -\left(\frac{c}{4\pi r f}\right)^2 \tag{4.2}$$

where L_s is the free space loss, c is the speed of light in m s^{-1}, r is the distance between the transmitter and receiver in m, and f is the frequency of the signal. To assume the worst-case scenario, the maximum distance between the glider and the orbiter, which will be discussed later in Section 7.3.2, will be assumed for the link budget.

The selection and performance of the receiving antenna on the orbiter will be elaborated on later in Section 8.3, only an overview of the performance will be stated in this paragraph. This high-gain antenna on the orbiter has a diameter of 4.0 m and will be pointed towards the glider when receiving the data and it will be pointed towards the Earth again to transmit the data after storing it on-board. The efficiency of this antenna is 55% and it will have a pointing loss of −0.12 dB. Using this antenna for the relay link minimises the need for an extra antenna, which means a decrease in mass. Having a receiving antenna with a high gain is preferable because this requires less power to be transmitted from the glider.

4.3.4 Link Budget

The link budget flows from the signal-to-noise ratio. The required transmitted power will be based on a margin of 3 dB for this ratio (Wertz et al., 2011), the required margin of 3 dB for deep space missions. The 405 MHz

Table 4.1: Design input variables for the glider to orbiter downlink

Design Input	Downlink
Transmitting power [W]	49.8
Receiving antenna diameter [m]	4.0
Frequency [MHz]	405
Transmitting antenna efficiency	0.76
Receiving antenna efficiency	0.55
Noise temperature [K]	103.34
Data rate [bps]	6373
Distance to receiver [m]	220.4×10^6

Table 4.2: Glider to orbiter relay design control table for downlink

Link Parameter	Design value [dB]
Transmitted power	16.97
Transmitting Gain	0.0
Receiving Gain	11.00
Transmitter loss	-1.19
Receiver loss	-2.60
Space loss	-191.5
Pointing loss	-0.12
Atmospheric attenuation	-0.02
Boltzmann constant	228.6
Data rate	38.04
Noise temperature	20.14
E_b/N_0 margin	3.02

signal will be used at an angle from boresight of 70° because this is the worst-case scenario. This margin will allow the disturbances in the direction of the antenna, the uncertainty in the displacement of the glider during the atmospheric flight and the uncertainty of the timing of the communication window. The signal-to-noise ratio is determined with the following equation, where the inputs and output are in dB:

$$\frac{E_b}{N_0} = P + G_t + G_r + L_l + L_r + L_s + L_{pr} + L_a - k - DR - T_s \tag{4.3}$$

where P is the transmitted power, G_t is the transmitting antenna gain, G_r is the receiving antenna gain, L_l is the transmitter loss factor, L_r is the receiver loss factor, L_s is the space loss, L_{pr} is the pointing loss, L_a is the atmospheric attenuation, k is the Boltzmann constant, DR is the data rate and T_s is the noise temperature. The data will be stored onboard outside of the communication window that will be discussed in Section 7.3.2. Together with the bit rate of 2251 bit s^{-1} in Section 3.3, this gives a required transmission bit rate of 6373 bit s^{-1}. An overview of the required inputs is shown in Section 4.3.4.

Table 4.2 confirms that each antenna will need 49.8 W of power. It is assumed that between the transceiver and the antenna a loss of 45% occurs due to the needed amplifiers (Simons et al., 2008). This brings the total power required by this subsystem to be 181 W.

The same thing can be done to show the required power for the RSE between the glider and Earth. The distance between the transmitter and receiver would then be as stated in Section 7.3. The gain of the VLBI network is the summation of the areas of the 72 receiving antennas[2], this gives an effective receiving diameter of 166.5 m. Because this network contains many antennas with different efficiencies and sizes, the average efficiency for a parabolic antenna of 55% is used (Wertz et al., 2011). An overview of the required input for the link budget tool is given in Table 4.3.

Table 4.4 shows that while the VLBI network has a large gain, the transmitting antenna would need to transmit 12 505 W or it would need to have a larger gain. A large enough gain would only be reached by accurate pointing and a small beam, this is not possible with the same system as the relay link due to the requirements set in Section 4.3.2.

Adding a separate system with these capabilities or storing the required extra power on the glider would increase the mass significantly. Because of this, it is chosen not to design for this experiment. However, when the Earth has a small angle from boresight, it could still be possible to receive the signal for short periods when the gain of the VLBI network increases in the future.

[2]URL https://planobs.jive.eu/ [cited 27 May 2023].

Table 4.3: Design input variables for the glider to Earth downlink

Design Input	Downlink
Transmitting power [W]	1205
Receiving antenna effective diameter [m]	166.5
Frequency [MHz]	326
Transmitting antenna efficiency	0.76
Receiving antenna efficiency	0.55
Noise temperature [K]	103.34
Data rate [bps]	100
Distance to receiver [au]	19.31

Table 4.4: Glider to Earth design control table for downlink

Link Parameter	Design value [dB]
Transmitted power	40.97
Transmitting Gain	0.0
Receiving Gain	49.40
Transmitter loss	-1.19
Receiver loss	-2.60
Space loss	-271.9
Pointing loss	-0.12
Atmospheric attenuation	-0.02
Boltzmann constant	228.6
Data rate	20.00
Noise temperature	20.14
E_b/N_0 margin	3.00

4.4 Aerodynamics Analysis

This chapter will cover the aerodynamic analysis of the glider selected to perform measurements of Uranus' atmosphere. As a first step, the subsystem requirements were identified and they are listed in Table A.18 (and a summary here below). Based on those, a detailed design of the aerodynamics subsystem can be performed.

In summary, the glider aerodynamic subsystem shall

- Be tested in conditions simulating the mission, by making used of a wind tunnel simulating the atmospheric and gravitational conditions of Uranus
- Have a negative C_{y_β}, C_{l_β}, C_{l_p},C_{n_p}, C_{n_r}, and C_{m_α}.
- Have a positive C_{n_β}, C_{y_p}, C_{y_r}, and C_{l_r}.
- Have eigenvalues with a negative real part of both symmetric and asymmetric eigenvalues; its value should be of the same order of magnitude as the rest of the eigenvalues in order to be considered relevant.
- Have a C_L/C_D ratio larger than 1.

In Section 4.4.1, the selection of the airfoil to be used for the glider's wings, horizontal stabilisers and vertical tail is described. Next the estimation of the parameters determining the geometry of the wing planform is detailed in Section 4.4.2. This is followed by an estimation of the flight performance and range in Section 4.4.3. Finally, the static and dynamic stability of the glider is analysed in Section 4.4.4 and Section 4.4.5, respectively.

4.4.1 Airfoil Selection

As stated above, this section will detail the airfoil selection process used by the team. This required the consideration of several aspects which will now be described.

Firstly, a screening process carried out to identify various airfoils applicable to the case being considered was performed. Next, an analysis of the aerodynamic characteristics of the various airfoils was carried out. Finally, a selection process was initiated to obtain the most appropriate airfoils for the glider.

Starting with the screening process, databases containing the geometry data of a plethora of airfoils were

Table 4.5: Airfoils considered in the Glider trade-off process

Wing Airfoil	Horizontal/ Vertical Stabiliser Airfoil
FX62-K-153/20	NACA0012
E431	NACA0010
E432	NACA0009
E435	-
E582	-
E582	-
E604	-
E654	-
E748	-
PSU-90-125WL	-
Wortmann FX79-K-144/17	-

identified[3] [4]. Next, since the type of aircraft being considered by the team is a glider, several airfoils used for the wings of gliders on Earth were obtained from such databases as well as from literature (Bessette, 2022). A similar process was performed for the screening process of the airfoils to be used for the horizontal and vertical stabiliser [5].

Next, as was stated above, an analysis of the various airfoils selected after the screening process, as shown by Table 4.5, was performed. In such an analysis, since the atmospheric vehicle is a glider which will be operating at low Mach numbers and Reynold's number, use was made of the aerodynamic analysis tool XFLR5.

By inputting the geometries of the various airfoils, which were obtained from the databases mentioned previously, various aerodynamic polars can be obtained for all airfoils, allowing for direct comparison of their aerodynamic properties. It should be noted that to ensure the highest possible accuracy for all aerodynamic polars, a sufficient number of panels representing the airfoil geometry as well as the correct density and kinematic viscosity of Uranus' atmosphere should be considered. An industry-standard number of 150 panels is used to ensure sufficient refinement of the airfoil mesh. The atmospheric density considered was at the most rarefied point, with a corresponding density of $0.05\,\mathrm{kg\,m^{-3}}$. Following from this, the kinematic viscosity was found to have a value of $2.25 \times 10^{-5}\,\mathrm{m^2\,s^{-1}}$. It should also be noted that XFLR has its inaccuracies as well; it was therefore considered pertinent to only consider the linear region of any aerodynamic polars obtained since this would minimise the effect of any such inaccuracies.

In this case, since a glider was selected, the aerodynamic characteristic considered to perform the trade-off process is $\frac{C_L}{C_D}$. By choosing an airfoil with a steep linear $\frac{C_L}{C_D}$-α curve the airfoil providing the biggest range for the glider can be selected. This was done for both the main wing and horizontal/vertical stabiliser trade-off process.

As can be seen by Figure 4.1a and Figure 4.1b, out of all the airfoils being considered, the FX62-K-153/20 airfoil discovered from literature, (Bessette, 2022), wins the trade-off process for the wing airfoil. It should be noted that only some of the wing airfoils are shown since if all were to be included, the graph would be illegible. Furthermore, the NACA0012 airfoil is also the clear winner for the horizontal and vertical stabiliser trade-off process. Figure 4.1c and Figure 4.1d show the geometry of the airfoils selected for the wing and stabilising surfaces respectively.

4.4.2 Aerodynamic Coefficient Determination and Wing Planform

Initially, the maximum $\frac{C_L}{C_D}$ ratio was used to maximise the gliding distance and time. However, the resulting gliding time posed problems for communication between the glider and the orbiter. From the orbit, it was determined that the maximum communication time was 12 h. By setting a velocity V and having the vertical distance h, the required lift over drag ratio $\frac{C_L}{C_D}$ could be determined. This was done by considering the vertical descent rate as a function of the flight path angle γ. The flight path angle is related to the $\frac{C_L}{C_D}$ by (Ruijgrok, 2013):

$$\frac{C_D}{C_L} = \sin\gamma \tag{4.4}$$

[3] URL https://m-selig.ae.illinois.edu/ads/coord_database.html [cited 17/06/2023]
[4] URL https://aerodynamics.lr.tudelft.nl/cgi-bin/afCDb [cited 17/06/2023]
[5] URL https://aerotoolbox.com/design-aircraft-tail/ [cited 17/06/2023]

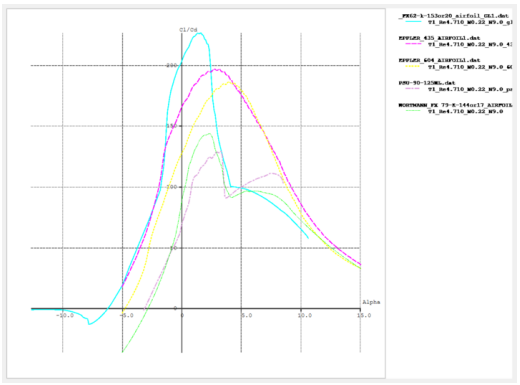

(a) $\frac{C_l}{C_d}$-α curves for the wing airfoils considered

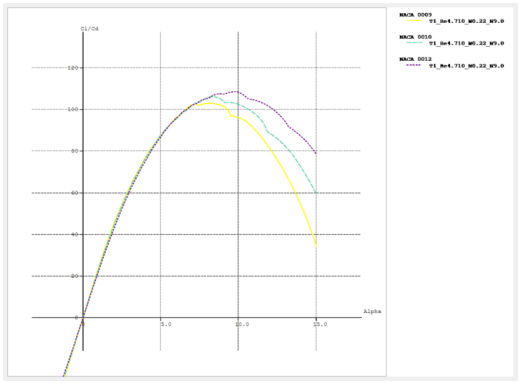

(b) $\frac{C_l}{C_d}$-α curves for the airfoils of the stabilising surfaces

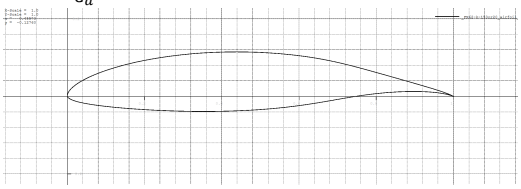

(c) Selected wing airfoil

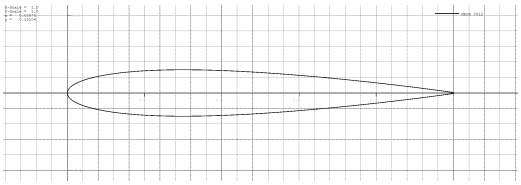

(d) Selected stabiliser airfoil

Figure 4.1: $\frac{C_L}{C_D}$-α curves for the airfoils considered in the trade-off and an outline of the relevant airfoils

This can be found by considering the performance of an aircraft in gliding flight. By considering the descent rate of an aircraft, the required $\frac{C_L}{C_D}$ is found through:

$$\frac{C_L}{C_D} = V\frac{t}{h_{range}} \tag{4.5}$$

where V and h are the same as before, and t is the set flight time. To have not any compressible flow effects, V was set to 200 m s^{-1}, which is slightly below a third of the speed of sound. By also considering the pressure range from 0.1 bar to 20 bar (a vertical distance of 197 km) it was found that $\frac{C_L}{C_D} = 43.2$. Furthermore, because of the gliding flight, the optimum lift coefficient C_L and drag coefficient C_D can be found through (Ruijgrok, 2013):

$$C_L = \sqrt{\pi ARe C_{D_0}} \tag{4.6}$$

$$C_D = C_{D_0} + \frac{C_L^2}{\pi ARe} \tag{4.7}$$

where AR is the aspect ratio, $e = 0.8$ is the Oswald efficiency factor, and C_{D_0} = is the zero lift drag. The optimum drag in gliding flight can be found by substituting Equation (4.6) into Equation (4.7), resulting in:

$$C_D = 2C_{D_0} \tag{4.8}$$

By using the equation for the lift drag polar, C_L can be expressed in terms of $\frac{C_L}{C_D}$ through:

$$C_L = 2C_{D_0}\frac{C_L}{C_D} \tag{4.9}$$

where the parameters are the same as before. By using the calculated value for $\frac{C_L}{C_D}$ and the value of 0.0089 for C_{D0}, C_L was calculated to be 0.71 From here the aspect ratio of the wing can be determined by rewriting Equation (4.6), resulting in:

$$AR = \frac{C_L^2}{\pi e C_{D_0}} \tag{4.10}$$

where the parameters are the same as before. It was calculated to be 26.4 Next, the wing loading was calculated. This was done by assuming that the lift is equal to the weight:

$$\frac{W}{S} = \frac{1}{2}\rho V^2 C_L \tag{4.11}$$

where $\frac{W}{S}$ is the wing loading, ρ is the atmospheric density, V is the velocity, and S and C_L are the same as before. The wing loading has a value of 845.85 N m^{-2}. From here the wing span and mean chord can be calculated through:

$$b = \sqrt{SAR} \tag{4.12}$$

$$\bar{c} = \frac{b}{AR} \tag{4.13}$$

where the b is the wing span, $\bar{c}$ is the mean chord, and the other parameters are the same as before. The glider has a span of 8.63 m and a mean chord of 0.33 m. Next, the root chord C_r and the tip chord C_t can be calculated with:

$$C_r = \frac{3}{2}\bar{c}\frac{1+\lambda}{1+\lambda+\lambda^2} \tag{4.14}$$

$$C_t = C_r\lambda \tag{4.15}$$

where λ is the taper ratio of the wing and the other variables are the same as before. The taper ratio has to be chosen. It was chosen that the glider will not have swept wings, meaning that the quarter chord sweep angle $\Lambda_{c/4}$ is 0°. The taper ratio is then calculated (Torenbeek, 2013):

$$\lambda = 0.2\left(2 - \Lambda_{c/4}\frac{\pi}{180}\right) \tag{4.16}$$

This results in a taper ratio of 0.4. This resulted in a root chord of 0.44 m and a tip chord of 0.176 m.

4.4.3 Flight Performance and Time of Flight

With $\frac{C_L}{C_D}$ calculated in Section 4.4.2, the maximum flight range can be calculated with:

$$R_{glide} = \left(\frac{C_L}{C_D}\right)_{max} h_{range} \tag{4.17}$$

where R is the range and h is the vertical distance. Similarly, the time of flight (ToF) t can be calculated with:

$$t = \sum \Delta h\sqrt{\rho_{avg}}\sqrt{\frac{1}{2\frac{W}{S}}}\frac{C_L^{3/2}}{C_D} \tag{4.18}$$

where Δh is the difference in altitude, W/S the wing loading, ρ_{avg} the average density between the altitudes considered, and C_L and C_D are the same as before. The ToF that is calculated with Equation (4.18) is expected to differ from the ToF given as input. This is due to the fact that the density change was not taken into account previously. By using the previously determined values for h and $\frac{C_L}{C_D}$ the glider is calculated to have a range of 8541 km. Similarly, by using the previously estimated values for the wing loading, lift and drag coefficient, the ToF can be calculated. The density between the respective pressure levels was calculated by using the GRAM model for Uranus (Justh et al., 2021). This resulted in a ToF of 4 d, 1 h, and 15 min. It should be noted, however, that the model used does not take into account any of the winds that are present in the atmosphere.

4.4.4 Glider Stability Analysis

Moving on to the glider stability analysis, since no active control surfaces were considered it was especially important for the glider to be statically and dynamically stable. Furthermore, since the stability of an aircraft is affected by various parameters pertaining to the glider geometry and mass, a tool ensuring fast iteration was required. As such, to perform the analysis while considering as many design choices as possible, XFLR5 was used for the airfoil selection.

Before a stability analysis could be started, some parameters had to be estimated based on the results obtained for the wing planform in Section 4.4.2.

$$\Gamma = 3 - \frac{\Lambda_{c/4}}{10} \tag{4.19}$$

$$\tan\Lambda_{c/2} = \tan\Lambda_{c/4} - \frac{4}{AR}\frac{1}{4}\frac{1-\lambda}{1+\lambda} \tag{4.20}$$

Starting with the estimation of the half-chord wing sweep and dihedral angle, using Equation (4.20) and Equation (4.19) respectively (Torenbeek, 2013), an initial value for the two quantities was found.

$$\varsigma_{h/v_{glider}} = \left(\frac{\varsigma_{h/v}}{\varsigma_w}\right)_{GL1}\varsigma_{w_{glider}} \tag{4.21}$$

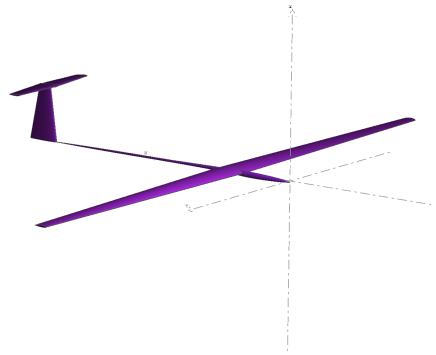

Figure 4.2: Final glider configuration

Then using Equation (4.21), an estimate for the horizontal and vertical stabiliser wing span, root chord and tip chord was found, where $\varsigma_{h/v_{glider}}$ is the quantity to be calculated, $\left(\frac{\varsigma_{h/v}}{\varsigma_w}\right)_{GL1}$ is the ratio of the quantity to be calculated over the same quantity for the wing obtained from literature (Amalia et al., 2018) and $\varsigma_{w_{glider}}$ is the known wing quantity for the CAELUS glider.

$$\frac{m_h}{m_w} = 0.1 \qquad\qquad m_v = m_h - 1 \tag{4.22}$$

Finally, to calculate the weights of both stabilising surfaces, Equation (4.22) was used. From literature, it was found that the mass of the vertical stabiliser is usually smaller than the horizontal stabiliser. Moreover, since the chords of the stabilising surfaces do not differ much the approximation stated in Equation (4.22) was deemed appropriate. This was not the case for the span of the horizontal stabiliser, since it is approximately twice the size of the vertical stabiliser.

After the previous estimation, the analysis could then begin. This began by considering the position of the centre of gravity of the aircraft as a whole, $x_{c.g.}$, which had to be determined in such a way that the moment coefficient vs. angle of attack,C_m-α curve has a negative slope. This ensures a stable equilibrium position. Furthermore, since a target α was obtained from the range and time-of-flight analysis the intercept of the curve with the α axis also had a target value. To accomplish the first condition, the following relation was used to ensure a stable equilibrium position:

$$x_{c.g.} \leq xa.c. \tag{4.23}$$

After iterating with different glider geometries and mass positions, while still keeping in mind Equation (4.23), a final configuration of the glider for static equilibrium was found. From the final $x_{c.g.}$ position obtained through the iterative process, the neutral point associated with the glider configuration obtained was found. This was done through an iterative process where the centre of gravity position was moved without affecting the chosen configuration until the c_m vs. α slope became equal to 0.

$$x_{c.g._{new}} = (SM\bar{c}) - x_{n.p.}) \tag{4.24}$$

Upon identifying the value of $x_{n.p.}$, by using Equation (4.24), a new location of the centre of gravity was consequently found. This location includes a static margin which ensures the static stability of the aircraft.

Once the static stability of the aircraft was ensured, an analysis of the dynamic stability of the glider was carried out using the appropriate function in XFLR5. This function follows a linearised analysis, in which the various eigenmotions belonging to an aircraft in flight can be analysed, [6]. The eigenmotions that can be obtained from the function are four longitudinal modes: two phugoid modes and two short-period modes; and four lateral modes: a spiral mode, a roll damping mode and two Dutch roll modes. To ensure both longitudinal and lateral dynamic stability, the eigenvalues characteristic of such motions were analysed and their real component was confirmed to be smaller than 0 to ensure the motion converges over time. This is vital since the glider has no active control. A final configuration of the glider geometry and centre of gravity location ensuring dynamic and static stability was identified after an iterative process where various parameters were varied. These parameters are the wing dihedral, wing sweep, horizontal stabiliser angle of incidence, and height of the centre of gravity with respect to the axis of symmetry of the aircraft.

For visualisation purposes, a model of the final configuration can be seen in Figure 4.2. Furthermore, Table 4.6 and Table 4.7 show the values obtained for the various relevant parameters and their masses respectively.

$$\omega_n = \sqrt{Re(\lambda_n)^2 + Im(\lambda_n)^2} \qquad\qquad \zeta = \frac{-Re(\lambda_n)}{\sqrt{Re(\lambda_n)^2 + Im(\lambda_n)^2}} \tag{4.25}$$

[6]URL: https://ebrary.net/59623/engineering/analyzing_decode_with_xflr5_stability [cited 20/06/2023]

Table 4.6: Overview of the aerodynamic parameters of the glider

(a) The aerodynamic parameters of the wing and other aerodynamic dimensions

Wing parameters	
b [m]	8.63
c_r [m]	0.44
c_t [m]	0.176
Γ [deg]	1
Λ_{c2} [deg]	1
AR [-]	28.0
Static Margin [%]	0.15
$\bar{c}$ [m]	0.33
Other parameters	
l_f [m]	1.675
d_f [m]	0.7
$l_{connection}$ [m]	1.675

(b) The aerodynamic parameters of the horizontal and vertical stabiliser

Vertical stabiliser parameters	
b_v [m]	0.777
c_{r_v} [m]	0.44
c_{t_v} [m]	0.161
Horizontal stabiliser parameters	
b_h [m]	1.57
c_{r_h} [m]	0.289
i_h [deg]	3
c_{t_h} [m]	0.162

Table 4.7: Final configuration mass parameters

m_w [kg]	m_f [kg]	$m_{payload}$ [kg]	m_{power} [kg]	m_{comms} [kg]	$m_{thermal}$ [kg]	$m_{connection}$ [kg]	m_h [kg]	m_v [kg]
164	7.35	28.2	57.1	1.4	0.2	4	16.4	15.4

Table 4.8: Critical eigenmotion parameters and eigenvalues

Phugoid Motion		
Eigenvalue	**Frequency [Hz]**	**Damping**
-0.000503 ±0.05223i	0.052	0.01
Short-Period Motion		
Eigenvalue	**Frequency [Hz]**	**Damping**
-0.308 ±2.231i	2.25	0.137
Dutch Roll Eigenvalue		
Eigenvalue	**Frequency [Hz]**	**Damping**
-0.00454 ±1.97i	1.97	0.0023
Roll Damping Eigenvalue		
Eigenvalue	**Frequency [Hz]**	**Damping**
-0.7598	[-]	[-]

Finally, Table 4.8 presents relevant parameters associated with the most critical eigenmotions in the longitudinal and lateral directions, obtained by performing a dynamic stability analysis using XFLR5. It should be noted that using Equation (4.25) enables for the estimation of the damping ratio and frequency associated with a particular complex eigenvalue, where Re() and Im() represent the real and imaginary part of the eigenvalue.

4.4.5 Verification, Validation and Sensitivity Analysis

Before making any meaningful conclusions about the obtained values, verification and validation of the used code is important. Through this process, one can be that the values that are calculated are actually realistic.

Verification

Verification has been done for the various codes used. Since the code consisted in implementing the equations above, performing unit tests on these functions proved to be sufficient. This was done by taking random values for the inputs and comparing the outputs from the numerical results and the hand calculations. Additionally, the XFLR5 software does not need explicit verification and validation. A paper (Güzelbey et al., 2018) talks specifically about the verification and validation of XFLR5 and was considered as such.

Validation

For the validation of XFLR5, the data computed with XFLR5 was compared to the actual experimental data of the chosen airfoil. For the wing platform, the GL-1 glider, an actual glider designed for thermal updraft conditions in Indonesia, was considered for validation (Amalia et al., 2018). For this, only the $\frac{C_L}{C_D}$ ratio will be validated,

as the other parameters directly flow down from this value. For a given condition the glider has a velocity of 24.3 m s^{-1}, a ToF of 7.5 min, and an altitude of 458 m. From this, a $\frac{C_L}{C_D}$ of 23.8 was found, which is within 1 % of the stated value, which is 24.

A paper on an autonomous glider in Uranus' atmosphere was used for the range validation (Lebeau et al., 2015). In the paper, they consider a large glider and a small glider. For validation, only the small glider was considered. It has a span of 6 m, a wing area of 4.8 m^2, a mass of 162.1 kg, and a $\frac{C_L}{C_D}$ of 22.9 A significant difference was noticed between the altitude ranges in which either glider operates. While they have an altitude of 170 km, GRAM gives an altitude of nearly 200 km, even though the same pressure range is considered. For validation, the 170 km was chosen. This resulted in a range of 3893 km, while the paper has a range of 3800 km. These values have a 2.5 %, which is considered acceptable.

4.5 Structures and Materials

In this section, an overall structural analysis of the glider will be performed. First of all, it is important to analyse the functions and requirements related to this specific subsystem, which can be found in Table A.15.

In summary, the glider Structure subsystem shall

- Withstand axial, vibrational, lateral and separation loads.
- Withstand the space environment without degradation.
- Withstand aerodynamic peak pressures.
- Perform unfolding.
- Have a volume of 3 mx3 mx3 m when in the folded configuration.
- Have a wing span not exceeding 8 m.
- Have a length not exceeding 3 m.
- Provide an interface to the glider subsystems.
- Have a natural frequency in the range described in the launch catalogue.
- Be evaluated in a test campaign.
- Include redundancy in the design.
- Stay within the mass and cost budget of 1000 kg (total of both glider and capsule) and M€ 340 respectively, with a reliability of 99.4%

Once the subsystem requirements have been established, the detailed design of the subsystem can begin. To do so in an efficient way, a couple of general assumptions have been made, together with some more specific ones that will be presented in due time. The analysis will be split into two main parts: one for the design of the wings, performed in Section 4.5.1, and one for the fuselage, performed in Section 4.5.2.

Before actually performing the different load analyses, appropriate materials shall be selected for the structure: without the material, no proper stress calculations can be done since they involve material properties such as the elastic modulus, the yield normal stress and the yield shear stress. Furthermore, these last two properties will be used as failure criteria for the different load cases. Hence, they will be the main criteria driving the materials selection process, since they will be the limiting values that must not be exceeded by the structure.

When material science is involved in aerospace engineering, it comes with no surprise that aluminium (and its alloys) is by far the most used material in the industry: its great material properties, combined with its low density, make it suitable for practically almost any application. This is indeed the case for aircraft as well: as it is mentioned in (Chatterjee & Bhowmik, 2019), aluminium is used in almost every structural component of aircraft wings, such as spars, ribs, and upper and lower skins. For wing skin, in particular, the alloy Al-Cu 2024 is mentioned. In addition to this, another aluminium alloy was considered for the selection, namely Ti-6Al-4V, which was used for the preliminary sizing of the conceptual design during the midterm phase. All the relevant properties needed for the stress analysis of both the wings and the fuselage are collected in Table 4.9. Unfortunately, no information could be found with respect to the corresponding temperatures at which these values are to be applied nor how the performance of the materials is at the low temperatures the glider will encounter; however, it is mentioned in (Yu et al., 2022) that, when the alloy Ti-6Al-4V is rolled at very low temperatures (cryorolled), very similar to the ones that will be encountered on Uranus, the hardness and strength values of the alloy increased: this, combined to the fact that the two alloys mentioned in Table 4.9 were and are still vastly used in the space industry, allows assuming with a certain degree of safety that the materials will not experience major performance flaws. Hence, the whole glider structural design will be performed assuming the values in Table 4.9 to be valid, since the cold temperatures shall not play a major role in the material performance. Please note that these were not the only two alloys considered: Al-Cu 2324-T39 and Al-Cu 2224-T351X were also considered, as they were recommended in (Bergmann et al., 1998), however not all the properties needed

Table 4.9: Key mechanical properties of the two aluminium alloys selected for the design. Sources: [2]: (Martin, 2006); [3]: (Hibbeler, 2018)

Al Alloy	E [GPa]	G [GPa]	σ_y [MPa]	τ_y [MPa]	ρ [kg m^{-3}]	Cost [€/kg]
Al-Cu 2024	73 [2]	27 [3]	455 [a]	172 [3]	2770 [2]	1.85 [b]
Ti-6Al-4V	120 [3]	44 [3]	924 [3]	508	4430 [3]	43 [c]

[a] URL https://www.theworldmaterial.com/2024-aluminum-alloy/ [cited 16 June 2023]
[b] URL https://markets.businessinsider.com/commodities/aluminum-price [cited 14 June 2023, value fluctuates on a daily basis]
[c] URL https://www.stindia.com/titanium-grade-5-supplier.html#price [cited 14 June 2023]

could be found, and the few ones found were very similar to Al-Cu 2024, if not identical, making it pointless for them to be considered. They were hence discarded.

As can be seen in Table 4.9, no source is mentioned for the yield shear stress of Ti-6-Al-4V: this is because the parameter was not found when performing literature research (since it was not mentioned anywhere), but it was estimated by assuming that the ratio between the yield and ultimate normal stress is the same as the ratio between yield and ultimate shear stress. If the material is considered to be isotropic (as is often the case for metals), then this assumption may be considered valid, because the main parameters that govern normal and shear stress, namely the elastic modulus E and the shear modulus G, are linearly related by the Poisson's relation (Hibbeler, 2018):

$$G = \frac{E}{2(1+\nu)} \tag{4.26}$$

Equation (4.26) is indeed valid for Ti-6-Al-4V since $G = \frac{120}{2(1+0.36)} = 44.1$ MPa (with Poisson's ratio value found in (Hibbeler, 2018)), hence τ_y can be found to be the value presented in Table 4.9.

One last consideration needs to be made with regard to the safety factors: for every load case considered, safety factors will be applied to either the thickness or the stress values computed during the analysis. For this, the ECSS-E-30 standards will be followed: a factor of 1.3 will be applied to any thickness calculated (meaning that the final value will be multiplied by this number) and a factor of 1.1 will be applied to stress (meaning that 1.1 times the stress value computed has to be lower than the critical value, namely the yield stress of the material) (ESA, 2000).

4.5.1 Wings Analysis

The wings structural analysis and design can be rather complicated since one has to take into account different distributions of the aerodynamic forces, numerous structural elements needed and various types of loading and failure modes that flow down from the force distributions. To simplify the analysis such that it can be performed with a high level of accuracy, while also complying with the Design/Synthesis Exercise timeline, it has been assumed that the main force contribution is from the lift, which will be computed by multiplying the wing loading by the relevant wing surface area: both of the lift and wing surface area will be given by the aerodynamic analysis of the glider (geometrical wing properties will be given, which will then be used to calculate the area). Moreover, the load considered will always be assumed to be uniformly distributed on the wing, meaning that it will always be assumed as a rectangular load distribution, even though the wing cross section is not rectangular. Additional considerations will be presented in the corresponding load analyses regarding this.

Speaking of other forces, such as the drag, it is mentioned in (Bessette, 2022) that the drag coefficient values computed during the verification procedure are much lower compared to the lift coefficients: based on this consideration, the effect of drag on the structure will be not as significant as the one lift would cause, hence it has not been taken into account for this analysis.

Additionally, it is highly suggested to thoroughly read Section 11.2, where more considerations, assumptions and consequent recommendations for this analysis are presented.

Cross-section Geometry

To ease the computations and reduce the overall degree of complexity, the cross-section of the wing has been approximated in the way presented in Figure 4.3a. The lift distribution and the resultant lift force are presented as well in Figure 4.3b: for simplicity, it has been assumed that the resultant force acts halfway through the horizontal section.

As it can be seen, the geometry of the airfoil has been approximated using thin-walled, simple geometric figures (all with the same thickness t_t): a half circle (1), a rectangle (2) and an isosceles triangle (3). By doing so, all the stress analyses that will be done can be significantly simplified for many different reasons: first, the computation of key geometrical properties such as the centroid location, the cross-sectional area and moments of inertia are easier to compute because the section is symmetrical with respect to the X axis; in this way, only one location (the X location, x_c in the figure) for the centroid needs to be computed, and the computation of

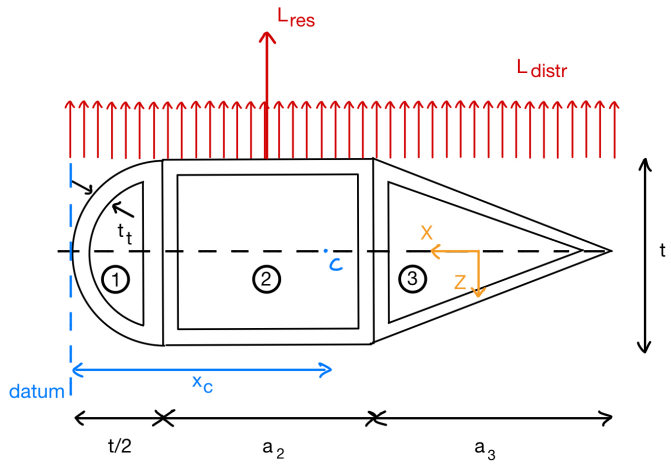

(a) Geometrical sketch representing the simplified cross-section of the wings used for the analysis

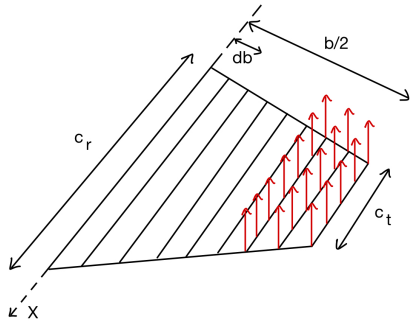

(b) 3-D Representation of the lift distribution used for the analysis. Note that the lift is distributed over the whole wing (not only on the portion shown in the sketch). db represents the span increment

Figure 4.3: Overall simplified geometry of glider wings

the moment of inertia with respect to the X axis (I_{xx}) will not need parallel axis theorem terms, because all the geometries already lay on the X axis. In addition, the moment of inertia I_{xz} is equal to 0 because of an axis of symmetry. Furthermore, the stress analysis due to bending is simplified as well, because no neutral axis has to be calculated since the section is symmetric (at least along the X-axis).

Please note that this simplification, since it reduces the complex geometry of the airfoil to a symmetric section, will intuitively be more accurate for symmetric airfoils than cambered ones: for the case in which an asymmetric airfoil is selected from the aerodynamics analysis, the edge of the airfoil with the lowest camber will be mirrored around the X axis such that symmetry is once more obtained and the aforementioned simplification can be applied. Although the new geometry would be certainly different, by using the edge with the lowest camber for the approximation the structural stiffness of the airfoil will be underestimated, leading to an overdesigning of its structure, which is preferred over an underdesigning. One final consideration is with regards to the dimensions t, a_2 and a_3 seen in Figure 4.3a: besides t, which corresponds to the maximum thickness of the airfoil, the other two dimensions are not generally given in the specifics; they must be computed by geometrically inspecting the specific airfoil selected.

Shear Stress due to Torsion Caused by Lift

The first step for this analysis was to estimate the torque caused by the lift: by looking at Figure 4.3b, remembering the assumption made at the beginning of the section regarding the point of action of L_{res}, it is clear that the largest torque that will ever be encountered in this idealisation is given by the resultant force times the moment arm, given by $|x_c - \frac{t}{2} - \frac{a_2}{2}|$, keeping in mind once more the assumption that the resultant lift force acts halfway through a_2. The second and last step consists of rearranging the formula for the shear of thin-walled closed sections to find the required thickness to sustain the yield stress of the material:

$$\tau_y = \frac{T}{2A_m t_t} = \frac{L_{res}|x_c - \frac{t}{2} - \frac{a_2}{2}|}{2A_m t_t} \tag{4.27}$$

where A_m represents the area enclosed by the cross-section. Solving for t_t and iterating for all the different chord values gives all the corresponding required thickness values, among whose the largest one will be considered.

Shear Stress due to Transverse Shear Caused by Lift

The shear due to transverse force analysis is by far the most complicated to implement. Even when using the simplified representation as seen in Figure 4.3a the definition of shear flow would have been rather complicated to define, since not only does the section present different geometries, but one of them is a half-circle, for which it is more complicated to estimate the variation of shear flow. Therefore, as it is commonly done when analysing wing boxes and airfoils, the section was further simplified by making it an idealised structure, using zero-thickness skins and point area booms as displayed in Figure 4.4. The procedure followed was the following: first, the boom areas were calculated using the general formula $B = \frac{t_{skin} b}{6}\left(2 + \frac{\sigma_2}{\sigma_1}\right)$, where for this case $t_{skin} = t_t$ and b is either equal to t or to a_2. Note that the skin thickness contribution is still taken into account when

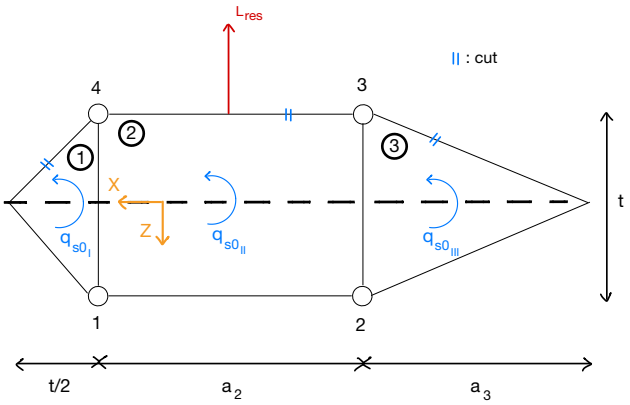

Figure 4.4: Idealised airfoil cross-section used for the transverse shear analysis

calculating the booms areas and that the area of each boom is given by the contribution of each adjacent one; as an example, $B_1 = B_{12} + B_{14}$.

After calculating the boom areas (which turned out to all be equal), the moment of inertia had to be recalculated using $I_{xx} = \Sigma z_i^2 B_i$. Following this, the shear flow for each segment of the section had to be estimated, but since this is a closed section the shear flow had to be divided into two components: one given by the equivalent open section, found by placing imaginary cuts on the section as shown in Figure 4.4, known as the basic shear flow q_b, and another contribution given by the fact that the section is indeed closed. This means that there must be an overall shear contribution that counteracts the open-section effect, found by applying moment equivalence between the shear flows and the external shear force. This contribution is often referred to as q_{s_0}. The full procedure is represented by Equation (4.28) and Equation (4.29).

$$q_s = q_b + q_{s_0} = -\frac{V_z I_{zz} - V_x I_{xz}}{I_{xx} I_{zz} - Ixz^2} \Sigma z_i B_i - \frac{V_x I_{xx} - V_z I_{xz}}{I_{xx} I_{zz} - Ixz^2} \Sigma x_i B_i + q_{s_0} = -\frac{V_z}{I_{xx}} \Sigma z_i B_i + q_{s_0} \tag{4.28}$$

$$(ccw+) \Sigma M_{35} : 2A_I q_{s_{0_I}} + 2A_{II} q_{s_{0_{II}}} + 2A_{III} q_{s_{0_{III}}} - a_2 t q_{b_{26}} = -\frac{a_2}{2} L_{res} \tag{4.29}$$

The last thing left to quantify is the deflection for each section, namely $\left(\frac{d\theta}{dz}\right)_I$, $\left(\frac{d\theta}{dz}\right)_{II}$ and $\left(\frac{d\theta}{dz}\right)_{III}$, which are all equal since the airfoil always undergoes the same torsion, hence $\left(\frac{d\theta}{dz}\right)_I = \left(\frac{d\theta}{dz}\right)_{II} = \left(\frac{d\theta}{dz}\right)_{III} = \left(\frac{d\theta}{dz}\right)$. Finding the deflection for each portion, setting them equal to each other and applying Equation (4.29) gives a system of four equations with four unknowns, $q_{s_{0_I}}$, $q_{s_{0_{II}}}$, $q_{s_{0_{III}}}$ and $\left(\frac{d\theta}{dz}\right)$. This finally allows one to find the shear flow for each segment of the airfoil cross-section, for which the largest has to be taken, allowing one to find the maximum thickness needed by the airfoil to resist shear loads using $\tau_y = \frac{q_{max}}{t_t}$.

An analogous analysis to the one just performed was done for the YZ plane of the wings as well: the geometry of the wing (as seen from the front) was approximated to be a thin-walled rectangle, with height equal to the thickness of the airfoil at the tip. In this way, although the analysis was for an idealised structure, it enabled an overestimation of the thickness, rather than an underestimation for the case where the root thickness would have been used.

Normal Stress due to Bending Caused by Lift

The general procedure that will be followed here is to estimate the moment in the X direction caused by the lift distribution among the wing and then apply the general formula for normal stress due to bending, simplified by the assumptions earlier mentioned:

$$\sigma_y = \frac{(M_x I_{zz} - M_z I_{xz})z + (M_z I_{xx} - M_x I_{xz})x}{I_{xx} I_{zz} - I_{xz}^2} = \frac{M_x z}{I_{xx}} \tag{4.30}$$

where I_{xx} is linearly dependent from t_t since the section is thin-walled. Starting from z, namely the vertical distance from the neutral axis (which coincides with the axis of symmetry), it is clear that it will have a maximum value at the horizontal edge of section (2) in Figure 4.3a, which will lead to the maximum value for the thickness needed to sustain the yield stress. Hence, for this analysis, a value of $z = \frac{t}{2}$ will be used. The only thing left to be identified is the moment M_x as a function of the spanwise location: to do so, the wing has been approximated

to be a cantilever beam (seen from the YZ plane) with a distributed rectangular lift force on top. Integrating the lift force with respect to the Y location gives the bending moment:

$$L(y) = L_{distr} yc(y) \rightarrow M_x(y) = -\frac{2}{3}\frac{(c_r - c_t)}{b} L_{distr} y^3 + \frac{c_r}{2} L_{distr} y^2 \tag{4.31}$$

with $c(y) = -2\frac{(c_r - c_t)}{b} y + c_r$ the geometric chord value as a function of the spanwise location. Now everything is known from Equation (4.31): rearranging to find t_t, which is included in I_{xx}, and iterating upon different Y locations and corresponding chord values, allows to find the required thickness for each cross-section to resist the maximum stress due to bending. Once more, only the largest value will be considered, since that allows for an overestimation.

Buckling Caused by Lift

Regarding buckling, the only analysis that has been performed is for the wing spars: this is because the only force considered for this whole structural analysis is the lift force, which acts perpendicular to the skin surface, meaning that the buckling is in the thickness direction; the skin thickness, however, is so thin (in the order of 1 mm) that it is safe to assume that buckling would never happen in that direction.

Having made this assumption, the buckling of the wing spars will be estimated using Euler buckling, which is described by the following formula: $P_{crit} = \frac{\pi^2 EI}{L^2}$, with P_{crit} the critical load applied (for this case equal to the lift) and L the length of the beam. As it is mentioned by (Chatterjee & Bhowmik, 2019), it is fairly common for spars to have an I-beam cross-section: the buckling will then be calculated on an I-beam spar of height equal to t, the maximum thickness of the airfoil as shown in Figure 4.3a. When considering the I beam, and assuming it to be thin-walled as well, it is intuitive to say that the horizontal portions of the I will not experience any buckling, for the same reason given for the skin thickness. Hence, the only effective part of the spar cross-section that will carry buckling is the vertical portion, which has a height of $t - 2t_I$, with t_I the thickness of the cross-section. Applying the equation previously presented, applying the thin-walled approximation (hence neglecting all high-order terms of t_I) and solving for t_I allows one to find the thickness required for the spars to sustain the buckling caused by lift.

Thermal Stresses due to Temperature Differences

The last load case that was analysed for the wings is the thermal loads caused by the differences in pressure that the glider will have to face during its descent inside Uranus's atmosphere. To estimate this, the strain due to thermal loads needed to be found, which then multiplied by the Young's modulus yields the stress caused by thermal differences; if it is lower than the yield stress of the material, then the structure will survive thermal loads. In formulas: $\sigma_{thermal} = E\epsilon = E\alpha\Delta T < \sigma_y$, where α represents the coefficient of thermal expansion of the material. As ΔT, the largest temperature difference that the glider will have to undergo was used, namely the one between the 1 bar and the 20 bar pressure levels.

4.5.2 Fuselage Analysis

The next structural element that must be analysed is the glider's fuselage. Its geometry and size will be determined based on the size of the payload as presented in Chapter 3. From such constraints, it can be computed that the length and diameter of the fuselage will, respectively, equal to 1.67 m and 0.7 m.

Once the main parameters of the fuselage have been determined, its thickness can be computed based on the two main loads that will be applied to the fuselage during operations: torque loads and differences in pressure. Regarding the first, these will be induced by the aerodynamic loads generated by the horizontal and vertical stabiliser and due to the small size of such surfaces, this specific load scenario will not be driving the sizing. A different situation arises when looking at the hoop stresses in the fuselage. These will lead to a higher minimum required thickness and therefore a higher overall weight of the glider. As a result, similarly to what has been done with the wing, holes will be drilled along the length of the fuselage to make sure that no difference in pressure is felt by the fuselage skin.

4.5.3 Results

All the load analyses presented in Section 4.5.1 and Section 4.5.2 allowed to find values for the thickness of the wings and fuselage such that the different stresses could be sustained; the largest out of all of these values is the one selected for the final design, both for the wings and fuselage; another important value for the thickness was taken into account, namely the minimum value that allows for manufacturability of thin metal sheets: according to sciencedirect.com [7], metal sheets cannot be manufactured to a thickness lower than 0.8 mm. This effectively means that any thickness value lower than this will not be critical in any way, because it is lower than the minimum value needed for the sheet to actually be manufactured, and hence applied.

[7] URL https://www.sciencedirect.com/topics/materials-science/ti-6al-4v [cited 18/06/2023]

Regarding the wings, the least constraining load turned out to be the stress due to transverse shear in the XZ plane: the maximum value of thickness required from the wings is lower than 0.8 mm, hence not driving the analysis. Shear due to transverse force in the YZ and shear due to torque in the XZ plane gave thicknesses in the same order of magnitude, around 10^{-1}mm, but still not the most constraining. Finally, normal stress due to bending gave a thickness value of 1.7 mm, which makes it the most driving out of all the load cases.

Regarding the fuselage, the torque was not driving in any way, since it gave values in the order of 10^{-3} mm. With this taken into account, the thickness of the structure is only limited by manufacturing and therefore will be limited to 0.8 mm.

Having values for thicknesses, it was then possible to estimate the total mass of the glider structure, found by simply calculating the volumes of wings and fuselage, multiplying them by the respective densities and adding them together: this led to a mass of 244 kg. It was then possible to estimate the total cost: the material cost could be found by simply multiplying the cost per kilo of the material by the amount of mass needed, while the other costs such as development, testing and manufacturing costs could be found using cost estimations from (Wertz et al., 2011). The total cost of the structure was found to be M€ 7.2.

Concerning the correctness of the results, the calculations and the tools developed were checked using unit tests, to confirm that the computations were correctly performed, and system tests, to confirm that the different functions were correctly interfaced and giving reasonable results. These tests highlighted numerous mistakes in the derivation of the different formulas, together with a conceptual mistake in the approach used for the estimation of the shear stress due to transverse force.

4.6 Thermal Management

As the glider will be travelling in the ”Ice-cold” atmosphere of Uranus (53 K to 193 K), care must be taken in maintaining the temperature of the onboard subsystems and payload equipment. Requirement CNRS01.66-A-TM states that the payload shall be kept between 253 K-300 K, while requirement ESA04.32-A-TM states that the subsystems shall be kept between 273 K and 293 K. Many similar constraints are present, as a result, before starting the detailed design of the subsystem, all subsystem requirements have been identified and are presented in Table A.17.

In summary, the glider Thermal Management subsystem shall

- Supply temperature data to the OBC at 1 Hz for internal temperature regulation.
- Keep the payload subsystem within a temperature range of 253 K to 300 K throughout the mission phases.
- Keep the glider subsystems within a temperature range of 273 K to 293 K throughout the mission phases.
- Remain within the mass, cost, and power values with a reliability of 99%.

To assess the required thermal management subsystem elements, the thermal influences in the Uranus atmospheric environment must be identified and consequently quantified. There are sources of heating and sources of heat loss. The thermal assumption is made that the skin surface of the glider is the same temperature as the outside air temperature, or equal to 3 K when travelling to Uranus. The payload and subsystems are suspended by rods within the glider fuselage, such that they are not in contact with the moving air of Uranus' atmosphere. Since the glider fuselage is not pressurised, however, there is still gas within the fuselage which only conducts heat, meaning there is no convection. For the thermal analysis, the payload instruments and subsystems are both assumed to be contained in cylinders whose centre is aligned with the centre of the fuselage. The payload dimensions mentioned in Section 3.3 are used by summing the maximum instrument depths to be the length of the cylinder, and the second largest width or height to be the radius of the cylinder. The length of the cylinder is then

$$L_{cylinder} = 19.5 + 10.5 + 20 + 0.47 + 0.25 = 50.72\,\text{cm}$$

The largest width dimension is 20 cm, taking the distance from the centre of that 20x20 cm^2 square yields a radius of $r_{clearance}$ equal to14.2 cm. Placed in the middle of the fuselage the payload thus has a distance of

$$r_{clearance,payload} = r_{fuselage} - r_{payload} = 0.28 - 0.142 = 0.138\,\text{m}$$

The surface area of this cylinder $A_{payload}$ is equal to 0.579 m^2. The same calculations are done for the subsystems contained in the glider fuselage, which are dominated by the batteries mentioned in Section 4.7. The subsystem cylinder is 0.8 m in length and has a radius of 0.1 m. The surface area of the subsystems $A_{subsystems}$ is equal to 0.565 m^2, and $r_{clearance,subsystems}$ is equal to 0.18 m.

Table 4.10: The heat flux values for radiation, conductivity, thermal inefficiency, and the thermal management system when the payload is held at 276.5 K and the subsystems are held at 283 K

Heat flux [W m^{-2}]	T = 3 K (vacuum)	T = 53 K	T = 193 K
$Q_{\text{rad,pl}}$	5.76	5.76	5.76
$Q_{\text{rad,subsys}}$	6.17	6.17	6.17
$Q_{\text{cond,str,pl}}$	1.02	0.84	0.31
$Q_{\text{cond,str,subsys}}$	1.05	0.86	0.34
$Q_{\text{cond,air,pl}}$	N/A	0.49	0.18
$Q_{\text{cond,air,subsys}}$	N/A	0.38	0.15
$Q_{\text{ineff,eff=0.98}}$	5.11	5.11	5.11
$Q_{\text{req,eff=0.99}}$	11.44	11.93	10.35
$Q_{\text{req,eff=0.98}}$	8.88	9.37	7.79
$Q_{\text{req,eff=0.97}}$	6.32	6.81	5.23

The thermal management subsystem either adds heat with a heating system or removes heat by radiating it away such that the equilibrium temperature remains within the operational temperature range of the payload and subsystems. The albedo, solar, and infrared radiation, are neglected, since they hit the skin of the glider, which instantly cools down as it interacts with the atmosphere. The remaining heat flux components are therefore thermal radiation, conduction through the structure, conduction through the air in the fuselage, and heating due to inefficient power management.

The heat flux due to the thermal radiation of an object is given by the following equation:

$$\dot{Q}_{rad} = \varepsilon \sigma A T^4 \tag{4.32}$$

where ε is the emissivity of the object, σ the Stefan-Boltzmann constant in W m^{-2} K^{-4}, A the surface area of the payload or subsystems in m^2, and T the temperature of the payload or subsystems in K. This heat flux is lost to the environment.

The next source of heat loss is conduction. Conduction through a gas, liquid, or solid follows from:

$$\dot{Q}_{cond} = \frac{kA}{l}(T - T_{atm}) \tag{4.33}$$

where k is the coefficient of thermal conductivity in W m^{-1} K^{-1}, A the area exposed to the air in m^2, or the cross-sectional area of the structural support rods, l the distance through which the heat flux moves in m, and T_{atm} the temperature of the skin and air inside the fuselage in K. In this case, l, for the structural rods and layer of gas in the fuselage is equal to $r_{clearance}$. This heat flux is also lost to the environment.

Following these components is a heating factor. Since the power subsystem is not perfectly efficient in distributing electrical power, some waste heat is generated. The waste heat emitted is equal to

$$\dot{Q}_{ineff} = P(1 - \eta)$$

Then, to arrive at the wished-for equilibrium temperature, another heat flux is added. It is added to the heat flux of the inefficiency, which has to be balanced with the heat flux into the surroundings. This balance is shown in the following equation:

$$\dot{Q}_{ineff} + \dot{Q}_{th.management} = \dot{Q}_{cond,subsys} + \dot{Q}_{cond,pl} + \dot{Q}_{rad,subsys} + \dot{Q}_{rad,payload} \tag{4.34}$$

The calculation of all these values is done for the temperatures $T_{payload}$ equal to 276.5 K, and $T_{subsystems}$ equal to 283 K to stay in the middle of the safe temperature ranges. The heat flux values are shown in Table 4.10

The low radiation values are due to the wrapping of the subsystems and payload in a thermal blanket made with the method of multi-layer insulation (Wertz et al., 2011). This blanket has a very low thermal emissivity factor ε of 0.03, which vastly reduces the heat lost to radiation. The thermal power generated as waste heat by the power subsystem is calculated using an efficiency η of 0.98 for total power usage (excluding the thermal management subsystem) of 255.6 W. This is a well-informed yet assumed value for the efficiency; if the efficiency varies by $\pm$ 1%, $\dot{Q}_{ineff}$ changes drastically. Therefore the required power for higher and lower efficiency is also calculated and shown at the bottom of the table. As can be seen, the minimum power generation at all times is 5.23 W. No matter where the spacecraft is, this is its constant heat flux requirement.

This constant heating required by the system is calculated for active use of the subsystems and payload, but the longest part of the Ouranos mission is spent in the aeroshell. In this situation, there are no measurements taken, and communication is not constant. The heating unit of the thermal management subsystem has to be able to heat the glider in this situation, to keep the payload and subsystems safe. In a vacuum, no other

Table 4.11: Average Power Budget During Atmospheric Flight

Subsystem	Average Power[W]
Thermal	6.1
Communication	181
Payload	95.8
Aerodynamics	1.0
Total	291.8

subsystems or payload is active. The power consumption is then essentially zero. The factor $\dot{Q}_{ineff}$ becomes zero, meaning the heating unit has to compensate for this. Looking back at Table 4.10 and adding $\dot{Q}_{ineff,eff=0.98}$ to $\dot{Q}_{req,eff=0.98}$ yields a new heating requirement $\dot{Q}_{req}$ equal to 14.0 W. This means, in conclusion, that the thermal management subsystem should generate at all times at least 5.23 W, and should be able to generate during almost the entire mission 14.0 W.

To provide the thermal minimum of 5.23 W a Radioisotope Heating Unit (RHU) is selected. The University of Leicester is developing an RHU with a mass of 200 g that generates 3 W of thermal energy per second (Barco et al., 2022). This requires less mass than storing the required energy that is required during the flight. On top of that, no additional energy storage is needed to heat the spacecraft between the separation from the orbiter and the start of the atmospheric flight. This further substantiates the selection of an arrival trajectory with an early separation, which results in the need for less propellant. The selected RHU uses americium-241, which has a half-life of 430 years. This means that upon arrival at Uranus, the RHU still generates 97% of its original output.

Since the RHUs come in a given size of 200 g the remaining 11 W will have to be generated by heating elements onboard the glider. Heating elements are very cheap and lightweight. Their mass is likely in the order of tens of grams. During the transfer to Uranus, their power will be supplied by the orbiter, and after capsule separation, the onboard battery will supply the thermal power until the end of the atmospheric mission.

4.7 Power

This section will discuss the power system of the glider. The different options for the power source will first be discussed in Section 4.7.1 and then the selected components will be discussed in Section 4.7.2.

In summary, the glider Power subsystem shall

- Be tested in conditions simulating the mission.
- Be designed with a safety factor of 1.2 with regard to peak load.
- Provide power to all the glider subsystems.
- Provide power to the aeroshell.
- Stay within the mass, power and cost budgets with a reliability of 99.4%

4.7.1 Source Selection

The main contributors to the required power are the communication subsystem and the payload. Because the thermal management subsystem partially generates its own required power, limited power is needed from the power subsystem. This results in minimum limitation on the moment of separation from an energy storage perspective. The time between separation and atmospheric entry requires limited energy storage because the systems will be hibernating. The average power budget during the atmospheric flight is given in Table 4.11.

For the flight time of 97.25 h as determined in Section 4.4.3 and the time between separation and atmospheric entry of 20.7 h, when 8.5 W for heating is needed, which will be discussed in Section 7.3.2, this gives a total required energy storage of 33.8 kW h. For the small amount of power that is needed from the moment of separation until the end of the atmospheric flight, RTGs could be considered due to this power being required for a larger amount of time. To prevent being too dependent on radioactive material with high specific energy, it was decided to go for batteries. The time between separation and the atmospheric entry requires 227.7 W h. Because the best possible specific energy provision by RTGs is 5.4 W kg^{-1} (Bennett et al., 2008), the flight time requires a battery with a specific energy of 525 W h kg^{-1} to perform equally. Solar arrays are not an option due to the large distance from the Sun.

4.7.2 Components

The non-rechargeable lithium carbon monofluoride battery from EaglePicher, a battery provider for NASA, is selected to store the required energy of the glider. The batteries will also store the required power for the

Table 4.12: Battery Performance

Component	Specific Energy [W h kg^{-1}]	Energy Density [W h L^{-1}]	Mass [kg]	Volume [L]	Capacity [kW h]
Single Battery	710	1000	0.072	0.051	0.051
Total (795 Batteries)	710	1000	57.1	40.5	33.8

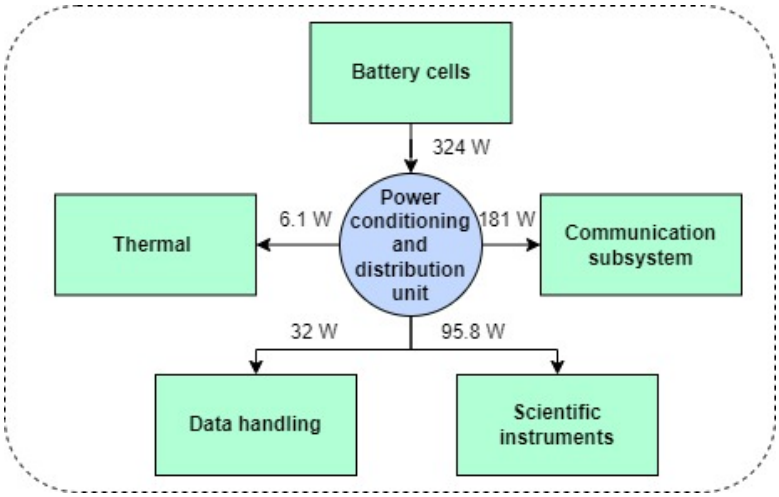

Figure 4.5: The electrical power diagram of the glider

aeroshell. This system only requires a small amount of power for a short amount of time. Having a separate power conditioning and distribution unit would add extra mass and more points of possible failure. The selected battery has a specific energy of 710 W h kg^{-1}, an energy density of 1000 W h L^{-1} and a capacity of 51 W h.[8]. The efficiency of 98% of the cables (Wertz et al., 2011) and a 20% margin is added to the required capacity for when the glider glides longer than expected or when the instruments use more power. To store the required amount of energy, 795 batteries are needed. Due to the number of batteries, a wide number of combinations of parallel and series connections are possible to provide the desired A and V by the system. Having this many small batteries allows for optimally filling the free space in the complex shape of the glider that is not used. An oversight of the performance of the batteries is given in Table 4.12.

A combined power conditioning and distribution unit is selected to regulate the output from the batteries. The SuperNova PCDU from Bradford Space can handle up to 1.5 kW and has a mass of less than 1.0 kg and is capable of handling the required number of outputs.[9]

4.7.3 Electrical power diagram

For the power system, a diagram fig. 4.5 was made to visualise the flow of power in the glider. This shows how power is provided by the batteries, distributed by the power conditioning and distribution unit and provided to all subsystems.

4.8 Sensitivity Analysis

To determine which variables will have the biggest influence on the design and to what degree, a sensitivity analysis was performed on every tool of the different subsystems. The communications are discussed in Section 4.8.1. This is followed bySection 4.8.2 which discusses the aerodynamics. The structures are discussed in Section 4.8.3, which is followed by the thermal management in Section 4.8.4. Finally, the power is treated in Section 4.8.5.

4.8.1 Communications

The communications subsystem has three inputs which are considered the main inputs. These are the bit rate, the maximum distance between the glider and the orbiter and the diameter of the receiving antenna. Starting with the bit rate, an increase of 10 % results in a decrease of 9 % for the signal energy. This percentage decrease changes to 33 % when increasing the bit rate by 50 %. Varying the maximum distance has a small influence on the actual value for the free space loss in dB. However, having an increase of 10 % in the maximum distance

[8]URL https://www.eaglepicher.com/sites/default/files/LCF-514%200222.pdf [cited 18/06/2023]
[9]URL https://satsearch.co/products/bradford-supernova-pcdu [cited 18/06/2023]

already causes the signal-to-noise ratio to be too low. It changed from 3.02 dB to 2.18 dB. Something similar happens when varying the diameter of the receiving antenna. A 10 % decrease causes the signal-to-noise ratio to change from 3.02 dB to 2.10 dB

4.8.2 Aerodynamics

In order to determine the variable having the biggest influence on the sizing and stability of the glider; a sensitivity analysis was performed. From this, it was found that the mass of the different subsystems making up the glider would be influencing the stability analysis the most. This is due to the fact that the larger the mass values of certain subsystems are with respect to the total mass of the glider the larger their influence on the position of the centre of gravity.

Furthermore, the total mass of the glider also had a big influence on the wing platform and its geometry, as shown in Section 4.4.2, which, in turn, influenced the stability analysis and the amount by which other parameters such as sweep, dihedral and elevator inclination angle had to be changed in order to achieve stability.

Lastly, the overall sizing is mostly influenced by the C_L and the input mass of the glider. Varying the C_L has a direct influence on the wing-loading, and thus the wing dimensions. This also directly influences the time of flight, although not massively. This is due to the fact that C_L is related to the power of 3/2, while the wing loading has a power of -1/2.

4.8.3 Structures and Materials

The structure calculations take the wing dimensions as the main inputs. These will be varied for the sensitivity analysis. Starting with the span, it became clear that the total structure mass is very sensitive to this. An increase if 10 % of the span results in an increase of 21.6 %. This becomes even worse when increasing the span by 50 %. Then the total structure mass increases by 204 %. The root chord has less, but still large influence on the structure mass. Increasing it with 10 %, results in a mass increase of 7.6 % . An increase of 50 % results in an mass increase of 39 %. Varying the tip chord actually results in an mass increase. However, the percentage changes are still relatively large. −13.5 % for a 10 % increase and −38.6 % for a 50 % increase. This shows that the mass of the structure is very sensitive to any changes to its input.

4.8.4 Thermal Management

A more detailed sensitivity analysis has been performed in Section 4.6 and will be summarised here. A change of ±1 %, results in drastic changes for $\dot{Q}_{ineff}$. These changes range from 20 to 50 %.

4.8.5 Power

Although the glider power has several different inputs, they all flow down from external factors. Similar to the battery, one would choose a well-performing battery instead of a badly performing one. Because of this, the ToF was seen as the most influential input to the battery sizing. When doubling the ToF, only the number of batteries doubles. Both the battery volume and mass multiply by a factor of 1.8. This means that the battery sizing is not very sensitive, as there is a nearly one-to-one factor increase from ToF to battery sizing.

5. Atmospheric Entry

To ensure that the glider safely reaches the measurement location, it was found to be necessary to design a capsule around the glider to protect the glider during atmospheric entry. To ensure the capsule survives entry into the Uranus atmosphere it was deemed necessary to create a simulation of the atmospheric entry to calculate all parameters necessary for the capsule design. This simulation was split into two major parts, a model for the atmosphere, which is outlined in Section 5.1 and the trajectory model which is elaborated on in Section 5.2. In Section 5.3 the calculation method for one of the major design parameters, the drag coefficient of the capsule, influencing the entry will be explained. After the explanation of both models, Section 5.4 outlines all steps taken to verify and validate the combined Entry model. This is then followed by a timeline of the entry into the atmosphere of Uranus in Section 5.5.

5.1 Atmospheric Model

The main purpose of the Atmospheric model is to provide all the following atmospheric parameters for Uranus, as a function of the altitude, that are listed in Table 5.1.

As Uranus has not yet been visited with the express intent to measure the atmospheric properties, a lot of the atmospheric models are based on formation methods of the ice giants and validated against the data gathered during the flyby of Voyager (Helled et al., 2010). As the team knew beforehand that the time to create the Atmospheric model was very limited it was decided to use an existing model. Following this, the team decided to request access to the NASA General Reference Atmosphere Model (GRAM) Suite (Justh et al., 2021). This model uses a list of altitude, latitude and longitude coordinate points as its input and outputs all atmospheric parameters for each of those coordinates. Table 5.1 also shows a minimum and maximum value for each of the atmospheric parameters for the altitude ranges from 7000 km above 1 bar and 200 km below 1 bar. The upper altitude is the limit altitude of the GRAM while the lower altitude is slightly below the 20 bar until where the atmospheric measurements are to be taken.

Another feature that some GRAM have are wind models, but due to a lack of data, the Uranus GRAM does not have a wind model implemented. To simplify the model and reduce run time the assumption was made that throughout entry the changes in latitude and longitude do not significantly influence the atmospheric parameters.

5.2 Trajectory Model

The Trajectory model simulates how the capsule moves over time. This is also a problem that has been tackled before by teams with a lot more time and knowledge, so it was decided to use Tudat[1] for simulating the movement of the capsule as well as the orbiter as outlined in Section 7.2. For this model specifically, the inputs necessary are:

- Distance from planetary centre r [m]
- Latitude [rad]

[1] URL https://docs.tudat.space/en/latest [cited 27/06/2023]

Table 5.1: Required Atmospheric parameters and their value range throughout the considered atmospheric segment

Description	Value Range	Unit
Pressure	$3.44 * 10^{-8} - 3.95 * 10^{6}$	$N\,m^{-2}$
Density	$1.045 * 10^{-14} - 5.036$	$kg\,m^{-3}$
Temperature	$53 - 800$	K
Specific Heat ratio	$1.39 - 1.66$	-
Gas constant	$3188 - 4122$	$J\,kg^{-1}\,K^{-1}$
Average Molecular mass	$2.02 - 2.61$	-
Gravitational acceleration	$5.14 - 8.79$	$m\,s^{-2}$
Speed of Sound	$560 - 2140$	$m\,s^{-1}$
Hydrogen mass fraction	$63.9 - 99.9$	-
Helium mass fraction	$0.0 - 26.8$	-
Methane mass fraction	$0.07 - 12.5$	-

- Longitude [rad]
- Velocity v [m s^{-1}]
- flight path angle γ [rad]
- heading angle [rad]

For the gravity model of Uranus it was decided to use the NASA SPICE library's newest version of the Uranus Empherisis. This generates a central gravity field for Uranus based on the coefficients provided by SPICE. As discussed in Section 5.1 the Uranus GRAM was used to gather the necessary atmospheric properties. The last setup step for the simulation was to include the rotation rate of the planet in the simulation.

One of the major assumptions made in the model is that the decreasing mass of the capsule does not significantly influence the trajectory. Furthermore, it is assumed that the angle of attack of the capsule is constant throughout the descent and equal to zero. This in combination with the assumption that the capsule does not generate lift, results in a pure ballistic entry.

Lastly, it was decided to use Runge-Kutta 4 integrator.

5.3 Capsule Drag Coefficient

For the capsule's drag coefficient C_D, a modified Newtonian Flow Analysis method was used (Skeen, 2013). This method starts from the point that:

$$C_D = \frac{\int P_{front} dA_x}{\frac{1}{2}\gamma M_\infty^2 A_x P_\infty} + \frac{P_{back}}{\frac{1}{2}\gamma M_\infty^2 A_x P_\infty} \tag{5.1}$$

where P_{front} is the pressure acting on the projected frontal area A_x. Conversely P_{back} is the pressure acting on the projected back area. Lastly, M_∞ is the freestream Mach number. This equation is only valid under the assumption that P_{back} is constant over the whole back area and that the specific heat ratio does not significantly change due to the temperature increase on the surface of the heat shield. Furthermore, this equation is simplified by assuming that P_{back} is equal to P_∞ as proposed by Skeen.

To calculate P_{front} the following equation is used:

$$\begin{aligned}\overline{P}(s) = \overline{P}_\infty + (1-\overline{P}_\infty)\cos\beta^2 - (1-\overline{P}_{FD})\left(\frac{\cos\beta^2 - \overline{P}^*}{1-\overline{P}^*}\right) \\ + \left(1-\frac{R_N}{R_{max}}\right)\left[\sin\beta^2\left(1-\frac{s}{s^*}\right) + \frac{1}{2}\frac{s}{s^*}\left\{\overline{P}_{FD} - 1\frac{s}{s^*}\sin\beta^2 + (1-\overline{P}_{FD})\left(\frac{\cos\beta^2-\overline{P}^*}{1-\overline{P}^*}\right)\right\}\right]\end{aligned} \tag{5.2}$$

where any overlined pressure is normalised by the stagnation point pressure. This equation gives the pressure at any distance s away from the stagnation point. This equation contains four variables which are dependent on the heat shield geometry. The first one of those is the surface angle β at point s. Another geometric parameter that is dependent on s is the surface normal radius R_N. There are also two geometric parameters independent of s, the first of these is the surface distance from the stagnation point of the sonic point s^*. To simplify the equation it was assumed that the sonic point is located at the edge of the heat shield. The other independent geometric property is the maximum surface normal radius R_{max}. Next to the geometric parameters, there are also different pressures which affect the total pressure. The first of these pressures is calculated using the following equation:

$$\overline{P}_\infty = \frac{1}{1+\frac{1}{2}\gamma M_\infty^2 C_{p,0}} \tag{5.3}$$

For $\overline{P}_\infty$, the only new parameter is the pressure coefficient at the stagnation point $C_{p,0}$ which can be calculated using the following equation derived from isentropic and shockwave relations:

$$C_{p,0} = \frac{1}{\frac{1}{2}\gamma M_\infty^2}\left[\frac{\left(\frac{\gamma+1}{2}M_\infty^2\right)^{\frac{\gamma}{\gamma-1}}}{\left(\frac{2\gamma}{\gamma+1}M_\infty^2 - \frac{\gamma-1}{\gamma+1}\right)^{\frac{1}{\gamma-1}}} - 1\right] \tag{5.4}$$

Another pressure used in Equation (5.2) is the pressure at the sonic point $\overline{P}^*$. For this pressure, it is assumed that the flow between the stagnation point is isentropic which allows for the use of the following equation:

$$\overline{P}^* = \left(\frac{2}{\gamma+1}\right)^{\frac{\gamma}{\gamma-1}} \tag{5.5}$$

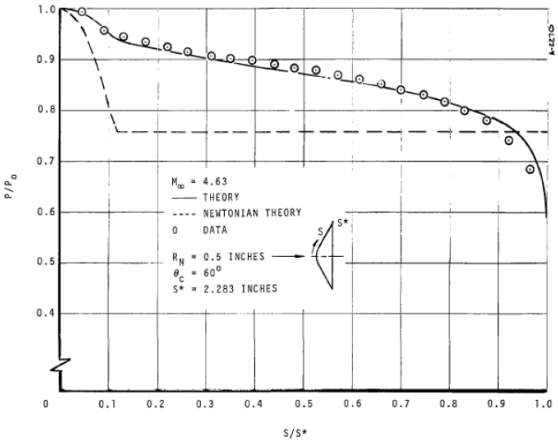

(a) Pressure distribution over the Heat shield (Moyer et al., 1970)

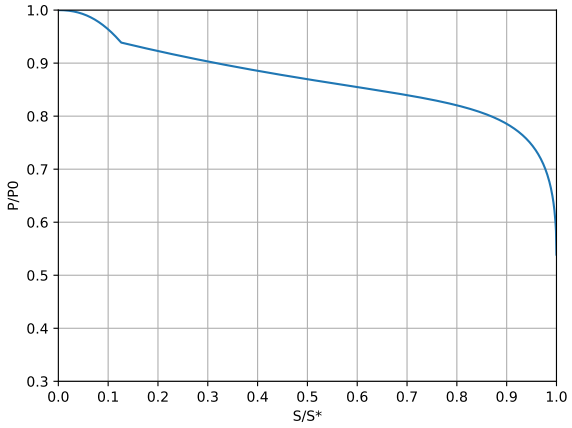

(b) Pressure distribution obtained using method outlined in Section 5.3

Figure 5.1: Pressure distribution over the heat shield from original source and own work

The last pressure, $\overline{P}_{FD}$ is a correction based on energy considerations and can be calculated using:

$$\overline{P}_{FD} = 1 - e^{-\lambda}(1 - \overline{P}^* - \frac{1}{16}\left[\left(\frac{s}{s^*}\right)^2 - e^{-\lambda}\right] \tag{5.6}$$

where λ is calculated using the following equation:

$$\lambda = 5\sqrt{ln\left(\frac{s}{s^*}\right)} \tag{5.7}$$

Combining all of the above equations it is then possible to numerically integrate over the whole heat shield surface to calculate the drag coefficient.

5.4 Verification and Validation

The focus for verification and validation was laid on the calculations for the drag coefficient. This was deemed appropriate as the Uranus GRAM was provided to the team in a state where it was validated against the data gathered during the Voyager 2 flyby. On the other hand, the usage of Tudat was first familiarised with the examples provided by the Tudat team and these examples are then adapted to the needs required. In this specific case, the baseline for the Entry model was the Reentry example [2].

During verification of the drag coefficient calculations, that Equation (5.7) dictates that real results are only returned if the ratio of s to s^* would be larger than one. This results in no real solutions existing over the whole heat shield. After some investigation, the original source for the calculation method was found which provided the equation for λ as shown here (Moyer et al., 1970):

$$\lambda = 5\sqrt{ln\left(\frac{s^*}{s}\right)} \tag{5.8}$$

After this error was corrected, the software was given the geometric shape shown in Figure 5.1a. For this geometry, the pressure distribution over the heat shield was then plotted in Figure 5.1b to compare it to the pressure distribution found by Moyer. The only potentially significant difference found is the visible discontinuity at the point where the simulation leaves the curved segment and continues to the straight segment.

As another validation step, the simulation was given the shape parameters of the Mars Surface Laboratory (MSL) (Dyakonov et al., 2012) and the result was compared against the drag coefficient that could be calculated from the ballistic coefficient of 135 kg m^{-2}, the mass of 3300 kg and surface area of 15.9 m^2. This simple calculation provided a drag coefficient of 1.536 and the method outlined in Section 5.3 resulted in a drag coefficient of 1.535.

[2] URL https://docs.tudat.space/en/latest/_src_getting_started/_src_examples/notebooks/propagation/reentry_trajectory.html [cited 16/06/2023]

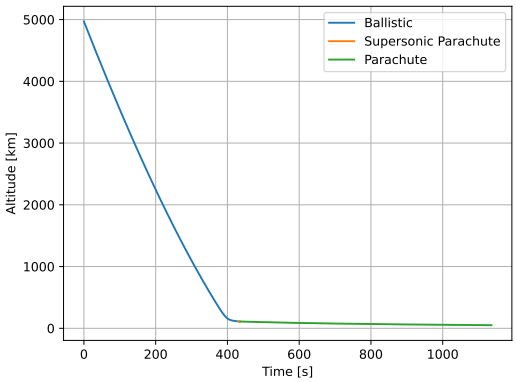

(a) Altitude vs time graph of the entry capsule

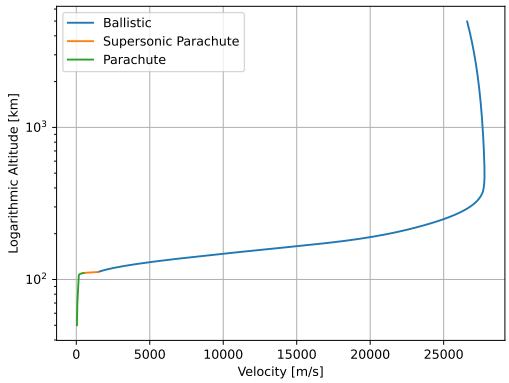

(b) Velocity vs Logarithmic Altitude graph of the entry capsule

Figure 5.2: Altitude and velocity graphs for Capsule decent

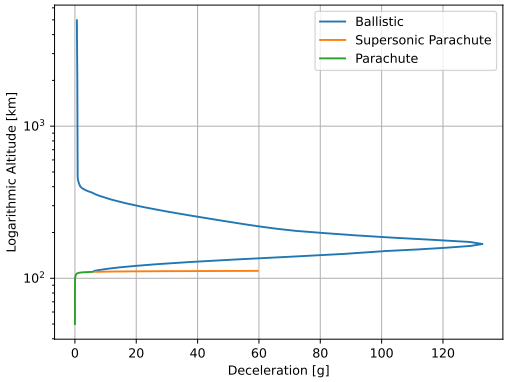

(a) Deceleration normalised by Earths gravitational acceleration vs Logarithmic Altitude graph of the entry capsule

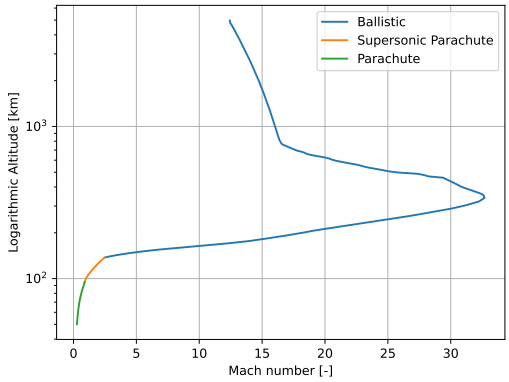

(b) Mach number vs Logarithmic Altitude graph of the entry capsule

Figure 5.3: Deceleration and mach number graphs for capsule decent

5.5 Entry Timeline

The entry is split into three segments that were considered. First the ballistic entry of the capsule, then decent under parachute at supersonic speeds and lastly decent under parachute at subsonic speeds. For the first segment, all methods were previously explained in this chapter and for the segments under the parachute, the method used will be explained in Section 6.2. For atmospheric entry, the upper entry point was considered to be 5000 km above the 1 bar surface line and the end of the entry simulation was set to be at 55 km where the pressure is 0.1 bar. Furthermore, the heat shield is intended to be released slightly after the deployment of the parachute.

As can be seen from Figure 5.2a, the whole entry phase lasts for 1100 s of which the capsule spends more than half of the decent time under ballistic entry conditions and only descends a relatively short amount of time with a parachute in supersonic conditions. From Figure 5.2b it can be seen that the velocity of the capsule initially still increases as the acceleration due to gravity is stronger than the deceleration due to atmospheric drag.

As can be seen in Figure 5.3b, the capsule flies at a peak Mach number of 32 at an altitude of 300 km and it can also be seen that the Mach number first increases. This is due to a decrease in the speed of sound compared to higher altitudes. There are two notable observations that can be drawn from Figure 5.3a, first until an altitude of 200 km the capsule atmospheric deceleration is negligible compared to the acceleration due to gravity. But then in a very short segment of altitude, the capsule reaches a peak deceleration of 125 g. The second observation that can be made from this timeline of deceleration is the discontinuity at parachute deployment. This is due to the significant increase in drag by the parachute as well as the shock loads from deployment.

6. Aeroshell Design

To enable the glider to reach its measurement location it is necessary for it to survive the harsh environment of entering an atmosphere at interplanetary speeds. For this purpose, the team decided to encase the glider in a protective capsule. This capsule will have three purposes. The first is to protect the glider from the extreme heat of entry. This is done using a heat shield and the calculations used for sizing this heat shield are outlined in Section 6.1. Once the Capsule has decelerated to a certain point it is necessary to employ a decelerator to further reduce the speed of the capsule. For this purpose, it was chosen to use a parachute which is sized in Section 6.2. During entry and under parachute descent the capsule and glider will be subjected to severe loads based on which the structure can be sized in Section 6.3. During entry, it is important that the capsule is oriented correctly. To ensure this, in Section 6.4 the stability of the capsule is determined, based on the previously calculated parameters. Lastly, once the capsule has decelerated sufficiently the glider needs to be deployed from the capsule. Section 6.5 elaborates on how it is planned to deploy the glider from the capsule to start its mission.

6.1 Heat Shield

The main purpose of the capsule is to protect the glider from the loads and heat of atmospheric entry. Multiple requirements are related to the heat shield design and they are presented in Table A.19.

In summary, the Aeroshell Heat Shield shall

- Stay within the mass, power and cost budget with a reliability of 99.4%
- Withstand a peak heat flux of 20 MW m^{-2}.
- Withstand a total heat load of 300 MJ m^{-2}.
- Have a diameter of less than 4.5 m.

To begin the design, the descent simulation outlined in Chapter 5 was extended to include calculations for the heat flux on the heat shield. This was split into two parts: the heat flux q_c due to the convective heating of the heat shield and the heat flux q_r due to the radiative heating of the heat shield. Two effects that were not considered during the design are the heat flux q_{rerad} out of the heat shield due to reradiation and the heat flux $q_{\dot{m}}$ out of the heat shield due to ablation. This is seen as a very conservative assumption as both heat fluxes that are not considered reduce the total heat load h on the heat shield.

For the convective heat flux q_c, the following equation is used (Ritter et al., 2006):

$$q_c = 2004.2526 \frac{1}{\sqrt{\frac{2R_N}{0.6091}}} \left(\frac{\rho}{1.22522}\right)^{0.4334341} \left(\frac{v}{3048}\right)^{2.9978867} \tag{6.1}$$

where ρ is the free stream density, v is the velocity of the capsule and R_n is the effective nose radius. This radius is dependent on the angle of the heat shield cone and increases past the radius of the heat shield itself. To stay with a conservative estimate it was decided that the effective nose radius is equal to the actual nose radius.

The other heat flux, the radiative heating q_r, is calculated using the following equation (Ritter et al., 2006):

$$q_r = 9.7632379^{-40} (2R_N)^{-0.17905} \rho^{1.763827469} v^{10.993852} \tag{6.2}$$

Both Equation (6.1) and Equation (6.2) were originally optimised for Jovian entry and are therefore not necessarily indicative of the heating in the atmosphere of Uranus, but both Uranus and Jupiter are gas giants with an atmosphere that is primarily made up of hydrogen and helium. The decision was made that despite the differences between the atmosphere of Uranus and Jupiter, the equations are to be used for the heat flux. Furthermore, both equations also only calculate the heat flux at the stagnation point. During entry, there is also the possibility that the heat flux at another point exceeds that of the stagnation point. One such point identified by the team is the edge of the heat shield and it was decided to increase the thickness at the edge to account for such a potential case. As this effect of increased heat flux is well understood for the shape of the MSL heat shield, it was decided to use a shape very similar to that heat shield (Meurisse et al., 2018).

As can be seen in Figure 6.1a the radiative heat flux has a larger magnitude than the convective heat flux. Furthermore, the convective heat flux has a significantly larger altitude range over which it is affecting the capsule.

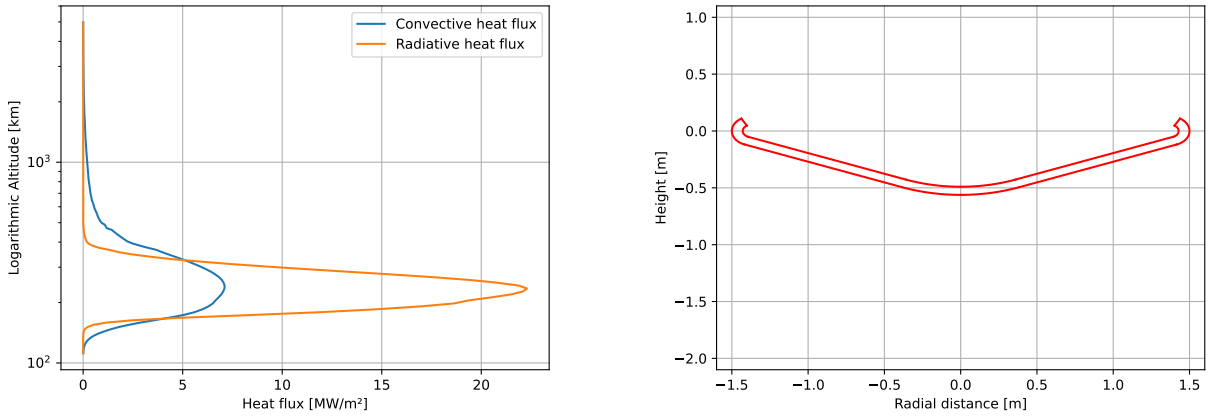

(a) Altitude vs Heat flux graph during entry

(b) Shape of the heat shield including thickness

Figure 6.1: Heat flux and required heat shield shape

To validate the heat flux values gained for the capsule it was compared to the values obtained by Ritter for a Jovian entry. The Jovian entry had an entry velocity of 47.4 km s^{-1} and resulted in a peak heat flux of 619 MW m^{-2}. Compared to the Ouranus mission which is entering at 26 km s^{-2}, resulting in a peak heat flux of 22 MW m^{-2}. This difference of more than two orders of magnitude is attributed to the nearly doubled entry speed which in Equation (6.2) is taken to the power of nearly eleven.

Now that the total heat flux has been calculated for every point in the entry trajectory it is numerically integrated to reach a total heat load of 571 MJ m^{-2}. With this total heat load, it is now possible to calculate the required thickness of the heat shield based on the chosen heat shield material PICA. The choice of PICA is based on two considerations, the first is that PICA is a well-understood material for interplanetary missions as it has been used on MSL and the second is its relatively low density for heat shields. For this purpose, a Mass Estimation Relationship (MER) for the PICA heat shield material is used (Sepka & Samareh, 2015):

$$TH = 1.8696\left(\frac{h}{v^2}\right)^{0.1873} \tag{6.3}$$

where TH is the heat shield thickness given in cm, h is the heat load in J cm^{-2} and lastly v is the entry velocity in km s^{-1}. For this relation, Sepka et al. indicate that it has only been generated with entry trajectories that result in a peak heat flux of less than 1200 W cm^{-2}, which is below the peak heat flux calculated for this capsule. Despite this, it was decided to use the relation. To ensure the thickness of the heat shield is conservative a safety factor of 11.7 % was added to the result given by Equation (6.3). This value is based on the maximum underestimation of the MER compared to the traditional calculation method. After including this safety factor, the heat shield thickness was calculated to be 7.14 cm.

Now that the heat shield thickness and its shape are known, the last step is to calculate the volume and resulting weight. For this purpose, another model was created to numerically integrate the heat shield thickness along the outer edge of the heat shield. For this purpose the shape shown in Figure 6.1b was used and revolved around the axis of symmetry of the capsule. This heat shield weighs a total of 232 kg.

This results in the heat shield making up 42 % of the total mass of the capsule. This was expected as for example the Galileo entry probe into Jupiter had a heat shield mass fraction of nearly 60 %.

Once the entire geometry of the heat shield has been determined, its total cost can be computed. This consists of the material cost and the manufacturing cost and it can be estimated based on literature estimations derived from previous deep-space heat shields. The relationship that has been determined to be the most appropriate for the analysed system was the cost estimation for high-density phenolic nylon systems. To calculate the final cost, the only data that is required from the thermal shield design is the number of tiles needed to cover the entire bottom shell surface. Such value could be determined by applying a linear proportion with the number of tiles (64) and the diameter (4.5 m) of the MSL thermal shield. Finally, assuming the presence of 43 thermal panels, the total cost of the heat shield results in K€ FY22 60.8.

6.2 Parachute

For the design of the parachute for the capsule, three main considerations were taken into account. First, the created shock loads during deployment, second the significant increase in stability and third the ability to act

as a backup descent method in case of failed glider deployment. These were all derived from the requirements presented in Table A.19 and summarised below.

In summary, the Aeroshell Decelerator shall

- Be tested in conditions simulating the mission.
- Reduce the vehicle velocity to 45 m s^{-1}.
- Stay within the mass, power and cost budget with a reliability of 99.9%.
- Generate shock loads not exceeding 150g.
- Generate shock loads for less than 1 s.
- Have a volume of less than 0.5 mx0.5 mx0.5 m.

As it is expected that the capsule will not be stable during the transonic phase of flight it was determined necessary that the parachute is deployed at supersonic conditions to allow for stabilising during the transonic flight regime. This already limits the selection down to only a few designs which are capable of being deployed at supersonic speeds (Britting et al., 2022). Of the designs presented by Britting et al., the Disk-Gab-Band (DGB) was selected for both its capability to be deployed at supersonic speeds as well as its simplicity in design and manufacturing. Furthermore, it has a comparatively good range of drag coefficients in both the supersonic as well as the subsonic regime.

Based on this choice of parachute it was decided to deploy the parachute at a Mach number of 2.5 which is higher than the deployment mach number of the MSL which deployed its DGB parachute at a Mach number of 1.7 (Skeen, 2013) but still below the limit for DGB deployment (Britting et al., 2022).

For the purpose of the descent analysis, the trajectory tool described in Section 5.2 was used. Here the assumption was made that the drag due to the parachute is orders of magnitude higher than the drag of the capsule which is neglected in the simulation. Furthermore, as mentioned previously, the parachute shall act as a backup descent option in case glider deployment fails so the parachute sizing was performed such that the capsule remains above 20 bar for at least 4 h. This gave the parachute a target decent time for which its diameter could be sized. This resulted in a necessary parachute diameter of 11.4 m at a C_D of 0.4 under subsonic conditions.

From this diameter, it was then possible to calculate the weight based on the assumption that the amount of fabric used was equal to the surface area of a hemisphere with the same diameter as the parachute. This estimate is considered conservative as it does not take into account the reduction of surface area due to the gap. For the parachute, the PIA.C-44378 Type III [1] fabric was used which has a surface weight of 35 g m^{-2} resulting in a total fabric weight of 5.1 kg.

The second part of the parachute that needs to be considered is the suspension lines connecting the parachute to the capsule. For this, it was decided to use 8-strand nylon ropes[2] with a diameter of 0.5 cm. The reason to go for a lower diameter rope despite its lower strength-to-weight ratio is one of redundancy as for a parachute with a high number of thin lines it is easier to add a few redundant lines to decrease loads than for a parachute with fewer but thicker lines. For the parachute in question, it was decided to use a safety factor of 3 on the line count to ensure that nonuniform load distributions during parachute inflation do not lead to the failure of the system. This resulted in the parachute needing a total of 54 lines. Comparing this to MSL with its 84 lines and a significant larger mass and larger parachute gave the team the impression that the number of lines calculated is reasonable. To calculate the mass of these lines, the length of the lines first needs to be calculated. This presents another design problem as it is now necessary to find the distance behind the capsule to place the parachute canopy. This parameter is commonly given as multiples of the parachute diameter and was found to be close to 2.5 for MSL(Clark et al., 2022). This length plus an additional segment of the lines inside the DGB results in a total weight of the lines of 22.2 kg.

The cost of the parachute was mainly determined by the cost of the individual materials. Based on a cost of 6.14 €/m^2 for the parachute fabric [3] and a cost of 0.41 €/m for the lines [4] the total material cost for the parachute is 5520 €. It is well understood that this is a severe underestimation of the cost as the higher fraction of the cost is due to the high labour cost for producing parachutes of this size and importance.

[1] URL: https://delcotex.de/en/products/parachute-fabric-piac-44378-type-iii [cited 18/06/2023].
[2] URL: https://www.engineeringtoolbox.com/nylon-rope-strength-d_1513.html [cited 18/06/2023].
[3] URL: https://www.amazon.co.uk/emma-kites-152x273cm-Repellent-Inflatable/dp/B096K4F6BC/ref=sr_1_9?keywords=kite%2Bfabric&qid=1687858863&sr=8-9&th=1 [cited 27/06/2023].
[4] URL: https://www.amazon.com/Nylon-Rope-inch-Solid-Braid/dp/B01G5ZOU7C/ref=sxin_17_pa_sp_search_thematic_sspa?content-id=amzn1.sym.45725740-bcaf-449c-812b-5eb1e0afbded%3Aamzn1.sym.45725740-bcaf-449c-812b-5eb1e0afbded [cited 27/06/2023].

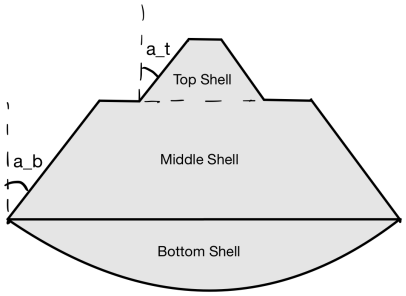

Figure 6.2: Sketch of the idealised geometry of the top shell structure.

6.3 Structures and Materials

In this section, the structural analysis of the aeroshell will be presented. The starting point of such an analysis is the list of requirements shown in Table A.19 and presented here below.

In summary, the Aeroshell Structure shall

- Withstand aerodynamic pressures, peak axial loads, heat loads and vibrational loads present during entry.
- Perform separation with the atmospheric vehicle without creating any damage to its subsystems.
- Stay within the mass budget of 1000 kg (total of both glider and capsule), with a reliability of 99.4%
- Separate from the glider at the right moment during entry.
- Separate from the glider with a relative velocity of 60 m s^{-1}.
- Allow the glider to take scientific measurements after heat shield separation.
- Have a volume of less than 4.5 m × 4.5 m × 3 m

The aeroshell presents two main elements, the thermal shield which has been presented in Section 6.1 and the backshell which is analysed in this section. The backshell architecture is subsequently divided into three parts based on the loads, the top, the middle and the bottom shell. The first two, based on the shape of the entry capsule of previous missions (i.e., MSL), were assumed to have a geometry which consisted of a trapezoidal shape with a specific taper ratio that defines the difference between the base and top radius of the trapezoid. The shape of the top and the middle shell is presented in Figure 6.2 where also the two taper angles a_t and a_b are shown.

This geometry has different constraints based on the size of the glider, the size of the decelerator, and the entry characteristics. Based on the height of the folded wings, the height of the middle shell element can be derived, while for the radius, this has been optimised to achieve the lowest entry loads while having an acceptable entry trajectory. Regarding the top shell, both its upper radius and height flow down from the size of the folded parachute which, with margin, results in 0.5 m. The other dimensions of the geometry can be easily calculated using the taper ratio which in this case has been selected to be 0.66 derived from the entry capsule of MSL (Dyakonov et al., 2012).

The top and middle shells will experience two different main loads: axial shock loads from the parachute deployment and the pressure loads due to the atmosphere of Uranus. Pressure loads will be analysed first. While entering the atmosphere, a weak shock wave will be generated around the capsule and this will allow to reduce the amount of pressure loads upon the top of the back shell. The pressure in the atmosphere will still be present and the minimum thickness required to withstand such hoop load can be calculated when assuming the top part of the capsule is made of two distinct truncated cones (ASME, 2019) using:

$$t_{required} = \frac{P_{atm} d_{base}}{2 \cos a (\sigma_y + 0.4 P_{atm})} \tag{6.4}$$

where P_{atm} equal to 0.1 bar is the highest atmospheric pressure encountered by the capsule during operations (at the altitude the glider is deployed), d_{base} is the base diameter of the truncated cone, σ_y is the yield strength of the capsule material and a is as defined above. This calculation can be performed for both the top and middle shell, taking into account the different sizes. Afterwards, the stresses induced by the parachute deceleration peak loads have been determined. Such axial stresses will act at the top of the backshell and will limit the minimum surface area that can be present in the geometry. As a result, the smaller radius of the top shell was

determined to be the largest value between the folded parachute size and the one computed using the formula below (Hibbeler, 2018):

$$r = \sqrt{\frac{F_{ax_{para}}}{\sigma_y \pi}} \tag{6.5}$$

where $F_{ax_{para}}$ is the axial force generated upon the backshell by the parachute inflation and σ_y is as defined previously. Once the size of both elements of the backshell has been determined, an additional structural analysis of the geometry using Euler's buckling formula was performed, to determine if such backshell panels would buckle under the compressive loads of entry. The entire analysis presented above was completed with the properties of the material used on the MSL capsule[5]. This is a panel of aluminium honeycomb with graphite epoxy whose mechanical properties are well-known in the industry (Czabaj et al., 2014) which combined the high strength of aluminium alloys with the low density of honeycomb structures.

The next element that had to be designed was the bottom shell. This will support the thermal shield and therefore share its shape. In this case, the main loads that should be analysed are the ones that derive from the axial entry accelerations and the atmospheric pressures surrounding the capsule during descent. The weak shock wave will not divert such pressures which is why they have to be taken into account for these computations. Regarding the axial loads, this will generate both axial and bending stresses. Due to the large surface area of the thermal shield, the second load scenario will be more critical. Bending stresses can be calculated with the following equation:

$$\sigma_{cr} = \frac{-EI\frac{d^2v}{dx^2}y}{I_{xx}} \tag{6.6}$$

where E is Young's modulus of the selected material in Pa, I is the area moment of inertia in m^4 and v is the maximum deflection defined by the presented relation (Hibbeler, 2018):

$$v = \frac{Px}{48EI}(3L^2 - 4x^2) \tag{6.7}$$

where L is the diameter of the thermal shield, x is the distance from the left fixture (here it is equal to half the thermal shield length as that is where the maximum deflection occurs), and P is the axial force applied on the structure. In a similar way, the stresses due to the entry pressure can be computed, the only difference stands on how the deflection is defined (Hibbeler, 2018):

$$v = \frac{wx}{24EI}(L^3 - 2L^2 + x^3) \tag{6.8}$$

where w is the pressure along the structure and all other parameters are as defined previously. Putting together Equations (6.6) to (6.8), the bottom shell minimum thickness to withstand the entry loads could be computed to be 4 cm.

The capsule will enter the atmosphere at a very high velocity, which makes the thermal loads very significant for structural analysis. This type of load scenario will have significant influences on the bottom shell geometry since it is directly in contact with the thermal shield. The thermal stresses can be computed with:

$$\sigma_{thermal} = \alpha \Delta T E \tag{6.9}$$

where α is the coefficient of thermal expansion of the selected material in °C, ΔT=200 °C^{-1} is the largest temperature change during entry given by the atmospheric entry calculations and E is as defined previously. Firstly, it was decided to use a different material for the bottom shell than the top shell. This was done to withstand high thermal stresses but was later deemed infeasible as it led to a too-high capsule structural mass. To solve this issue a thermal insulation layer between the thermal shield and the bottom shell was implemented. After a thorough literature review, the best material to survive the specific harsh conditions of Uranus's entry was a hypocrystalline ceramic aerogel which presents a very low coefficient of thermal expansion (1.2×10^{-7} °C^{-1} compared to the 70×10^{-6} °C^{-1} of aluminium) and quite a low density of 55 kg m^{-3}(Guo et al., 2022). It was calculated that for such thermal loads, the insulation layer should be 3 cm over the entire surface of the thermal shield. In contrast, a thicker portion of 7 cm was required towards the centre of the capsule surface since most stresses concentrate there due to the centre of mass, peak pressures and peak temperatures. With such a plane to manage the thermal loads, the bottom shell structure analysis can be limited to all bending stress reported previously. Using Euler's buckling formula and the resulting geometry was needed to check if the surface would buckle during operations. For a cheaper and easier manufacturing process, it was decided to use the same material selected for the top shell.

[5]URL: https://spaceflight101.com/msl/msl-aeroshell-and-heat-shield/ [cited 17/06/2023].

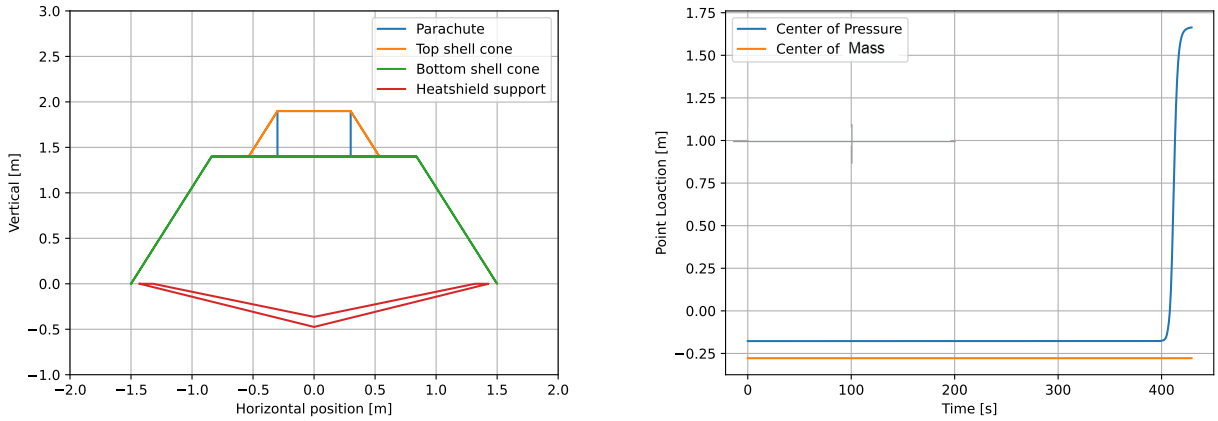

(a) Geometry considered for CM calculations

(b) Location of CM and CP throughout entry

Figure 6.3: CM and CP graphs

The final step in the design was to compute the total mass of the structure architecture. The top shell was calculated to have a thickness of 0.001 m, a bottom radius of 0.54 m and a top radius of 0.3 m. The middle shell ended up having a thickness of 0.001 m, a bottom radius of 1.5 m and a top radius of 0.84 m. The bottom shell and insulation thickness are, respectively, 0.04 m and 0.07 m, while their radius is exactly equal to the thermal shield radius of 1.5 m. With this geometry, the total subsystem mass results in 41.57 kg

6.4 Stability

To ensure that the capsule does not fly through the atmosphere in an incorrect orientation it must be checked that the capsule is stable in the desired orientation. For this purpose, the location of both the capsule's Centre of Mass (CM) and the Centre of Pressure (CP) was calculated and compared. This was necessary as a more aft location of the CP compared to the CM in flight direction is necessary for stability.

To improve the CM calculation speed the capsule was simplified to the shape shown in Figure 6.3a. The inclusion of the complete Heat shield for this is a non-conservative estimate as it moves the CM significantly downwards thought out the flight despite being ablated. The reason why it is believed that the assumption of constant CM is valid is that the ablation of the heat shield coincides with a significant shift of the CP backwards due to the increased pressures around the capsule. This shift would significantly increase the margin for the CM position and is assumed to allow for the ablation to be counteracted for stability.

For calculating the CM of the capsule the following equation has been used:

$$CM = \frac{\sum_{n=1} d_n m_n}{\sum_{n=1} m_n} \tag{6.10}$$

where d_n is the distance of subsystem n from the selected axis and m_n is the mass of said subsystem.

For the CP the following equation was used:

$$CP = \frac{\int y p(y) \hat{\boldsymbol{n}} \cdot \hat{\boldsymbol{x}} dy}{\int p(y) \hat{\boldsymbol{n}} \cdot \hat{\boldsymbol{x}} dy} \tag{6.11}$$

where y is the distance from the datum line as defined in Figure 6.3a, $\hat{\boldsymbol{n}}$ is the normal vector of the surface at height y, $P(y)$ is the pressure acting on the capsule at height y perpendicular to the surface and lastly $\hat{\boldsymbol{x}}$ is the vector parallel to the datum line. This equation was then split into two segments the contribution to the CP location due to the heat shield and the contribution due to the backshell. For the backshell, the pressure was assumed to be equal to the free stream pressure. This assumption was chosen despite being non-conservative for consistency with the pressure assumptions used in Section 5.3. For the pressure on the heat shield Equation (5.2) was used. As both the free stream pressure and the pressure on the heat shield depend on the decent conditions the location of the CP changes throughout the decent. This change can be seen in Figure 6.3b.

Based on both the calculations for CM and CP it is necessary to place additional mass of 114 kg in the bottom of the heat shield. which results in the CM shown in Figure 6.3b.

Additionally to ensure the capsule does not enter the atmosphere at a fixed angle of attack due to an laterally offset CM it was also necessary to add a mass of 38.2 kg. This mass is placed in line with the glider fuselage at the edge of the capsule ahead the glider.

6.5 Glider Deployment

In this section, the mechanism and procedure that will be implemented to deploy the glider into its operational configuration will be analysed. After using a parachute and the capsule to slow down during atmospheric entry, the glider has to detach and start its flight into the scientifically important region of the Uranus atmosphere while gathering data. The connection between the glider and the capsule will have to be strong enough to survive the entry accelerations but also capable of releasing the atmospheric vehicle with a certain velocity and precision without negatively influencing the glider's operations. The deployment procedure is very critical for the mission because without it, no scientific data could be gathered and the mission would have to be classified as failure. Three different mechanisms were idealised to fulfill the previously described functions.

First of all, it is important to understand at a high level what the general deployment procedure will look like. The glider will stay attached to the capsule during entry, in this way the backshell structure will carry all the loads and will allow for an appropriate load transfer into the glider. Then, once the thermal shield has been released and the deployment altitude has been reached, attachment points from the top and middle shell will release the glider and the bottom shell (still connected to the atmospheric vehicle) will open to an angle of 45°. At this point, the glider will slide onto a rail in the backshell and be released in the Uranus atmosphere with a specific initial angle of attack, allowing it to generate enough lift to achieve an appropriate flight profile.

Now, the different mechanisms can be described in more detail. In addition to its connection with the bottom shell, multiple attachment points between the capsule structure and the glider will be designed to keep the atmospheric vehicle in place during entry. Such stiffening elements will have a built-in pyro mechanism at their ends, which will fire when the glider has to deploy and become operational. This mechanism will require almost no power since a pyro can be ignited quite easily with an electric signal in a high resistance low voltage circuit.

Another mechanism that will be required during the deployment phase will be a rail on the bottom shell, letting the glider slide from the capsule to start its scientific investigation. The glider cannot slide directly on the metal surface because that will lead to the detriment of its fuselage. As a result, a small cart under such a structural element will be present and this will drive the glider along the bottom shell ramp until the end of the rail is reached and the vehicle enters flight. The cart will have a soft material at its extremity and will connect to the glider through attachment points present on the fuselage. Once the end of the rail is reached, the attachments will open and the entire vehicle will slide upon the cart, preventing the tail from striking against the bottom shell. A nylon wire will be used to hold the cart in its initial position, in this way, the mechanism can be started at any time with the use of a high change in temperature induced by a high resistance circuit.

Thirdly, a mechanism to open the bottom part of the capsule will be required. This consists of two different parts, one component is required for the bottom shell deployment and another to hold the glider in the meantime. Regarding the glider, a hinge mechanism will be implemented on its tail to keep it in position while deploying and until the rail mechanism is in place. This ensures the glider does not deploy if the wings do not properly unfold since the capsule will still take more than two hours to descend to the 20 bar pressure level, making sure CNRS03.04 is still met. Similarly, the bottom shell will open with a hinge on its side to create a ramp angle for the deployment of the glider, allowing the vehicle to generate enough horizontal velocity to begin its atmospheric flight.

The last mechanism that has to be analysed is related to the glider folding procedure. The 6 m span of the glider is too big to fit in the entry capsule (3 m diameter). As a result, the wings of the glider need to be folded on Earth during integration and then unfolded mid-air when preparing for deployment on the capsule rail. There are many different ways this issue can be solved but most of them would require splitting the wing into four parts, therefore negatively influencing both the aerodynamic characteristics and structural integrity. In fact, a lot of stress will concentrate on the mechanism during flight because of the discontinuity in the load path along the wing. Moreover, if a hinge mechanism is used, any type of vertical force applied to the wing during operation could lead to a partial folding of the wing itself. As a result, CAELUS determined that electroactive high-temperature shape memory alloys (SLA) should be used for the deployment mechanism. This specific alloy material (50.3% Nichel, 29.7% Titanium and 20% Hafnium) is able to fold in any necessary temporary configuration and then unfold into the final one when a thermal load is applied to it. This load will be generated through a change in temperature induced by an applied voltage through the material, as presented in the paper. As can be seen from the paper, the mechanism can unfold wings over an angle of 90°, and its performance can be developed even further. With this solution, the wing will be made of the material presented in Section 4.5 but it will present additional mechanisms both at a distance of 1 m and 2.4 m from the fuselage outer skin. This will consist of a titanium hinge line connected to SMA rotary tubes which have been trained previously to rotate when a specific heat load is applied. In this way, the wing will be folded into three sections and when in the folded configuration it will have dimensions: h_{folded} =1.4 m and $w_{folded} = 2r_{fuselage} + 2 = 2.6$ m (see Figure 6.4), which leaves a 0.4 m margin in case the fuselage has to be made bigger or any additional instrumentation has to be placed on the side. Shape memory alloys were selected because they present a very high power density and also because they would allow having a way smaller discontinuity in the wing with respect to an actual hinge mechanism. The other element of the glider that needs to fold is the tail. This is placed at a distance

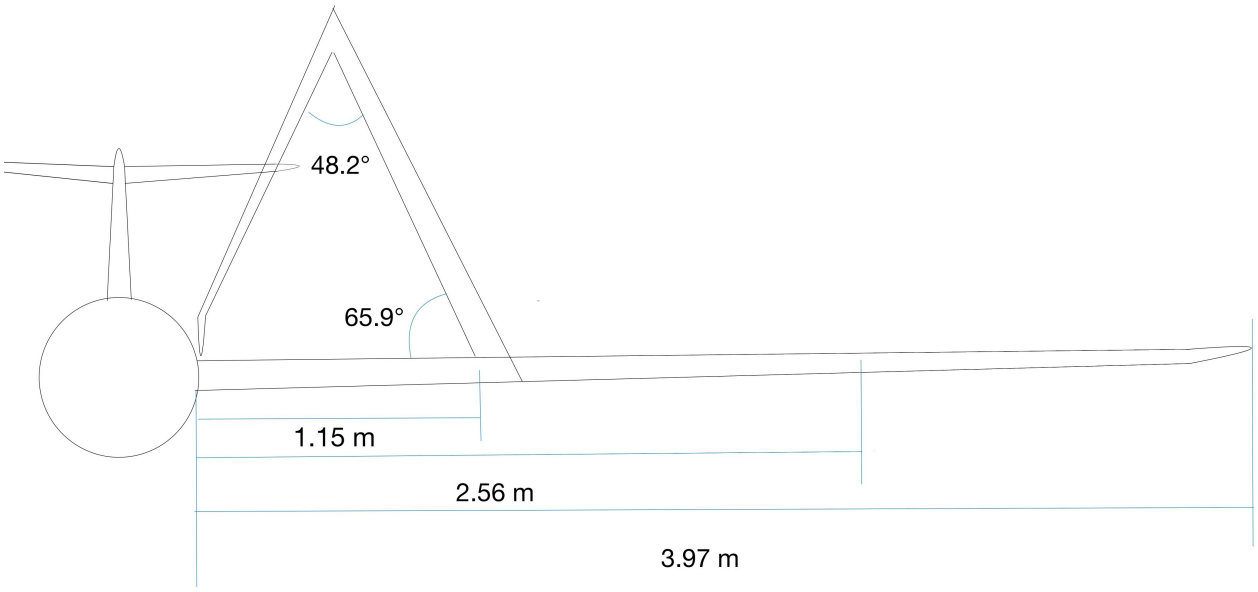

Figure 6.4: Geometry of the folding glider wings, front view

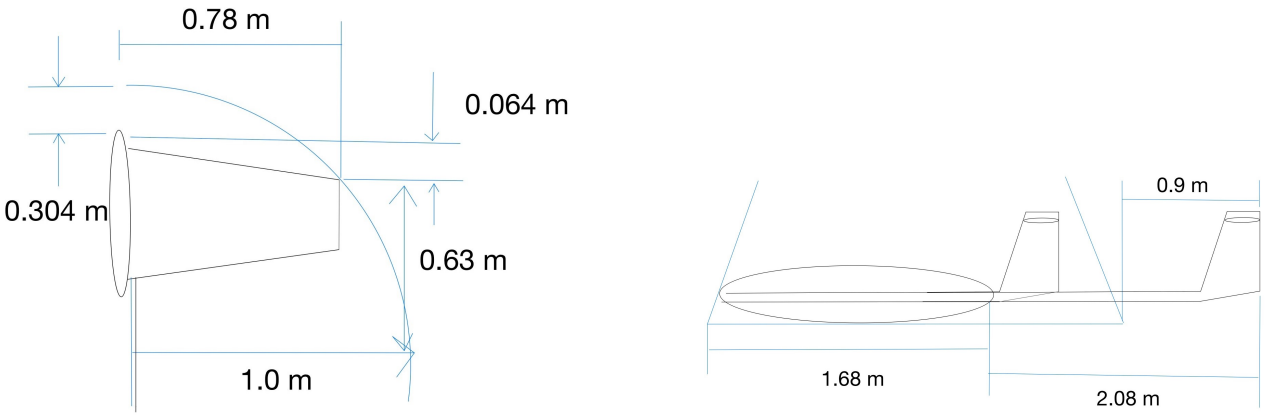

(a) Tail in the aeroshell, top view

(b) Geometry of the stowed glider tail, side view

Figure 6.5: Folding of the glider tail

from the fuselage with the use of a 1.7 m rod which will slide out of the fuselage and lock as soon the glider is unfolding. The locking mechanism will make use of compliant tabs which do not require any power. Different from the other lifting surfaces, the T-tail will not fold since it fits perfectly in the aeroshell structure.

Finally, it is important to understand how reliable all these mechanisms can be. Regarding the pyros and hinges, these mechanisms have very high reliability and TRL 9 since they have been used many times in space for the deployment of rovers, thermal shields, probes and more[6]. Rails are also quite standard in the space sector, especially for the deployment of solar panels, which therefore wields a TRL of 9 as well. Finally, despite shape memory alloys being a new technology and therefore less reliable, they have been already tested in a laboratory and in-flight ((Benafan et al., 2019)) and implemented in space for the deployment of instruments and solar panels in CubeSats(Guzik & Benafan, 2018). As a result, they are characterised by a TRL of 7.

[6]URL: https://www.nasa.gov/centers/wstf/testing_and_analysis/propellants_and_aerospace_fulids/pyrotechnic_device_evaluation.html [cited 18/06/2023].

PART III

SPACE MISSION

7. Astrodynamics Design

In this chapter, the astrodynamic trajectory design is described. It describes the model used for the simulations used in the trajectory design and the resulting trajectory options. Additionally, the encounter with Uranus is modelled, the atmospheric entry conditions are determined, and the communication distance and angle are determined. Both the trajectory of the orbiter and the capsule are designed to suit both the communication during the mission and the entry trajectory. The astrodynamics are treated in four parts. Firstly, in Section 7.1, describes the trade-off required for the launcher that will send the total system combination on a course to Uranus. Secondly, the interplanetary trajectory is detailed in Section 7.2, where several trajectories use one or more planets to decrease the required propellant mass to reach Uranus. A trade-off between the trajectories is done to choose the final trajectory. Thirdly, contained in Section 7.3 is the Uranus encounter, where the capsule and the orbiter part ways. Here the orbiter performs an insertion burn, and the capsule enters Uranus' atmosphere directly. And fourthly, in Section 7.4, the orbital mission performed at Uranus is analysed. All throughout the chapter cost is understood to mean ΔV cost.

7.1 Launcher

This section treats the selection of the launch vehicle to be used for the Ouranos mission. Various potential launch vehicles are compared and a single option is chosen. When the launcher is picked its capabilities still have to be assessed for the specific ΔV needs of the Ouranos mission, for which a function is set up to determine what payload mass can be launched for what ΔV.

7.1.1 Launcher Trade-off

For the launch selection, four candidates were identified. These are the Falcon Heavy (reusable and expendable), Vulcan, and Ariane 6. The trade-off is based on the following trade-off criteria:

Cost **Weight: 40%** The launch cost should be within the allocated budget. A launcher that by default is too expensive should not be considered.

Payload **Weight: 45%** The launcher should be able to launch the designed system. Similarly, having an estimate for the maximum payload sets a clear limit to the maximum payload mass.

Sustainability **Weight: 15%** Each launcher has different environmental impacts. This is both in emissions from the launch and the manufacturing. Both these factors and the sustainability requirements are taken into account.

As can be expected, the cost is the driving factor in the trade-off. This is due to the budget requirement LAU07, as this stipulates the maximum launch cost. The payload capabilities are driven by LAU07, as a maximum system mass is chosen. This means that the launcher should be able to launch said mass at a minimum. Service record and certification flow from ESA04. Having a good service record and the proper certification results in better reliability. Lastly, sustainability flows from the overall sustainability requirements of this mission. In Table 7.1 below the scoring of each launcher per criteria is shown. The scoring was done on a scale of 0 to 4, where 0 means it does not meet the requirement and 4 means it exceeds the requirement.

The Falcon Heavy scored first. In terms of cost, it was scored a 4 as it performs better than the constraint set by LAU08. In terms of payload, it was given a 2, as its payload capabilities are below the total system mass. Lastly, for sustainability, it scored a 3. This is due to the reusability of the launcher itself.

Next, the Falcon Heavy in its expendable configuration was scored. In the cost criterion, it was scored a 3, as it exactly meets the constraint set by LAU08. For payload, however, it was scored a 4, as it is capable to launch the total system mass and provide it with a large amount of ΔV. For sustainability, it scored a 2. This is due to the fact that the launcher cannot be reused in this configuration. However, it is not given a 1 since the boosters could have been reused and SpaceX aims to increase reusability over time.

Table 7.1: Launcher Trade-Off

Launcher	**Cost (40%)**	**Payload (45%)**	**Sust. (15%)**	**Total**
Falcon Heavy	4	2	3	2.95
Falcon Heavy Expendable	3	4	2	**3.3**
Vulcan	2	2	1	1.85

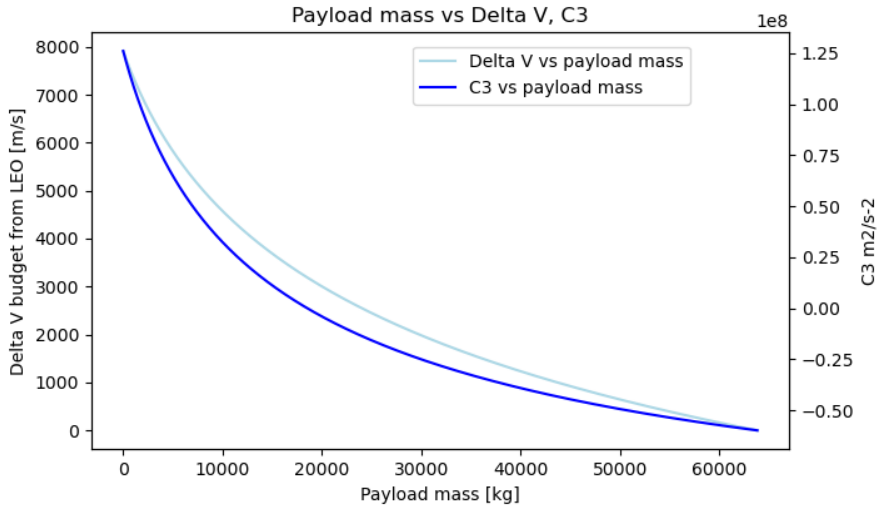

Figure 7.1: ΔV and C_3 plotted against payload mass for the Falcon Heavy launcher

Lastly, the Vulcan launcher was scored. For the cost, it was scored a 1. This is due to the massive estimated cost range thus making it unsure whether or not LAU08 can be met. For the payload, it was scored a 2, as it is not clear if it can launch the system. Last, for sustainability it scored a 1. This is due to it not being reusable and United Launch Alliance not having any track record or intention to make reusable launch vehicles in the future.

From the trade-off, it can be concluded that the Falcon Heavy in its expendable configuration is the preferred launcher. This decision mainly flows from the ΔV requirement. It should also be noted that the Vulcan is not fully rejected, as it has not yet flown at this time. It might still be a viable option in the future, provided the launcher is developed before the required launch date, as a backup launcher.

7.1.2 Launcher Trade-off Sensitivity Analysis

After the trade-off, a sensitivity analysis was performed. This is to test the rigour of the trade-off process. First, the weights were switched around. By switching cost and maximum payload, the reusable Falcon Heavy comes closer in score to its expendable configuration, but the expandable configuration still wins the trade-off. The same happens when switching cost and sustainability. The reusable configuration only wins when the payload weight is switched with the sustainability weight.

The second test was by removing criteria. Removing the cost still has the expendable configuration win the trade-off. The same happens when removing the sustainability category. The reusable configuration wins when the maximum payload category is removed.

7.1.3 Falcon Heavy Payload Mass

Since SpaceX's Falcon Heavy (FH) in its expendable configuration has a wide payload possibility, it is not clear how many kilograms of payload it can propel to a certain velocity. SpaceX reports that FH expendable can get a payload of 63.8 tons to Low Earth Orbit (LEO), and 3.5 tons to Pluto [1]. By the latter SpaceX means it can propel the payload to a transfer orbit to Pluto, which takes about 8.2 km s^{-1} from LEO. Knowing these two values, in combination with the mass fraction data known about FH, it is possible to set up a function that provides the maximum payload for a required ΔV. The results of this calculation are shown in Figure 7.1. On the x-axis is plotted the payload capacity of FH, whilst on the left y-axis is plotted the ΔV capacity from LEO, for that payload. As can be seen the 63.8 tons of payload has a corresponding ΔV of 0 m s^{-1}. It can also be noted that the payload for a Hohman transfer to Mars, which requires a ΔV of 3600 m s^{-1}, is correctly evaluated to be about 16.5 tons, corresponding to SpaceX's reported value of 16.8 tons. In the very high ΔV range the tool starts underestimating the possible payload: the ΔV without a payload tops out at about 7900 m s^{-1}, which conflicts with what SpaceX reports for Pluto as mentioned above. The tool is, therefore, accurate for ΔV ranges up to about 6000 m s^{-1}, and is conservative overall, meaning it can still safely be used up to 7000 m s^{-1}. This tool can then reliably be used during the design of the interplanetary trajectory.

[1] URL: https://web.archive.org/web/20220322170331/https://www.spacex.com/media/Capabilities&Services.pdf [cited 21/06/2023].

7.2 Interplanetary Trajectory

The interplanetary trajectory was designed using the Tudat package for modelling the trajectory and PyGMO for the optimisation. Section 7.2.1 covers the model used for the analysis of the astrodynamic trajectories, after which Section 7.2.2 covers how the trajectory problem is a global optimisation problem, and how PyGMO generates a numerical solution. Section 7.2.3 treats how the trajectory is designed, and finally, Section 7.2.4 details the verification of the interplanetary model.

7.2.1 Trajectory Model

The Tudat package, published and maintained by the aerospace faculty of the TU Delft, was used to determine the trajectory. From this library, the transfer_trajectory functions and classes define the trajectory. These functions allow for the direct design of the trajectory, with the package taking care of the loading of ephemeris data for the planets and the management of the system. First, the order of planets visited is defined, with an orbit around the departure body and the arrival body. Then, the time between each encounter is designed. Additionally, the minimum periapsis height is set for each planet to avoid the atmospheres and rings. This creates a system of nodes, which are at the encounters with the planets, and legs, which are sections of orbits between each node. The orbital characteristics of the legs are derived from the timing between the nodes. The legs are considered to be unpowered, and thus no additional characteristics are required. These legs are simulated as purely Keplerian motion, undisturbed by celestial objects other than the Sun. Then, at each node, the required periapsis of the flyby is determined to allow the change in orbit. If this is lower than the minimum periapsis height previously given, the flyby is adjusted to have a periapsis at the lowest option, and a burn at periapsis is determined to correct for the higher periapsis. The flyby of the planet is not simulated. Instead, the impact of the flyby on the heliocentric orbit is determined. As the node settings for the flybys are derived from the legs, no parameters for the nodes are set beforehand. The planets are here considered points in space. This results in the legs describing the heliocentric trajectory, and nodes with a defined periapsis and velocity change for the given trajectory. Furthermore, the states of the orbiter are given as the position in the x, y and z direction of the ECLIPJ2000 reference frame and the velocities in x, y and z of the same reference frame for each leg of the trajectory. For the final encounter, it should be noted that the gravity of the planets is neglected outside the calculations at the nodes, and thus the orbital model needs to take into account that it starts sufficiently early that the impact of this assumption is negligible.

7.2.2 Optimisation

While the previous module can determine the trajectory of the multiple gravity assist, it only determines it for a single set of transfer times. As an initial guess of the transfer times is unlikely to be the optimal set of transfer times, these values have to be optimised. For this purpose, the PyGMO module, published and maintained by ESA, was used (Biscani & Izzo, 2020).

The PyGMO module requires a problem class to be created. This problem class is initiated with the problem to be solved and the bounds on the parameters of the function. It then sets up the class with the bounds and sets up the number of parameters. Then, the function to be optimised is evaluated based on the list of input parameters. This results in a specific fitness score, which is the main output of the problem class.

as the optimisation algorithm, a differential evolution algorithm was used. This algorithm first uses a seed to generate a population of input parameters. Furthermore, the crossover probability and differential weight are set. The fitness of each value is then determined. Then, a new generation of solutions is generated. This is done by evolving all points. For each point x in a generation, 3 other points,a, b, and c from the same generation are selected. Each parameter x_i has a chance of the crossover probability to be changed. If the value is changed, then the new value is determined by:

$$y_i = a_i + F(b_i - c_i) \tag{7.1}$$

with y_i being the new value of the parameter and F being the differential weight. If the new point y has higher fitness than x, it will be used in the new generation. Otherwise, x is used for the new generation. This process is repeated for a set number of generations. Then, the best parameters and their fitness values are the output of the optimisation. This resulted in a The optimisation uses a crossover probability of 0.7 and a differential coefficient of 0.55. These values were found to generate better solutions than others but were still insufficiently consistent. To improve consistency, and ensure that the simulation found the global optimum, the simulation is run 25 times with random seeds, and the best result is stored. From investigation, this results in the global optimum being found with 95%, with a low variance of the outcomes. No optimisation of the population or number of generations was done, and populations of 20 individuals and 800 generations were used for all optimisations.

Table 7.2: Properties of the four most promising gravity assist trajectories and a direct transfer for reference.

Planets	**Earth manoeuvre ΔV** [m s^{-1}]	**ΔV transfer** [m s^{-1}]	**ΔV V_∞** [m s^{-1}]	**Flight time** [yr]
EU	8081[a]	1817 [b]	997	19.79
EJU	6395[c]	132 [b]	3260	21.62
EMJU	5695 [d]	170 [e]	4240	16.10
EVVEJU	4244 [d]	3 [e]	3220	26.26

[a] 6264 m s^{-1} provided by the launcher
[b] Remaining ΔV performed by the orbiter at Earth departure
[c] 6263 m s^{-1} provided by the launcher
[d] Fully provided by launcher at Earth departure
[e] ΔV provided by orbiter at planetary swingby

7.2.3 Trajectory design

There are many options for gravity-assist trajectories. Simple trajectories, with only a single flyby, are only a feasible option for Uranus if either Jupiter or Saturn is used. Gravity assist trajectories including the inner planets can lower the required propellant but usually have a cost of an increased transfer time. The inner planets are very unlikely to efficiently be able to bring the spacecraft to Uranus. Therefore, the only trajectories considered include either Jupiter, Saturn or both of them. Furthermore, to constrain the complexity of the analysis and to limit the flight time, only up to three flybys of the inner planets are considered. The limits of the flight times are given depending on the destination: to the inner planets, the flight time has to be between 30 and 500 days, while for Jupiter and Saturn, the flight time is between 400 and 2000 days. The time until the Uranus encounter is between 3 and 20 years. With these settings, the optimisation was run for the indicated trajectory options. From this, three promising trajectories were found: Here V refers to Venus, E refers to Earth, M refers to Mars, J refers to Jupiter and U refers to Uranus. All of these trajectories use the launcher for the largest part of their manoeuvre. Here, it is assumed that the launcher shall provide a burn of up to 6264 m s^{-1} of ΔV at the first departure of Earth, and this is subtracted from the transfer ΔV. The Jupiter gravity assist requires a small additional burst at Earth departure but has the smallest capture burn. The trajectory visiting Mars requires a larger capture burn but compensates for this with a much lower flight time. The long gravity assist trajectory has the lowest propellant required but has a much higher flight time. Considering the disadvantages of a longer mission, especially since RTGs shall be used and their power output decreases exponentially over time, the somewhat increased ΔV cost of the Earth-Mars-Jupiter-Uranus trajectory is considered the best choice. This would require a burn of 5695 m s^{-1} at Earth, done by the launcher, a burn of 170 m s^{-1} at Mars and a capture burn of 783 m s^{-1}.

7.2.4 Verification

The Tudat software is considered verified. The functions used have already been compared to the Cassini trajectory in the documentation. However, the specific implementation of the functions might still be faulty. Therefore, this implementation is also compared to the Cassini mission benchmark from (Vinkó et al., 2007). The output is a vector with the times of flight of the legs between planets and a ΔV value associated with the trajectory. When compared with this benchmark, the program output vector is (-792.7, 157.6, 449.4, 56.9, 1014.6, 4541.0), times given in days, with a ΔV of 4943.8 m s^{-1}, compared to the benchmark value of (−789.8, 158.3, 449.4, 54.7, 1024.7, 4552.8), again times given in days, with a ΔV of 4930 m s^{-1}. This shows that the model is slightly inefficient, but gets close to the optimal solution. This indicates that, while further optimisation of the trajectory to Uranus is possible, the model output is reliable.

7.3 Encounter and Insertion Burn

After the travel to Uranus, at a distance of 2.89 Million kilometres from Earth, the capsule and orbiter will arrive at Uranus. Here, their trajectories will split, with the capsule entering the Uranian atmosphere and the orbiter entering an orbit. The trajectories taken here are important for the design of the entry capsule, and determine the communication intervals during the atmospheric mission. Therefore, in this section, a model for these trajectories will be designed and the trajectories will be designed according to constraints of the entry capsule and the glider communication subsystem. Firstly the use of the model is described in Section 7.3.1, after which it is used in Section 7.3.2, leading to the selection of an orbit. Last of all, the model is verified by comparing the resulting angles and distances to expected values, and examining the output for a Uranostationary captured orbit.

Table 7.3: Orbital characteristics of the capsule trajectory up to entry around Uranus

V_∞ [m s^{-1}]	**Periapsis** [km]	**Atmospheric entry velocity** [m s^{-1}]	**Entry flight path angle** [°]
4240	19.400	26.600	-33.0

7.3.1 Model Architecture

The orbital model uses Tudat[2], published and maintained by the aerospace faculty of the TU Delft, to simulate the Keplerian motion of the capsule up to atmospheric entry, and to model the motion of the spacecraft up to the end of the glider mission. First of all, the velocity at an infinite distance V_∞, is determined from the interplanetary trajectory. A manoeuvre to change this hyperbolic velocity for the orbiter after separation was considered and implemented, but not selected. In addition, the inclination and initial argument of periapsis are determined from the interplanetary model. To simulate both bodies and determine the properties of a trajectory relevant to the atmospheric mission, the first 2 bodies were created. these are the orbiter and the capsule. The capsule will enter the atmosphere, and will thus require a periapsis low enough in the atmosphere that this will be achieved. For this purpose, the periapsis of the capsule orbit is set sufficiently deep into the atmosphere. The capsule trajectory is assumed to be the trajectory of the combined system from interplanetary space so that the capsule doesn't need to do any manoeuvres. Then, the orbiter's initial state is generated. This is assumed to be right after separation, but still far out. Furthermore, the orbiter is assumed to have done a manoeuvre to change its orbit and increase the periapsis, modify its semi-major axis and adjust the angle of periapsis. This is done by a manoeuvre changing the direction and magnitude of the velocity vector at this point. This allows for changing the V_∞ of the orbiter. This manoeuvre is also assumed to change the orbit from a retrograde one, which the capsule will take, to a prograde one. This proved to increase the communication window due to the change in location of the argument of periapsis. The manoeuvre is considered to be instantaneous. Using this manoeuvre, the semi-major axis and eccentricity are found directly, while the argument of periapsis and true anomaly are found by matching the initial position of the orbiter and the capsule.

First, the capsule trajectory is simulated up to atmospheric entry. This is done by Keplerian propagation up to periapsis. Then, it is determined at which point the capsule crossed a preset height above 1 bar, and the state of the capsule is given as an input to the atmospheric entry model. Then, the required manoeuvre for the orbiter to capture and enter a desired orbit is determined. This manoeuvre is assumed to be instantaneous. While this is an oversimplification, as the real manoeuvre will take approximately an hour, this spread-out burn could be leveraged to change the argument of periapsis to a more advantageous location. Options for a capture burn before or after the periapsis were implemented and considered, but not used. The orbiter state is then propagated up to its periapsis, where it is assumed to enter the desired orbit, at which point the orbiter will enter this orbit. Then, the orbiter state is propagated up to the end of the atmospheric mission. The glider is assumed to be stationary on the planet after atmospheric entry and to only move due to the rotation of Uranus. This is reasonable as the distance the glider travels is low in comparison to the circumference of Uranus.

7.3.2 Orbit Selection

First of all, a suitable trajectory for the capsule shall be designed. The main parameter to account for in this design is the entry angle: a too shallow angle would cause the capsule to leave the atmosphere, while a too steep entry would cause the capsule to enter the lower layers of the atmosphere with too much velocity. The bounds as determined by the entry simulation is between −30° and −35° This angle is controlled by setting the periapsis. The entry velocity and position follow from the orbit. Furthermore, the atmosphere was considered to start at 1000 km above the 1 bar altitude. This leads to the orbital characteristics given in table 7.3. The next orbit to design is the orbital trajectory of the orbiter. The orbiter will enter the Uranian system together with the capsule at an inclined orbit, but separate at some point before atmospheric entry. The ΔV for a manoeuvre to change the V_∞ after separation was considered too expensive. This point should be far away from Uranus, to decrease the ΔV cost of any correction manoeuvre. After this manoeuvre, the orbiter will continue the highly inclined hyperbolic orbit. A capture manoeuvre somewhere other than at periapsis was considered to adjust the final argument of periapsis, but this was also not worth the high ΔV cost. After periapsis, the orbiter is in a captured orbit. The required velocity increment is considered the main cost of a specific orbit. The trajectory of the orbiter is a major factor in the design of the communication system of the glider, and thus the communication windows during which the orbiter is within communication distance and the angle is acceptable are essential for this design. For this purpose, the distance between the glider and the orbiter and the angle between radial out at the glider and the vector from the glider to the orbiter are determined at all points of the entire atmospheric mission. These distances and angles are then cross-checked with constraints from the glider communication system. This results in a list of intervals at which communication will be possible or impossible. These intervals are then provided for the glider communication design to verify the feasibility of these orbits with regard to the

[2]https://docs.tudat.space/

Table 7.4: Orbital characteristics of the orbit the orbiter will enter during the atmospheric mission

V_∞ [m s^{-1}]	**Periapsis** [km]	**Apoapsis** [km]	**Inclination** [°]	**Argument of periapsis** [°]	Orbital period [h]
4240	26.900	240,000	81	118	35.3

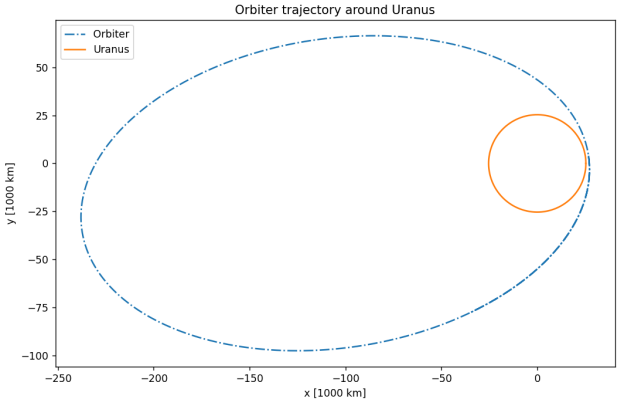

Figure 7.2: The chosen orbit, shown in its own orbital plane.

Table 7.5: Properties of the orbit relevant to the communication design

Mission share in contact with orbiter [%]	**Maximum distance** [km]	**Maximum angle** [°]
40	225.000 km	70

required bit rate. Another factor taken into account for the design of the orbit is that a lower orbit requires more ΔV, and complicates further options for missions after the atmospheric mission has been concluded. Furthermore, a long capture burn will place more strain on the propulsion system, increasing the risk of the manoeuvre. These two interests have been balanced to satisfy requirements for a low orbit to communicate and a high orbit for future mission potential and a smaller capture burn. The option to satisfy both options is an elliptic orbit, with a periapsis just above the atmosphere, and an apoapsis high enough to allow for future mission potential. Several iterations of orbits and communication system characteristics have been created and evaluated from a communications standpoint, a capture efficiency standpoint and considering the future mission. The orbital characteristics of the orbits satisfying these conditions are given in table section 7.3.2, and the final orbit is shown in fig. 7.2.

These trajectories lead to the properties of the communication windows as shown in Table 7.5:

7.3.3 Verification

In general, the orbital model is based on Tudat, which has already been verified. The application, however, could still be using it incorrectly. Therefore this section details some tests that were done to confirm the appropriate working of the model. First of all, the properties of the final orbit were examined. As the final orbital period is approximately 2 Uranian days, one would expect the distance and angle to behave approximately periodically over 2 Uranian days, or one orbit. The angle and distance plots are shown in fig. 7.3. Here, it is seen that the distance is clearly periodic with the same period as the orbit. Furthermore, while the angle seems irregular due to the two rotations in different planes, it too is periodic with the same period as the orbit. Next, a Uranostationary orbit was inserted. according to the following equation:

$$T = 2\pi \sqrt{\frac{a^3}{\mu}} \tag{7.2}$$

with T being the orbital period, a being the semi-major axis and μ being the Uranian gravitational parameter. From this equation the semi-major axis of a Uranostationary orbit by expressing this equation in the semi-major axis, as done in the next equation.

$$a = \left(\mu \frac{T^2}{4\pi^2}\right)^{\frac{1}{3}} \tag{7.3}$$

This leads to a semi-major axis of 82 686 km. Inserting this as the final apoapsis and periapsis of the orbiter, and setting the inclination to zero, should result in constant angle and distance. This is because the orbiter and

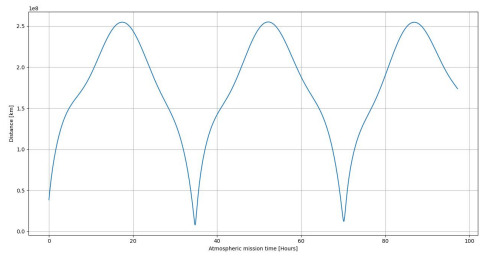

(a) Distance from the glider to the orbiter

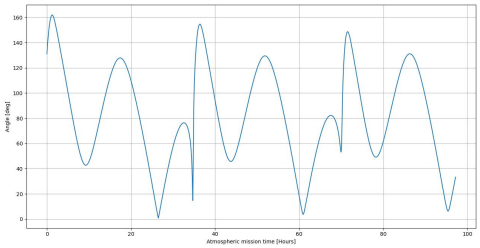

(b) Angle between pointing directly up and pointing to the orbiter at the glider location

Figure 7.3: The distance and angle of communication during the atmospheric mission. Both graphs show clear periodic behaviour during the atmospheric mission with the period of the orbiter, 35 h

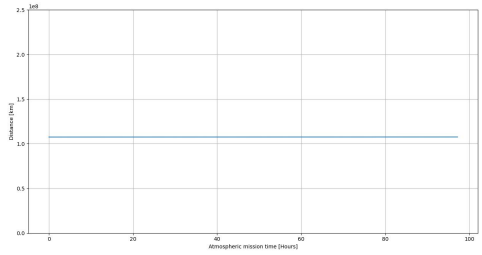

(a) Distance from the glider to the orbiter

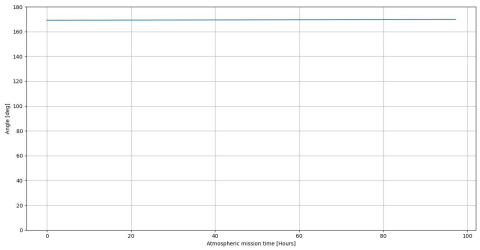

(b) Angle between pointing directly up and pointing to the orbiter at the glider location

Figure 7.4: The distance and angles for a Uranostationary orbit. While some drift occurs, the error in angle and distance remains small.

glider would move with the same period of one rotation. This results in the figures given in fig. 7.4. Here, a small drift can be observed, but the results are what would be expected from a Uranostationary orbit, meaning that the angle and distance remain almost the same over the atmospheric mission. A possible explanation for the drift is that different accuracies of the Uranian day are used when determining the semi-major axis and the movement of the glider.

7.4 Orbital Mission

After the atmospheric mission has been concluded, the orbiter will continue to investigate Uranus and its moons for 3 more years. In this section, this part of the mission is briefly discussed. This phase of the mission is analysed in less detail as it places considerably fewer demands on the design of the mission. It has, however, been kept in mind during the design due to the market analysis in section section 2.1. This analysis showed that an extended mission visiting the main moons of Uranus is required to make the mission competitive.

At the end of the atmospheric mission, the orbiter will initially have an orbital inclination of 81° relative to the equatorial plane of Uranus. This complicates manoeuvres to encounters with any of the Uranian moons. In addition, the low apoapsis places only Miranda and Ariel in range for an encounter, with Umbriel, Titania and Oberon having a higher orbit than the apoapsis of the orbiter. At this point, the orbiter is not properly positioned to investigate the moons, but useful science on the magnetic field and other properties of Uranus itself can be gathered from the polar orbit. To preserve fuel and avoid a major burn to change the inclination, it is advised to consider a swingby of either Miranda or Ariel. This will fulfil some scientific objectives and in addition, be able to raise the apoapsis and decrease the inclination of the orbit at a low cost. Low flybys are recommended, as these provide more scientific value and provide a more significant change in orbit. This encounter can be engineered by adjusting the orbit at either apoapsis or periapsis, modifying the orbital period to encounter the planet. Both from a scientific perspective and an efficiency standpoint, these manoeuvres should be repeated for the duration of the mission in Uranian orbit. While initially, the encounters will be harder to engineer, as due to the inclination the orbits need to have points close together and the timing needs to be correct. When the inclination has been decreased, the orbits will have points where they are close together, and only the timing needs to be arranged, which can be done by adjusting the orbital period of the orbiter. During these manoeuvres, the orbiter should take care to avoid the rings, as to not cause unnecessary risks. In the initial orbit, the inclination makes avoidance of the rings easier. As inclination decreases due to successive flybys, a manoeuvre to increase the periapsis higher than the rings should be considered to solve this problem.

8. Herschel Orbiter Design

In this chapter, the design of the Herschel orbiter for the Ouranos mission is considered. In Section 8.1 the payload onboard of the orbiter is analysed, after which the data handling subsystem of the orbiter is explored in Section 8.2. Next, in Section 8.3 the communication subsystem of the orbiter is described, after which the attitude determination and control subsystem used to ensure proper communication between the orbiter and the glider and Earth is detailed in Section 8.4. After this, the power and propulsion subsystems are analysed in Section 8.5 and Section 8.6 respectively, after which the structural analysis and thermal management are detailed in Section 8.7 and Section 8.8. Here below the main requirements of the orbiter system are presented and the same procedure will be implemented for the different subsystems described in this chapter. These boxes will not present any specific values due to their nature as summary boxes, for any more detail, the full lists of requirements are presented in Appendix A. The mass, power and cost of each subsystem are checked with the requirements and if it complies, then the requirement is checked off with an 'X' in the verification column in Appendix A.

In summary, the Orbiter shall

- Perform scientific measurements in a temperature range of 253 - 300 K
- Withstand the harsh condition of deep space
- Use less than 4.2 km s^{-1} for the total mission ΔV, while using less than 170 m s^{-1} and 0.6 km s^{-1} respectively for transfer and operations at Uranus
- Stay within the mass, power and cost budget with a reliability of 99.9%.
- Utilise the drag generated by Uranus' atmosphere
- Collect and process onboard housekeeping from all its subsystems and scientific data for transmission to Earth
- Be able to receive and process commands from Earth and data from the glider

8.1 Onboard Payload

The orbiter's payload suite has 5 instruments which are extensively discussed in Section 3.3. It consists of the magnetometer, the camera, Visible-IF Imaging Spectrometer, a Laser Altimeter, and the instruments for the Radio Science Experiments. Combined, it has a total mass of 75.3 kg, a power consumption of 147 W, and a data rate of 40 Mbit s^{-1}. It has an operational temperature range of 233 to 290 K. A customer requirement concerning the mission states that during flybys, the space system needs to be in Uranian-orbit-measuring-configuration. This means that these instruments will take measurements during the interplanetary phase, the arrival at Uranus, and in Uranian orbit until the end of life.

8.2 Data Handling

Similar to the glider, the orbiter also needs a data handling subsystem.

In summary, the Orbiter Data Handling subsystem shall

- Communicate commands to the orbiter subsystems
- Preprocess all data that shall be transmitted
- Be capable of handling program updates until the end-of-life phase
- Receive status assessments of all other orbiter subsystems
- Remain within the mass, power and cost budget with a reliability of at least 93%
- Withstand the harsh conditions of deep space

The orbiter payload suite given in Section 8.1 generates a maximum bit rate of 40 Mbits^{-1}, assuming that all the instruments take measurements at the same time. The camera is the most intensive instrument, data-wise. The mission phase where it will take the most measurements is during the moon flybys. During this manoeuvre, the orbiter will capture around 90 images in 1 hour after the example set by JUNO as part of its extended mission

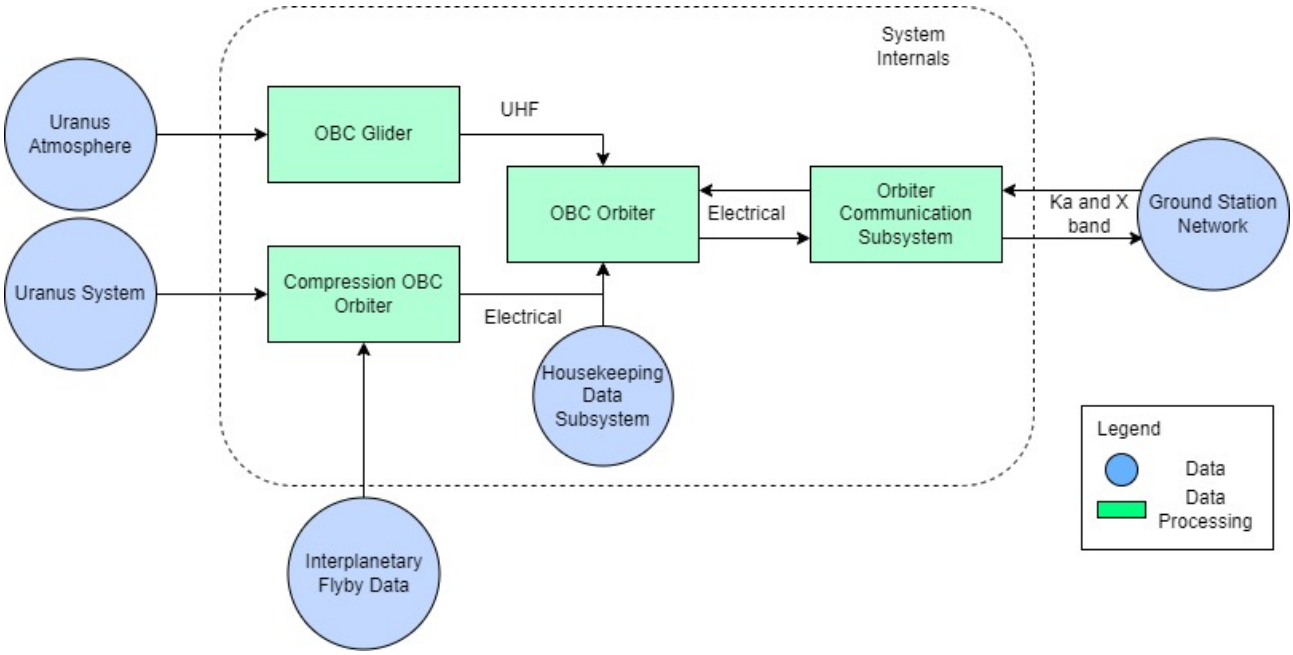

Figure 8.1: Data handling diagram

in the Jovian system[1]. The lossless data that this will generate will result in more than 600 MB.

Together with Edgise[2], different compression techniques were considered to deal with this high-measurement data. It was determined to use a rad-hard, long-distance Field-Programmable Gate Arrays (FPGA) design to perform onboard region-of-interest compression (ROIC) for the flyby images. It was calculated, for a flyby of Oberon with the closest approach of around 175 km, that the ROIC with common compression ratios for imaging measurements (Wertz et al., 2011) will result in a total of 35 MB per flyby. This calculation was a proof of concept of the compression technique and it is recommended to further investigate this for the mission planning of the orbiter.

The FPGA for the compression is the *NanoXplore NG-Large*[3] which can deal with the initial 600 MB (Leon et al., 2021). The onboard computer on the orbiter that deals with all the (compressed) scientific data and telemetry of the subsystems, is handled by the same OBC as the glider. Its specifications can be found in Section 4.2. The whole subsystem architecture for the data handling is portrayed as a diagram in Figure 8.1. It includes the data handling of the glider as well. There is a distinction made between outside sources and onboard data outside, all indicated by a blue circle. The different instruments are drawn as green blocks; the 3 types of OBCs and the communication subsystem hardware. They are connected through electrical cables or transmitted frequencies. The communications subsystem then sends a downlink to the ground station network.

8.3 Communications

The communications subsystem is responsible for sending all the gathered data to Earth. The design of this subsystem is constrained by the many requirements that have been identified during the requirements analyses of the systems, which are presented in Table A.5 and summarised here below.

[1]URL: https://www.planetary.org/articles/juno-io-flybys [cited 20/06/2023].
[2]URL: https://www.edgise.com/ [cited 20/06/2023].
[3]URL: https://nanoxplore.org/index.php/product/ng-large/ [cited 21/06/2023].

In summary, the Orbiter TT&C subsystem shall

- Have a high gain antenna with a gain of at least 59.9 dB
- Be able to receive the data from the atmospheric vehicle.
- Have a high gain antenna with a data transfer speed exceeding 34 kbit s^{-1}.
- Have a pointing accuracy of at least 159 arcsec.
- Be able to receive data via the X-band.
- Be able to transmit data via the Ka-band.
- Have a low gain antenna with a gain of at least 10 dB.
- Have a low gain antenna with a data transfer speed exceeding 1 kbit s^{-1}.
- Communicate all received data to the OBC.
- Have a signal-to-noise ratio of at least 7.23 dB.
- Operate in the harsh conditions of deep space.
- Stay within the mass, power and cost budget with a reliability of 99.9%

As mentioned in Section 8.1, the camera generates 40 Mbit s^{-1}. Using a data rate of 34 kbit s^{-1}, it is not possible to send all of this data. To put it into perspective, if the camera would take a picture every second for three years long, the total generated data, combined with the data of the other instruments, would be 1029.5 Tbit. This already includes a lossless compression factor of 5. It would take 960.1 years to send all of this back to Earth using a data rate of 34 kbit s^{-1}. This means that there will be a limit on the number of pictures that can be taken to be able to send all of the data back to Earth. The number of pictures that can be taken can be calculated by first calculating the total generated data from all the instruments except for the camera over a time span of three years. Again using a compression factor of 5, this value equals 0.1175 Tbit. Subtracting this from the total amount of data that can be sent over three years using a data rate of 34 kbit s^{-1}, the amount of data that can be used for the camera is found. Using a downlink time of 8 h, the total amount of data that can be sent in three years is 1.07 Tbit. This means that 0.955 Tbit remains to be used for camera data. By dividing this by the amount of data for one picture, the total amount of pictures that can be taken is found. This results in the capability of sending the data of 17 549 pictures, which means that every 90 min a picture can be taken.

Using this bit rate of 34 kbit s^{-1}, the antenna design can be done using Equation (4.3). Cassini and OCEANUS had a required signal-to-noise ratio of 0.31 dB. Cassini had a E_b/N_0 margin of 1.63 dB (Taylor et al., 2002), while OCEANUS has a margin of 7.23 dB (Saikia, 2016). The latter value is used as a required margin for this mission as well (requirement CNRS02.01-O-TTC.11).

The gain can be found using:

$$G = \frac{\pi^2 D^2}{\lambda^2 \eta} \tag{8.1}$$

where D is the diameter of the antenna, λ is the wavelength and η is the antenna's efficiency. The space loss can be calculated using Equation (4.2), where r is the distance between the orbiter and Earth.

The pointing loss is calculated with (Hodges et al., 2006):

$$L_{pr} = -12\left(\frac{eD}{70\lambda}\right)^2 \tag{8.2}$$

where e is the pointing accuracy. The value 70 is the taper factor in degrees which varies between 50 and 70, but for a parabolic antenna, this value is typically 70 degrees[4]. To have a pointing loss of less than 1 dB (Bocanegra-Bahamón et al., 2015), a pointing accuracy of 0.768 mrad is necessary.

Using the design input variables shown in Table 8.1, the downlink and uplink signal-to-noise ratio for the high gain antenna (HGA) can be calculated. The results for both are given in Table 8.2a and Table 8.2b respectively. The transmitted power, Boltzmann constant, data rate and noise temperature are converted to decibels. The gains, space loss and pointing loss are explained above, where the Deep Space Network (DSN) 34-meter antenna is used in the gain calculations. Finally, the transmitter loss, receiver loss and atmospheric attenuation are used from both Cassini and OCEANUS (Taylor et al., 2002) (Saikia, 2016).

The same can be done for the low gain antenna (LGA). The design input variables are shown in Table 8.3 and the downlink and uplink design control tables are given in Table 8.4a and Table 8.4b respectively. This time the DSN 70-meter antenna is used instead of the 34-meter one.

The same configuration as Cassini is used where one LGA is mounted on top of the HGA. A second LGA is placed on the other side of the orbiter. The HGA operates at X- and Ka-band, while the LGA operates only

[4] URL: https://www.researchgate.net/post/How_to_find_the_beam_width_of_the_parabolic_antenna10#:~:text=More%20accurate%20formula%20for%20the,when%20%CE%B8%20is%20in%20degrees. [cited 16/06/2023].

Table 8.1: Design input variables for chosen high gain antenna configuration (Taylor et al., 2002) (Saikia, 2016)

Design Input	Downlink	Uplink
Transmitting power [W]	50	20000
Transmitting antenna diameter [m]	4	34
Receiving antenna diameter [m]	34	4
Frequency [GHz]	32	7.2
Transmitting antenna efficiency [-]	0.55	0.76
Receiving antenna efficiency [-]	0.76	0.55
Noise temperature [K]	46.97	344.76
Data rate [bps]	34000	500
Distance to receiver [au]	19.32	19.32

Table 8.2: Design control tables for the downlink and uplink for the high gain antenna

Link Parameter	Design value [dB]
Transmitted power	16.99
Transmitting Gain	59.95
Receiving Gain	79.9
Transmitter loss	-1.35
Receiver loss	-0.8
Space loss	-311.8
Pointing loss	-0.983
Atmospheric attenuation	-0.5
Boltzmann constant	228.6
Data rate	45.31
Noise temperature	16.72
E_b/N_0 margin	8.05

(a) High gain antenna design control table for downlink

Link Parameter	Design value [dB]
Transmitted power	43.01
Transmitting Gain	65.58
Receiving Gain	48.39
Receiver loss	-2.20
Space loss	-298.8
Pointing loss	-0.12
Atmospheric attenuation	-0.5
Boltzmann constant	228.6
Data rate	-26.99
Noise temperature	-25.38
E_b/N_0 margin	31.6

(b) High gain antenna design control table for uplink

Table 8.3: Design input variables for chosen low gain antenna configuration (Taylor et al., 2002) (Saikia, 2016)

Design Input	Downlink	Uplink
Transmitting power [W]	60	20000
Transmitting antenna diameter [m]	0.08	70
Receiving antenna diameter [m]	70	0.08
Frequency [GHz]	8.425	7.2
Transmitting antenna efficiency	0.55	0.76
Receiving antenna efficiency	0.76	0.55
Noise temperature [K]	46.97	344.76
Data rate [bps]	1000	500
Distance to receiver [au]	1.5	19.32

at X-band. Up to and including the first gravity assist, the LGA will be used for communication between the spacecraft and Earth. Afterwards, the HGA will take over and be responsible for the communication and the LGA can be used in case of emergency. To transmit and receive X- and Ka-band, the Small Deep-Space Transponder is used. On top of this to receive UHF-band from the glider, the UHF transceiver II is selected [5]. Two travelling wave tube amplifiers (TWTA) are selected as well to amplify the radio frequency for the Ka-band and X-band. Both have an efficiency of 0.6 (Wertz et al., 2011), thus to have a transmitted power of 50 W, an input power of 84 W is required. On top of this, an ultra stable oscillator is selected to ensure as much frequency stability as possible. A diplexer is needed to be able to receive a certain frequency (X-band) while transmitting another frequency (Ka-band). A waveguide transfer switch is used to change the path of the electric wave between several sources. Finally, a telemetry control unit and command detector unit are selected. All of the specifications are shown in Table 8.5. The total subsystem mass is 121.1 kg and the peak power consumption is 116.6 W. The cost of the total subsystem is based on a SMAD estimation (Wertz et al., 2011) and results in a cost of M€ FY22 39.2.

The overview of the communication is given in a communication flow diagram. Here, the flow of information from the scientific instruments to the ground station, and the flow of commands from the ground station to the

[5]URL: https://satsearch.co/products/endurosat-uhf-transceiver-ii [cited 19/06/2023]

Table 8.4: Design control tables for the downlink and uplink for the low gain antenna

Link Parameter	Design value [dB]
Transmitted power	17.78
Transmitting Gain	14.38
Receiving Gain	74.62
Transmitter loss	-1.35
Receiver loss	-0.8
Space loss	-277.97
Pointing loss	-0.12
Atmospheric attenuation	-0.5
Boltzmann constant	228.6
Data rate	30
Noise temperature	16.72
E_b/N_0 margin	7.92

(a) Low gain antenna design control table for downlink

Link Parameter	Design value [dB]
Transmitted power	43.01
Transmitting Gain	71.86
Receiving Gain	14.42
Receiver loss	-2.2
Space loss	-298.8
Pointing loss	-0.12
Atmospheric attenuation	-0.5
Boltzmann constant	228.6
Data rate	-26.99
Noise temperature	-25.38
E_b/N_0 margin	3.89

(b) Low gain antenna design control table for uplink

Table 8.5: Overview of all the telecom instruments with their mass and power (Taylor et al., 2002) (Saikia, 2016)

Instrument	Power [W]	Mass [kg]
HGA	0	100.6
LGA x2	0	0.5
Small Deep-Space Transponder	19.5	3.2
X-band TWTA	84	0.965
Ka-band TWTA	84	1.495
Ultra stable oscillator	8	2
Waveguide Transfer Switch	0	0.44
Diplexer	0	3.4
Telemetry Control Unit	5.1	7.3
Command detector Unit	0	0.7
Total	116.6	121.1

orbiter are visualised. The bands used and data transfer rates of connections are also indicated next to the connecting lines.

All the calculations for the design of the communication subsystem were performed using software generated by the CAELUS team. This was verified using Pycharm's built-in tool to find bugs and with unit and integration tests to check if all the methods were implemented correctly and especially if their final addition to the orbiter design tool was performed flawlessly.

8.4 Attitude Determination and Control

The Attitude Determination and Control Subsystem (ADCS) of the orbiter is there to determine and adjust the orientation of the spacecraft during the mission. The ADCS is a complex subsystem with many different components that work together to guarantee pointing accuracy, accurate manoeuvring, and disturbance resistance. Firstly, the attitude determination components are selected based on the requirements presented in Table A.11 and summarised here below:

In summary, the Orbiter ADCS subsystem shall

- Be tested in conditions simulating the mission.
- Have redundancy in the design
- Determine the position, rotational rate and orientation of the orbiter
- Perform attitude correctional manoeuvres
- Stay within the mass, power and cost budget with a reliability of 99.9%.

Secondly, the attitude control components are selected based on what functions the orbiter has to be able to perform.

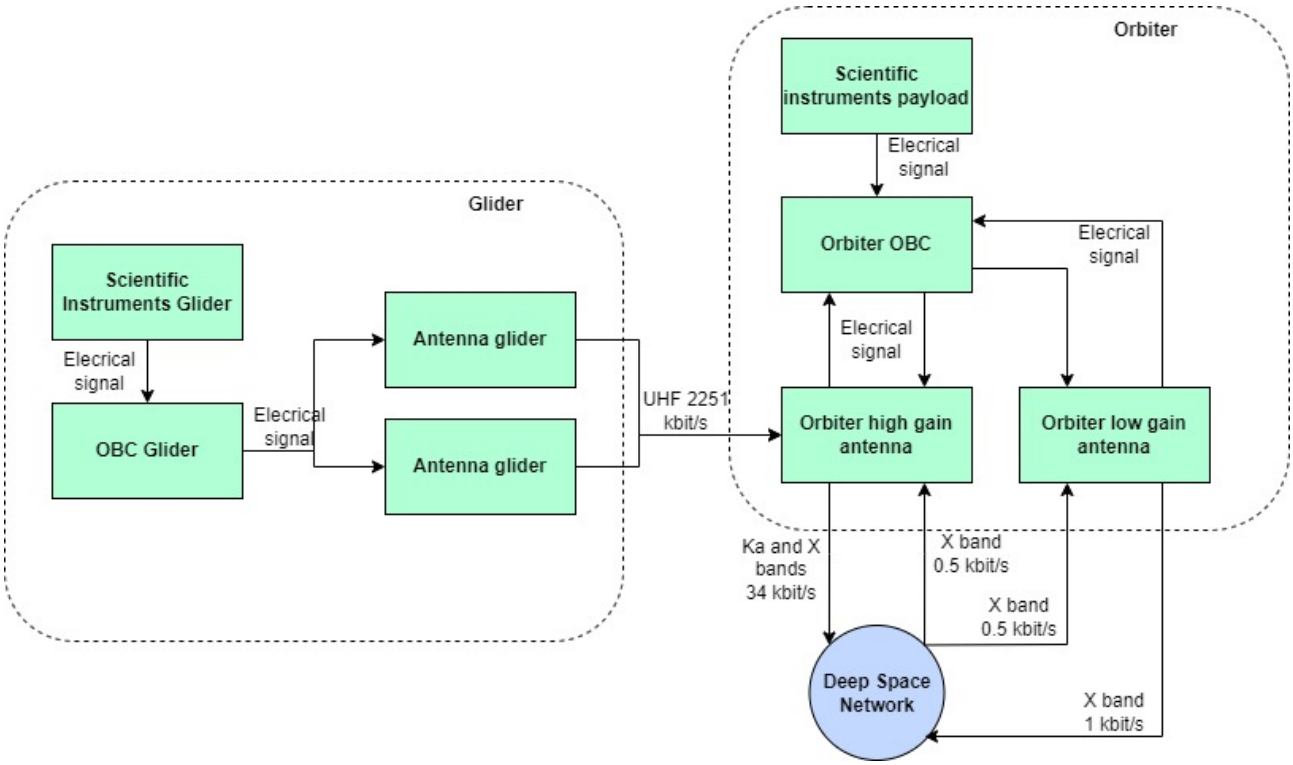

Figure 8.2: Communication diagram

8.4.1 Attitude Determination

The attitude determination of the orbiter is vital for it to perform accurate burns, communicate with Earth and the glider, and take precise scientific measurements over its 19-year lifespan. To make this possible the orbiter must know its orientation very accurately, down to 0.7 mrads, in line with requirement ESA04.06-O-ADCS.04 as listed in Appendix A. The orbiter is equipped with various attitude-determination instruments for redundancy and combined use.

The attitude will primarily be determined using star sensors and gyroscopes. On board will be three star sensors. Two star sensors aligned perpendicularly allow the spacecraft to determine its orientation to an accuracy of at least 0.01 degrees. A third star sensor is added for redundancy, perpendicular to the other two, still making full orientation knowledge possible in the case of a failure. Complementary to these are two Inertial Reference Units (IRUs), made up of two gyroscopes each. Two gyroscopes are enough for full attitude awareness, and make it possible to determine the speed or angle of rotation from an inertial reference point. They have the tendency to drift, and therefore require periodical information from the star sensors to calibrate, but serve their own special purpose for attitude determination during thruster firing when star sensors experience vibrations and can therefore not accurately keep track of the orbiters' orientation. In case these primary systems fail, or if a general system reboot occurs, the orbiter is equipped with three Sun sensors to help it re-obtain its attitude. These three Sun sensors offer lower accuracy in the order of 0.1 to 3 degrees but have lower mass and power requirements than star sensors and gyroscopes do.

8.4.2 Disturbance Torques

To quantify the magnitude of disturbance torques information on the mass and area distribution of the spacecraft is required in the form of mass moment of inertia (MMOI). For all activity around Uranus, the orbiter's propellant tanks are considered empty and the capsule is not attached. The MMOI of this configuration is (157, 324, 324) kg m^2.

The control part of the ADCS serves multiple functions. The first function is the re-orientation of the spacecraft. A re-orientation may be necessary to point the antenna, science instruments, or thruster. The second function is stability, since the position achieved has to be held for a certain time, depending on the function of the orientation, be it data transmission or engine thrusting. To determine the ADCS requirements periodical and non-periodical external disturbance torques are analysed. The disturbance torques at Uranus all use MMOI values for the (near)-empty-propellant-tank configuration. Periodical disturbance torques do not build up momentum over time, and therefore merely determine the size of momentum storage required. The first of the periodical disturbances is the gravity gradient torque, which occurs when a spacecraft's centre of gravity is not

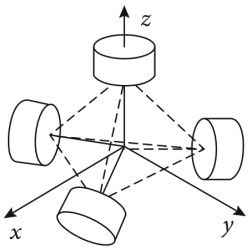

Figure 8.3: Four reaction wheels in tetrahedral formation to enable full 3-axis stabilisation in case of a single failure

aligned with its centre of mass (CoM) with respect to the local vertical (Wertz et al., 2011). It can be calculated with:

$$\bar{T}_g = \frac{3}{2}\frac{\mu}{a^3}(0, (I_{xx} - I_{zz})\sin 2\varphi, (I_{xx} - I_{yy})\sin 2\theta) \tag{8.3}$$

where μ is the gravitational parameter of Uranus, a the semi-major axis of the orbit about Uranus, φ and θ the angle difference by which the orbiter x-axis deviates from the gravitational vertical about the z and y axes, respectively. $\bar{\boldsymbol{T}}_{\boldsymbol{g}}$ is found to be (0, 1.19×10^{-7}, 1.19×10^{-7}) N m. The next periodic disturbance torque is the magnetic disturbance torque and it is calculated using:

$$T_m = DB \tag{8.4}$$

where D is the spacecraft's residual dipole moment, conservatively estimated to be 1 A m^2 (Wertz et al., 2011), and B is the magnetic field strength in T. This is found to be 1.1×10^{-4} N m. To accommodate both periodical disturbances, a reaction wheel should then have a momentum storage capability of at least 8.7 N m s (Wertz et al., 2011).

The first non-periodic disturbance torque is atmospheric drag. When flying high over a planet, traces of the atmosphere still exist, causing atmospheric drag. The drag disturbance torque can be found using:

$$T_a = \frac{1}{2}\rho C_D A V^2 (cp - cm) \tag{8.5}$$

where ρ is the atmospheric density, C_D the drag coefficient of the orbiter (conservatively equal to 2.5 (Wertz et al., 2011)), A the surface area in the wind, V the velocity at periapsis, cp_a the centre of pressure, and cm the CG of the orbiter. It is assumed that the drag acts from periapsis at 30 000 km where the density is 6.902×10^{-13} kg m^{-3}(Justh et al., 2021), where the spacecraft is for 15 minutes per orbit. T_a is found to be 1.37×10^{-3} N m. The second non-periodic disturbance torque is solar pressure. The light from the Sun impacts the orbiter, and due to a misalignment of the centre of pressure and mass, generates a torque. This torque can be found using:

$$T_s = \frac{\Phi}{c} A(1 + q)(cp - cm)\cos\varphi \tag{8.6}$$

where Φ is the solar flux at Uranus equal to 4.1 W m^{-2}, c the speed of light, and q the reflectivity of the spacecraft, assumed to be 1. T_s is equal to 3.44×10^{-5} N m.

There are also internal disturbances, the most significant of which is a misalignment of the CG and the thruster. According to (Wertz et al., 2011) this can be up to 3 cm. With a thrust of 425 N the main engine could therefore induce a torque of up to 12.75 N m around the y- and z-axis.

8.4.3 Attitude Control

Now that the disturbances are found and quantified, it is time to determine an attitude control configuration. Attitude control is not only meant to actively counteract disturbances but also to reorient the spacecraft when needed. Due to the high pointing accuracy required of the spacecraft, there is no other option than to have a 3-axis spin stabilised system. Such systems generally employ reaction wheels, which make use of the conversation of angular momentum to change the orientation of the spacecraft at will. Control Moment Gyroscopes are not feasible because of their short lifespan (Wertz et al., 2011). For redundancy, four reaction wheels are installed in a tetrahedral formation, as illustrated in Figure 8.3. The reaction wheels are not enough by themselves, however, since they get saturated over time. In that case, their momentum has to be dumped, which is done with Reaction Control System (RCS) thrusters. RCS thrusters are also able to counteract larger disturbances like the torque caused by the thrust misalignment mentioned above.

RCS thruster blocks can be fit on the corners of the spacecraft plus about 15 cm above the spacecraft bus where they can counteract the torque generated by the engine. Since the CG is found at 1.07 m above the base of the spacecraft, the moment arms of the RCS thrusters around the x-, y-, and z-axes are respectively

Table 8.6: Monopropellant thrusters considered for attitude control

Thruster	Thrust [N]	Mass [kg]	Isp [s]	TRL
Envisat/Helios Liquid AOCS thruster	3.5 - 16.5	0.355	232	9
MONARC-5	4.5	0.49	233	8
MRE-1.0	3.4 - 5	1	218	9
MR-111C	1.3 - 5.3	0.33	229	9
CHT-20	7.9 - 24.6	0.395	230	9

Table 8.7: Overview of the mass, power, and cost of the various ADCS components

Component	Mass [kg]	Power [W]
Reaction wheels[a]	15.2	60[b]
Gyroscopes	26	20[c]
RCS thrusters	5.68	0[d]
Star sensors[e]	1.8	7
Sun sensors[f]	3	0[g]
Total	**51.7**	**87**

[a]URL: https://www.rocketlabusa.com/assets/Uploads/Rocket-Lab-12-Nms-RW4-RW5-reaction-wheel-datasheet.pdf
[b]This value is three-quarters of the total since only 3 of 4 reaction wheels are active at a time
[c]The gyroscopes have a maximum power usage of 40 W, but due to redundancy only two of four are in use at a given time
[d]The reaction control thrusters are almost never used, but when they are there are at most four active at a time, with a max power usage of 54.6 W
[e]URL: https://sodern.com/en/viseurs-etoiles/
[f]URL: https://www.opticalenergytechnologies.com/our_products/sun-sensors-for-spacecraft/
[g]Since the sun sensors are only used in re-boot mode they use 0 W during normal operation. When active they use 6 W

(0.5 , 1.22, 1.22) m. This requires a thruster force of 10.46 N for each thruster pair. A single thruster thus has to provide a thrust of 5.23 N. For simplicity and reliability, monopropellant thrusters are considered. Several monopropellant thruster options are shown in Table 8.6. The thrusters are assessed based on their thrust, mass, specific impulse, and technology readiness level (TRL).

The multiple thrusters can comply with the 5.23 N thrust requirement. To apply a small safety margin on this, the thruster should be able to provide at least 5 N of thrust. The CHT-20 engine would overshoot at a mounting distance of 1.07 m above and below the CM, and would therefore have to be moved closer to the CG. This would, however, be inefficient. The mass of the thrusters is about the same, except for the poor mass of the MRE-1.0 thruster. The Isp is rather alike, with the MRE-1.0 thruster scoring the worst. The TRL is excellent for all, but MONARC-5 is merely flight certified, whilst the others are flight-proven. The choice is therefore between the MR-111C and Envisat thruster. The mass of the MR-111C is slightly lower, but its I_{sp} is also lower than that of the Envisat thruster. It is essentially an even choice between the Envisat thruster and the MR-111C. A fifth consideration is made based on age. The Envistat mission is quite old, and the Envisat thruster would therefore be difficult to obtain. The MR-111C is easier to obtain and is therefore chosen.

Four blocks of four thrusters are placed on the outer edges of the orbiter to give it full control. Although full control would be enabled by 12 thrusters, 16 thrusters are installed to make sure that a large misalignment torque is sufficiently countered. The accrued momentum over the three-year mission from the solar and aerodynamic disturbances at Uranus is found to be equal to 2126 N m s. To size the propellant mass required by the RCS thrusters to counteract a misalignment torque and to perform the required momentum dumping, the following equation is used:

$$m = t_{burn,RCS}\dot{m} = (t_{burn,me} + \frac{H_{RW}}{T_x})\frac{T/r_{arm}}{g_0 Isp} \tag{8.7}$$

where $t_{burn,RCS}$ is the RCS thruster burn time, $t_{burn,me}$ the burn time of the main engine, H_{RW} the total angular momentum stored in the reaction wheels over the mission-time at Uranus, and T_x the torque about the x-axis of the spacecraft, which is the worst case scenario. We find a propellant mass of 14.1 kg. Adding a safety margin of 10% yields a propellant mass of 15.5 kg. The ADCS system characteristics are summarised in Table 8.7

The estimated cost of the subsystem is based on statistical relations from (Wertz et al., 2011), which use the ADCS mass to estimate recurring and non-recurring costs. The recurring costs are estimated to be M€14.3 and the estimated non-recurring costs are estimated to be M€30.74, for a total cost of M€45.04.

8.5 Power

As discussed in the summary of the trade-off process in Section 3.1, a Radioisotope Thermoelectric Generator (RTG) was the most feasible option as the power source for the orbiter. Two trade-offs must be made to decide

Table 8.8: Power density of the different considered isotopes after 20 years

Isotope	Power density [W/g]	Half-life [years]	Power density @ 20 years [W/g]
Polonium 210	82	0.38	1.175×10^{-14}
Plutonium-238	0.41	86.4	0.35
Curium-242	98	0.4	8.704×10^{-14}
Strontium-90	0.24	28	0.1463
Americium-241	0.114	432.2	0.1104

Table 8.9: RTG specifications for the MMRTG, GPHS-RTG and the Next-Generation RTG (NASA, 2020) (Bennett et al., 2008) (NASA, 2022) (Werner et al., 2016)

RTG Type	BOL Power [W]	Mass [kg]	Power density [W/kg]	Cost [M€FY2022]
MMRTG	110	45	2.444	128.0
GPHS-RTG	300	55.9	5.367	138.6
Next-Gen-RTG	245	55.7	4.399	/

the final RTG choice, namely the isotope that will be used as a heat source. The options considered for this trade-off are polonium-210, plutonium-238, curium-242, strontium-90 and americium-241. This is a technical trade-off that will be based on the power density after a certain amount of time. Afterwards, the availability of the best isotope will be checked. The second trade-off is to decide the RTG type (Multi-Mission RTG, General-Purpose Heat Source RTG or Next-Generation RTG). This trade-off will be based on the beginning-of-life (BOL) power, the mass and the cost.

Before performing the trade-offs, it is important to determine what requirements will constrain the design space of the power subsystem. Such requirements are presented in Table A.9 and summarised here below.

In summary, the Orbiter Power subsystem shall

- Be tested in conditions simulating the mission.
- Be designed with safety factors with regard to peak load.
- Provide power to all the orbiter subsystems.
- Stay within the mass, power and cost budget with a reliability of 99.9%.

The first trade-off is to decide the isotope that will be used. The power density and the half-life for the different considered isotopes are shown in Table 8.8 [6] (Dustin & Borrelli, 2021). The power decay over time can be calculated using:

$$P = P_0 e^{\frac{-ln(2)t}{\tau_{1/2}}} \tag{8.8}$$

Using Equation (8.8), the power density after 20 years can be calculated. P_0 is the BOL power, t is the time that has passed and $\tau_{1/2}$ is the half-life of the isotope. As can be seen, plutonium-238 has a power density of 0.35 W/g after 20 years, which is more than double the second-best option and more than triple the third-best option.

The problem with plutonium-238 is its scarcity. It was found that NASA only has enough plutonium-238 left to make three GPHS-RTGs and this plutonium-238 is almost certainly already reserved for other missions. However, NASA started to produce more plutonium-238 and wants to have a production rate of 1.5 kg per year by 2026. At that rate, there will most likely not be enough for this mission but NASA can look into increasing this production rate if the demand is there[7]. On top of this, ESA will start producing plutonium-238 as well. Also on a small scale where they will produce 300 g per year, but they plan to perform more research to speed up the process (Parys & Spindler, 2022). This mission would increase the demand for plutonium-238. Thus if NASA increases their production rate and combines this with the ESA production, it is considered feasible to produce enough Plutonium-238.

The second trade-off is to decide the RTG type and this is based on the power density and cost. All of these specifications can be found for the three different RTG types in Table 8.9. NASA has not performed a cost estimation for the Next-Generation RTG yet, but it is assumed that the cost will be in the same range as the other two.

The power required for all the subsystems equals 466.3 W. This means that seven MMRTGs would be necessary compared to only three GPHS-RTGs or Next-Gen RTGs. This means that the MMRTG is discarded

[6] URL: https://ebookcentral-proquest-com.tudelft.idm.oclc.org/lib/delft/reader.action?docID=693314 [cited 16/06/2023]
[7] URL: https://spacenews.com/plutonium-availability-constrains-plans-for-future-planetary-missions/ [cited 15/06/2023]

Table 8.10: Comparison between plutonium-238 and americium-241 RTGs

	N_{RTG}	Power subsystem mass [kg]	Orbiter wet mass [kg]
Plutonium-238	3	217.1	2386.5
Americium-241	57	700.0	3724.1

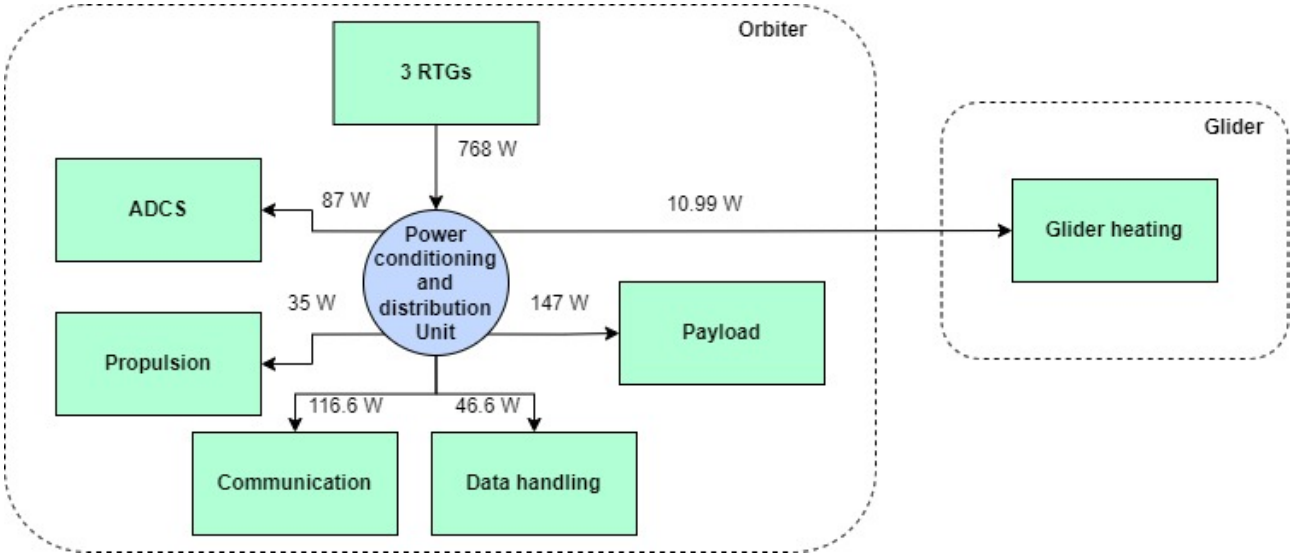

Figure 8.4: The electrical power diagram of the orbiter

because it results in a higher mass and cost. Because the mass of the GPHS and Next-Gen RTG is almost exactly the same and the same number of RTGs are necessary, it has been decided to go for the GPHS-RTG because it has a higher BOL power. This gives a bigger margin and if possible, the mission can be extended for longer. Thus three GPHS-RTGs will be used to provide up to 256 W each after 20 years. This results in a mass of 167.7 kg and a cost of M€437.

Americium-241 is considered the best alternative for plutonium-238 for deep space missions (Dustin & Borrelli, 2021). The University of Leicester developed an americium-241 RTG that can generate 10 W and it weighs 10 kg (Barco et al., 2022). To show why it was chosen to go for the plutonium-238 GPHS-RTGs, a comparison was made between these americium-241 RTGs and the plutonium-238 GPHS-RTGs to check the feasibility of using americium-241 RTGs. Plugging in the Leicester RTG values results in the values shown in Table 8.10. It can be seen that the power subsystem mass for americium-241 RTGs is almost triple the weight of the subsystem mass for plutonium-238 RTGs. This increase creates a snowball effect that requires more propellant, which then requires a bigger structure and thus heavier. This results in a total wet mass increase of 1338 kg.

Besides generating power, the power subsystem needs to distribute the power. For this, the Galileo power conditioning and distribution unit (PCDU) was selected (Terma, 2012d). It consists of three S3R shunt regulators (Terma, 2012f), three equipment power distribution modules (Terma, 2012a), six heater power distribution modules (Terma, 2012b), one propulsion power distribution module (Terma, 2012e), two thermal knives actuation modules (Terma, 2012g), two command and monitoring modules (Terma, 2012c) and one backplane module. All of these form the PCDU and it weighs 13.23 kg and consumes 23.05 W. Thus the power subsystem mass becomes 180.9 kg. The power is distributed to the other subsystems through cables, which are 20 % of the subsystem mass (Wertz et al., 1999). This brings the total power subsystem mass to 217.1 kg.

For the power system, Figure 8.4 was made to visualise the flow of power in the orbiter. This shows how power is provided by the RTGs, distributed by the power distribution unit and provided to all subsystems. It also shows the external connection to the glider, to provide power to heat the batteries and scientific payload during the transfer period. This connection will end when the capsule and orbiter separate. The power provided by the RTGs is taken as the peak power output when arriving at Uranus.

The team created a tool to perform the above explained power subsystem calculations. Unit and integration tests were performed using Pycharm's built-in tool to find bugs and to check that the tool was implemented correctly in the orbiter design tool.

Table 8.11: Main engines considered for the orbiter (Borgmeyer, 2019) (MOOG, 2013)

	Thrust [N]	Isp [s]	Mass [kg]	Power req [W]
Apogee motor S400-15	425	321	4.3	35
R-4D engine	490	312	3.76	46
Leros 1b apogee engine	635	317	4.5	40

8.6 Propulsion

The propulsion subsystem is there to perform manoeuvres during the mission. As it was done for all other subsystems, a list of subsystem requirements was generated and this is presented in Table A.7.

In summary, the Orbiter Propulsion subsystem shall

- Provide a total ΔV of at least 4.2 km s^{-1}.
- Perform multiple burns.
- Have a tank volume not exceeding 10.1 m × 4.5 m × 2.5 m.
- Have a nozzle not exceeding 4.5 m.
- Have a propellant mass not exceeding 2820 kg.
- Stay within the mass, power and cost budget with a reliability of 99.9 %.
- Provide a thrust of at least 400 N.
- Have a specific impulse of at least 300 s.
- Use a liquid propellant.
- Store the propellants at their operational temperatures.
- Not burn for more than 96 min.

As determined in Section 7.3, the biggest manoeuvre that needs to be performed is the orbit insertion, where a change in velocity of 1398 m s^{-1} is necessary. During the transfer, a ΔV of 170 m s^{-1} is required and for the exploration of the moons, 500 m s^{-1} is needed. On top of this an extra ΔV of 100 m s^{-1} is taken as a safety margin to have enough propellant. To perform all of these manoeuvres, a choice of propellant type needs to be made and a main engine needs to be selected. This will all be explained in this section.

To select the propellant type, requirement CNRS03.08-O-PRP.01 needs to be taken into consideration. It states that the propulsion system shall provide a minimum thrust of 400 N. The only type of propellant that can provide this amount of thrust is chemical propellant (Wertz et al., 1999). Multiple options were considered in the first place but a lot of them were quickly discarded. All options using fluoride as an oxidiser were discarded because it is too toxic and dangerous to work with. Hydrazine as a monopropellant was considered, but the specific impulse did not fulfil requirement CNRS03.08-O-PRP.02, which states that the propulsion subsystem shall have a specific impulse of at least 300 s. Water electrolysis is partly electrical and partly chemical. It fulfils both the thrust and specific impulse requirements but the problem is that it requires too much power. This leaves not a lot of options, but the two main ones that were investigated were bipropellant N_2O_4 as oxidiser and monomethylhydrazine (MMH) as fuel and the second option is a green monopropellant Advanced Spacecraft Energetic Non-Toxic (ASCENT). This monopropellant has a very similar performance and is even higher than hydrazine but the problem with it is that there are no thrusters yet for this green propellant that provide enough thrust to fulfil the requirements (Spores et al., 2013). Thus this leaves only the bipropellant N_2O_4/MMH as a suitable propellant for this mission.

Next up is the selection of the main engine. Again taking the thrust and specific impulse requirements into account, three possible engines were found. Their characteristics are shown in Table 8.11[8]. The propellant mass required depends on the specific impulse of the engine and can be found using:

$$m_{prop} = m_{final}\left(e^{\frac{dV}{gI_{sp}}} - 1\right) \tag{8.9}$$

where m_{final} is the final mass after the manoeuvre, dV is the required change in velocity, I_{sp} is the specific impulse and g is the gravitational constant of Earth. The selection of the engine also depends on the burn time of a single manoeuvre and if it complies with requirement CNRS03.08-O-PRP.07, which states that a single burn shall not be longer than 96 min. This value comes from Cassini's orbit insertion burn and it is used as the

[8]URL: http://www.astronautix.com/r/r-4d.html [cited 18/06/2023].

Table 8.12: Calculated burn time and propellant mass for the different considered engines

	Burn time [min]	Prop mass [kg]	Mass [kg]	Power required [W]
Apogee motor S400-15	40.2	915.2	4.3	35
R-4D engine	35.2	950.2	3.76	46
Leros 1b apogee engine	27.0	926.4	4.5	40

upper limit burn time for this mission [9]. The burn time can be found using:

$$t_b = \frac{m_{prop} I_{sp} g}{T} \tag{8.10}$$

The calculated burn time and propellant mass are shown in Table 8.12 together with the mass of the engine itself and the power required. All engines provide enough thrust to perform the biggest manoeuvre (orbit insertion) within the required 96 min. Because they all fulfil this requirement, the engine that requires the least amount of propellant and power is selected. Thus the Apogee motor S400-15 will be used for this mission. The required burn time was also checked with the allowed burn time for a single burn. For the S400-15 Apogee motor, it is maximum 150 min (Lescouzères et al., 2014) and thus acceptable.

Using Pycharms's built-in tool to find bugs, the tool created for the propulsion subsystem was verified. Performing unit and integration tests, it was checked if the tool was implemented correctly in the orbiter design tool.

8.7 Structures and Materials

This section will discuss the analysis of the structural elements present in the CAELUS mission space system. This analysis will be based on the requirements presented in Table A.6 and listed here below.

In summary, the Orbiter Structure subsystem shall

- Withstand vibrational, axial, lateral and peak loads.
- Perform separation from the atmospheric vehicle without any damage.
- Withstand the harsh conditions of deep space.
- Be designed applying safety margins depending on the analysed load.
- Have a volume of less than 4.5 m × 4.5 m × 10.1 m.
- Provide an interface for the orbiter subsystems.
- Have a natural frequency in the range described in the launch catalogue.
- Deploy the magnetometer at least 3.6 m from the orbiter main body.
- Separate from the launch vehicle without causing any damage.
- Be evaluated in a test campaign.
- Stay within the mass, power and cost budget with a reliability of 99.9%.

These consist of the two propellant tanks (N_2O_4, MMH), the stiffening elements and any type of structural sheet which have been idealised to assure the protection of the multiple orbiter subsystems. Before starting the analysis, it is important to understand that the properties of these specific subsystems mainly flow down from the launcher constraints, LAU01-03, which define the launch loads and the size of the subsystem, the main scientific requirement CNRS01 and the reliability requirement dictated by ESA, ESA04.

For the orbiter structure, it was decided to implement an integral structure, therefore having the tank surfaces as load-bearing elements. This design decision will allow to save on mass and cost since a lot less material will be required and the complexity of the design will decrease due to the reduction of required assemblies and joints. With this in mind, the tanks will be optimised to withstand any axial, lateral and pressure loads that could be encountered during operations.

The propellant tanks can have many different shapes but the best solution was determined to be a cylindrical body with two spherical caps. Such a geometry would allow for saving mass in the caps while still having a big enough aspect ratio to fit the orbiter in the payload fairing. The volume required to fit in the tanks results from the summation between the propellant volume and the pressurising gas necessary to reduce the pressure difference in the tanks during operations. For the first, the value can be easily calculated with the density of N_2O_4 and MMH, respectively, 1431 kg m^{-3} and 874 kg m^{-3}. Regarding the pressurising gas, the volume

[9] URL: https://sci.esa.int/web/cassini-huygens/-/34955-approach-and-arrival [cited 17/06/2023].

Table 8.13: Loads experienced by the orbiter during a launch with Falcon Heavy (X, 2021).

Load case	Load Factor (g)
Axial Tension	6
Axial Compression	2
Lateral	2
Shock	1000

required can be determined by assuming an isothermal expansion in the propellant tank and with the use of:

$$V_g = \frac{(p_{T_f}/p_{T_i})V_{prop}}{(1 - p_{T_f}/p_{T_i})} \tag{8.11}$$

where p_{T_f} is the tank pressure after the propellant has been completely drained in Pa, p_{T_i} is the tanks pressure before operations start in Pa, V_{prop} is the total propellant volume in m^3 and V_g is the pressurising gas volume in m^3. This volume constraint can be achieved with multiple values for the radius and length of the tanks, therefore an optimisation will be implemented to choose the combination of parameters that lead to the lowest possible tank mass.

Once the geometry has been defined, it is important to determine what are the loads that will act on the orbiter during operations. The orbiter will have to withstand many forces during operations but the greatest ones will be experienced during the launch phase due to the high accelerations induced by the launch vehicle. The axial, lateral and shock loads of the selected launcher, Falcon Heavy, are presented in Table 8.13.

The main load cases that will be analysed in this section are the hoop and hoop stresses due to the propellant present in the tanks and the axial, bending and buckling stresses during launch. First, a radius and length will be selected, then the minimum radius required will be determined based on the axial and hoop stresses and finally a buckling and lateral loads check will be performed on the geometry to make sure the selected parameters follow all the requirements. The required pressure necessary to store the propellant and drained it into the propulsion subsystem was determined from literature to be 3 MPa for both N2O4 and MMH (Muhammad et al., 2010). With this value, the required minimum thickness for both the cylindrical and spherical sections could be determined using

$$t_{cylinder} = \frac{\Delta p r_{tank}}{2\sigma_y} FOS \qquad t_{sphere} = \frac{\Delta p r_{tank}}{\sigma_y} FOS \tag{8.12}$$

where $t_{cylinder}$ is the thickness of the cylindrical section in m, t_{sphere} is the thickness of the spherical caps in m, Δp is the pressure difference across the tank walls in Pa, σ_y is the yield strength of the selected material in Pa, FOS is the factor of safety which was selected to be 1.1 as reported in the ECSS-E-30 standard (ESA, 2000) and r_{tank} is the tank radius in m. Once the pressure loads are analysed, the minimum thickness required to withstand the axial loads was determined with the following equation from SMAD (Wertz et al., 2011).

$$t_{axial} = \frac{(F_{axial} + 2M_{bending}/r_{tank} * FOS)}{2\pi r_{tank}\sigma_y} \tag{8.13}$$

where F_{axial} is the axial force that acts upon the structure which results to be equal to the mass of the entry capsule multiplied by the tensile axial launch acceleration presented in Table 8.13, $M_{bending}$ is the applied moment generated by the mass of the tank at the CG in N m due to the lateral launch accelerations presented in Table 8.13, r_{tank} is the radius of the tank in m and σ_y and FOS are as presented above. Of these two structural analyses, the minimum value, for both the cylindrical and spherical sections, should be implemented as the final tank thickness to make sure that both load scenarios can be withstood by the structure. To make this final selection, a material for the propellant tanks had to be chosen. From previous missions and market analysis, it was determined that the titanium alloy Ti-6Al-4V was selected due to the highest specific strength in all the aerospace materials that could be utilised. Moreover, since the minimum achievable thickness for metals is 0.8 mm, any result below such limit would have been increased to make sure the designed product was manufacturable.

After computing the thickness, the radius and the length of the tanks have been determined, it is important to check if these allow sustaining the bending loads present during the launch and the compression loads that could lead to buckling of the structure sheets. Regarding the bending loads, the maximum induced stress can be computed with:

$$\sigma_{cr_{bending}} = \frac{acc_y M_{bending} Lc}{I_{xx}} + \frac{acc_x M}{A} \tag{8.14}$$

Table 8.14: Final propellant tanks dimensions

Propellant	Tank Radius [m]	Tank Length [m]	Tank Thickness [mm]
N2O4	0.5	0.05	1.8
MMH	0.5	0.04	1.8

where acc_y is the lateral launch acceleration in m s^{-2}, acc_x is the axial tensile acceleration in m s^{-2}, I_{xx} is the area moment of inertia in m^4 and A is the cross-sectional area of the structure in m^2. At the same time the critical buckling load can be determined using the following equation from SMAD (Wertz et al., 2011):

$$\sigma_{cr_{buckling}} = 0.61\left(-0.901\left(1 - e^{1/16\sqrt{r_{tank}/t}}\right)\right)\frac{Et}{r_{tank}} \tag{8.15}$$

with r_{tank} and t as described before and E=113.8 × 10^9 Pa is the Young's Modulus of the Ti-6Al-4V alloy. Computed these critical loads, it was checked if they had a magnitude below 90% of the yield stress of the selected material to have some safety margin in case any unexpected loads are encountered during operations.

The last step of the analysis is to determine if the idealised structure can withstand the vibrational loads of the rocket launch. This can be determined by checking that the natural frequency of the structure is outside the critical ranges specified by the launch catalogue. In the case of Falcon Heavy, the lateral frequency should be above 10 Hz and the axial frequency should be above 25 Hz[10]. If the structure is assumed to be a beam with a mass placed at its tip, its natural frequencies can be computed using eqations from (Wertz et al., 2011):

$$f_{ax} = 0.160\sqrt{\frac{AE}{m_{AV}L + 0.333m_{orb}L}} \qquad f_{lat} = 0.276\sqrt{\frac{EI}{m_{AV}L^3 + 0.236m_{orb}L^3}} \tag{8.16}$$

where m_{av} is the mass of the atmospheric vehicle on top of the orbiter and m_{orb} is the mass of the orbiter, both in kg. The final structure axial and lateral frequencies end up being, respectively, 27 and 1067 Hz.

Finally, the final dimensions of the propellant tanks are presented in Table 8.14: The spherical caps of the propellant tanks are surrounded by thin plates to have interfaces and protection for the other orbiter subsystems. These will present the same minimum thickness as the tanks and will lead the structure subsystem's total mass to 49.3 kg. With the total mass, the total cost of the subsystem can be derived, this consisted of the material cost (42.795 $/kg[11]) and the development cost which can be estimated from SMAD (Wertz et al., 1999). The total cost results in M€ FY22 2.3.

All the calculations presented above were completed using a design tool generated by the CAELUS team which was thoroughly verified and validated. First, a Pycharm built-in tool was run to fix all low-level bugs and typos that could not be seen when analysing the methods at a higher level. Then, the correctness of every method and its integration was analysed with the use of unit and system tests. Finally, as a validation of the code, the same design inputs and constrained presented in (Muhammad et al., 2010) were inserted in the code and the returned tanks' mass was compared with the study. This validation test was passed by the algorithm since an error of only 6% was computed and it probably derives from the fact that in the presented paper, the same hoop stress formula was used for the cylindrical and spherical tanks (resulting in a doubled spherical caps thickness) to be more conservative in the calculations.

8.8 Thermal Management

In this section, the thermal management of the CAELUS space system will be analysed. Before beginning the detailed design, multiple subsystem requirements have been identified, listed in Table A.10 and presented below.

In summary, the Orbiter Thermal Management subsystem shall

- Maintain the payload at a temperature of 283 K during operations.
- Have an emissivity not exceeding 0.05.
- Have an absorptivity of at least 0.42.
- Stay within the mass, power and cost budget with a reliability of 99.9%.
- Keep the orbiter subsystems within their operating temperature ranges.

[10] URL:https://www.spacex.com/media/falcon-users-guide-2021-09.pdf [cited 15/06/2023].
[11] URL:https://www.navstarsteel.com/titanium-grade-5-sheet.html [cited 16/06/2023]

The designed orbiter will be travelling to Uranus for many years and in the meanwhile will encounter two different planets. As a result, first, the orbiter thermal management will be designed for the operational conditions at Uranus, and then some heat dissipation strategies will be developed to handle the situations when the orbiter is closer to the Sun. The requirements of the thermal subsystem flow down from the main science requirement, CNRS01, the mission lifetime requirement CNRS03, and the driving reliability requirement from ESA, ESA04.

The thermal balance of the spacecraft can be investigated using the thermal balance equation from SMAD (Wertz et al., 2011):

$$\dot{Q}_{absorbed} + \sum P_{dissipated} = \dot{Q}_{emitted} \tag{8.17}$$

where $\dot{Q}_{absorbed}$ is the flow of energy coming to the spacecraft from outer space, $P_{dissipated}$ is the heat dissipated by the various power devices on board the spacecraft and $\dot{Q}_{emitted}$ is the power emitted by the spacecraft during operations. All these quantities are in W. The absorbed power consists of three different components: the solar radiation coming directly from the Sun, the solar radiation reflected by a certain planet (albedo radiation) and the infrared energy radiated by the planet itself. First, the Sun radiation, which depends on the distance of the spacecraft from the Sun, can be computed with:

$$J_s = \frac{P}{4\pi d^2} \tag{8.18}$$

where P=3.856 × 10^{26} W is the total power emitted by the Sun and d is the distance between the orbiter and the Sun. This quantity will change throughout the transfer phase and will be at a minimum value when the spacecraft reaches Uranus. Differently, the albedo radiation can be identified using:

$$J_a = aJ_sF \tag{8.19}$$

where a is the albedo factor as presented in the ECSS-E-ST-10-04C standard (ESA, 2008) (which equals 0.15 for Mars, 0.52 for Jupiter and 0.51 for Uranus), J_s is the solar radiation computed with Equation (8.18) and F is the visibility factor which represents the ratio between the orbit (or gravity assist) radius and the planet radius. As for the solar radiation, also this quantity will change based on the nearest planet to the orbiter and the solar radiation coming directly from the Sun. Third, the planet flux can be computed using:

$$J_{IR} = \sigma T_{IR}^4 F \tag{8.20}$$

where σ=5.67 × 10^{-8} W/m^{2}K^4 is the Boltzmann constant, T_{IR} is the effective radiating temperature of the planet given by the ECSS-E-ST-10-04C standard (ESA, 2008) (which equals 210.1 K for Mars, 109.5 K for Jupiter and 58.2 K for Uranus) and F is as presented above.

Looking at Equation (8.17), the other parameter that can be computed is the emitted heat flux ($\dot{Q}_{emitted}$), which can be calculated with:

$$\dot{Q}_{emitted} = \epsilon\sigma A_e T^4 \tag{8.21}$$

where ϵ is the emissivity of the orbiter structure material, $A_e = 2\pi r_{orbiter} l_{orbiter} + \pi r_{orbiter}^2$=5.2 m^2 is the emitting area, T is the operating temperature required in the spacecraft in K, which can be determined based on the operational conditions of the payload on board, σ is as defined previously. Finally, with all the formulas defined above, the thermal balance equation can be rewritten as:

$$\alpha_s J_s A_i + \alpha_s J_a A_i + \epsilon_{IR} J_{IR} A_i + \sum P_{dissipated} = \epsilon\sigma A_e T^4 \tag{8.22}$$

where α is the absorptivity of the spacecraft material, A_i=$l_{orbiter} d_{orbiter}$=1.5 m^2 is the projected area receiving the solar, albedo and IR radiations and all the other parameters are as defined before. With Equation (8.22), the power required to maintain the payload at its operational condition can be computed for the different phases of the mission. The most important one is at Uranus, which is also the condition in which the spacecraft will be in the coldest environment possible. To determine an appropriate thermal management plan for operations, the orbit apoapsis was considered since it would lead to the lowest possible albedo and IR radiation encountered throughout the entire mission. Before starting the calculations, it is important to determine what type of multilayer insulation will be used because it highly influences the thermal balance. Due to the large distances from the Sun, the orbiter will need insulation that allows a very high absorptivity and very low emissivity. As a result, after a thorough literature review, aluminised Kapton foil was selected because it presented the highest absorptivity to emissivity ratio and due to its usage in previous space missions[12]. Its inner metal layer blocks the heat to be dissipated away from the spacecraft with $\epsilon = 0.05$, while the external golden polyimide film makes sure that all possible external radiations are absorbed ($\alpha = 0.42$). Consequently, the calculation result

[12]URL: https://solarsystem.nasa.gov/missions/cassini/thermal-blankets/ [cited 21/062023].

in an absorbed power of 3.28 W, an emitted power of 133.8 W and a required thermal power of 130.6 W to heat up the spacecraft. This amount of heat can be generated by the spacecraft RTGs which, due to the power generation inefficiency, emits 4500 W each. As a result, using the same relation presented in Equation (8.18), the distance between the RTG and the orbiter can be computed as 2.7 m.

With the thermal plan just described, the spacecraft will have the ability to maintain nominal temperatures during operations at Uranus, even in the worst-case scenario. Nevertheless, during the transfer phase, the spacecraft will be a lot closer to the Sun and therefore it will absorb radiation with higher magnitudes than the ones at Uranus. As a result, if the RTGs are kept in the same position for the entire mission, a radiator will be needed to dissipate the exceeding heat. The values of the exceeding heat will be 215.4 W at Mars and 19.53 W at Jupiter. These values are very different, therefore it was decided that the spacecraft will have a deployable radiator that leads to nominal conditions at Mars and then use louvres to limit its performance throughout the mission. Louvres are metal strips paced upon the radiator whose hinge is forced to open or close by a torque generated by a specific thermal heat. As a result, such elements will be designed to close as the spacecraft temperature goes down while travelling further away from the Sun.

After determining the thermal plan necessary for the different phases of the mission, the total weight of the thermal subsystem can be determined. Regarding the radiator, a deployable unit can radiate 180 $W\,m^{-2}$ and has a surface density of 15 $kg\,m^{-2}$. As a result, to dissipate the amount of power required at Mars, the total radiator mass will be 50 kg. The louvres are assumed to be a 1 mm thick aluminium plate, therefore their mass results in 11.4 kg. Finally, the Kapton foil mass can be computed as 8 kg using a density of 1550 $kg\,m^{-3}$ and a thickness of 1 mm[13]. The total mass of the subsystem ends up being 69.8 kg. The last step in the analysis is to calculate the price of the subsystem. This consists of the material price of the material plus the manufacturing price which, using a relation presented on SMAD based on past missions, results in a value of M€ FY22 2.65.

8.9 Sensitivity Analysis

The last step in the overview of the orbiter is to perform a sensitivity analysis of the generated design. In the case of the orbiter design tool, the main inputs are the mass of the atmospheric vehicle and the total ΔV for transfer and operations, while the main output is the total wet mass. Applying the same relative change to any of these parameters (10%), the operational ΔV comes up to be the most relevant with a change in the wet mass of 5%. This is a very important result because it shows CAELUS that the amount of manoeuvres that the orbiter can complete during the operational phase is limited by the consequent increment in mass and the launcher payload mass constraint. Another aspect that was investigated was the maximum mass the glider and aeroshell architecture could have to still have a feasible mission (therefore complying with the launcher requirements). After multiple iterations of the orbiter design tool, the highest atmospheric vehicle mass was found to be 4000 kg.

For the communications, another sensitivity analysis was performed. The effect on the signal-to-noise ratio was checked when certain parameters were increased by 10%. The parameters that were increased were the transmitted power, the distance between the spacecraft and Earth, the orbiter antenna size and the data rate. This resulted in an increase or decrease of 5.1%, -10.3%, 8% and -5.2% respectively. It was also checked what the effect was of using the DSN 70-meter antenna instead of the 34-meter one. This resulted in an increase in the signal-to-noise ratio of 77.9%.

Regarding the structure, the main input of the design of the subsystem is the propellant mass. In fact, this influences the geometry of the tanks and consequently their mass. By increasing the propellant, the tanks will become either more cylindrical and tall or more spherical and wide. As a result, there will be a certain quantity of propellant which will not be acceptable anymore because it would lead to a tank geometry which does not fit in the payload fairing of the selected launcher.

[13] URL: https://www.dupont.com/content/dam/dupont/amer/us/en/ei-transformation/public/documents/en/EI-10175-Kapton-100CRC-Data-Sheet.pdf [cited 16/06/2023].

PART IV

ASSEMBLY, OPERATIONS, AND ORGANISATION

9. Complete Configuration

Before the assembly, operations, and organisation is discussed, it is useful to give a complete overview of the space system. Section 9.1 gives a summary of each system. Then, Section 9.2 covers the reliability budget. Finally, Section 9.3 present the final cost budget.

9.1 Systems Summary

With the design of the orbiter, glider and capsule described in detail, it is beneficial to summarise the most important values of these subsystems. The overview will be given in the same order as each system was presented and discussed in this report.

9.1.1 Glider

The glider carries a net flux radiometer, a nephelometer, an atmospheric structure instrument, a mass spectrometer, a tunable laser spectrometer and a radio science experiment; as explained in Section 4.1. To process the data obtained from the payloads analysing the Uranian atmosphere, three rad-hard RAD720 OBCs are used, resulting in a total bit rate of 2251 bit s^{-1}. To communicate with the orbiter, a one-way link using a frequency 405 MHz, and no compression of the data is established. Moreover, to allow communication at a large range of angles from boresight, an omnidirectional quadrifilar helix antenna with a maximum angle from boresight of 70°, a transmission frequency of 330 MHz, an antenna efficiency of 55 % and a pointing loss of −0.12dB. Lastly, a margin of 4 dB for the signal-to-noise ratio and a loss of 45 % were considered for the link budget, yielding a total power of 160 W. To estimate the aerodynamic characteristics of the glider, various analyses using XFLR5 with 150 panels, at a density of 0.05 kg m^{-3} and a kinematic viscosity of 2.25×10^{-5} m^2 s^{-1} were performed. To maximise the gliding capabilities of the atmospheric vehicle, which has no active control, a FX62-K-153/20 airfoil, for the main wing, and a NACA0012 airfoil, for both the horizontal and vertical stabiliser, were selected. Furthermore a wing area of 2.12 m^2, with an aspect ratio of 26.2 , a span of 7.45 m, a mean chord of 0.302 m, no quarter chord sweep, a taper ratio of 0.4 and root and tip chord of 0.407 m and 0.163 m, respectively, were chosen. This allowed for the determination of the time of flight and glide range, which were found to 4 d, 1 h and 12 min, and 8541 km correspondingly. For the structures and materials, an aluminium alloy Al-Cu 2024 and a titanium alloy Ti-6Al-4V were chosen, where, per the ECSS-E-30 stands, a safety factor of 1.3 was added to any thickness estimations and a factor of 1.1 applied to stress estimations. This resulted in a fuselage length of 1.68 m, a fuselage diameter of 0.7 m, a fuselage thickness of 1 mm, a wing thickness of 1.4 mm and a total mass for the glider structure of 110.3 kg. A summary of these masses can be found in Table 9.1b. Additionally in Table 9.1c shows the resulting position of the glider CM and the non-zero moments of inertia of the glider. Lastly, the power required for thermal management was found for a payload operating temperature of 276.5 K and a subsystem temperature of 283 K. From the subsystems, the minimum power generation at all times was determined to be 5.234 W, for which a Radioisotope Heating Unit, using the isotope americium-241, having a half-life of 430 yr and a mass of 360 g, is used. Moreover, the remaining 8.76 W will be generated by heating elements onboard the glider. Finally, for the total flight time of 97.25 h and the time between separation and entry being 20.7 h, the total, required energy storage is 31.3 kW h, and 227.7 W h, respectively, for which a battery of specific energy of 710 W h kg^{-1} was selected. An outline of the glider power budget can be found in Table 9.1a. In Chapter 4, the electric power diagram for the glider can be found. Similarly, the software and communications diagram was implemented for the glider-orbiter architecture in Chapter 8.

The glider has a skin of aluminium. This skin envelops most of the other systems. First of all, the net flux radiometer and nephelometer have parts that protrude out of the nose of the glider, to be exposed to the atmosphere. Second of all, both transmission antennas protrude out of the top of the fuselage. All other components are fully inside the structure. The core of the nephelometer and net flux radiometer, other instruments and batteries are inside a thermal isolation blanket. The inside of this isolated environment has temperature regulation by a radiative heating unit. This environment was positioned to locate the centre of gravity in the correct location. The battery system was not included in the render as it is too spread out into small sections. The glider presented in the technical drawings was implemented using a model from externals[1] and can be found in Figure 9.1 and Figure 9.2.

9.1.2 Capsule

Next, the capsule design is summarised. Its purpose is to protect the glider during entry, and eventually deploy it in the atmosphere. Its heat shield has a thickness of 5.98 cm and is made up of PICA material. During entry,

[1] URL: https://www.cgtrader.com/3d-print-models/hobby-diy/mechanical-parts/glaser-dirks-dg-100 [cited 27 June 2023].

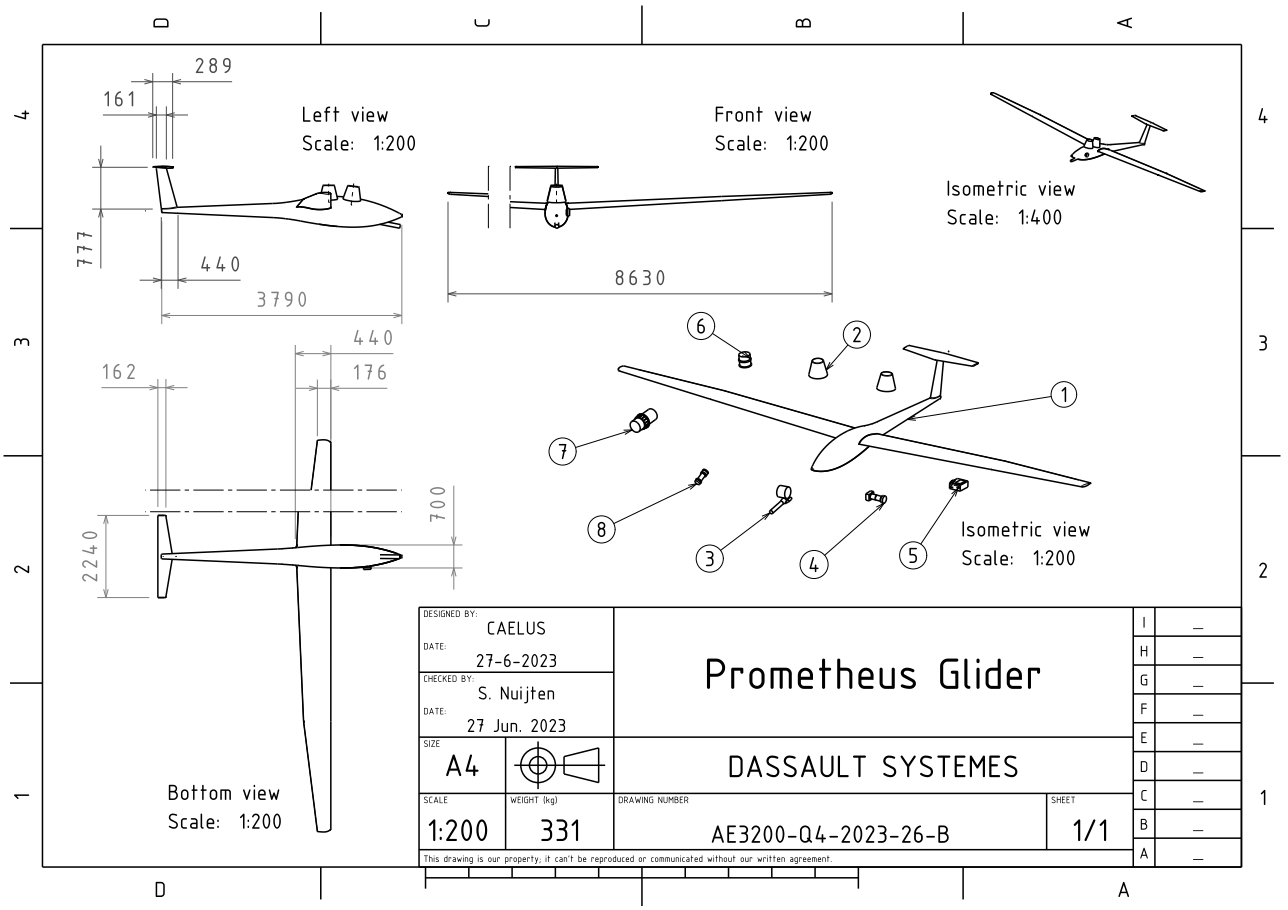

Figure 9.1: Technical drawing of the Prometheus glider

it will deploy its supersonic parachute, which will happen at Mach 2.0. As a backup to the glider, the parachute will have a diameter of 11.2 m, as to descend over the 20 bar in 4 h. The parachute is made up of the PIA.C-44378 Type III fabric. The mass of the different subsystems can be found in Table 9.2. The elements with the highest mass are the glider and the offset stability. Furthermore, to ensure the stability of the capsule, a small mass of 38.2 kg has to be added. Finally, it will deploy the glider into the atmosphere of Uranus.

The capsule has two main elements. First of all, there is the thermal shield at the bottom. The backshell is attached to the top. At the top of the backshell, the parachute is installed. The technical drawing of the entry capsule can be found in Figure 9.3. Inside of the capsule, the glider is mounted with its wings folded in half. The glider is held in place by the glider deployment subsystem.

9.1.3 Orbiter

Finally, the orbiter mass budget is presented in Table 9.3b. As expected, the atmospheric vehicle and the propellant mass contribute the most to the total mass of the orbiter. The shape of the orbiter should also be considered. Overall, the orbiter has a cylindrical form with a radius of 0.5 m and a length of 2 m. Furthermore,

Table 9.1: Glider power and mass budgets

(a) Glider power budget

Subsystem	Value [W]
Structure	0
Communications	181
Payload	95.8
Data Handling	32.2
Power	0
Thermal	14
Total	***323***

(b) Glider mass budget

Subsystem	Value [kg]
Structure	243.4
Communications	1.4
Payload	28.2
Data Handling	0.5
Power	57.1
Thermal	0.2
Total	***330.8***

(c) Inertial Parameters

Inertia	Value [kg m^2]
I_{xx}	633.5
I_{yy}	279.7
I_{zz}	892
I_{xz}	41.57
Centre of Mass	**Value [m]**
x_{cg}	0.971
y_{cg}	0.000
z_{cg}	0.083

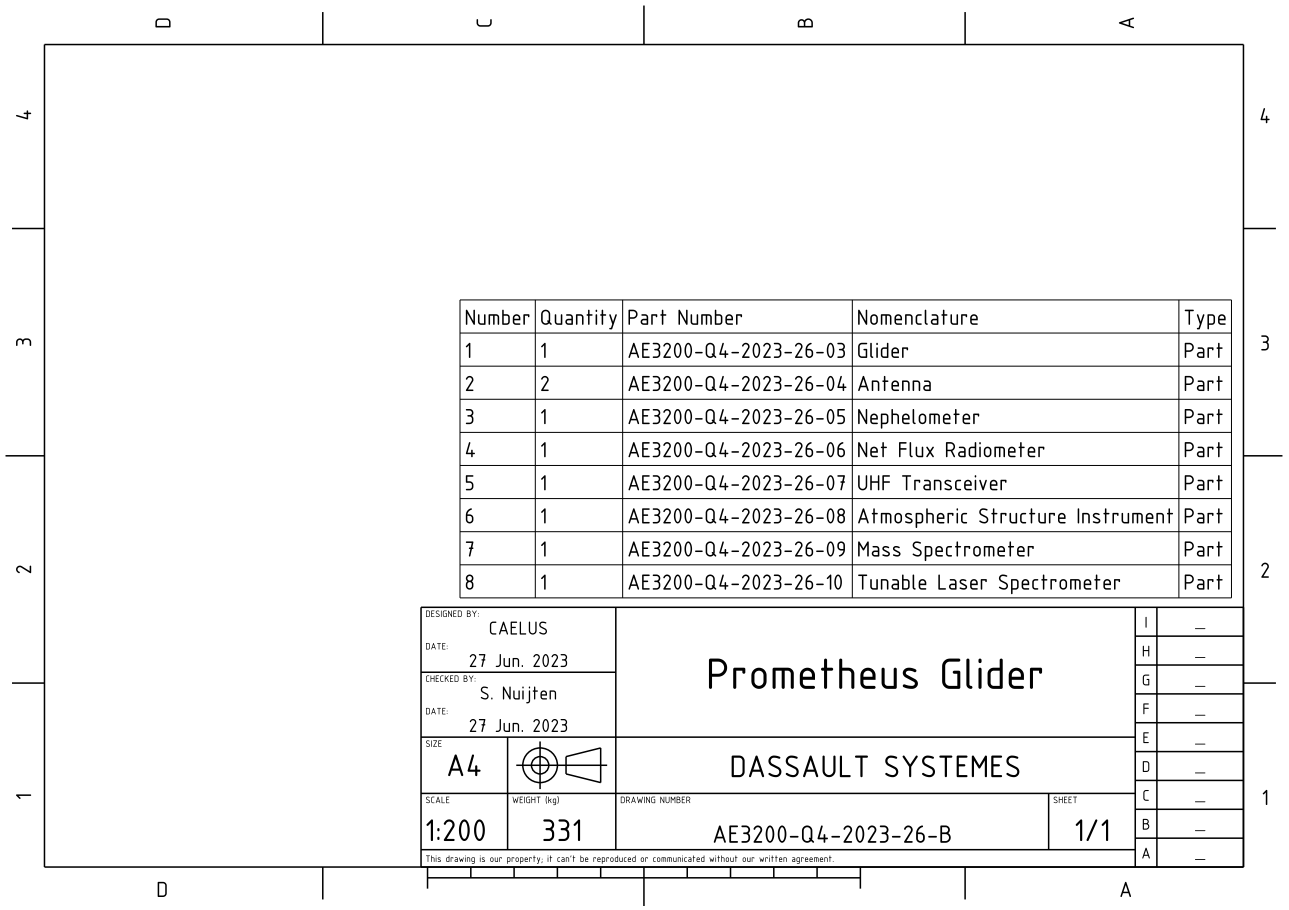

Figure 9.2: Technical drawing of the Prometheus glider

Table 9.2: Capsule mass budget

Subsystem	Value [kg]
Thermal Shield	232
Structure	41.6
Decelerator	57.3
Off-set Stability	152.2
Glider Mass	330.8
Total	***813.9***

it has an antenna with a diameter of 4.0 m(Presented in the render using the 3D model from NASA[2]) and it will perform two gravity assist. Its ADCS system determines and adjusts its orientation over the course of the mission. Its power source is three RTGs that use plutonium-238 as their source. The power required for the specific subsystems can be found in Table 9.3a. As expected the communications and the payload subsystems require the most power, 116.6 W and 147.1 W, respectively. The power and communication diagram of the orbiter can be found in Chapter 8.

The core of the orbiter is made up of 2 fuel tanks incorporated into a cylindrical structure. The three RTGs are mounted on poles on the side of the cylinder. These poles are used to reduce the heating effect of the RTGs on the rest of the orbiter. The high-gain antenna is mounted on the other side of the cylinder. At the end of this, one of the low-gain antennas is mounted. The other low-gain antenna is mounted on the same side as the RTGs. At one end, the thruster is mounted. On the other end, the capsule is mounted during the interplanetary phase. The magnetometer is mounted to extend between the capsule and the antenna. The gyroscope, present inside the spacecraft configuration, was implemented using a model for externals[3]. Similarly, the sun sensors were implemented in the orbiter[4]. The technical drawing of the Herschel orbiter can be found in Figure 9.4.

[2]URL: https://solarsystem.nasa.gov/resources/2401/cassini-3d-model/ [cited: 27 June 2023].
[3]URL: https://grabcad.com/library/gyroscope-with-dynamic-simulation-1 [cited 27 June 2023].
[4]URL: https://satsearch.co/products/tensortech-fss-15-fine-sun-sensor [cited 27 June 2023].

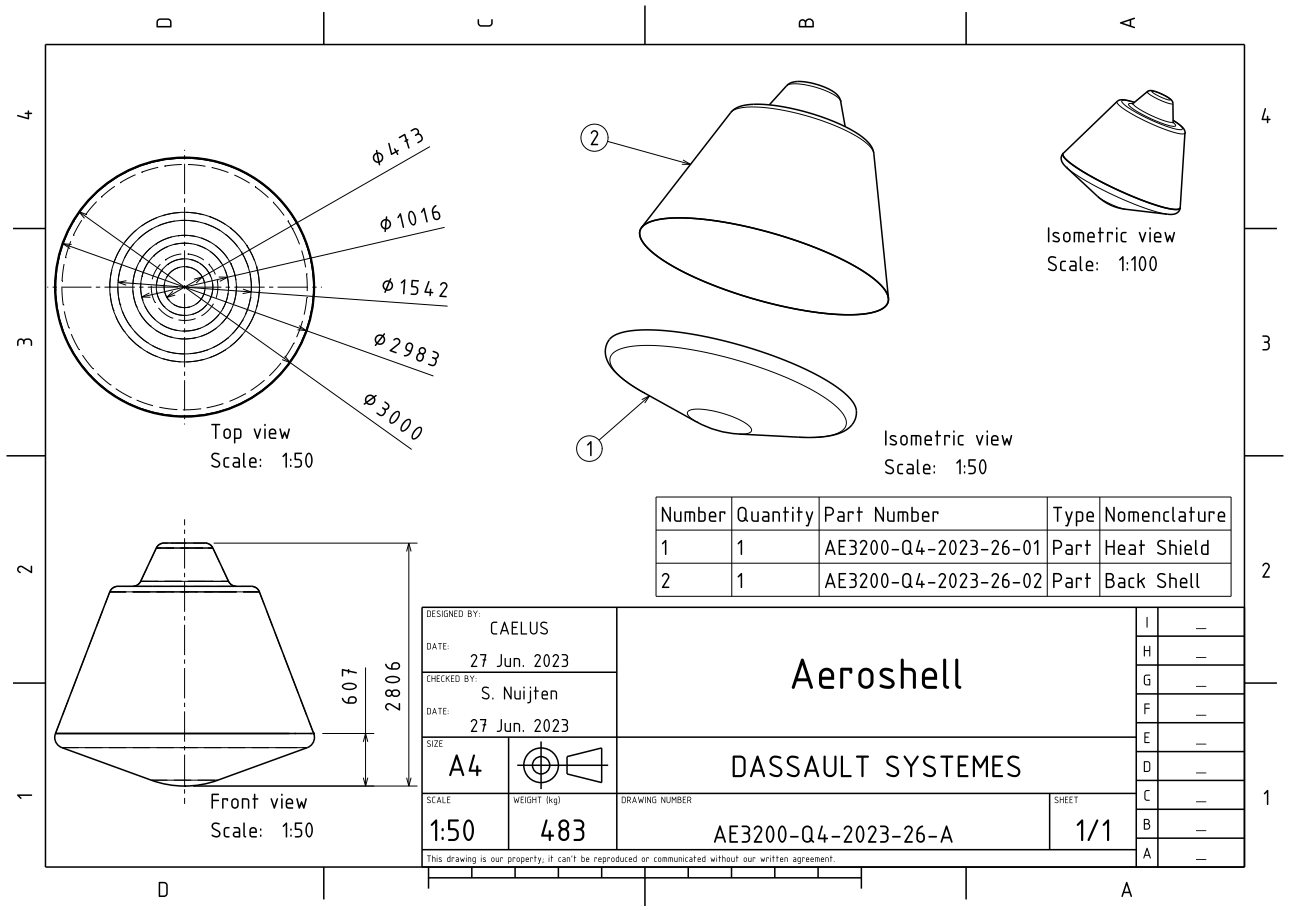

Figure 9.3: Technical drawing of the entry capsule

Table 9.3: Orbiter power and mass budget

(a) Orbiter power budget

Subsystem	Value [W]
Structure	0
Communications	116.6
Payload Instruments	147.1
Data Handling	46.6
ADCS	87
Power	23.05
Thermal	11
Propulsion	35
Total	***466.3***

(b) Orbiter mass budget

Subsystem	Value [kg]
Structure	49.3
Communications	121.1
Payload Instruments	75.3
Atmospheric Vehicle	813.9
Data Handling	1
ADCS	51.7
Power	217.1
Thermal	70.3
Propellant	923.8
Total Dry (w/ 25% Margin)	1785.3
Total Wet	***2709***

9.2 Reliability Budgets

The system has a required reliability of 95 %. Considering that an atmospheric mission into the Uranian atmosphere has never been done before, and only one mission has entered the atmosphere of a gas giant, significant importance should be placed on the reliability of the entire system. To assist in this, a reliability budget has been made. Here, the minimum reliability of all subsystems of the orbiter, glider and capsule was established.

For the orbiter, more previous designs exist and more proven systems can be referenced. Therefore, this section of the system is considered the most reliable. According to SMAD (Wertz et al., 2011), after 10 years, the parts most likely to cause failure are either TT&C or the Attitude control. For TT&C, a backup low-gain antenna is included in the mission. In addition, the main antenna has already been used in a deep space mission, namely Cassini (Taylor et al., 2002). These factors increase the reliability of the system. With regard to attitude control, several redundant components are used. In addition, all components have been used many times in a

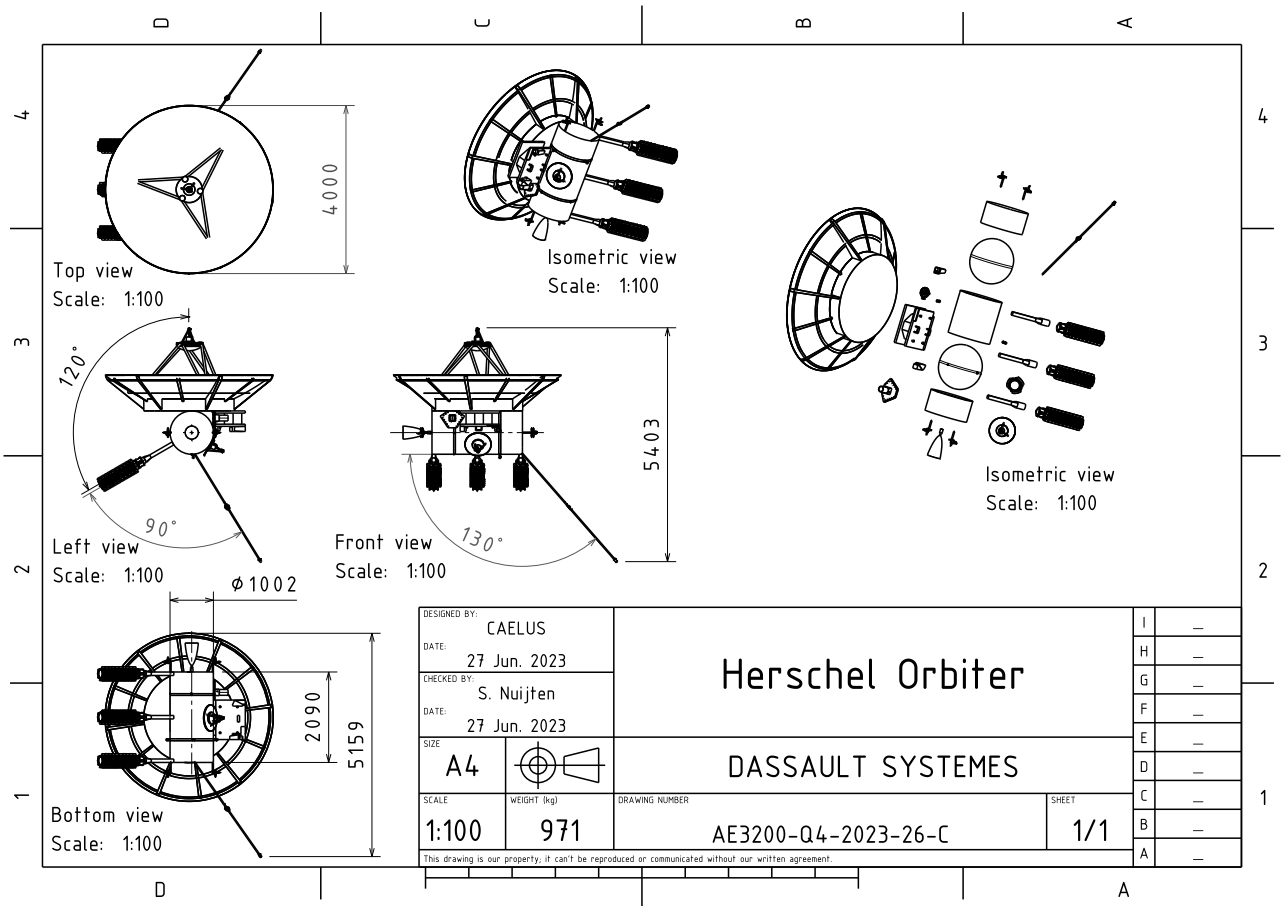

Figure 9.4: Technical drawing of the Herschel orbiter

Table 9.4: Reliability characteristics

(a) Reliability budget of the orbiter

Subsystem	Reliability[%]
Structure	99.99
Communications	99.90
Payload Instruments	99.90
Data Handling	99.5
ADCS	99.95
Power	99.99
Thermal	99.90
Electronics	99.99
Propulsion	99.99
Total orbiter reliability	**99.43**

(b) Reliability budget of the capsule

Subsystem	Reliability[%]
Heat shield	99.50
Decelerator	99.00
Glider deployment	99.90
Structure	99.99
Total capsule reliability	98.31

space environment. Some other causes of failure are the electrical system and thruster and fuel system. With regard to the electrical system, the RTGs have already been used in a space environment. Furthermore, one RTG could fail without causing a deficit of power. With regard to the thruster system, the thruster has already been used in a mission to the outer planets. These considerations lead to the reliability allocations given in Table 9.4a

The entry into the Uranian atmosphere is one of the moments of great risk. Only one previous mission has entered the atmosphere of a gas giant, meaning that there is little experience concerning this area. Some notes can be taken from re-entry capsules for Earth, or capsules designed for Mars or Venus. These are dissimilar, however, as the entry velocities are lower, the uncertainties about the atmosphere are lower and the time of travel is lower. Especially the risk of any damage to the heat shield is a dangerous prospect. Secondly, proper functioning of the decelerator is required for the successful deployment of the glider. Therefore, the reliability budget for these components is lower. the reliability budget for the capsule is given in Table 9.4b.

While on Earth, gliders are well understood, the situation for a glider on Uranus is different. The atmo-

Table 9.5: Reliability budget of the glider

Subsystem	Reliability[%]
Power	99.50
Structures	99.50
Data handling	99.90
Communications	99.50
Thermal management	99.50
Electronics	99.99
Control	99.50
Payload	99.90
Total glider reliability	97.32

Table 9.6: Cost Budgets

(a) Orbiter Cost Budget

Subsystem	Value [M€ FY22]
Structure	2.3
Communications	39.2
Data Handling	41.4
ADCS	45
Power	437.1
Thermal	2.65
Propulsion	0.69
Launch	150
Operations	236.8
Assembly	12.9
Total Hardware	581.3
Total (with 20% margin)	***1162***

(b) Glider Cost Budget

Subsystem	Value [M€ FY22]
Structure	7.2
Communications	0.3
Data Handling	41.4
Thermal	0.04
Power	1.8
Total (with 20% margin)	***61***

spheric conditions are not only very different but also not entirely known. In addition, the glider will be stored in the capsule for over 16 years, with its wings folded up. Specifically, the lateral control, power, structure and communication subsystems are expected to face difficulties. The lateral control will not be actively controlled, but will still be important for maintaining the flight path angle, ensuring the glider doesn't descend too quickly or exceeds its flight envelope. For the Uranian atmosphere, this design is expected to face more risks. The power subsystem will operate in an atmosphere that is too cold for it. While it will be protected by the thermal subsystem, it is still expected to face significant risks. The structure shall face the aerodynamic forces, that will be difficult to model with great certainties. In addition, the wind gusts will cause significant challenges for the structural design. The communication subsystem, too, is expected to face difficulty due to the atmosphere. These considerations lead to the reliability budget given in table 9.5.

9.3 Cost Budgets

After the design of the different subsystems was completed, the cost of the orbiter, glider and capsule could be computed with a bottom-up cost estimation. All the costs are presented in Tables 9.6a and 9.6b. All the presented values were determined either by searching off-the-shelf components' costs or by computing the material cost and adding a manufacturing cost taken from SMAD (Wertz et al., 2011). Regarding the capsule, the components were very specific, therefore their cost was very difficult to estimate. As a result, its overall cost could be determined based on previous planetary entry capsules (Galileo and Huygens) as M€ 600. The CAELUS team understand that this value is very high and probably not correct since the technologies improved from the Galileo and Huygens missions. Anyways, since the total mission budget is lower than the 2.5 billion euros set by ESA, the cost of the aeroshell should fit inside the budget. Another element that influences the total cost is the operations which have been further analysed in Section 10.2. Table 9.6 shows the mission cost budget, where the total cost for the orbiter is estimated by adding the launch, operations, assembly, and total hardware costs and applying a 20 % margin to the value found as presented in the NASA Green Book. In the cost budget, the cost of the payload is not included because it was determined from a private conversation with Dr. Lebreton, that ESA does not pay for the scientific instruments for their own missions. As a result, if the payload cost exceeds the amount of money NASA will contribute to the Ouranos mission, CAELUS will have to look for external sources of income, such as private companies, universities, or scientific institutions. The total cost of the scientific instruments should range between M€ FY22 500 and 1000, from a private meeting

between Dr. Lebreton and the team. Finally, as can be seen in Tables 9.6a and 9.6b and adding a capsule cost of M€ FY22 300, and a payload cost of M€ FY22 500, it can be determined that the total mission cost will be M€ FY22 2428.

10. Project Management

In this chapter, the project management aspects of the Ouranos mission are analysed. Section 10.1 details the reliability, availability, maintainability and safety traits of the selected design. Section 10.2 and Section 10.3 describe the operations and logistics and the production plan respectively. Finally, Section 10.4 and Section 10.5 detail an analysis of the sustainability aspects of the mission and the Gantt chart reflecting the mission timeline, respectively.

10.1 RAMS Characteristics

This section will discuss the Reliability, Availability, Maintainability, and Safety (RAMS) characteristics of the selected design. First, the reliability will be discussed in Section 10.1.1, then the availability in Section 10.1.2, the maintainability in Section 10.1.3 and finally the safety in Section 10.1.4.

10.1.1 Reliability

Reliability: ”The probability of an item to perform a required function under given conditions for a given time interval” (ECSS, 2012). The reliability of the glider, aeroshell, and orbiter has been discussed in Section 9.2.

10.1.2 Availability

Availability: ”Ability of an item to be in a state to perform a required function under given conditions at a given instant of time or over a given time interval, assuming that the required external resources are provided” (ECSS, 2012). It is of more interest to look at the availability of the individual subsystems than at the total system, since the design will be used once. Because the design has a long mission duration with limited support from outside, the total system should have an extremely high availability once it is completely assembled. The availability of the subsystems is mainly determined by them being off-the-shelf or custom designed. Off-the-shelf components and subsystems will always be preferred due to the cost decrease. This also results in better availability because custom-designed subsystems will only have availability once they are produced. However, delays could occur when an item is not available in time.

Glider

The glider requires little development time. Most of the subsystems, for example, do not require new technologies. The payload does have limited availability. However, due to the selection of instruments that have been used on past missions, the development time of these is still limited. The only component that is relatively new, is the RHU. This component is still under development and thus has limited availability. However, the americium-241 for the RHU is easily available because it is used on an industrial scale. The structure of the glider needs to be custom-made. This type of structure is nevertheless often made which results in it still having a high availability.

Aeroshell

The structure needs to be custom-made. It is a standard type of structure, thus it still has a high availability. The thermal management components have a lower availability. The gel between the heat shield and the rest of the structure is relatively hard to find and the heat shield itself also has a lower availability. Another component that is limited available is the parachute. There are not that many companies that produce custom-made parachutes for this purpose. Thanks to the collaboration with NASA, the availability of the components that are needed for thermal control and to decelerate the aeroshell increases.

Orbiter

The payload on the orbit has limited availability but limited development time as well, just like the glider. Most other subsystems have high availability. They are either easy to produce even though they are custom-made or they are off the shelf. The only other subsystem with limited availability is the power system. The scarcity of plutonium-238 was discussed in Equation (8.8).

10.1.3 Maintainability

Maintainability: ”Ease of performing maintenance on a product” (ECSS, 2012). Due to the spacecraft being physically isolated from the ground station, it is impossible to perform maintenance on the hardware when the spacecraft is launched. Errors in the software can be present and stay undetected until after the launch, but they can also get introduced due to space radiation. Better software updates could get developed while the

spacecraft is already in space. The ground station can then send data to the spacecraft to check, repair, or update the software[1].

However, physical maintenance of the hardware is still possible while on Earth. During the assembly process, it is necessary to check the performance of the different systems and subsystems to ensure that they are working as intended. It could be that a system gets damaged due to the assembly process, or the reliability over time decreases quicker than expected. Maintenance could detect this and ensure that proper actions are taken. A component can then get replaced in time to minimise delays and to ensure the proper functioning of the complete assembly.

Glider
The subsystem on the glider with the lowest maintainability is the structure. Due to the integration of the other subsystem in and on it, maintenance would require removing other subsystems as well. This requires time, but should not be too complicated. The only component that would be difficult to maintain is the RHU. Due to the radiation, extra safety measures need to be taken into account when people need to be close to it.

Aeroshell
The things that mostly make maintenance of the aeroshell difficult, are the explosives that are used to release the parachute and the heat shield. They should be handled with extra care. Maintenance of the heat shield itself is also difficult. Repairing or replacing of one part usually means the replacement of the total heat shield, due to the parts being glued to each other. The remaining part of the structure is easy to maintain.

Orbiter
Maintenance of the orbiter is similar to that of the glider. Maintaining the structure is easy, but also often requires the removal of other subsystems. The orbiter has components that require extra care as well, the RTGs. They are also radioactive and require extra safety measures during maintenance. The workers need to be shielded from the radiation when they are close to the RTGs.

10.1.4 Safety
Safety: ”State, where an acceptable level of risk is not exceeded” (ECSS, 2012). Possible risks for the spacecraft and how they can be mitigated are discussed in Section 3.6. However, the spacecraft itself could pose risks to the environment as well. The highest risks are present before and during the launch. During the production phase of the spacecraft, possibly dangerous situations or exposure to harmful substances could occur. These risks are all at acceptable levels due to proper precautions. If a launch failure would occur, the negative effects of possible debris are limited due to the location of the launch sites. The direction of the launch is always such that debris would fall into water or areas with a low population density. At higher altitudes, most of the spacecraft will burn up which lowers the risks as well. To prevent contamination of other celestial bodies, the spacecraft is also carefully sterilised. All the safety measures thus ensure the safety of the spacecraft and the environment.

Glider
The main components on the glider that could cause harm to the environment, are the RHUs. When the radioactive material gets exposed, it poses possible safety issues. This risk however is low due to the high amount of safety testing (Barco et al., 2022) and regulations. The glider itself is not quickly affected on Earth because it is built to withstand harsh conditions.

Aeroshell
The explosives that are used to release the parachute and the heat shield, are the main components that could cause harm. It is hard to detonate them but proper caution should be used at all times to minimise the possible risk of detonation.

Orbiter
The radioactive RTGs could harm the environment as well. When this radioactive material gets exposed, it also poses risks. This risk however is extremely low due to the high amount of safety measures (Kastenberg & Wilson, 2004). The hydrazine onboard is highly toxic but it is easier to handle.

10.2 Operations and Logistics
This chapter will focus on the operations and logistics that are necessary to support the CAELUS mission. The first is linked to the functions that the spacecraft has to perform and the way the scientific data are transmitted

[1] URL: https://www.esa.int/esapub/bulletin/bullet91/b91deni.htm [cited 25/05/2023].

back to Earth while the second is mostly related to the facilities and activities to be implemented on Earth. In this chapter, the logistics will be discussed before the operations to follow what is the real timeline of the mission.

When talking about logistics, the first thing that has to be analysed is the testing facilities necessary to understand if the designed systems fulfil the generated requirements. As a result, CAELUS will use the European Space Agency (ESA) testing facilities at the European Space Research and Technology Centre (ESTEC at Noordwijk, The Netherlands) for the tests of the main orbiter and glider subsystems and integration, which consist of a clean room, various test stands and environments and the Phoenix thermal vacuum chamber[2]. Regarding the capsule, its test campaign will be partially conducted at ESTEC, but development testing can be performed at the Langley Research Centre due to the expertise of the personnel, who worked on the Orion capsule[3], and the state-of-the-art wind tunnel. Moreover, to complete the parachute testing, the National Full-Scale Aerodynamics wind tunnel facility will be required because of the size of the parachute to be inflated (11 m) and the many different flow conditions that can be simulated in such state-of-the-art facility(Zell, 1993). Once the testing phase has been completed and all systems have been integrated successfully, the spacecraft needs to be delivered at the Kennedy Space Centre (KSC) four weeks before launch as described by the Falcon Heavy User Manual (X, 2021). The transfer of all the hardware can be done via air link using the Space Shuttle landing strip at KSC. Space X will be in charge of moving the spacecraft to the Horizontal Integration Facility (HIF). The HIF will be used to complete the final checkouts and to integrate the system into the rocket launcher. Space X will be in charge of such a process but a member of the CAELUS team will supervise the entire operation.

After integration with the launcher, the main logistics that still need to be analysed are related to communication and operations. Three main facilities are critical and these are the Spacecraft Operations Control Centre (SOCC), the Payload Operations Control Centre (POCC) and the Mission Control Centre (MCC). All of these will be located at the European Space Operations Centre (ESOC at Darmsdat, Germany) since ESA is the main customer. Also since the main scientific customer is from Europe, a data user room will be set up at the MCC to allow a more smooth information flow. Moreover, since the launch site is quite far away from the MCC, an additional SOCC will be set up at the Launch Control Centre at KSC, and this will be responsible for final checkouts and first in-orbit checks after launch. After that, the responsibility will shift to the ESOC facilities. The communication between the two centres will be constant and can be implemented using ESA L-sat geostationary satellite constellation as reported in SMAD (Wertz et al., 1999). Another important aspect is the redundancy of the operations facilities. In case a failure occurs at ESOC, it is important to have the possibility to still communicate with the space systems. As a result, NASA's Christopher C. Kraft Jr. Mission Control Centre in Houston will act as a redundant MCC, SOCC and POCC. Finally, the last facility required for this mission will be all the ground station locations of the deep space network and VLBI which will allow to communicate constantly with the spacecraft throughout the whole mission.

Finally, the operations behind the CAELUS mission can be analysed. These consist of all the people and activities necessary to make the spacecraft and atmospheric vehicle fulfil the pre-selected functions and mission objectives. Throughout the mission, a very different amount of people will be required to work at the MCC, SOCC and POCC depending on the phase of the mission. The most crowded phases will be the launch and early mission operations due to the many checks and in-orbit tests, the two fly-bys at Mars and Jupiter where many measurement data will be gathered and finally during operations at Uranus. This last phase will be the longest one, therefore leading to a very high operational cost.

The complexity and the cost of operations can be estimated at a high level by looking at four main mission elements: the mission design, the payload and spacecraft design, the communications and ground system design and operational risk policies. The more complex these architecture segments are, the more complex and expensive the operations will end up being. As described in the previous chapters, even though the mission objectives are well defined, the mission timeline ends up being very complex due to the presence of multiple phases, many one-time-only activities and the presence of the new space environment. Similarly, the system and payload design ends up being very complex since many different sensors and instruments will be required and a high amount of new technologies will be implemented. Different are the risks policies and the ground systems design. The fact that the spacecraft is so far away from Earth and travels for so many years, makes downlinks and uplinks a lot more rare. At the same time, the delay in communications will require the spacecraft to be autonomous when it comes down to errors and risk handling. As a result, both these elements will be less complex.

Using SMAD (Wertz et al., 2011), the total cost of operations can be estimated using Level-of-Effort estimating techniques. This takes into account the following elements:

- Project Management and System Engineering: assumed to be 15% of the total operations cost.
- Space software maintenance: the cost can be estimated using the formula $Cost_{s/w} = Salary_{eng} n_{SLOC}/16000$. With $Salary_{eng}$ being the salary of one single engineer and n_{SLOC} being the number of single lines of code.

[2]URL: https://www.esa.int/Enabling_Support/Space_Engineering_Technology/Test_centre/Phenix_Thermal_Vacuum_Chamber [cited 18/062023].

[3]URL: https://www.nasa.gov/feature/wind-tunnel-testing-prepares-orion-for-return-to-earth [cited 19/06/2023].

- Mission operations: assuming on average through the entire mission the presence of eight engineers and four technicians with an annual full-time equivalent cost of, respectively, € FY22 268K and 201K.
- Ground hardware and software maintenance: the cost can be estimated using the formula $Cost = Salary_{tech} n_{SLOC}/16000$. Where $Salary_{tech}$ is the salary of a technician and n_{SLOC} is as defined before.
- Facilities: assuming a cost of € FY22 1.7K per square meter with a facility of 1000 m^2

The number of lines of code can be determined to be 59000 using the relations presented in (Wertz et al., 2011). This is the worst-case scenario, therefore when no line of code is actually recycled from previous missions. As a result, the software and ground hardware maintenance can be computed to be M€ FY22 1.

With the cost described above, the cost per year of mission for operations will be derived to be 5.6 M€/year. Moreover, another additional cost will come from the ground station maintenance through the mission years, which from (Wertz et al., 2011) results in $M_{ground} = 2.01 M_{dh} = 83.2$ M€ FY22. Finally, with a total mission duration of 20 years, including the transfer phase of the operations at Uranus and the extended mission phase, a total operations cost of M€ FY22 244.

10.3 Production Plan

In this section, the production plan, for the manufacturing process of the orbiter and atmospheric vehicle, is analysed. The systems selected for the Ouranos mission present different structural elements:

- Glider wing
- Glider fuselage
- Glider T-tail
- Backshell Structure
- Thermal Shield
- Orbiter Structure

The processes behind the production of each of them will now be analysed in more detail.

First, the glider wing. This is made of four skin panels (two for the right and two for the left half wing), and four wing ribs and should be made of Ti-6Al-4V. Two manufacturing processes will be used for the two elements due to the different structural characteristics and geometry. Regarding the wing skin, these are flat panels that can be manufactured using separation by mechanical removal from a bigger panel with constant thickness. In fact, this last one is not required to change through the span of the wing as presented in Section 4.5. Once the separating process is completed, post-processing should consist in removing any type of burr or inaccuracy at the edges of the panels by sanding. Differently, the ribs of the wings should be a lot thicker and with a very specific and complex shape. As a result, in this case, extrusion will be used to apply to the fluid metal alloy the commonly used ”I” cross-section. For this specific process, it is very important to take into account the shrinkage of the material, therefore the mould should be made bigger than the final required dimensions. Both the processes described for the wing require very little time and people and they are both very cheap. In fact, separating will only require cutters and paper sand which are commonly available, and extrusion can use machines that are already implemented in aircraft manufacturing, therefore cutting the cost of tooling. Once the skin panels and the ribs have been manufactured, they have to be assembled together. First of all, the two skin panels can be linked using Frictions Stir Welding and the ribs can be connected to the skin using common welding.

The next structural element that should be investigated is the glider fuselage. This is a cylindrical thin-walled structure made of Al-Cu-2024. To achieve the curved shape required, rolling manufacturing can be used and material after the metal sheet has been separated. In case during rolling, a too-long sheet is found, cutting or milling can be used to remove such inaccuracies. Moreover, the sheet after rolling can be closed using friction stir welding or common welding techniques. With the same process, the nose of the fuselage can be connected to the cylindrical section. This manufacturing process could not be too accurate therefore it is very important to take into account any possible spring back of the metal. Moreover, due to the small dimensions of the fuselage, the entire structure can be made out of one single metal sheet.

Thirdly, the production of the glider T-tail should be analysed. Due to the similarities between loads and geometry, the same manufacturing processes used for the wing can be applied to this structure. The use of the same type of process allows for saving time and improving the quality of the product since the workers will be already used to the required tasks and actions.

The next structure to be analysed is the backshell of the aeroshell. This is a structural element that will go through very high aerodynamic, pressure and thermal loads, therefore choosing the right manufacturing process is critical. Due to the presented load case scenario, the structure should be made an integral structure to avoid any heat or cracks propagating through the backshell. As a result, the only manufacturing method that can be used is metal forming, where a personalised mould should be created for this specific occasion. Nevertheless, since different thicknesses are necessary at different locations of the backshell, forming should

be implemented with the maximum necessary thickness and then machining can be applied in the specific sections that should be more lightweight. This manufacturing process is very specific to the type of product that the Ouranus mission requires, for example, a personalised mould will have to be designed, and this will make the manufacturing costs of the backshell a lot higher than other elements.

Regarding the thermal shield, the required manufacturing process can be determined based on previous deep space missions or entry capsules. More specifically, due to the similarity between the type of panels that will be used in the Ouranos missions and the Space Shuttle (Phenolic/Nylon based), the manufacturing process can be derived from such a system (Dulak & Cecka, 1970). In the presented paper, the required processes are described in more detail and it consists of two parts: production of the panels and assembly. During the first, curing will be performed to achieve the necessary densities and strength to withstand thermal loads while surface dressing and spraying to protect the material from external chemical agents. Once this is completed, the different panels can be linked together using high thermal glues. Based on the size and number of tiles of MSL, it could be estimated that the Ouranos mission will require 43 thermal panels for its aeroshell.

Finally, the orbiter structure has to be produced. As presented in Section 8.7, it was decided to make it an integral structure with the propellant tanks. Since this is an element that is commonly used in the space industry, its manufacturing can be addressed by a private company. In this case, the process used will be casting since the tanks have a significant size and thickness. As for the extrusion in the wing ribs, while performing casting, it is very important to take into account the material shrinkage including some allowance. Before casting can be performed, a personalised mould should be designed to avoid hot tears, gas spots and other inaccuracies in the material. Moreover, since the tanks are made of spherical caps and cylindrical sections, friction stir welding will be required to connect such curved and non-curved parts (Meisnar et al., 2023). Due to the high availability of the material and the highly used manufacturing process, the cost of the process should not be too high. Moreover, the manufacturing time will be kept low because the casting process will not require more than a couple of hours.

10.4 Sustainability

This chapter discusses the sustainability aspect associated with the Ouranos mission within the final design phase. Section 10.4.1 discusses the impact of sustainability on the mission, reflected in the requirements. Following this, the impact on the sustainability of the final design phase is analysed in Section 10.4.2. Then in Section 10.4.3, the manufacturing aspect of the mission and its impact on sustainability is analysed. This is followed by a discussion on the launch vehicle selected and its sustainability, in Section 10.4.4. Next, in Section 10.4.5, the sustainability of the end-of-life phase of the mission is discussed. Finally, in Section 10.4.6, the impact of operation and logistics on the overall sustainability of the mission is examined.

10.4.1 Impact on Requirements

Similarly to what was mentioned in the midterm report, some of the requirements set for the system took sustainability into account. From the midterm report, their feasibility when applied to the Ouranos mission was explored. Starting from requirement ESA03, stating ”The usage of toxic materials shall be minimised”, a reformulation into a constraint from the original customer requirement of complete disallowance to minimisation of their use was done. This reflects its infeasibility based on the use of protective coatings for the atmospheric vehicle to resist the damaging environment of Uranus, although it does have the positive impact of reducing the mass of the atmospheric vehicle since the least amount of protective coatings will be used. Moreover, the use of limit testing for the protective coating can be further used to determine the need for their use or to avoid over-using protective coatings. However, depending on whether this testing is destructive or not, it could have a negative impact since destructive would lead to higher material wastage.

On the other hand, ESA03.05 states that it will be ensured that all external contractors will implement sustainable manufacturing methods. This reflects a positive impact on the sustainability of the mission since it does not influence the design of the systems but rather ensures the sustainability of their manufacturing. The only other requirement that could be considered problematic during the baseline report was ESA03.07, which states ”The launch vehicle shall be reusable”. After the final design was performed, the total launch mass was found to interfere with this requirement. This is due to the fact that the total amount of ΔV required to perform the required interplanetary trajectory is too high. As such, the use of a Falcon rocket, which is the most prominent re-usable launch vehicle, in its expandable configuration was eliminated. The remaining requirements were found to not have any impact on the sustainability of the Ouranos mission. It should be noted, however, that the impact is minimal for both requirements.

10.4.2 Design Phase

Moving on to the design phase impact, it is important to note that the decisions made during the design phase significantly impact the overall sustainability of the final mission design. This is due to the fact that some parts of both the mission phase and system trade-off process made use of sustainability as a trade-off criterion. In

the case of the mission phases, sustainability was especially prominent for the interplanetary trajectory and the end-of-life potential of the mission. Meanwhile, sustainability was viewed as a separate criterion for the system design, especially when considering the trade-off between kick stage vs no kick stage, chemical vs electrical propulsion, the manufacturability of the different atmospheric vehicles, and the end-of-life potential of the different space systems and atmospheric vehicles.

Starting with the trade-off between having a kick stage and no kick stage, the presence of a kick stage would imply an increased amount of fuel. This would imply that, depending on the type of fuel used, the sustainability of the interplanetary trajectory would worsen if a kick stage was present as more fossil fuels would have to be used. As such, since no kick-stage was selected for the final design, the influence on the sustainability of the mission due to this design choice can be said to be reduced when compared to the option of having a kick-stage.

Moving on to the trade-off between chemical and electrical propulsion, similar to what was said previously for the trade-off between kick-stage and no kick-stage, the impact on sustainability would depend on the type of fuel being used (fossil fuel or not). If fossil fuel is to be used, then the impact it would have on the mission would be bigger than electrical propulsion. It should be further noted, however, that depending on the ΔV required for the interplanetary trajectory, the amount of fuel required would vary and its availability would also have an impact on the sustainability.

In the case of the Ouranos mission, the final design choice for the type of propulsion system to be used and the type of fuel being used by such a system is chemical propulsion using monomethylhydrazine and nitrogen tetroxide. From this, it is possible to see the negative impact the choice of propulsion system has sustainability since both compounds, especially hydrazine, are extremely toxic to the Earth's environment.

Furthermore, the power required to operate the orbiter and its payload is obtained from three RTGs, requiring 33 kg plutonium-238. This has a negative effect on the sustainability of the mission since plutonium-238 is a scarce and radioactive material meaning that not only its production but also its decay will affect the Earth's environment, especially when such large quantities are required.

10.4.3 Manufacturing

Continuing with the impact of the manufacturing phase, this will be similar to what was described in the baseline report and midterm report. The atmospheric vehicle, the orbiter, and their combination are very complex systems. However, the clear outlier in this is the atmospheric vehicle since the manufacturing of space systems, such as the orbiter, has a very high manufacturing readiness level due to decades of space exploration. The problem with the manufacturing of the glider system is that it is a very novel concept, therefore, not having many previous manufacturing experiences to refer to. However, when looking into Earth-based aircraft, it can be noted that the manufacturing of aircraft and gliders is very well developed. This would make the manufacturing of the atmospheric vehicle more sustainable, due to the amount of time spent on optimisation of the manufacturing processes. Furthermore, due to the novelty of the design, it should be noted that extensive testing at conditions similar to the mission conditions will have to take place. As such, multiple scaled models will have to be built and tested, hence increasing the amount of material used but also allowing for further refinement of specific manufacturing processes. In the case of the manufacturing plan of the Ouranos mission systems, since their structural characteristics are extreme, the processes used will result in a lot of material waste. This will have a negative impact on the sustainability of the mission.

10.4.4 Launch Vehicle

As mentioned above, by choosing the correct launch vehicle the overall sustainability of this project can be vastly increased. With the burning of the fuel, the launcher has one of the most direct and visible effects on Earth's environment. However, it should be, simultaneously, recognised that the selection of launchers might be very restricted due to the payload mass and ΔV required for the chosen interplanetary trajectory. Taking the above into consideration, the most obvious launchers are SpaceX's Falcon launcher series as they have been specifically developed to return to Earth and, after inspection, used in subsequent launches. Although from a fuel point of view, this would not necessarily be more sustainable than other launchers, it would heavily impact the other use of Earth's resources, as it prevents a new launcher from being built after every launch. At the same time, these launchers have an expendable configuration allowing for a higher ΔV and, thus, payload mass to be launched, which would imply that the stages have no re-usability. This is similar to other launchers considered (Ariane 5, Atlas 5 551) in the trade-off process, hence heavily impacting the overall sustainability of the mission. Moreover, the Ariane 5 launch vehicle uses liquid hydrogen and oxygen as a fuel, which in itself is a clean fuel, as it does not produce any CO_2 when burned. This would imply that it would be a more sustainable option than the expendable Falcon launchers since those use RP1 and liquid oxygen. In the case of the final design choice for the Ouranos mission, since a Falcon-heavy, expendable launch vehicle was selected, the effect on the sustainability of the mission is negative.

10.4.5 End-of-life Phase

Moving on to the end-of-life phase of the Oruanos mission, both the mission and system concepts are generally similar. Hence, to consider the impact on sustainability, the potential of the end-of-life phase of both the mission and system concept selected after the trade-off was analysed.

To perform the analysis, a differentiation was considered between the space part and the atmospheric flight part. For the space part, the possibility of secondary scientific missions was considered. This is dependent on the final orbit around Uranus since different secondary missions will be possible. In the case of the Ouranos mission, the final orbit selected is highly elliptical with an apoapsis at 240 000 km. This would allow for the exploration of the two moons, Miranda and Ariel, as a secondary mission through flybys, thus, having a positive impact on the sustainability of the mission. Furthermore, separate from the secondary mission of the orbiter, its disposal was also considered. In the case of the orbiter, it was concluded that it will most likely burn up in the atmosphere, however, the method chosen for de-orbiting could be done via a burn or aerobraking (drag de-orbiting). Since aerobraking was the method chosen for the de-orbiting of the orbiter of the Ouranos mission, when compared to a de-orbit burn, it can be said to have a positive impact on sustainability since it would allow for an extension of the orbiter's lifetime and, therefore, for a secondary mission while not needing any extra fuel. This is reflected by requirements CNRS04.01 and CNRS03.05, stating that an extended mission shall be defined should the system exceed nominal life and that the EOL phase mission phase shall last at least 10 years, respectively.

In the case of the atmospheric segment, however, different aspects were taken into consideration. In this case, the potential for a mission extension is the most critical impact the end of life will have on sustainability. This aspect is dependent on the combination of the flight profile and the atmospheric vehicle selected. Since the flight profile chosen is one of gradual descent while the atmospheric vehicle chosen is a glider, the possibility of a secondary mission is more likely than a rotorcraft and orbiter or blunt body and orbital combination. This is due to the fact that no active propulsion and control mechanisms are present in the glider, meaning that the duration of the mission becomes a design variable and, thus, it becomes possible to design for an extended mission. A rotorcraft on the other hand would have to have an increased battery size, and therefore mass, to keep both the propellers and payload active during the extended mission. Furthermore, in the case of a blunt body, while the rate of descent can be controlled via the deceleration mechanism, the extent to which the mission duration can be customised, with respect to a glider, is much lower. Consequently, it can be said that the impact of the orbiter and glider combination on sustainability is the lowest out of all combinations considered for the trade-off. It should also be further noted that considering the fact that the mission being designed is effectively a flagship mission, it is of interest to have as many data points, with as much variation as possible. Therefore, both the glider and rotorcraft concept combinations yield a higher level of sustainability. However, when taking into consideration the argumentation above, it is clear to see that the glider concept's end-of-life phase impact on sustainability is the best out of all concept combinations considered. Similarly to the space segment, this is further reflected by requirement CNRS03.05, stating that the EOL phase of the mission shall last at least 10 years.

10.4.6 Operations and Logistics

As a final consideration, the operations and logistics of the Ouranos mission are analysed. The SOCC, POCC and MCC are all in the same location, however, when compared to a scenario where all three are at different locations, not much of a difference is seen in terms of the impact the location has on sustainability. This is due to the fact that the distance between the system while travelling en route to Uranus and at Uranus and the Earth is so much bigger than the hypothetical distances between control centres if they were to be separate, that any increase in resource usage brought about by this distance is negligible. As a further point of reflection, the testing facilities to be used for the orbiter and glider are located in Europe, whereas the parachute and development testing of the capsule is to be performed in America. Therefore, when compared to a scenario where all testing would occur in Europe, a smaller carbon footprint is created as the number of systems to be transported to the KSC is smaller.

10.5 Gantt Chart

This report has presented the preliminary exploration of what it would take to send a space mission to Uranus to take in-situ atmospheric measurements. The further phases of realising the Ouranos mission lay ahead, and are detailed in Figure 10.1. The Gantt chart starts with the work already done, which is the mission analysis and identification, feasibility analysis, and preliminary design. The next phase is the detailed design, where the entire mission and system architecture are defined down to the level of detail required for production. The phase that follows is the Qualification and Production phase, where first the subsystems are produced and thoroughly tested. When they pass their tests they shall gain qualification. After subsystem qualification, the subsystems are integrated into the spacecraft system. This is again followed by another round of extensive testing to certify the entire system. After the end of the certification process, the preparations for launch start.

Four weeks before launch the spacecraft is integrated into the launcher fairing. On 18 February 2031, 10 years after Perseverance arrived at Mars, the Ouranos mission is kicked off by its launch from Earth. It will arrive at Mars on May 21st for its first planetary flyby. The next leg will take until September 17th 2033 when the spacecraft arrives at Jupiter, after which it slingshots around, taking another 14 years to travel to Uranus. 20 days before the closest approach of Uranus, the spacecraft splits into the orbiter and capsule. The capsule will enter the atmosphere and deploy the glider. At this point, the atmospheric mission starts. It lasts four days, in which the orbiter receives data when in view of Earth. When not receiving data from the glider, the orbiter will start transmitting data to Earth. When the atmospheric mission is done, the orbiter continues on a secondary mission of the Uranus system, including visits to the moons, on April 1st, 2047. When this 36-month mission is done, and the spacecraft is still operational, an extended mission is possible. At the end of the extended mission, the orbiter is de-orbited and disposed of in the atmosphere of Uranus.

ID	WBS	Start	Duration
1		Mon 4/24/23	1 wk
2	A	Mon 5/1/23	4 wks
3	B	Mon 5/29/23	5 wks
4	C	Mon 7/3/23	32 mons
5	**D**	**Sat 3/21/26**	**1736 days**
6	D.4	**Sat 3/21/26**	18 mons
7	D.1	Thu 9/30/27	6 mons
8	D.2	Mon 4/3/28	4 mons
9	D.6	Sat 8/5/28	14 mons
10	D.5	Sat 10/13/29	8 mons
11	D.7	Tue 6/18/30	6 mons
12	F	Sat 12/21/30	4 wks
13	**E**	**Tue 2/18/31**	**10544 days**
14	E.1	Tue 2/18/31	10 mins
15	**E.2**	**Tue 2/18/31**	**5883 days**
16	E.2.1	Tue 2/18/31	92 days
17	E.2.2	Wed 5/21/31	1 day
18	E.2.3	Thu 5/22/31	849 days
19	E.2.4	Sat 9/17/33	0.65 days
20	E.2.5	Sat 9/17/33	4919 days
21	E.2.6	Thu 3/7/47	0 days
22	E.2.7	Thu 3/7/47	21 days
23	**E.3**	Wed 3/27/47	**15 days**
24	E.3.1	Wed 3/27/47	15 mins
25	E.3.2	Wed 3/27/47	5 mins
26	E.3.3	Wed 3/27/47	3.9 days
27	E.3.4	Sun 3/31/47	0 days
28	**E.4**	**Wed 3/27/47**	**139 mons**
29	**E.4.1**	**Wed 3/27/47**	**4 days**
30	E.4.1.1	Wed 3/27/47	50 mins
31	E.4.1.2	Wed 3/27/47	14 hrs
32	E.4.1.3	Wed 3/27/47	12 hrs
33	E.4.1.4	Thu 3/28/47	8 hrs
34	E.4.1.5	Thu 3/28/47	14 hrs
35	E.4.1.6	Fri 3/29/47	12 hrs
36	E.4.1.7	Fri 3/29/47	9 hrs
37	E.4.1.8	Fri 3/29/47	14 hrs
38	E.4.1.9	Sat 3/30/47	12 hrs
39	**E.4.2**	**Wed 3/27/47**	**36 mons**
40	E.4.2.2	Wed 3/27/47	7.2 mons
41	E.4.2.3	Tue 11/5/47	7.2 mons
42	E.4.2.4	Mon 6/15/48	7.2 mons
43	E.4.2.5	Sun 1/24/49	7.2 mons
44	E.4.2.6	Sun 9/5/49	7.2 mons
45	E.4.5	Sat 4/16/50	1 day?
46	**H**	**Wed 1/1/59**	**1 day**
47	H.1	Wed 1/1/59	1 day?

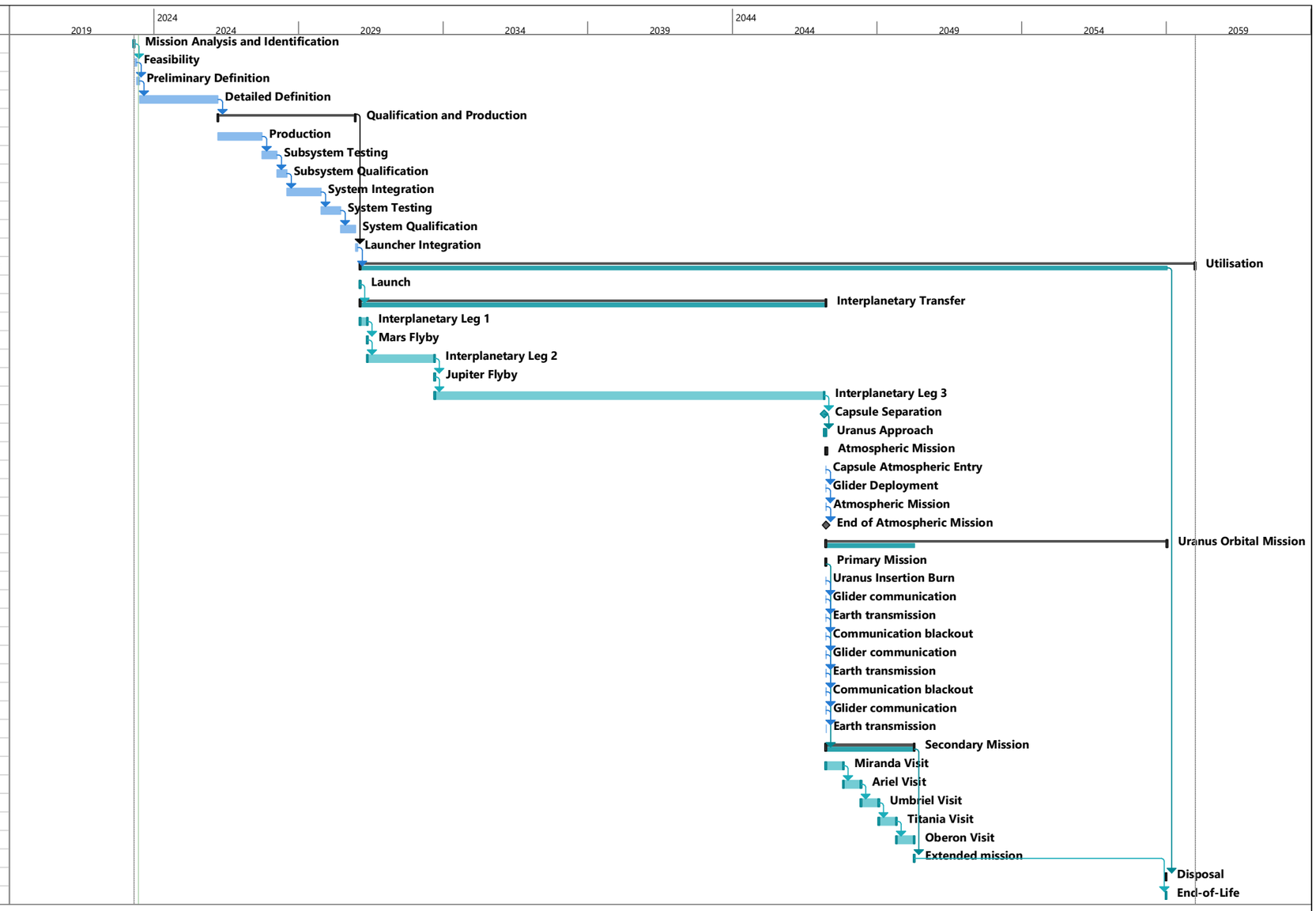

Project: Ouranos Mission Plann
Date: Wed 6/21/23

Task	Project Summary	Manual Task	Start-only	Deadline
Split	Inactive Task	Duration-only	Finish-only	Progress
Milestone	Inactive Milestone	Manual Summary Rollup	External Tasks	Manual Progress
Summary	Inactive Summary	Manual Summary	External Milestone	

Page 1

Figure 10.1: Gantt Chart for the Ouranos mission, from first development to mission termination

11. Conclusions and Recommendations

After presenting the different analyses of the glider, orbiter and aeroshell, it is important to summarise the results and present the recommendations. This is done in Section 11.1 and 11.2 respectively.

11.1 Conclusions

The scientific community has indicated that a mission to Uranus would greatly expand the understanding of both the planet itself and the formation of the solar system. After missions to Mercury, Venus, Mars, Jupiter and Saturn, a mission to Uranus will next push the boundary of our knowledge of our solar system. This report documents the design proposal of a mission to Uranus that shall perform detailed in-situ measurements of the atmosphere to fulfil this need. This will further the knowledge of the Uranian system and by extension the solar system, with orbital measurements.

To fulfil the need for this mission, a trade-off of both the system and mission concept has been performed in a previous stage of the design. This resulted in the selection of a custom orbital platform, referenced in this report as the orbiter, and a glider. To protect the glider during atmospheric entry, a capsule was included in the design. For the mission concept, a gravity assist trajectory was chosen to reach Uranus. A gradual descent was chosen for the flight path inside the Uranian atmosphere. These concepts were further developed in this report.

In this report, both the design process and the outcome of this process for all relevant systems and subsystems are described. The result of these analyses is a design of an orbiter, entry capsule and glider with critical components already selected. These components indicate the main functioning of the systems involved in this system and provide the basis for any further design.

Out of all concepts, the glider provides the best opportunity to measure the atmospheric properties of Uranus. This is due to the fact that the glider has a minimum glide time of 4 days, making it possible to collect vast amounts of scientific data. Additionally, secondary science missions can be added to the primary mission. By using gravity assists, measurements of the passed planets can be done, as well as science missions within the Uranian system can be performed. Within the Uranian system, a margin of propellant allows for manoeuvres to gather science on Uranus and its rings and moons.

The outcome of this design is that the projected cost of this system is lower than the expected budget for this mission. This is in addition to the fact that the expected budget is lower than numerous other missions with a similar scope. In addition, the wet mass of the orbiter can be increased by over a ton, which means two things. Either the payload can be increased, or the total cost can be reduced. The latter could be done by selecting a partially reusable Falcon Heavy, which only expends the centre core. With either option, the design as outlined in this report demonstrates that this mission is not only feasible but has the potential for even better advancement of our understanding of both Uranus and the entire solar system.

11.2 Recommendations

Throughout the whole design process, many assumptions and simplifications had to be performed such that the final product could be finished within the time limit. In addition to that, many alternative solutions to certain design choices had to be discarded because of a lack of information on the current state-of-the-art. In this section, all these aspects are presented for all the subsystems where these choices were performed, together with some potential solutions that would make the design more precise.

With regards to the orbiter communication subsystem, for the communication between the orbiter and Earth, VLBI can be considered. By summing up the antenna areas, the effective diameter of these antennas combined can be found. The European VLBI network Ka-band antennas and the ones from the Pacific VLBI network have an effective diameter of 150 m (Jacobs et al., 2012). This increases the receiving gain to 92.8 dB. Because of this the data rate can for example be increased to 550 kbit s^{-1}. Another option is to decrease the compression rate to decrease the bit error. The effects can be further investigated to find the optimal configuration.

Regarding the orbiter propulsion subsystem, the use of the green monopropellant ASCENT could be considered, as it was discussed before. The problem with it was that there are no thrusters yet that can provide enough thrust for this mission. From the moment a 100 N thruster is developed, it can be considered to cluster four of these together and function as the main engine to provide enough thrust. If a 400 N thruster is developed, then just one would be enough to provide the thrust required. A second, redundant main engine should be considered because it might not be proven yet in spaceflight before the time the spacecraft is launched.

Speaking of the orbital tool, the interplanetary model assumes the planetary flybys are nodes, and thus simplifies these flybys. While the model has been verified, further analysis of this trajectory is recommended.

Furthermore, the verification showed that the optimisation had suboptimal convergence. Therefore, more gains could be achieved by further analysis and improvements of the optimiser. With regard to the orbits, the model assumed instantaneous manoeuvres. This is no problem for the initial manoeuvre, as here the conditions do not change quickly. However, for capture, the orbiter shall move a significant amount during the expected burn time. This could, however, also be used to change the argument of periapsis, which would have a positive impact on the communication windows. A more detailed analysis of this manoeuvre should be done. Furthermore, possibilities of gravity assist by the Uranian moons should be investigated, either to ease the capture around Uranus or to lower the ΔV cost of the later mission of the orbiter.

Moving on to the aeroshell, specifically, the heat shield, quite some recommendations could be made. First, Computational Fluid Dynamics (CFD) could be used to quantify the highest heat flux and locate its point of action. Following this, a non-constant thickness for the heat shield could be used depending on the heat flux simulated from CFD. After that, using an asymmetric heat shield could be investigated, which would give the capsule a non-zero lift coefficient. Linked to this, other materials might also be considered. Furthermore, micrometeorites have not been taken into account during the design: a risk analysis of their potential impact could be performed. Finally, the possibility of using the heat shield regression rate to measure atmospheric properties in the upper atmosphere shall be investigated.

Regarding the aeroshell parachute, deployment methods shall be investigated to finalise the design. Using a pilot chute could also be used to move the deployment of the main parachute to subsonic conditions, which would decrease the deployment loads. Alternatively, reefing could also be considered. After that, parachute clustering might be investigated to decrease risks. Finally, the use of tension cones shall be analysed for stability purposes.

Moving on to the glider, more specifically the power and communications respectively, one recommendation per subsystem can be appointed: regarding the first, RTGs could be considered as the power source for the glider once enough radioactive material would be available since it can not only provide a higher energy density but would also help the thermal management subsystem because it radiates quite some heat. Regarding communications, the RSE between the glider and Earth had to be discarded because of many factors, one being the large distance between Earth and Uranus: it could be reconsidered when the two planets are closer to one another.

The glider structural analysis required a lot of assumptions, and consequently, a lot of recommendations can be derived. First, horizontal and vertical stabilisers were not analysed because no tail loading could be found in due time; the analysis, however, would be very similar to the one performed for the wings, once the loading is found. Secondly, vibrational loads were not analysed due to time constraints, however, a good initial approach, especially for the wings, would be to assume the structure to be a cantilever beam and perform a basic natural frequencies analysis. The same applies to loads due to launch, atmospheric entry and deceleration. Many geometrical components and properties had to be neglected as well, such as the presence of ribs and stringers in the wings, and the effect of sweep and dihedral: they should all be taken into account for a safer and more complete result. Thirdly, in case during future iterations, the hoop stress due to pressure turns out to be the most driving, then it might be considered drilling holes on the wings structure to nullify the pressure difference, and hence the stress. A more detailed stress analysis would then have to be performed to quantify the peak stresses caused by the holes, together with the maximum size allowed for the holes. Fourthly, as explained already in Section 4.5, the effect of drag on the structure was neglected because of the much lower influence compared to the lift contribution: to perform a more complete design, the drag shall be quantified and its effects are taken into account in the structure. Fifthly, in the structural analysis of the glider, only single load cases were analysed, but no combination of different loads was analysed, which is what would actually happen in real life: this leads to an overall underestimation of the structure. To take this into account, the superposition of all the load cases shall be performed. Another very important aspect that had to be left out due to time constraints is the analysis of the load transfer between wings, tail and fuselage: that is something that should be seriously designed for since that is where usually peak stresses arise. As a final remark, to get more accurate results overall, non-symmetrical sections shall be used for the wings cross-section analysis, more detailed lift distributions shall be used (not rectangular), and a finite element analysis (FEM) shall be used to validate and confirm the results.

As a recommendation for the design of the thermal management of the glider, it is suggested to vary the thermal insulation such that the thermal power required in the vacuum and atmosphere is closer together: in this way, an RHU can take care of it, which would reduce the size of the batteries. In addition to that, an actual model using thermal nodes could be used to get more accurate results over the whole structure.

Regarding the glider aerodynamics, a wider range of airfoils should be investigated to further optimise the design. Furthermore, to make the stability analysis more comprehensive, all velocities and densities experienced throughout the time of flight should be considered rather than just the worst-case scenario. Finally, it is recommended to use CFD rather than XFLR5 to obtain more accurate estimations for the aerodynamic characteristics of the glider, since the influence of the glider body was not taken into consideration.

Concerning the cost estimations, it is recommended to estimate the capsule cost appropriately. This was

attempted by CAELUS, however, the value obtained was found based on previous missions. Therefore, although a realistic value was obtained, it is recommended to re-estimate this cost by considering the material costs as well as the labour and manufacturing costs involved with the production of the capsule. Additionally, cost estimations shall be analysed more in detail by e.g. performing bottom-up cost analyses.

The last recommendations are with respect to the payload: regarding the definition of cost, mass, power, and operational temperature, it shall be considered to contact the manufacturers for further information. From this, it can be assessed if further funding needs to be considered as NASA will not provide more than M€ 500. The same could be done for information with respect to the state-of-the-art instruments used, which are not published on the web yet.

Bibliography

Amalia, E., Moelyadi, M. A., Julistina, R., and Putra, C. A. (2018). Aerodynamics characteristics of glider GL-1 based on computational fluid dynamics. *Journal of Physics: Conference Series*, *1130*. https://doi.org/10.1088/1742-6596/1130/1/012006

Anderson, B. J., Acuña, M. H., Lohr, D. A., Scheifele, J., Raval, A., Korth, H., and Slavin, J. A. (2007). The magnetometer instrument on MESSENGER. *Space Science Reviews*, *131*, 417–450. https://doi.org/10.1007/s11214-007-9246-7

Aslam, S., Achterberg, R. K., Calcutt, S. B., Cottini, V., Gorius, N. J., Hewagama, T., Irwin, P. G., Nixon, C. A., Quilligan, G., Roos-Serote, M., Simon, A. A., Tran, D., and Villanueva, G. (2020). *Advanced net flux radiometer for the ice giants* (1). Springer. https://doi.org/10.1007/s11214-019-0630-x

ASME. (2019). *Rules for construction of pressure vessels 2019 ASME boiler and pressure vessel code an international code*. https://www.asme.org/shop/certification-accreditation.

Atkinson, D. H., Mousis, O., Spilker, T. R., and Ferri, F. (2020). *Reference model payload for ice giant entry probe missions* (8). Springer Science; Business Media B.V. https://doi.org/10.1007/s11214-020-00738-y

Atreya, S. K., Hofstadter, M. H., In, J. H., Mousis, O., Reh, K., and Wong, M. H. (2020). *Deep atmosphere composition, structure, origin, and exploration, with particular focus on critical in situ science at the icy giants* (1). Springer. https://doi.org/10.1007/s11214-020-0640-8

Barco, A., Ambrosi, R. M., Fongarland, C., Brunet, P., Guguin, Y., and Stephenson, K. (2022). Impact tests and modelling for the ESA radioisotope power systems. *Journal of Space Safety Engineering*, *9*, 56–71. https://doi.org/10.1016/j.jsse.2021.11.001

Batygin, K., Adams, F. C., Brown, M. E., and Becker, J. C. (2019). *The planet nine hypothesis*. Elsevier B.V. https://doi.org/10.1016/j.physrep.2019.01.009

Bauer, S. J., Block, B., and Israel, G. (1997). *The gas chromatograph mass spectrometer aboard Huygens*. https://www.researchgate.net/publication/4692494

Benafan, O., Moholt, M. R., Bass, M., Mabe, J. H., Nicholson, D. E., and Calkins, F. T. (2019). Recent advancements in rotary shape memory alloy actuators for aeronautics. *Shape Memory and Superelasticity*, *5*, 415–428. https://doi.org/10.1007/s40830-019-00260-3

Bennett, G. L., Lombardo, J. J., Hemler, R. J., Silverman, G., Whitmore, C. W., Amos, W. R., Johnson, E. W., Zocher, R. W., Hagan, J. C., and Englehart, R. W. (2008). The general-purpose heat source radioisotope thermoelectric generator: A truly general-purpose space RTG. *AIP Conference Proceedings*, *969*, 663–671. https://doi.org/10.1063/1.2845028

Bergmann, C. P., Malandruccolo, A., and Gialanella, S. (1998). *Topics in mining, metallurgy and materials engineering series editor: Aerospace alloys*. http://www.springer.com/series/11054

Bessette, É. (2022). *Mission analysis and navigation design for Uranus atmospheric flight*. http://resolver.tudelft.nl/uuid:f9686e4c-ba52-455d-8f78-8b7d75efa2af

Biscani, F., and Izzo, D. (2020). A parallel global multiobjective framework for optimization: Pagmo. *Journal of Open Source Software*, *5*, 2338. https://doi.org/10.21105/joss.02338

Bocanegra-Bahamón, T., Bracken, C., Sitjà, M. C., Dirkx, D., Gerth, I., Konstantinidis, K., Labrianidis, C., Laneuville, M., Luntzer, A., Macarthur, J. L., Maier, A., Morschhauser, A., Nordheim, T. A., Sallantin, R., and Tlustos, R. (2015). MUSE - mission to the Uranian system: Unveiling the evolution and formation of ice giants. *Advances in Space Research*, *55*, 2190–2216. https://doi.org/10.1016/j.asr.2015.01.037

Borgmeyer, S. C. (2019). *Chemical bi-propellant thruster family 10N, 200N, 400N*. https://www.satcatalog.com/component/s400-15-biprop-thruster/

Britting, T., Toussaint, W. L. J. R., Vukosavljević, K., Sujahudeen, M. S., Knöll, N. E., Pepermans, L., and Hadji, Y. P. (2022). *Selection criteria for parachutes of student-built sounding rockets*. Delft Aerospace Rocket Engineering.

Brown, M. E., and Batygin, K. (2021). The orbit of planet nine. *The Astronomical Journal*, *162*, 219. https://doi.org/10.3847/1538-3881/ac2056

Cappellin, C., Jørgensen, E., Meincke, P., Borries, O., Nardini, C., and Dreyer, C. (2015). *Detailed pattern computations of the UHF antennas on the spacecraft of the ExoMars mission*. https://www.ticra.com/detailed-pattern-computations-uhf-antennas-spacecraft-exomars-mission/

Castillo-Rogez, J., Weiss, B., Beddingfield, C., Biersteker, J., Cartwright, R., Goode, A., Daswani, M. M., and Neveu, M. (2023). Compositions and interior structures of the large moons of Uranus and implications for future spacecraft observations. *Journal of Geophysical Research: Planets*, *128*. https://doi.org/10.1029/2022JE007432

Chatterjee, B., and Bhowmik, S. (2019). *Evolution of material selection in commercial aviation industry*. Elsevier. https://doi.org/10.1016/B978-0-12-816564-5.00009-8

Clark, I. G., O'Farrell, C., Sackier, C. V., Karlgaard, C., Zumwalt, C. H., and Way, D. W. (2022). Reconstructed performance of the Mars 2020 parachute decelerator system. *IEEE Aerospace Conference Proceedings*, *2022-March*. https://doi.org/10.1109/AERO53065.2022.9843441

Czabaj, M. W., Zehnder, A. T., Davidson, B. D., and Singh, A. K. (2014). Compressive strength of honeycomb-stiffened graphite/epoxy sandwich panels with barely-visible indentation damage. *Journal of Composite Materials*, *48*, 2455–2471. https://doi.org/10.1177/0021998313499949

Dulak, R. E., and Cecka, A. M. (1970). *Low cost ablative heat shields for Space Shuttles*. Jet Propulsion Laboratory. https://ntrs.nasa.gov/citations/19800019917

Dustin, J. S., and Borrelli, R. A. (2021). Assessment of alternative radionuclides for use in a radioisotope thermoelectric generator. *Nuclear Engineering and Design*, *385*. https://doi.org/10.1016/j.nucengdes.2021.111475

Dyakonov, A. A., Schoenenberger, M., and Norman, J. W. V. (2012). *Hypersonic and supersonic static aerodynamics of Mars Science Laboratory entry vehicle*. NASA. AIAA Member. https://ntrs.nasa.gov/citations/20120011936

ECSS. (2012). *ECSS system glossary of terms*.

ESA. (2000). *Space engineering mechanical-part 2: Structural*.

ESA. (2008). *Space engineering space environment*.

Ferri, F., Colombatti, G., Aboudan, A., Bettanini, C., Debei, S., Harri, A.-M., Lebreton, J.-P., Montmessin, F., Berthelier, J.-J., Gall, A. L., al The and Harri, A. M. (2020). The atmospheric structure of the ice giant planets from in situ measurements by entry probes. *Space Sci Rev*, *216*, 118. https://doi.org/10.1007/s11214-020-00749-9ï

Gaulme, P., Mosser, B., Schmider, F.-X., Guillot, T., and Jackiewicz, J. (2014). Seismology of giant planets. https://doi.org/10.1017/CBO9781107300668.017

Goldreich, P., Murray, N., and Kumar, P. (1994). Excitation of solar p-modes. *The Astrophysical Journal*, *424*, 466–479. https://doi.org/10.1086/173904

Guillot, T. (2022). Uranus and Neptune are key to understand planets with hydrogen atmospheres. *Experimental Astronomy*, *54*, 1027–1049. https://doi.org/10.1007/s10686-021-09812-x

Guo, J., Fu, S., Deng, Y., Xu, X., Laima, S., Liu, D., Zhang, P., Zhou, J., Zhao, H., Yu, H., Dang, S., Zhang, J., Zhao, Y., Li, H., and Duan, X. (2022). Hypocrystalline ceramic aerogels for thermal insulation at extreme conditions. *Nature*, *606*, 909–916. https://doi.org/10.1038/s41586-022-04784-0

Güzelbey, İ. H., Eraslan, Y., and Doğru, M. H. (2018). Numerical investigation of different airfoils at low reynolds number in terms of aerodynamic performance of sailplanes by using XFLR5. *Karadeniz Fen Bilimleri Dergisi*, *8*, 47–65. https://doi.org/10.31466/kfbd.423932

Guzik, A. T., and Benafan, O. (2018). *Design and development of cubesat solar array deployment mechanisms using shape memory alloys*. http://www.sti.nasa.gov

Helled, R., Anderson, J. D., Podolak, M., and Schubert, G. (2010). Interior models of Uranus and Neptune. *The Astrophysical Journal*, *726*, 15. https://doi.org/10.1088/0004-637X/726/1/15

Hibbeler, R. (2018). *Mechanics of materials tenth edition in si units*. www.pearsonglobaleditions.com/hibbeler

Hodges, R. E., Sands, O. S., Huang, J., and Bassily, S. (2006). *High-capacity communications from martian distances part 4: Assessment of spacecraft pointing accuracy capabilities required for large Ka-band reflector antennas*.

Hussmann, H., Palumbo, P., Jaumann, R., Dougherty, M., Langevin, Y., Piccioni, G., Barabash, S., Wurtz, P., van den Brandt, P., Gurvits, L., Bruzzone, L., Plaut, J., Wahlund, J., Cecconi, B., Hartogh, P., Gladstone, R., Iess, L., Stevenson, D., Kaspi, Y., … and Fletcher, L. (2014). *JUICE JUpiter ICy moons Explorer exploring the emergence of habitable worlds around gas giants definition study report european space agency*.

Jacobs, C. S., Bach, U., Colomer, F., García-Miró, C., Gómez-González, J., Gulyaev, S., Horiuchi, S., Ichikawa, R., Kraus, A., Kronschnabl, G., López-Fernández, J. A., Lovell, J., Majid, W., Natusch, T., Neidhardt, A., Phillips, C., Porcas, R., Romero-Wolf, A., Saldana, L., … and Zharov, V. (2012). *The potential for a Ka-band (32 GHz) worldwide VLBI network*. http://ivscc.gsfc.nasa.gov/publications/gm2012/jacobs.pdf

Justh, H. L., Cianciolo, A. M. D., Hoffman, J., and Allen, G. A. (2021). *Uranus global reference atmospheric model (Uranus-GRAM): User guide*. NASA. http://www.sti.nasa.gov

Kastenberg, W. E., and Wilson, R. (2004). Risk of nuclear powered space probes. *Reliability Engineering and System Safety*, *86*, 53–59. https://doi.org/10.1016/j.ress.2003.12.006

Keller, H. U., Barbieri, C., Lamy, P., Rickman, H., Rodrigo, R., Wenzel, K. P., Sierks, H., A'Hearn, M. F., Angrilli, F., Angulo, M., Bailey, M. E., Barthol, P., Barucci, M. A., Bertaux, J. L., Bianchini, G., Boit, J. L., Brown, V., Burns, J. A., Büttner, I., … and Zaccariotto, M. (2007). OSIRIS - the scientific camera system onboard Rosetta. *Space Science Reviews*, *128*, 433–506. https://doi.org/10.1007/s11214-006-9128-4

Lebeau, R. P., Bramesfeld, G., Palotai, C., Dreas, J., Krofta, J., Kirwen, J., and Reyes, P. (2015). *Examining conditions to explore the atmosphere of Uranus with autonomous gliders*.

Leon, V., Stamoulias, I., Lentaris, G., Soudris, D., Gonzalez-Arjona, D., Domingo, R., Codinachs, D. M., and Conway, I. (2021). Development and testing on the european space-grade BRAVE FPGAs: Evaluation of NG-Large using high-performance DSP benchmarks. *IEEE Access*, *9*, 131877–131892. https://doi.org/10.1109/ACCESS.2021.3114502

Lescouzères, R., Wolf, M., Wollenhaupt, B., Goodburn, S., Peukert, M., Biehler, T., Abele, M., Pastorino, M., and Walloschek, T. (2014). *Propulsion system development and verification activities for the 2016 ExoMars trace gas orbiter*.

Mahaffy, P. R., Webster, C. R., Cabane, M., Conrad, P. G., Coll, P., Atreya, S. K., Arvey, R., Barciniak, M., Benna, M., Bleacher, L., Brinckerhoff, W. B., Eigenbrode, J. L., Carignan, D., Cascia, M., Chalmers, R. A., Dworkin, J. P., Errigo, T., Everson, P., Franz, H., … and Mumm, E. (2012). The sample analysis at mars investigation and instrument suite. *Space Science Reviews*, *170*, 401–478. https://doi.org/10.1007/s11214-012-9879-z

Martin, J. W. (2006). *3.1 general strengthening mechanisms: The effect of processing*.

Meisnar, M., Bennett, J. M., Andrews, D., Dodds, S., Freeman, R., Bellarosa, R., Kelleher, J., Graham, A., Norman, A. F., Rohr, T., and Ghidini, T. (2023). Advanced manufacturing of titanium propellant tanks for space applications part 2: A comparative study of residual stresses. *CEAS Space Journal*, *15*, 139–149. https://doi.org/10.1007/s12567-021-00398-w

Meurisse, J. B., Lachaud, J., Panerai, F., Tang, C., and Mansour, N. N. (2018). Multidimensional material response simulations of a full-scale tiled ablative heatshield. *Aerospace Science and Technology*, *76*. https://doi.org/10.1016/j.ast.2018.01.013

MOOG. (2013). *Upper stage engines*.

Mousis, O., Atkinson, D. H., Cavalié, T., Fletcher, L. N., Amato, M. J., Aslam, S., Ferri, F., Renard, J. B., Spilker, T., Venkatapathy, E., Wurz, P., Aplin, K., Coustenis, A., Deleuil, M., Dobrijevic, M., Fouchet, T., Guillot, T., Hartogh, P., Hewagama, T., … and Villanueva, G. L. (2018). *Scientific rationale for Uranus and Neptune in situ explorations*. Elsevier Ltd. https://doi.org/10.1016/j.pss.2017.10.005

Moyer, C. B., Anderson, L. W., and Dahm, T. J. (1970). *A coupled computer code for the transiend thermal responce and ablation of non-charring heat shields and nose tips*. Langley Research Center.

Muhammad, N., Muhalim, F. B., and Krishnan, S. (2010). *Design of nitrogen-tetroxide / monomethyl-hydrazine thruster for upper stage application*.

NASA. (2019). *Mars exploration program Mars relay description for discovery 2019 proposals*.

NASA. (2020). *Multi-mission radioisotope thermoelectric generator (MMRTG)*. www.nasa.gov

NASA. (2022). *Next generation radioisotope thermoelectric generators*. www.nasa.gov

Parys, R. V., and Spindler, B. (2022). *Pu-238 production feasibility study*. Tractebel Engie.

Renard, J.-B., Mousis, O., Berthet, G., Geffrin, J.-M., Levasseur-Regourd, A. C., Rannou, P., and Verdier, N. (2020). The LONSCAPE instrument, a light optical nephelometer sizer and counter for aerosols in planetary environments. *EGU General Assembly*, *2020*. https://doi.org/10.5194/egusphere-egu2020-3495ï

Ritter, H., Franck, M., Santovincenzo, A., and Atzei, A. (2006). *Jupiter entry probe feasibility study from the ESTEC CDF team, heat flux evaluation and TPS definition*. ESA-ESTEC.

Rodmann, J., Miller, A., Traud, M., Bunte, K. D., and Millinger, M. (2021). Micrometeoroid impact risk assessment for interplanetary missions. In J. Rodmann, A. Miller, M. Traud, K. Bunte and M. Millinger (Eds.). ESA Space Debris Office. http://conference.sdo.esoc.esa.int,

Ruijgrok, G. J. (2013). *Elements of airplane performance* (2nd ed.). Delft Academic Press.

Ryschkewitsch, M. G. (1992). *Mission design activities section 1. introduction 1.1 purpose of the guide 1.2 the new-start process for NASA missions*. NASA EMC. http://www.everyspec.com

Saikia, S. J. (2016). *Oceanus mission to explore Saturn and Uranus*.

Sepka, S. A., and Samareh, J. A. (2015). *Thermal protection system mass estimating relationships for blunt-body, earth entry spacecraft*. AIAA. https://ntrs.nasa.gov/search.jsp?R=20160004208

Simon, A., Nimmo, F., and Anderson, R. C. (2021). *Journey to an ice giant system*. www.nasa.gov

Simons, R. N., Wilson, J. D., and Force, D. A. (2008). *High power and effi ciency space traveling-wave tube amplifiers with reduced size and mass for NASA missions*. http://www.sti.nasa.gov

Skeen, M. A. (2013). *Conceptual modeling and analysis of drag-augumented supersonic retropropulsion for application in mars entry, decent, and landing vehicles*.

Spores, R. A., Masse, R., Kimbrel, S., and Mclean, C. (2013). *GPIM AF-M315E propulsion system*.

Taylor, J. (2014). *Deep space communications*.

Taylor, J., Sakamoto, L., and Wong, C.-J. (2002). *Cassini orbiter/Huygens probe telecommunications*.

Terma. (2012a). *Equipment power distribution module*. www.terma.com

Terma. (2012b). *Heater power distribution module*. www.terma.com

Terma. (2012c). *MIL-STD-1553 interface module*. www.terma.com

Terma. (2012d). *Modular medium power unit*. www.terma.com
Terma. (2012e). *Propulsion power distribution module*. www.terma.com
Terma. (2012f). *S3R shunt regulation module*. www.terma.com
Terma. (2012g). *Thermal knives actuation module*. www.terma.com
Torenbeek, E. (2013). *Advanced aircraft design : Conceptual design, analysis and optimization of subsonic civil airplanes* (1st ed.). John Wiley; Sons, Incorporated.
Vinkó, T., Izzo, D., and Bombardelli, C. (2007). Benchmarking different global optimisation techniques for preliminary space trajectory design. *58th International Astronautical Congress*. www.esa.int/gsp/ACT/mad/op/GTOC/index.html
Werner, J. E., Johnson, S. G., Dwight, C. C., and Lively, K. L. (2016). *Cost comparison in 2015 dollars for radioisotope power systems-Cassini and Mars Science Laboratory*. http://www.inl.gov
Wertz, J. R., Everett, D. F., and Puschell, J. J. (2011). *Space mission analysis and design*. Space Technology Library.
Wertz, J. R., Larson, W. J., Kirkpatrick, D., and Klungle, D. (1999). *Space mission analysis and design*. Microcosm.
X, S. (2021). Falcon Heavy user guide.
Yu, F., Zhang, Y., Kong, C., and Yu, H. (2022). Microstructure and mechanical properties of Ti–6Al–4V alloy sheets via room-temperature rolling and cryorolling. *Materials Science and Engineering A*, *834*. https://doi.org/10.1016/j.msea.2022.142600
Zell, P. T. (1993). *Performance and test section flow characteristics of the national full-scale aerodynamics complex 80- by 120-foot wind tunnel*.

A. Requirements

Appendix A lists all the requirements related to the mission and systems. In the table, the abbreviation SC (System Compliance) is related to the requirements linked to engineering budgets. In fact, in specific cases, some subsystems do not comply with the subsystem requirements, but when the general system is analysed, the other subsystem can compensate for such inconsistency.

Table A.1: Stakeholder Requirements

Req ID	Requirement Description	Verification
CNRS01	The system shall gather data on Uranus' atmosphere.	
CNRS02	The system shall allow for data transfer to Earth.	
CNRS03	Mission duration shall be of at least 20 years.	
ESA01	Launch date shall be chosen such that it allows a favourable orientation of the planets	X
ESA02	The mission cost shall not exceed M€ 2500, including launch and operations.	
ESA04	The system shall have a reliability of at least 94%, excluding launch operations.	
ESA05	The system transportation shall be organised in a safe manner.	X
ESA06	The system shall be able to perform measurements during the transfer phase.	X
CUST01	The scientific instrument volume shall not exceed the volume of the payload allocated space in the system.	X
CUST02	The scientific instrument shall be able to interface with the system without influencing its nominal operations.	X

Table A.2: Constraints

Req ID	Requirement Description	Verification
LAU01	The system volume shall not exceed the specified measures in the launch catalogue.	X
LAU02	The system shall survive the launch phase without any damage.	
LAU03	The system shall be able to interface with the launcher without influencing the nominal operations of the subsystems.	
LAU04	The system shall be transported to the launch site at least 4 weeks before the launch date.	X
LAU07	The total mission mass budget shall be less than 6000 kg	X
LAU08	The launch target cost shall not exceed 6% of the mission cost	X
ESA03	The usage of toxic materials shall be minimised	X

Table A.3: Mission Requirements

Req. ID	Requirement Description	Verification
CNRS01.47	The system shall measure the zonal winds	X
CNRS01.48	The system shall investigate the acoustic oscillating modes of Uranus	X
CNRS01.49	Previously used and tested science devices shall be used when feasible	X
CNRS01.50	The system shall gather data about the gravitational field of Uranus.	X
CNRS01.51	The system shall gather data about the magnetic field of Uranus.	X
CNRS01.52	The system shall measure the atmospheric helium abundance	X

Continued on next page

Table A.3 – *Continued from previous page*

CNRS01.53	The system shall measure the abundance of the noble gases	X
CNRS01.54	The system shall measure the reservoirs for the main isotopes of H, He, N, C, O, and heavy noble gases	X
CNRS01.55	The system shall measure the pressure and temperature	X
CNRS01.56	The system shall measure the fraction He/H2	X
CNRS01.57	The system shall measure the vertical distribution of chemical species	X
CNRS01.58	The system shall measure the dynamical structure of Uranus's atmosphere	X
CNRS01.59	The system shall measure the radiative energy balance	X
CNRS01.37	The chosen atmospheric vehicle shall be operational from pressures of 0.1 bar until 10 bar	X
ESA04.04	Sufficient corrections to the orbital trajectory shall be used if the deviation from the trajectory would cause mission failure	X
CNRS04.01	Technical requirements shall come from research and negotiations with clients and potential users (scientists).	X
ESA02.02	The operational cost shall be less than 53% of the target cost of the total mission	X
ESA02.03	Financial budget reviews shall be organised with ESA to accommodate updated expenses	
ESA02.04	CAELUS shall be able to increase the mission budget if ESA cannot accommodate updated expenses.	X
ESA02.05	The total mission cost shall be less than M€2500.	X
ESA02.06	A 20% cost margin shall be maintained for the overall budget	X
ESA01.01	The system shall be launched in the 2030 launch window.	X
CNRS02.03	The orbit architecture at Uranus shall allow for communication with Earth	X
CNRS03.03	The transfer time shall be less than 20 years	X
CNRS03.04	The operations at Uranus shall last no less than 2 hours	X
CNRS03.05	The EOL mission phase shall last at least 10 years	X
CNRS01.74	The system shall have an atmospheric interface velocity of 26.6 km s^{-1}	X
CNRS01.75	The system shall have an atmospheric interface angle between 30° and 45°	X
CNRS01.76	The system shall have an atmospheric interface angle of at maximum 45°	X
CNRS01.77	The system shall have an orbit with a semi-major axis of 133 400 km	X
CNRS01.78	The system shall have an orbital inclination between 80° and 100°	X
CNRS01.81	The system shall have an orbit with a periapsis that exceeds 26 400 km	X
CNRS01.82	The orbiter instruments shall be in flight operating calibration during the planetary flybys	X
CUST03.01	A market analysis shall identify the secondary mission and/or science objectives to reduce development and operational costs.	X
ESA04.01	An extended mission shall be defined for the case that the system will exceed nominal life.	X
ESA03.04	The system shall have a clear end-of-life strategy.	X
ESA03.05	CAELUS shall assure that all external contractors implement sustainable manufacturing methods	X
ESA04.39	The orbiter shall at no point have an altitude lower than 300 km above Venus	X
ESA04.40	The orbiter shall at no point have an altitude lower than 300 km above Earth after having entered solar orbit	X
ESA04.41	The orbiter shall at no point have an altitude lower than 200 km above Mars	X
ESA04.42	The orbiter shall at no point have an altitude lower than 100 000 km above Jupiter	X
ESA04.43	The orbiter shall at no point have an altitude lower than 50 000 km above Saturn	X

Table A.4: Orbiter Requirements

Req ID	Requirement Description	Verification
CNRS02.01	All science data shall be transmitted to Earth.	
CNRS02.02	All housekeeping data shall be transmitted to Earth	X
CNRS01.39	The Orbiter shall perform scientific measurements in a temperature range of 253 - 300 K	X
CNRS03.06	The Orbiter shall withstand the harsh condition of deep space.	
CNRS01.40	The total mission delta V shall be less than of 4.2 $km\,s^{-1}$	X
CNRS01.41	The total BOL power budget of the Orbiter shall be no more than 900 W	X
CNRS01.42	The ΔV for the transfer to Uranus shall be less than 170 $m\,s^{-1}$	X
CNRS01.43	The ΔV for the operations at Uranus shall be of 0.6 $km\,s^{-1}$	X
CNRS01.44	The EOL manoeuvre shall utilise the drag generated by the Uranus atmosphere.	X
CNRS02.04	The Orbiter shall be able to process onboard scientific data for transmission to Earth	X
CNRS02.05	The Orbiter shall be able to collect housekeeping data from all its subsystems	
CNRS02.06	The Orbiter shall be able to receive commands from Earth	
CNRS02.07	The Orbiter shall be able to receive data from the atmospheric vehicle	X
CNRS02.08	The Orbiter shall be able to process commands received from Earth	X
LAU07.01	The Orbiter shall have a total mass budget of less than 6000 kg	X
LAU07.02	The Orbiter shall have a total dry mass of less than 3180 kg	X
LAU02.01	The Orbiter shall withstand maximum launch loads defined by the launch catalogue	
CNRS01.45	The Orbiter shall be able to separate from the atmospheric vehicle upon arrival at Uranus	
CNRS01.61	The orbiter shall have dimensions not exceeding 5.2 x 5.2 x 11.1 m^3	X
CNRS03.08	The Orbiter shall be able to produce a thrust level of at least 400 N	
ESA04.02	Regular housekeeping checks shall be performed during transfer to Uranus	
ESA04.03	The Orbiter shall be evaluated in a testing campaign simulating the mission	
ESA04.05	There shall be a margin of 4% ΔV for emergency manoeuvres or correction burns	X
ESA04.06	The spacecraft position shall be determined with sufficient accuracy to verify the space trajectory and allow for correction burns	X
ESA04.22	The Orbiter shall withstand chemical exposure of chemicals known to be present in Uranus's atmosphere	
ESA04.30	The Orbiter shall have a reliability of at least 99.0%	
LAU03.01	The Orbiter shall be designed such that the interface with the launcher does not have any mismatch	X
LAU03.02	The Orbiter shall be designed such that the interface with the launcher does not cause any damage	
ESA03.06	The Orbiter shall comply with the Planetary Protection Guidelines	X
CNRS01.68	The Orbiter shall sense Uranus's gravitational field with an accuracy of at least 2 $\mu m\,s^{-1}$	X
CNRS01.69	The Orbiter shall measure Uranus' gravitational field in different regions of space	X
CNRS01.70	The gravitational field of the Uranian system shall be measured continuously during operations	X
CNRS01.71	The magnetic field of the Uranian system shall be measured continuously during operations	X
CNRS01.72	The Orbiter shall measure Uranus' magnetic field in different regions of space	X
CNRS01.73	The Orbiter shall sense Uranus's magnetic field with an accuracy of at least 0.1 nT	X
LAU05.01	The Orbiter components shall be easily transportable	X
ESA02.01	The development cost of the Orbiter shall not exceed M€ 835	X

Table A.5: Orbiter TT&C Requirements.

Req ID	Requirement Description	Verification
CNRS02.01-O-TTC.01	The orbiter shall have a high gain antenna with a gain of at least 61.5 dB	X
CNRS02.01-O-TTC.02	The orbiter communication subsystem shall be able to receive the data from the atmospheric vehicle	X
CNRS02.01-O-TTC.03	The orbiter high gain antenna shall have a data transfer speed exceeding 34 kbit s^{-1}	X
CNRS02.01-O-TTC.04	The orbiter shall have a pointing accuracy of at least 159 arcsec	X
CNRS02.01-O_TTC.05	The orbiter shall be able to receive data via the X band	X
CNRS02.01-O-TTC.06	The orbiter shall be able to transmit data via the K band	X
CNRS02.01-O-TTC.07	The orbiter shall have a low gain antenna with a gain of at least 16.3 dB	X
CNRS02.01-O-TTC.08	The orbiter shall have a low gain antenna with a data transfer speed exceeding 1 kbit s^{-1}	X
CNRS02.01-O-TTC.09	The orbiter TT&C high gain subsystem shall communicate all received data to the data handling subsystem	
CNRS02.01-O-TTC.10	The orbiter TT&C low gain subsystem shall communicate all received data to the data handling subsystem	
ESA04.30-O-TTC.01	The reliability of the Orbiter communication subsystem shall exceed 99.9%	X
CNRS01.41-O-TTC.01	The Orbiter communication subsystem shall have a required power of less than 162 W	X
LAU07.02-O-TTC.01	The Orbiter communication subsystem shall have a mass not exceeding 223 kg	X
CNRS03.03-O-TTC.01	The Orbiter communication subsystem shall be able to operate at a temperature of at least 4 K	X
CNRS03.03-O-TTC.03	The Orbiter of the communication subsystem shall be able to operate in the vacuum of space	X
ESA02.01-O-TTC.01	The total cost of the communication subsystem shall not exceed M€ 25	SC
CNRS02.01-O-TTC.11	The signal to noise ratio margin shall be at least 7.23 dB	X

Table A.6: Orbiter Structure Requirements

Req ID	Requirement Description	Verification
LAU02.01-O-STR.01	The structure subsystem shall withstand longitudinal vibrational loads with an amplitude of at least 1g	X
LAU02.01-O-STR.02	The structure subsystem shall withstand axial loads of at least 6g	X
LAU02.01-O-STR.03	The structure subsystem shall withstand lateral loads of at least 2g	X
CNRS01.45-O-STR.01	The structure subsystem shall be able to perform separation from the atmospheric vehicle without any damage	
CNRS01.45-O-STR.03	The structure subsystem shall withstand separation loads of at least 1000g	X
CNRS02.01-O-STR.01	The structure subsystem shall deploy the antenna in its operational position with an accuracy of 1 mrad at a temperature level of at least 4 K	
CNRS03.06-O-STR.02	The structure subsystem shall withstand without degradation temperatures of at least 4 K	

Continued on next page

Table A.6 – *Continued from previous page*

ESA04.30-O-STR.01	A safety margin of 10% shall be implemented for loads in the structure subsystem design	X
ESA04.30-O-STR.02	A safety margin of 30% shall be implemented for thicknesses in the structure subsystem design	X
LAU01-O-STR.01	The structure subsystem shall have a volume of less than 4.5 x 4.5 x 10.1 m^3	X
LAU02.01-O-STR.06	The structure subsystem shall provide an interface for the communication subsystem	X
LAU02.01-O-STR.07	The structure subsystem shall provide an interface for the power subsystem	X
LAU02.01-O-STR.08	The structure subsystem shall provide an interface for the payload subsystem	X
LAU02.01-O-STR.09	The structure subsystem shall provide an interface for the propulsion subsystem	X
LAU02.01-O-STR.10	The structure subsystem shall provide an interface for the data handling subsystem	X
LAU02.01-O-STR.11	The structure subsystem shall provide an interface for the ADCS subsystem	X
LAU02.01-O-STR.12	The structure subsystem shall have a lateral natural frequency above 10 Hz	X
LAU02.01-O-STR.13	The structure subsystem shall have a longitudinal natural frequency above 25 Hz	X
LAU02.01-O-STR.14	The structure subsystem shall withstand shock loads of 1000g	X
LAU02.01-O-STR.15	The structure subsystem shall withstand longitudinal vibrational loads with an amplitude of at least 0.9g	
CNRS01.41-O-STR.01	The structure subsystem shall have a power required of less than 9 W	X
CNRS01.51-O-STR01	The structure subsystem shall deploy the magnetometer at least 3.6 m from the orbiter main body	X
LAU03.02-O-STR.01	The structure subsystem shall separate from the launch vehicle without causing any damage to the other subsystems	
ESA04.03-O-STR.01	The structure subsystem performance shall be evaluated in a fatigue cycle test	
ESA04.03-O-STR.02	The structure subsystem performance shall be evaluated in a radiation test	
ESA04.03-O-STR.03	The structure subsystem performance shall be evaluated in thermal test	
ESA04.03-O-STR.04	The structure subsystem performance shall be evaluated in an ultimate load test	
ESA02.01-O-STR.01	The structure subsystem cost shall not exceed M€ 23.1	X
LAU07.03-O-STR01	The structure subsystem shall have a mass of less than 795 kg	X

Table A.7: Orbiter Propulsion Requirements

Req ID	**Requirement Description**	**Verification**
CNRS.01.40-O-PRP.01	The propulsion subsystem shall provide a total delta V not exceeding 4.2 km s^{-1}	X
CNRS.01.40-O-PRP.02	The propulsion subsystem shall be able to perform multiple burns	X
CNRS01.61-O-PRP.01	The propellant tank volume shall not exceed 10.1 x 4.5 x 2.5 m^3	X

Continued on next page

Table A.7 – *Continued from previous page*

LAU03.01-O-PRP.02	The propulsion subsystem nozzle shall not exceed a diameter of 4.5 m	X
LAU07.01-O-PRP.01	The total propellant mass shall be less than 2820 kg	X
LAU07.02-O-PRP.01	The propulsion subsystem mass shall be less than 414 kg	X
ESA02.01-O-PRP.01	The propulsion subsystem cost shall be less than M€ 23.3	X
ESA04.03-O-PRP.01	The propulsion subsystem shall have a reliability of at least 99.9%	X
CNRS03.08-O-PRP.01	The propulsion subsystem shall provide a thrust of at least 400 N	X
CNRS03.08-O-PRP.02	The propulsion subsystem shall have a specific impulse of at least 300 s	X
CNRS03.08-O-PRP.04	The propulsion subsystem shall use a liquid propellant	X
CNRS03.08-O-PRP.05	The fuel storage temperature shall be lower than 221 K	
CNRS03.08-O-PRP.08	The oxidizer storage temperature shall be lower than 264 K	
CNRS03.08-O-PRP.09	The throat temperature shall not exceed 1853.15 K	
CNRS03.08-O-PRP.07	A single burn shall not be longer than 96 min	X
CNRS01.41-O-PRP.01	The propulsion subsystem shall have a total power required of less than 99 W	X

Table A.8: Orbiter Data Handling Requirements

Req ID	**Requirement Description**	**Verification**
CNRS02.06-O-DH.01	The data handling subsystem shall be able to communicate commands to all other orbiter subsystems	
ESA04.30-O-DH.01	The data handling subsystem shall be able to hibernate	
CNRS02.06-O-DH.02	The data handling subsystem shall have a processing speed exceeding 10 MHz	X
CNRS02.01-O-DH.01	The data handling subsystem shall have a storage capacity exceeding 2 GB	X
CNRS02.04-O-DH.01	The data handling subsystem shall preprocess all data that shall be transmitted	X
ESA04.30-O-DH.02	The data handling subsystem shall be capable of handling program updates until the end of life phase	
ESA04.02-O-DH.01	The data handling subsystem shall be able to receive status assessments of all other orbiter subsystems	
CNRS01.41-O-DH.01	The data handling subsystem power consumption shall not exceed 99 W	X
ESA04.30-O-DH.03	The data handling subsystem reliability shall exceed 99.9%	X
LAU07.02-O-DH.01	The data handling subsystem mass shall not exceed 128 kg	X
ESA02.01-O-DH.01	The data handling subsystem cost shall not exceed M€ 16	SC
CNRS03.03-O-DH.01	The data handling subsystem shall be able to operate in temperatures of at least 252 K	
CNRS03.03-O-DH.02	The data handling subsystem shall be able to operate in the vacuum of space	

Continued on next page

Table A.8 – *Continued from previous page*

CNRS02.01-A-DH.03	The Command & Data Handling subsystem shall have a data compression ratio of 5:1 for relevant data	X
CNRS02.01-A-DH.03	The Command & Data Handling subsystem shall have a data compression ratio of 80:1 for non relevant data	X

Table A.9: Orbiter Power Management Requirements

Req ID	Requirement Description	Verification
ESA04.03-O-PW.01	The power subsystem shall be tested in conditions simulating the mission	
ESA04.30-O-PW.01	The power provision shall include a safety factor of 10% with regard to peak load	X
ESA04.30-O-PW.02	The power subsystem shall have a reliability of 99.9%	X
CNRS01.41-O-PW.01	The power subsystem shall provide a power of at least 162 W to the TTC subsystem	X
CNRS01.41-O-PW.02	The power subsystem shall provide a power of at least 99 W to the PRP subsystem	X
CNRS01.41-O-PW.03	The power subsystem shall provide a power of at least 99 W to the DH subsystem	X
CNRS01.41-O-PW.04	The power subsystem shall provide a power of at least 135 W to the TM subsystem	X
CNRS01.41-O-PW.05	The power subsystem shall provide a power of at least 66 W to the ADCS subsystem (TBC)	X
CNRS01.41-O-PW.06	The power subsystem shall provide a power of at least 198 W to the PLD subsystem	X
ESA02.01-O-PW.1	The power subsystem shall have a maximum cost of M€ 22	SC
LAU07.02-O-PW.1	The power subsystem shall have a mass of 668 kg	X
CNRS01.41-O-PW.01	The power subsystem shall have a power required not exceeding 90 W	X

Table A.10: Orbiter Thermal Management Requirements

Req ID	Requirement Description	Verification
CNRS01.39-O-TM.01	The payload shall be kept at a temperature of at least 283 K during operations	X
CNRS01.41-O-TM.01	The thermal management shall have a maximum power usage of 135 W	X
CNRS03.06-O-TM.01	The orbiter shall have an emissivity of at least 0.05	X
CNRS03.06-O-TM.02	The orbiter shall have an absorptivity of at least 0.42	X
ESA02.01-O-TM.01	The thermal management system shall have a maximum cost of M€ 5	X
ESA04.02-O-TM	The thermal managment subsystem shall supply temperature data to the OBC	
ESA04.02-O-TM.01	The propulsion subsystem temperature data shall be obtained upon request	
ESA04.02-O-TM.02	The communication subsystem temperature data shall be obtained upon request	
ESA04.02-O-TM.03	The payload subsystem temperature data shall be obtained upon request	

Continued on next page

Table A.10 – *Continued from previous page*

ESA04.02-O-TM.04	The structure subsystem temperature data shall be obtained upon request	
ESA04.02-O-TM.05	The power subsystem temperature data shall be obtained upon request	
ESA04.02-O-TM.06	The data handling subsystem temperature data shall be obtained upon request	
ESA04.02-O-TM.07	The ADCS subsystem temperature data shall be obtained upon request	
ESA04.03-O-TM.01	The thermal management shall have a reliability of 99.9%	X
ESA04.32-O-TM.01	The fuel shall be kept below 221 K during operation	X
ESA04.32-O-TM.07	The oxidiser shall be kept below 264 K during operations	X
ESA04.32-O-TM.02	The communications subsystem shall be kept at a temperature of 253 - 333 K during operations	X
ESA04.32-O-TM.03	The structure mechanisms shall be kept at a temperature of 273 - 323 K during operations	X
ESA04.32-O-TM.05	The data handling subsystem shall be kept above 252 K during operations	X
ESA04.32-O-TM.06	The ADCS thrusters subsystem shall be kept between 243 - 338 K during operations	X
LAU07.02-O-TM.01	The thermal management subsystem shall have a mass not exceeding 191 kg	X

Table A.11: Orbiter ADCS Requirements

Req ID	**Requirement Description**	**Verification**
ESA04.03-O-ADCS.01	The ADCS subsystem shall be tested in conditions simulating the mission	
ESA04.30-O-ADCS.01	There shall be a redundancy in the attitude determination subsystem	X
ESA04.06-O-ADCS.04	The ADCS subsystem shall determine the orientation with an accuracy higher than 140 arcsec	X
ESA04.04-O-ADCS.01	The ADCS subsystem shall perform any attitude correctional manoeuvres with a pointing accuracy exceeding 159 arcsec	X
ESA04.01-O-ADCS.01	The ADCS subsystem shall have a maximum cost of M€ 40.4	SC
LAU07.02-O-ADCS.01	The ADCS subsystem shall have a mass of less than 191 kg	X
ESA04.30-O-ADCS.01	The ADCS subsystem shall have a reliability of at least 99.9%	X

Table A.12: Atmospheric Vehicle Requirements

Req. ID	**Requirements Description**	**Verification**
CNRS01.38	The Atmospheric Vehicle shall gather scientific data for at least 2 hours between 1 bar and 20 bar pressure levels	
CNRS02.09	All science data shall be transmitted to the Orbiter	X
CNRS02.10	All housekeeping data shall be transmitted to the Orbiter	X
CNRS01.66	The Atmospheric Vehicle shall perform scientific measurements in a temperature range of 252 K-300 K	X

Continued on next page

Table A.12 – *Continued from previous page*

CNRS03.07	The Atmospheric Vehicle shall withstand the harsh condition of deep space	
CNRS01.67	The total BOL power budget of the Atmospheric Vehicle shall be no more than 375 W	X
CNRS02.11	The Atmospheric Vehicle shall be able to process onboard scientific data for transmission to the Orbiter	
CNRS02.12	The Atmospheric Vehicle shall be able to collect housekeeping data from all its subsystems	
LAU07.03	The Atmospheric Vehicle shall have a total mass budget of less than 1000 kg, including the aeroshell	X
LAU02.01	The Atmospheric Vehicle shall withstand maximum launch loads defined by the launch catalogue	
CNRS01.60	The Atmospheric Vehicle shall have a volume of less 4.5 mx4.5 mx4 m	
CNRS01.62	The Atmospheric Vehicle capsule shall be able to put itself on course for atmospheric entry	X
CNRS01.63	The Atmospheric Vehicle shall have a ballistic coefficient of less than 100 kg m^{-3} during entry	X
CNRS01.64	The Atmospheric Vehicle shall survive entry conditions	
CNRS01.65	The Atmospheric Vehicle shall be able to separate from the aeroshell after entry into Uranus	
ESA04.36	Regular housekeeping checks shall be performed during transfer to Uranus	
ESA04.37	The Atmospheric Vehicle shall be evaluated in a testing campaign simulating the mission	
ESA04.12	The software used shall be able to be changed at least up to the start of the re-entry phase	X
ESA04.38	The Atmospheric Vehicle shall withstand chemical exposure of chemicals known to be present in Uranus's atmosphere	X
ESA04.23	A safety factor of 2 in density shall be taken into account when designing the atmospheric phase	X
ESA04.24	A safety factor of 2 in pressure shall be taken into account when designing the atmospheric phase	X
ESA04.31	The Atmospheric Vehicle shall have a reliability of 95% after entering Uranus atmosphere	X
ESA04.32	The atmospheric vehicle shall keep its subsystems within their operating temperatures during operations	X
ESA04.33	The atmospheric vehicle shall keep its subsystems within safe temperatures under extreme conditions	X
ESA04.34	The atmospheric vehicle shall keep its subsystems within safe temperatures during hibernation	X
ESA03.07	The Atmospheric Vehicle shall comply with the Planetary Protection Guidelines	X
LAU04.01	The Atmospheric Vehicle shall be delivered at the launch site 4 months before launch	
LAU05.01	The Atmospheric Vehicle components shall be easily transportable	X
LAU04.02	The glider shall fit inside the entry capsule	X
ESA02.07	The development cost of the Atmospheric Vehicle shall not exceed M€ 340	

Table A.13: AV Data Handling Subsystem Requirements

Req. ID	**Requirement Description**	**Verification**
ESA04.11-A-DH.01	The total data processor reliability shall be of at least 99.4% over mission duration	X

Continued on next page

Table A.13 – *Continued from previous page*

ESA04.12-A-DH.02	The software used shall be able to be changed at least up to the start of the re-entry phase	X
CNRS02.12-A-DH.01	The Command & Data Handling subsystem shall collect all subsystem data	
CNRS01.38-A-DH.01	The Command & Data Handling subsystem shall activate all glider subsystems upon arrival at Uranus	
ESA04.04-A-DH.01	The Command & Data Handling subsystem shall determine any trajectory changes required for atmospheric flight	
ESA04.04-A-DH.02	The Command & Data Handling subsystem shall send all required trajectory changes to the ADCS subsystem	
CNRS02.11-A-DH.01	The Command & Data Handling subsystem shall process all measurement data for Earth transmission	
CNRS02.09-A-DH.01	The Command & Data Handling subsystem shall have at least 2 GB of data storage	X
CNRS02.09-A-DH.02	The Command & Data Handling subsystem shall have at least 250 MB of program memory	X
CNRS01.38-A-DH.02	The Command & Data Handling subsystem shall be able to process at least 110 MHz	X
ESA02.07-A-DH.01	The Command & Data Handling subsystem cost shall not exceed M€ 1.9	SC
LAU07.03-A-DH.01	The Command & Data Handling subsystem shall have a mass of less than 115 kg	X
CNRS01.67-A-DH.01	The Command & Data Handling subsystem shall have a power required not exceeding 41.25 W	X

Table A.14: AV TT&C Subsystem Requirements

Req ID	**Requirement Description**	**Verification**
CNRS02.01-A-TTC.01	The atmospheric vehicle shall be equipped with a low gain antenna of diameter not exceeding 3 m	X
CNRS02.01-A-TTC.02	The atmospheric vehicle shall transmit data to the Orbiter at a minimum data rate of at least 6373 kbit s^{-1}	X
CNRS02.01-A-TTC.04	The atmospheric vehicle shall be able to communicate with the Orbiter	X
CNRS02.01-A-TTC.05	The atmospheric vehicle shall transmit data using UHF frequency bands	X
ESA04.29-A-TTC.01	The TTC system shall be tested in conditions simulating the mission	
ESA04.31-A-TTC.01	The communication subsystem shall transmit data to the orbiter with a reliability of at least 99.4%	X
ESA02.07-A-TTC.01	The communication subsystem cost shall not exceed M€ 2.2	X
LAU07.03-A-TTC.01	The communication subsystem shall have a mass of less than 21 kg	X
CNRS01.67-A-TTC.01	The communication subsystem shall have a power required not exceeding 67.5 W	SC

Table A.15: AV Structure Subsystem Requirements

Req. ID	**Requirement Description**	**Verification**
LAU02.01-A-STR.01	The structure subsystem shall withstand longitudinal vibrational loads with an amplitude of at least 1g	

Continued on next page

Table A.15 – *Continued from previous page*

LAU02.01-A-STR.02	The structure subsystem shall withstand axial launch loads of at least 6g	X
LAU02.01-A-STR.03	The structure subsystem shall withstand lateral launch loads of at least 2g	X
CNRS01.65-A-STR.01	The structure subsystem shall withstand separation loads with an amplitude of at least 0.9g	
CNRS03.07-A-STR.02	The structure subsystem shall withstand without degradation temperatures of at least 4 K	
CNRS01.37-A-STR.01	The structure subsystem shall withstand aerodynamic peak pressures of at least 20 bar	X
CNRS01.37-A-STR.02	The structure subsystem shall withstand bending loads along the wings of at least 806 N m	X
CNRS01.60-A-STR.01	The structure subsystem shall perform unfolding	X
LAU01-A-STR.01	The structure subsystem shall have a volume of 3 mx3 mx3 m when in the folded configuration	X
LAU01-A-STR.01.01	The structure subsystem wings shall have a span that does not exceed 8 m	X
LAU01-A-STR.01.03	The structure subsystem main body shall have a length that does not exceed 3 m	X
ESA04.31-A-STR.01	A safety margin of 10% shall be implemented for loads in the structure subsystem design	X
ESA04.31-A-STR.02	A safety margin of 30% shall be implemented for thicknesses in the structure subsystem design	X
LAU02.01-A-STR.06	The structure subsystem shall provide an interface for the communication subsystem	X
LAU02.01-A-STR.07	The structure subsystem shall provide an interface for the power subsystem	X
LAU02.01-A-STR.08	The structure subsystem shall provide an interface for the payload subsystem	X
LAU02.01-A-STR.09	The structure subsystem shall provide an interface for the data handling subsystem	X
LAU02.01-A-STR.10	The structure subsystem shall provide an interface with the aeroshell	X
LAU02.01-A-STR.12	The structure subsystem shall have a lateral natural frequency above 10 Hz	X
LAU02.01-A-STR.13	The structure subsystem shall have a longitudinal natural frequency above 25 Hz	X
LAU02.01-A-STR.14	The structure subsystem shall withstand shock loads of 100g	
ESA04.03-A-STR.01	The structure subsystem performance shall be evaluated in a fatigue cycle test	
ESA04.03-A-STR.02	The structure subsystem performance shall be evaluated in a radiation test	
ESA04.03-A-STR.03	The structure subsystem performance shall be evaluated in thermal test	
ESA04.03-A-STR.04	The structure subsystem performance shall be evaluated in an ultimate load test	
ESA04.09-A-STR05	Critical elements of the structure subsystem shall include redundancy	X
ESA04.31-A-STR.01	The unfolding mechanism shall have a reliability of at least 99.4%	X
ESA02.07-A-STR.01	The structure subsystem cost shall not exceed M€ 4	X
LAU07.03-A-STR.01	The structure subsystem shall have a mass of less than 138 kg	X

Table A.16: AV Power Management Subsystem Requirements

Req ID	Requirement Description	Verification
ESA04.29-A-PW.01	The power subsystem shall be tested in conditions simulating the mission	
ESA04.26-A-PW.01	The power provision during the atmospheric phase shall include a safety factor of 1.2 with regard to peak load	X
CNRS01.67-A-PW.01	The power subsystem shall provide a power not exceeding 67.5 W to the TTC subsystem	X
CNRS01.67-A-PW.03	The power subsystem shall provide a power not exceeding 41.25 W to the DH subsystem	X
CNRS01.67-A-PW.04	The power subsystem shall provide a power not exceeding 56.25 W to the TM subsystem	X
CNRS01.67-A-PW.06	The power subsystem shall provide a power not exceeding 82.5 W to the PLD subsystem	X
CNRS01.67-A-PW.07	The power subsystem shall have an energy storage capacity of at least 51 W h	X
CNRS01.67-A-PW.08	The power subsystem shall have a maximum discharge time of 76 h	X
CNRS01.60-A-PW.01	The power subsystem shall have a volume not exceeding 0.52 m^3	X
CNRS03.02-A-PW.01	The power subsystem shall have a cycle life of at least 1 cycle	X
ESA04.31-A-PW.01	The power subsystem shall transmit power to the various subsystems with a reliability of at least 99.4%	X
ESA02.07-A-PW.01	The power subsystem shall have a cost not exceeding M€ 2.1	X
LAU07.03-A-PW.01	The power subsystem shall have a mass not exceeding 63 kg	X
CNRS01.67-A-PW.01	The power subsystem shall have a power required not exceeding 37.5 W	X

Table A.17: AV Thermal Management Subsystem Requirements

Req. ID	Requirement Description	Verification
ESA04.36-A-TM.01	The TM subsystem shall supply temperature data to the OBC	X
ESA04.36-A-TM.02	The ADCS subsystem temperature data shall be obtained upon request	
ESA04.36-A-TM.03	The communication subsystem temperature data shall be obtained upon request	
ESA04.36-A-TM.04	The payload subsystem temperature data shall be obtained upon request	
ESA04.36-A-TM.05	The structure subsystem temperature data shall be obtained upon request	
ESA04.36-A-TM.06	The power subsystem temperature data shall be obtained upon request	
ESA04.36-A-TM.07	The data handling subsystem temperature data shall be obtained upon request	
ESA04.36-A-TM.09	The capsule subsystem temperature data shall be obtained upon request	
ESA04.36-A-TM.10	The decelerator subsystem temperature data shall be obtained upon request	
CNRS01.66-A-TM.01	The payload subsystem shall be kept at a temperature of 252 K-300 K during entry	X
ESA04.32-A-TM.01	The subsystems shall be kept between 273 K-293 K during operation	X

Continued on next page

Table A.17 – *Continued from previous page*

ESA04.32-A-TM.02	The ADCS subsystem shall be kept between 273 K-303 K during operation	X
ESA04.32-A-TM.03	The communications subsystem shall be kept at a temperature of 253 K-333 K during operations	X
ESA04.32-A-TM.04	The structure mechanisms shall be kept at a temperature of 273 K-323 K during operations	X
ESA04.32-A-TM.05	The power subsystem shall be kept between 273 K-293 K during operation	X
ESA04.32-A-TM.06	The data handling subsystem shall be kept at a temperature of at least 252 K	X
ESA02.07-A-TM.01	The thermal management subsystem cost shall not exceed M€ 0.53	X
LAU07.03-A-TM.01	The thermal management subsystem mass shall not exceed 18 kg	X
ESA04.31-A-TM.01	The thermal management subsystem shall have a reliability of 99.4%	X
CNRS01.67-A-TM.01	The thermal management subsystem shall have a power required not exceeding 56.25 W	X

Table A.18: AV ADCS Subsystem Requirements

Req ID	**Requirement Description**	**Verification**
ESA04.29-A-ADCS.01	The ADCS subsystem shall be tested in conditions simulating the mission	
ESA04.13-A-ADCS.02	There shall be a redundancy in the attitude determination subsystem	X
CNRS03.02-A-ADCS.01	The stability derivative Cy_beta shall be positive	X
CNRS03.02-A-ADCS.02	The stability derivative Cl_beta shall be negative	X
CNRS03.02-A-ADCS.03	The stability derivative Cn_beta shall be positive	X
CNRS03.02-A-ADCS.04	The stability derivative Cy_p shall be negative	X
CNRS03.02-A-ADCS.05	The stability derivative Cl_p shall be negative	X
CNRS03.02-A-ADCS.06	The stability derivative Cn_p shall be negative	X
CNRS03.02-A-ADCS.07	The stability derivative Cy_r shall be positive	X
CNRS03.02-A-ADCS.08	The stability derivative Cl_r shall be positive	X
CNRS03.02-A-ADCS.09	The stability derivative Cn_r shall be negative	X
CNRS03.02-A-ADCS.10	The stability derivative Cm_alpha shall be negative	X
CNRS03.02-A-ADCS.11	The real component of the eigenvalues of the symmetric equations of motion shall all be negative	X
CNRS03.02-A-ADCS.12	The real component of the eigenvalues of the asymmetric equations of motion shall all be negative	X
CNRS03.02-A-ADCS.13	The L/W ratio shall be larger than 1	X

Table A.19: AV Capsule Requirements

Req ID	Requirement Description	Verification
ESA04.29-A-CAPS-ADCS.01	The ADCS subsystem shall be tested in conditions simulating the mission	
ESA04.13-A-CAPS-ADCS.01	There shall be a redundancy in the attitude determination subsystem	X
CNRS01.58-A-CAPS-ADCS.01	The ADCS subsystem shall send the decelerator activation command upon reaching a dynamic pressure of 6000 Pa	
ESA04.31-A-CAPS-ADCS.01	The ADCS subsystem shall have a reliability of 99.4%	X
ESA04.29-A-CAPS-ADCS.01	The ADCS system for the space phase shall be tested in conditions simulating the mission	
CNRS01.62-A-CAPS-ADCS.03	The ADCS shall be operational after 20 years	X
CNRS01.62-A-CAPS-ADCS.04	The ADCS shall activate at least once	X
ESA04.35-A-CAPS-ADCS.01	The ADCS activation mechanism shall have redundancies	X
LAU07.03-A-CAPS-HS.01	The heat shield subsystem shall have a mass of less than 500 kg	X
ESA02.01-A-CAPS-HS.01	The heat shield subsystem shall cost less than M€ 0.11	
CNRS01.64-A-CAPS-HS.01	The heat shield subsystem shall withstand a peak heat flux of 20 $MW\,m^{-2}$	X
CNRS01.64-A-CAPS-HS.02	The heat shield subsystem shall withstand a total heat load of 300 $MJ\,m^{-2}$	X
CNRS01.60-A-CAPS-HS.01	The heat shield subsystem shall have a diameter of less than 4.5 m	X
CNRS01.64-A-CAPS-STR.01	The capsule structure shall withstand aerodynamic pressures of 0.1 bar	X
CNRS01.64-A-CAPS-STR.02	The capsule structure shall withstand peak loads from parachute inflation of at least 925 $m\,s^{-2}$	X
CNRS01.64-A-CAPS-STR.03	The capsule structure shall withstand thermal heat loads of at least 523 K	X
CNRS01.64-A-CAPS-STR.04	The capsule structure shall withstand vibrational loads with an amplitude of at least 0.9g	
CNRS01.65-A-CAPS-STR.01	The capsule structure shall perform separation with the atmospheric vehicle without creating any damage to its subsystems	
LAU07.03-A-CAPS-STR.01	The capsule structure shall have a mass of less than 175 kg	X
ESA02.07-A-CAPS-STR.01	The capsule structure cost shall not exceed M€ 5.1	
CNRS01.65-A-CAPS-STR.03	The capsule shall only separate from the glider when the glider status check is nominal	
CNRS01.65-A-CAPS-STR.04	The capsule shall physically separate from the glider with a minimum relative velocity of 60 $m\,s^{-1}$	X
CNRS01.65-A-CAPS-STR.06	The glider contained in the capsule after heatshield separation shall be able to take scientific measurements	X
CNRS01.60-A-CAPS-STR.01	The capsule structure shall have a volume of less than 4.5 x 4.5 x 3 m^3	X
ESA04.29-A-CAPS-DEC.01	The Decelerator subsystem shall be tested in conditions simulating the mission	
ESA04.13-A-CAPS-DEC.01	The Decelerator subsystem shall have a reliability of at least 99.9%	X
CNRS01.38-CAPS-A-DEC.03	The Decelerator subsystem shall reduce the vehicle velocity to 45 $m\,s^{-1}$	X
ESA02.01-A-CAPS-DEC.01	The Decelerator subsystem shall cost less than M€ 0.15	

Continued on next page

Table A.19 – *Continued from previous page*

LAU07.03-A-CAPS-DEC.01	The Decelerator subsystem shall weight less than 100 kg	X
CNRS01.64-CAPS-A-DEC.06	The Decelerator subsystem shock loads shall be less than 150g	X
CNRS01.60-A-CAPS-DEC.01	The Decelerator subsystem shall have a volume of less than 0.5 x 0.5 x 0.5 m^3	
CNRS01.64-CAPS-A-DEC.08	The Decelerator subsystem shock loads shall last for less than 1 s	

B. Scientific Traceability Matrix

Appendix B is related to all the scientific aspects of the mission. First, the scientific requirements of the orbiter (Table B.1) and glider (Table B.2) are given, After that, the scientific traceability matrix is presented in Table B.3.

Table B.1: Orbiter Payload Requirements

Req ID	Requirement Description	Verification
CNRS01.47-O-PLD.01	The speed of sound shall be measured with an accuracy of at least 1%	X
CNRS01.47-O-PLD.02	the altitude profile of atmospheric dynamics, including horizontal winds, waves, and convection shall be measured	X
CNRS01.48-O-PLD.01	The photometric light curve shall be measured for oscillations of the planet	X
CNRS01.49-O-PLD.01	The orbiter shall use previously used and tested science devices when feasible	X
CNRS01.51-O-PLD.01	The orbiter shall measure the internal magnetic field structure with an accuracy of at least 0.1 nT	X
CNRS01.51-O-PLD.02	The orbiter shall measure charged particle concentration over different ranges of space and time with an accuracy of at least 0.1 nT	X
CNRS01.51-O-PLD.03	The orbiter shall measure the energetic particle flux in different orbital ranges with an accuracy of at least 0.1 nT	X
LAU07.02-O-PLD.01	The payload subsystem shall have a mass of less than 477 kg	X
CNRS01.41-O-PLD.01	The payload subsystem shall have a power required of less than 198 W	X

Table B.2: AV Payload Requirements

Req ID	Requirement Description	Verification
CNRS01.52-A-PLD.01	The atmospheric helium abundance shall be measured with an accuracy of at least 2%	X
CNRS01.53-A-PLD.01	The abundance of the noble gases Ne shall be measured with an accuracy of at least 10%	X
CNRS01.53-A-PLD.02	The abundance of the noble gases Xe shall be measured with an accuracy of at least 10%	X
CNRS01.53-A-PLD.03	The abundance of the noble gases Kr shall be measured with an accuracy of at least 10%	X
CNRS01.53-A-PLD.04	The abundance of the noble gases Ar shall be measured with an accuracy of at least 10%	X
CNRS01.54-A-PLD.01	The ratio of nitrogen $^{15}N/^{14}N$ shall be measured with an accuracy of at least 5%	X
CNRS01.54-A-PLD.02	The D/H ratio of hydrogen shall be measured with an accuracy of at least 3 %	X
CNRS01.54-A-PLD.03	The helium isotope ratio $^{3}He/^{4}He$ shall be measured with an accuracy of at least 5%	X
CNRS01.54-A-PLD.04	The noble gas isotope ratio $^{20}Ne/^{22}Ne$ shall be measured with an accuracy of at least 1%	X
CNRS01.54-A-PLD.05	The noble gas isotope ratio $^{35}Ar/^{38}Ar$ shall be measured with an accuracy of at least 1%	X
CNRS01.54-A-PLD.06	The noble gas isotope ratio ^{132}Xe/Total Xe shall be measured with an accuracy of at least 1%	X

Continued on next page

Table B.2 – *Continued from previous page*

CNRS01.54-A-PLD.07	The noble gas isotope ratio ^{131}Xe/Total Xe shall be measured with an accuracy of at least 1%	X
CNRS01.54-A-PLD.08	The noble gas isotope ratio ^{129}Xe/Total Xe shall be measured with an accuracy of at least 1%	X
CNRS01.54-A-PLD.09	The isotope ratios of oxygen ^{18}O/^{17}O/^{16}O shall be measured with an accuracy of at least 1%	X
CNRS01.54-A-PLD.10	The isotope ratios of carbon ^{13}C/^{12}C shall be measured with an accuracy of at least 1%	X
CNRS01.55-A-PLD.01	The atmospheric pressure shall be measured with an accuracy of at least 1%	X
CNRS01.55-A-PLD.02	The atmospheric temperature shall be measured with an accuracy of at least 0.1 K in the upper troposphere	X
CNRS01.55-A-PLD.03	The atmospheric temperature shall be measured with an accuracy of at least 1 K at deeper atmospheric levels	X
CNRS01.56-A-PLD.01	The fraction He/H_2 shall be measured with an accuracy of at least 2%	X
CNRS01.57-A-PLD.01	The vertical profile of elemental abundance relative to hydrogen of the cosmological abundant species carbon from its primary host molecule CH_4 shall be measured with an accuracy of at least 10%	X
CNRS01.57-A-PLD.02	The vertical profile of elemental abundances relative to hydrogen of the cosmological abundant species nitrogen from its primary host molecule NH_3 shall be measured with an accuracy of at least 10%	X
CNRS01.57-A-PLD.03	The vertical profile of elemental abundances relative to hydrogen of the cosmological abundant species sulphur from its primary host molecule H_2S shall be measured with an accuracy of at least 10%	X
CNRS01.57-A-PLD.04	The vertical profiles of elemental abundances relative to hydrogen of the cosmological abundant species oxygen from its primary host molecules H_2O shall be measured with an accuracy of at least 10%	X
CNRS01.57-A-PLD.05	The tropospheric abundances of CO shall be measured with an accuracy of at least 5%	X
CNRS01.57-A-PLD.06	The tropospheric abundances of PH_3 shall be measured with an accuracy of at least 5%	X
CNRS01.57-A-PLD.07	The troposphere abundance of AsH3 abundances shall be measured with an accuracy of at least 10%	X
CNRS01.57-A-PLD.08	The troposphere abundances of GeH_4 shall be measured with an accuracy of at least 10%	X
CNRS01.58-A-PLD.01	The altitude structure and properties of clouds, including determination of the aerosol optical properties, size distributions, number/mass densities, and possibly composition shall be measured	X
CNRS01.58-A-PLD.02	The altitude structure and properties of haze layers, including determination of the aerosol optical properties, size distributions, number/mass densities, and possibly composition shall be measured	X
CNRS01.59-A-PLD.01	The altitude profile of the net radiative balance between solar visible insulation and upwelling thermal infrared radiation shall be measured	X
CNRS01.49-A-PLD.01	The orbiter shall use previously used and tested science devices when feasible	X
LAU07.03-A-PLD.01	The payload subsystem mass shall not exceed 93 kg	X
CNRS01.67-A-PLD.01	The payload subsystem shall have a power required that does not exceed TBD W	X

Table B.3: Science traceability matrix

Science goal	Science objective	Science question	Priority	Science measurement	Instrument	Identifier Code
Studying the magnetospheres	Determine how it was formed	What is the internal magnetic field structure?	2	Magnetic particles and fields	MAG (orbiter)	CNRS01.73
		Which material is the core made of?	2	Gravitational perturbations	RSE (orbiter)	CNRS01.68 - CNRS01.70
	Determine how it interacts with the solar wind	How do charged particles concentration and fields change over ranges of time (spin, solar wind variability)	2	Magnetic particles and fields	MAG (orbiter)	CNRS01.73
		How do charged particles concentration and fields change over ranges of space (distance, latitude, local time)	2	Magnetic particles and fields	MAG (orbiter)	CNRS01.72
	Determine how the magnetic field interacts with the upper atmosphere	How do the energetic patricle fluxes change in different orbital ranges	2	Magnetic particle fluxes	MAG (orbiter)	CNRS01.71-CNRS01.73
Studying the atmospheres		What is the radiative energy balance of the atmosphere?	1	The altitude profile of net radiative balance between solar visible insulation and upwelling thermal infrared radiation	NFR (glider)	CNRS01.59-A-PLD.01
	Determine the compositional thermal, and dynamical structure of Uranus' atmosphere	What is the vertical structure, composition and properties of Uranus' cloud and haze layers?	1	Aerosol optical properties, size distribution, number/mass densities, and possibly composition. The altitude profile of atmospheric dynamics.	Visible-IR imaging spectrometer, Camera, Nephelometer (orbiter, glider)	CNRS01.58-A-PLD.01, CNRS01.58-A-PLD.02
		Does Uranus have acoustic oscillating modes?	2	The photometric light curve	Camera (orbiter)	CNRS01.48-O-PLD.01
		What is the vertical structure of Uranus' atmospheric temperatures and stability? How do atmospheric winds and wave phenomena vary as a function of depth?	1	Pressure, temperature from the upper atmosphere to 10 bar. Profile of descent glider telemetry Doppler frequencies zonal winds from 0.1-10 bar	Visible-IR imaging spectrometer, RSE, ASI (orbiter, glider)	CNRS01.47-O-PLD.01, CNRS01.47-O-PLD.02, CNRS01.55-A-PLD.01 - CNRS01.55-A-PLD.03
Sampling the planetary composition		How do convective motions and vertical mixing shape the vertical distribution of chemical species?	1	Vertical profiles of CH_4, NH_3, H_2S, and H_2O	TLS (glider)	CNRS01.57-A-PLD.01 - CNRS01.57-A-PLD.04
		How do convective motions and vertical mixing shape the vertical distribution of chemical species?	1	Vertical profiles of CO, PH_3, AsH_3, GeH_4	MS, ASI (glider)	CNRS01.57-A-PLD.05 - CNRS01.57-A-PLD.08
	Determine the composition of Uranus' well-mixed atmosphere beneath the clouds	What are the most important reservoirs for the main isotopes of H, He, N, C, O, Ne and heavy noble gases?	1	$^{14}N/^{15}N$, $^{12}C/^{13}C$, D/H, $^{3}He/^{4}He$, Ne, Ar, Kr and Xe isotopes, $^{18}O/^{17}O/^{16}O$	MS, ASI (glider)	CNRS01.54-A-PLD.01 - CNRS01.54-A-PLD.10
		What are the well-mixed abundances of the noble gases?	1	He, Ne, Xe, Kr, Ar	MS, ASI (glider)	CNRS01.52-A-PLD.01 - CNRS01.52-A-PLD.04
		What is the abundance of helium to H_2?	1	He/H_2	MS (glider)	CNRS01.56-A-PLD.01
Studying the major moons	Determine how it was formed	What is the internal magnetic field structure?	2	Magnetic particles and fields	MAG (orbiter)	CUST03.01
		What is the core made of?	2	Gravitational perturbations	RSE (orbiter)	CUST03.01
	Investigate the surface	What is the height profile?	2	Time-of-flight of a laser pulse	Laser Altimeter (glider)	CUST03.01
		What is the composition?	2	Measure the albedo	Laser Altimeter, Visible-IR imaging spectrometer	CUST03.01
		What are the physical properties?	2	Ices, salts, minerals, organic compounds	Visible-IR imaging spectrometer	CUST03.01
Studying the rings	Determine the structure	How do the rings influence the radio signals?	2	Transmitted radio signals	RSE (orbiter)	CUST03.01
	Determine the composition					
Studying the outer Solar System	Investigate planets during flybys	Similar to all the previously mentioned priority 2 questions	3	Similar to all the previously mentioned priority 2 measurements	Orbiter payload	CUST03.01
	Investigate the possibility of Planet 9's existence	How much does the spacecraft diverge from the nominal interplanetary flight path?	3	Radial velocity of the spacecraft during Jupiter and Uranus transfer	Antenna dish (orbiter)	CUST03.01